Quantum Information Processing with Non-classical Light

A dissertation submitted to Queen's University, Belfast for the degree of Doctor of Philosophy

by

Hyunseok Jeong, M.S., B.S.

School of Mathematics and Physics
Queen's University, Belfast

November 16, 2003

Dedicated to my parents.

Abstract

The main purpose of this dissertation is to suggest and investigate various schemes for quantum information processing utilising non-classical light. We define a qubit basis with coherent states and develop quantum information processing schemes based on it. Teleportation via a mixed entangled coherent state was investigated with Bell-state measurement using linear optical elements. Universal quantum computation with coherent states is suggested based on the teleportation and Bell-measurement schemes. Proposals for entanglement concentration of pure entangled coherent states and purification of mixed entangled coherent states are found to distil highly entangled coherent states even in a noisy environment. We briefly discuss how to generate cat states which are used as qubits in our suggestions. A scheme to simulate quantum random walks with classical fields is suggested using linear optical devices. The majority of quantum information applications have been developed based on simple two-dimensional systems while continuous-variable states are useful in optical experiments. Our suggestions try to bridge this gap and bring quantum information applications closer to experimental realisations in optical systems. Our approach has merits particularly in simplicity compared with others for practical implementations of quantum information processing.

The dissertation is also dedicated to studies on quantum entanglement, quantum nonlocality and decoherence for various quantum states. We investigate entangled coherent states in the framework of 2×2 Hilbert space. It is found that the quantum nonlocality of an entangled coherent state persists longer when considered in 2×2 Hilbert space. When it decoheres it is found that the entangled coherent state fails the nonlocality test, which contrasts with the fact that the decohered entangled state is always entangled. Previous studies on quantum non-locality for continuous variables based on dichotomic observables are re-examined. It is shown that it does not have to be a maximally entangled state to give the maximal violation of the Bell's inequality. This is attributed to a generic problem of testing the quantum non-locality of an infinite-dimensional state using a dichotomic observable.

Acknowledgements

It is my great pleasure to thank many people who have contributed to this dissertation. I would like to thank my supervisor Dr Myung Shik Kim for his excellent guidance and advice during my doctoral course. This dissertation would never have been completed without his patient guidance. I am grateful to my other supervisor Professor Stuart Swain for his warm help and support as the leader of the quantum optics and quantum information theory group at Queen's. I am also thankful to Professor Young-Jai Park, Professor Andrew Whitaker and Dr Jim McCann who have been extremely kind to support me. I thank Professor Jaejun Yu for all his great help through exciting discussions during the first year of my masters course.

I would like to thank my collaborators. This dissertation is a collaborative product with Dr Myung Shik Kim, Dr Jinhyoung Lee, Derek Wilson, Wonmin Son and Mauro Paternostro. Dr Jinhyoung Lee has often surprised me with his insight into many physics and mathematics problems. It was Dr Lee who made a decisive influence on my choosing quantum computation and quantum information theory for my postgraduate study. My office mate Derek Wilson has always kindly helped me in many aspects during my stay at Queen's. Lots of inspiring discussions have been had with Wonmin Son. Mauro Paternostro, a passionate person from Sicily, has impressed me with his ideas and ardour for physics. I feel extremely lucky that I have been able to work with them. I thank those researchers who spent their precious time for the helpful discussions during their visit to Queen's or who kindly answered my email questions — Professor Ian Walmsley, Dr Vlatko Vedral, Professor Klaus Mölmer, Professor Kyuman Cho, Dr Zhi Zhao, Dr Bill Munro, Dr Friedrich König and more. I thank James McAuley and Peter Cowan for their reading my dissertation as non-specialists and making a lot of useful comments. I will not forget James and Peter's friendship. I would like to thank Lawrence Lau, Dennis and Annie Rankin, Jinlu Wu, W. H. Lam, Stewart Wilson and Gregory Neville (and many more) for their warm friendship. I deeply appreciate Tony Yu, Eileen Nugent and Helen McAneney's help and kindness.

I am greatly indebted to my family for their love and support to me. My parents and brother have always been my best supporters. Many thanks go to my beloved wife for her devotional love and care. I deeply thank God who has led me so far.

List of Publications

[1] H. Jeong, M. Paternostro, and M. S. Kim, *"Simulation of quantum random walks using interference of classical field"*, to be published in Phys. Rev. A.

[2] H. Jeong, W. Son, M. S. Kim, D. Ahn, and C. Brukner, *"Quantum nonlocality test for continuous-variable states with dichotomic observables"*, Phys. Rev. A **67**, 012106 (2003).

[3] H. Jeong and M. S. Kim, *"Entanglement purification for entangled coherent states"*, Quantum Information and Computation **2**, 208 (2002).

[4] D. Wilson, H. Jeong and M. S. Kim, *"Quantum nonlocality for a mixed entangled coherent state"*, J. Mod. Opt. **49**, 851 (Special Issue for QEC 15, 2002).

[5] H. Jeong and M. S. Kim, *"Efficient quantum computation using coherent states"*, Phys. Rev. A **65**, 042305 (2002).

[6] H. Jeong, M. S. Kim and J. Lee, *"Quantum-information processing for a coherent superposition state via a mixed entangled coherent channel"*, Phys. Rev. A **64**, 052308 (2001).

[7] J. Lee, M. S. Kim and H. Jeong, *"Transfer of nonclassical features in quantum teleportation via a mixed quantum channel"*, Phys. Rev. A **62**, 032305 (2000).

[8] H. Jeong, J. Lee and M. S. Kim, *"Dynamics of nonlocality for a two-mode squeezed state in a thermal environment"*, Phys. Rev. A **61**, 052101 (2000).

Contents

List of Figures

Chapter 1

Introduction

The tremendous progress in the understanding of nature in the last century owes much to the epoch-making success of quantum mechanics. Despite its incredible success in understanding the microscopic world and predicting experimental results, quantum mechanics has puzzled scientists because it requires a revolutionary change of their viewpoint on nature. In quantum mechanics, a quantum system experiences two completely distinguished processes. One is unitary evolution (U) which is a deterministic process, and the other is reduction of the state vector (R) which is a probabilistic process. It is assumed that a closed quantum system always undergoes U processes, and R processes occur only when measurements by an observer are applied. During U processes, the quantum system can be in a superposition of possible measured-out states and the interference between the superposed states makes various non-classical phenomena. This picture of nature including the intrinsic probability involved with measurements seemed unsatisfactory to some of the pioneers of quantum mechanics. Einstein, as one of those, expressed this dissatisfaction saying 'God does not play dice'. Schrödinger's cat paradox is an illustration of how strange this picture is: If the postulates of quantum mechanics are applied to macroscopic systems, there must exist, for example, a linear superposition of dead cat and alive cat states. Another example of the oddness of quantum mechanics is nonlocal correlation or quantum entanglement between distant physical systems. Einstein, Podolsky, and Rosen argued that quantum mechanics is an incomplete theory because it contradicts the idea of local reality, which is called EPR paradox [1]. Bell suggested an inequality which enables experimental tests on this paradox [2]. Ironically, it is not completeness of quantum mechanics but

the idea of local reality that has been abandoned among scientists.

Nowadays, another remarkable innovation in science and technology is on the move based on quantum mechanics. The recent development of quantum information theory has brought about advances in the fundamental understanding of quantum mechanics and the possibility of wide applications for future technology. The promise of new technologies like quantum computation [3, 4, 5, 6], quantum teleportation [7, 8, 9], and quantum cryptography [10, 11] has attracted considerable attention not only among physicists but also among the public audience. The inventors of quantum mechanics could not have dreamed, for example, that the characteristics of U and R processes of quantum mechanics or entanglement of the EPR state can be useful for factoring large integers or secure key distribution. Furthermore, quantum information theory has led to a deeper understanding of quantum mechanics itself. For example, fundamental features of quantum mechanics have been intensively reconsidered in terms of quantum entanglement. It is an important subject in quantum information theory how to define, quantify and utilise quantum entanglement, which is not only a crucial nature of quantum mechanics but also a useful resource for quantum information processing. There has been great progress on understanding and manipulating quantum entanglement in recent years.

Quantum information technologies are expected to overcome limitations of classical information technologies. The idea of quantum computing originated in the fact that computers are physical systems and computation processes are physical processes (See Fig. 1.1). The doubling of the number of transistors per integrated circuit every couple of years has been maintained for more than 30 years, as was predicted by Moore [12]. Even though it has recently been slowed down and shown some sign of saturation, at some point, it will be unavoidable to apply the law of quantum mechanics to information processing in computation. Feynman firstly observed, in the 1980's, that certain quantum mechanical effects cannot be simulated efficiently on a classical computer [3]. In 1990's, it has been found that the quantum parallelism based on the characteristics of U processes enables faster computation in problems like factoring large integers [4] and database search [5]. It is worth noting that quantum mechanics enables reversible gate operations in computation without heat dissipation because of the reversibility of U processes. This can be a remarkable advan-

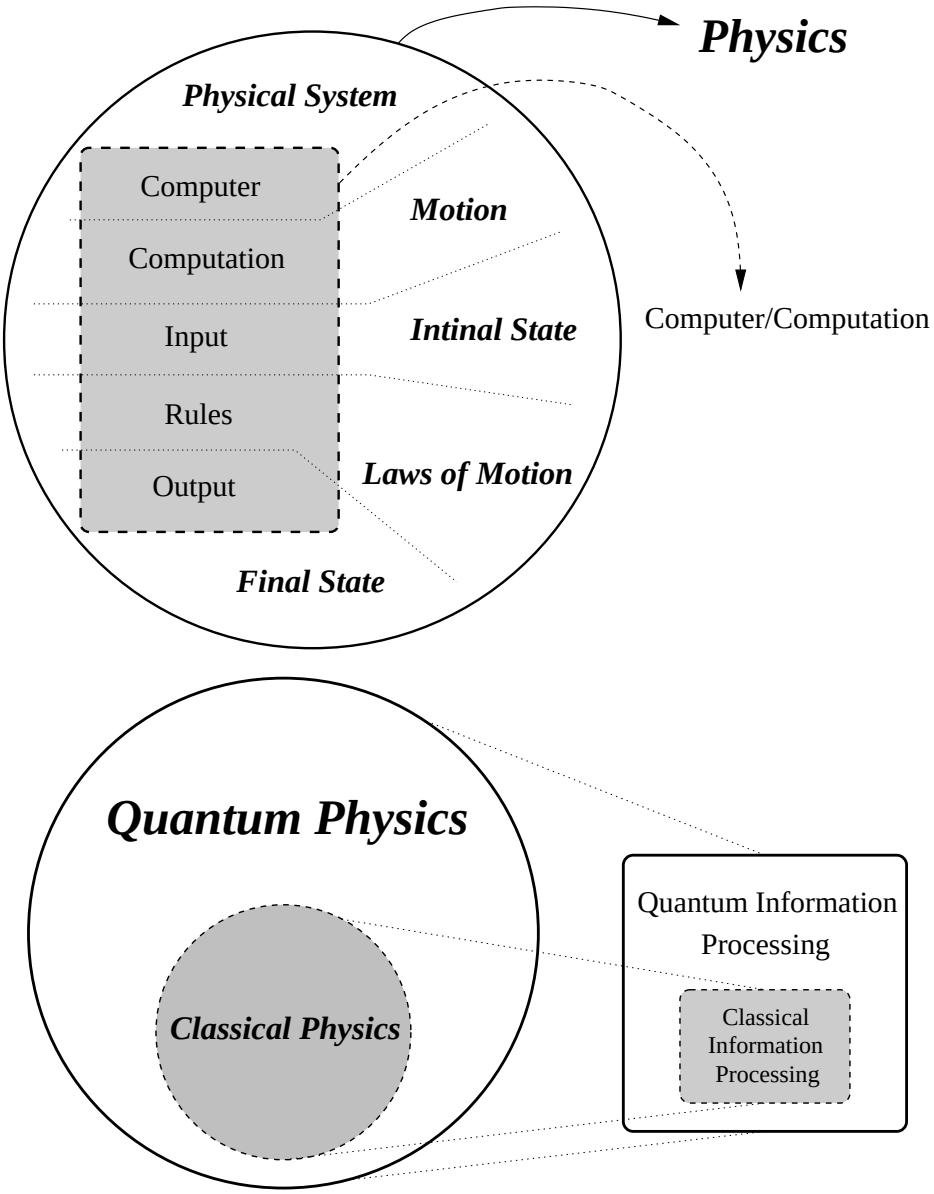

Figure 1.1: Why *physics* for quantum information processing? Two diagrams to show that a computer is a physical system and computation is a physical process. If classical physics is a limiting case and subset of quantum physics, classical information processing should also be a subset of quantum information processing. We notice that there remains a wide unexplored area for quantum information processing. The upper diagram is based on Deutsch's lecture [13].

tage to implement physical computation on such a small scale. Communication and cryptography technologies have also been explored based on quantum mechanics. Quantum key distribution can allow for secure communication, which can never be performed by a classical way. The nonlocal property of quantum mechanics enables a striking phenomenon called quantum teleportation. By quantum teleportation, an unknown quantum state is disintegrated in a sending place and its perfect replica appears at a distant place. Teleportation is not only a demonstration of quantum mechanics but also a useful tool for quantum computation and communication. High precision measurement and lithography utilising quantum entanglement have been studied to increase the resolution limit beyond the standard uncertainty limit. It is quantum coherence that plays the crucial role in all the quantum information technologies discussed above.

In spite of the striking developments in this field over the past 10 years, there is still a long way to go before the realisation of quantum information processing for practical use. For quantum computation, researchers must find a scalable physical qubit system, universal set of gate operations, and qubit initialisation/readout methods. Furthermore, unavoidable errors occur due to decoherence and imperfect operations during quantum computation processes: Quantum error correcting methods [14, 15] are necessary for an implementation of a reliable quantum computer. There are several different approaches to the implementation of a quantum computer. Nuclear magnetic resonance (NMR), ion trap, neutral atom, optical and solid state systems have been studied as such candidates with their own particular strengths. So far, the most advanced demonstrations of quantum computing have not gone beyond manipulating more than 7 qubits, which means they are still at the basic stage. In 1998, Chuang *et al.* reported a two-qubit realisation of a simple quantum algorithm (Deutsch-Jozsa algorithm), achieved using the bulk NMR technique [16]. In the same year and the following year, there were several similar experimental demonstrations; for example, Jones and Mosca created a liquid-based two-qubit device, where the two qubits were stored in the nuclear spins of hydrogen atoms [17]. Most recently, Vandersypen *et al.* developed a seven-qubit device using NMR to demonstrate Shor's factoring algorithm in 2001 [18]. Now in 2003, there are optimistic researchers like Stoneham who believes that he can make a viable desktop quantum computer based on the silicon approach

by 2010 [19]. Long-distance quantum entanglement is the key ingredient for quantum cryptography and communication. Over the past 20 years, many optical experiments have demonstrated nonlocal effects in the laboratory [20, 21] and more recently over ranges of up to 10 km in optical fibres [22]. Most recently, Aspelmeyer *et al.* showed that entanglement of the photon polarisation can be maintained in *free space* over a separation of 600 metres [23]. Quantum cryptography is known as one of the most promising quantum information applications for successful commercialisation in the near future. Even though limitations of real physical devices and the inclusion of noise sources may be obstacles, remarkable experimental progress has been made since the original quantum cryptography experiment over 32 centimetre was performed [24]. In 2003, Shields *et al.* were able to demonstrate quantum cryptography over optical fibres longer than 100 kilometres [25], which should be enough to cover a large metropolitan area. According to some media coverage, it is expected that we will see commercial quantum cryptography products in the marketplace in no more than a couple of years[1]. There are lots of challenging problems in this rapidly developing field.

In this dissertation, we address quantum information theory and quantum information processing via continuous variables in optical systems. Quantum optics is a young field which has been developed based on quantum theory of light and there have been endeavours to apply the knowledge of quantum optics to quantum information processing. Optical systems have some remarkable advantages as a candidate for the implementation of quantum computation [26]. For example, most of the operations may be performed at room temperature, and coherence time of photons is long compared with operation time typically required. In particular, we investigate quantum information processing utilising optical coherent states. In our framework, quantum computation, quantum teleportation and entanglement purification are developed using coherent states and their superposition and entanglement. The single-photon based approach and continuous-variable approach based on Gaussian states have been studied for various quantum information processing applications. Recently, Knill *et al.* showed that universal gate operations for quantum computation can be implemented using only linear devices [27]. Gaussian continuous-variable states have been studied particularly for quantum cryptography [28, 29, 30]

[1] A. Shields, BBC news, 5 June 2003.

and teleportation [31, 32]. Our approach is different from those two approaches and has its own particular merits when compared to the others. In the single-photon approach, the requirement for resources becomes very demanding for near-deterministic quantum computation and nonlinear effect is required for a complete Bell-state measurement. The majority of quantum information applications have been developed based on simple two-dimensional systems, which cannot be directly applied to continuous-variable states. In our approach, we deal with superposition and entanglement of coherent states, which are non-Gaussian continuous-variable states, in the framework of simple two-dimensional systems. In this framework, Bell state measurements are simply performed using linear optical devices so that simpler schemes can be constructed for quantum teleportation and quantum computation. This approach may be powerful with pre-arranged *propagating* optical coherent superposition states (so called cat states). However, it should be noted that the generation of an optical cat state requires a strong nonlinear interaction, which is very demanding in current technology. We therefore develop a scheme to generate a coherent superposition state with a relatively small nonlinear effect and conditional measurements. Besides the applications for quantum information processing, we study nonlocal properties of continuous variable states which are used for quantum information processing, which provides deeper understanding of Gaussian and non-Gaussian continuous-variable states.

The dissertation is organised as follows. Chapter 2 contains an introduction to basic concepts of quantum information theory and frameworks of our work for the development of quantum information processing schemes in this dissertation. The entangled coherent states and Bell measurement scheme with linear optical devices are introduced. Nonlocality of continuous-variable states, which are used as quantum channels for our approach, is studied in Chapters 3, 4 and 5. We investigate the dynamic behaviour of quantum nonlocality for continuous-variable states and find out some interesting phenomena. Chapters 6 to 9 are devoted to the implementation of quantum information processing. Quantum teleportation, computation and entanglement purification schemes are investigated. A coherent state qubit is found to be a strong candidate for quantum information applications. Quantum random walks with all-optical devices are addressed in Chapter 10. We show that quantum random walks can be simulated with classical light and linear optical devices. In Chapter 11, we

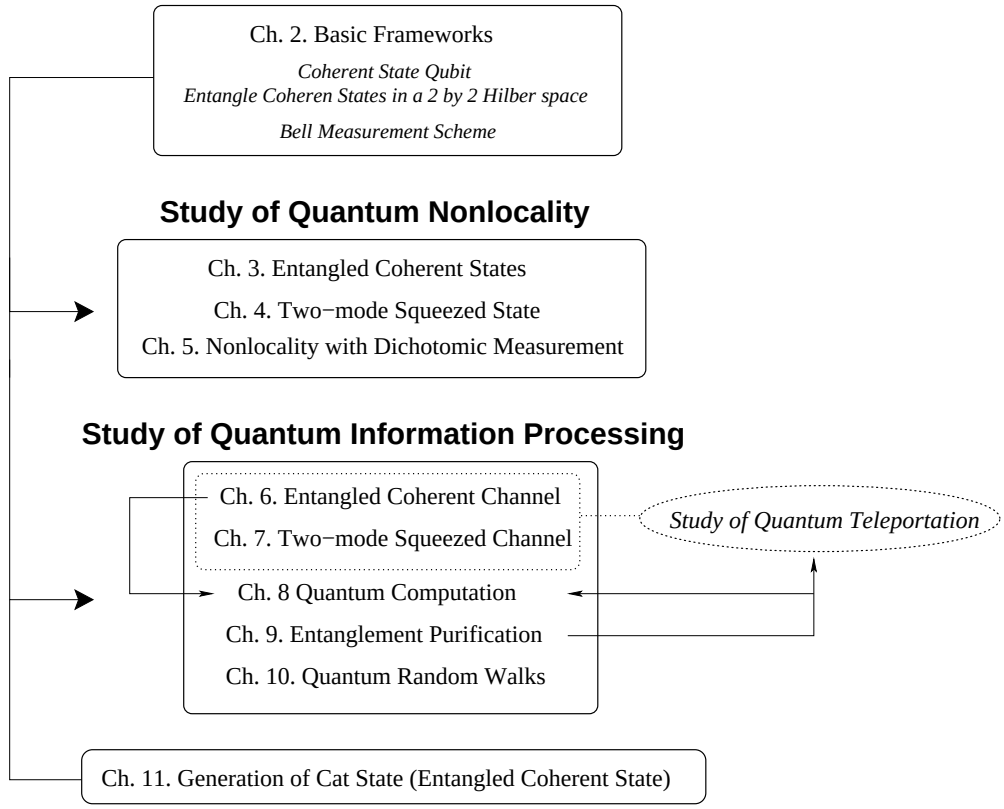

Figure 1.2: An outline of the dissertation.

study the generation of cat states, which is a crucial requirement for most of our schemes. We conclude with some final remarks and prospects in Chapter 12. It is assumed that readers of this dissertation have basic knowledge and experience of quantum mechanics and quantum optics.

Chapter 2

Basic Concepts and Frameworks

2.1 Qubit

The basic unit of classical information is the 'bit'. A bit can take either 0 or 1 for its value and contains the smallest amount of information. A classical bit can be realised in a simple physical system. For example, one can imagine an electric signal which is either 'on' or 'off'. Classical information processing is concerned with how to encode, decode, store, transmit, and protect classical information which can be expressed by bits, in efficient ways. Shannon, in his pioneering work, dealt with how to compress and reliably transmit classical information [33].

Quantum mechanics introduces two crucial tools to describe nature: observables and state vectors. In quantum mechanics, there exists a Hermitian operator, called observable, for every measurable quantity and the state of a physical system is represented by a state vector defined in a Hilbert space. Differently from classical physics, quantum physics allows a linear superposition (or linear combination) of two different states. It should be noted that there is no classical analogy of a linear superposition state. Such a state must be distinguished from a case of a statistical mixture of two different states or any other classical situation. Let us consider a quantum particle labelled A and suppose that $|x_1\rangle$ represents the state of the particle being around the position x_1 and $|x_2\rangle$ the state of its being around x_2[1]. One of the possible linear superposition

[1]For example, we can suppose two potential wells separated each other as depicted in

states where particle A can be is

$$\frac{1}{\sqrt{2}}(|x_1\rangle + e^{i\varphi}|x_2\rangle), \tag{2.1}$$

where the overall $1/\sqrt{2}$ factor is for the normalisation of the total probability and φ is the local phase factor. Once we measure the position of particle A to find out where it 'really' is, the state (2.1) will collapse and particle A will be found either around x_1 or around x_2 with the equal probability 1/2. One of the remarkable features of the superposition state (2.1) is that the interference between the states $|x_1\rangle$ and $|x_2\rangle$ can affect the probability distribution of the position measurement on the state (2.1). The interference pattern varies according to the value of φ. Eq. (2.1) does not mean that particle A is either around x_1 or around x_2 and their probabilities are equal (a case of the statistical mixture[2]), nor that particle A is somewhere between x_1 and x_2. It is also dangerous to say that particle A is both around x_1 and around x_2 at the same time, *i.e.,* it is spread, because no one can verify it by any type of direct measurement. There have been number of paradoxical examples to demonstrate the strangeness of this 'principle of linear superposition'. Schrödinger's cat paradox shows how odd the quantum mechanical description of nature could be when it is applied to macroscopic physical systems. The gedanken experiment of a double slit explains the interference effect of a *single* quantum particle in a superposition state [34]. Hardy's paradox illustrates how a quantum superposition produces a nonsensical result when it is involved with the interaction between matter and anti-matter [35]. All these examples show how a quantum superposition of two states, say $|A\rangle$ and $|B\rangle$, can give the 'third' experimental result by quantum interference that can never be obtained from $|A\rangle$, $|B\rangle$ nor a classical mixture of $|A\rangle$ and $|B\rangle$. These effects (for example, the interference fringe in the double slit gedanken experiment) disappear when any measurement is performed to trace the trajectory of the quantum phenomenon. There are still controversies over the origin of this oddity [36, 37] including some inspiring experimental en-

Fig 2.1. To be precise, the component states $|x_1\rangle$ and $|x_2\rangle$ should not be position eigenstates but be 'moderately' localised states like Gaussian wave packets. While a classical particle should be in one or the other well, a quantum particle can be in a superposition state of the two states until a measurement is performed to find out its position.

[2]A state corresponding to a statistically mixed state of $|x_1\rangle$ and $|x_2\rangle$ with equal probabilities should be represented by a density operator $N(|x_1\rangle\langle x_1| + |x_2\rangle\langle x_2|)$, where the normalisation factor N is determined by the overlap between $|x_1\rangle$ and $|x_2\rangle$.

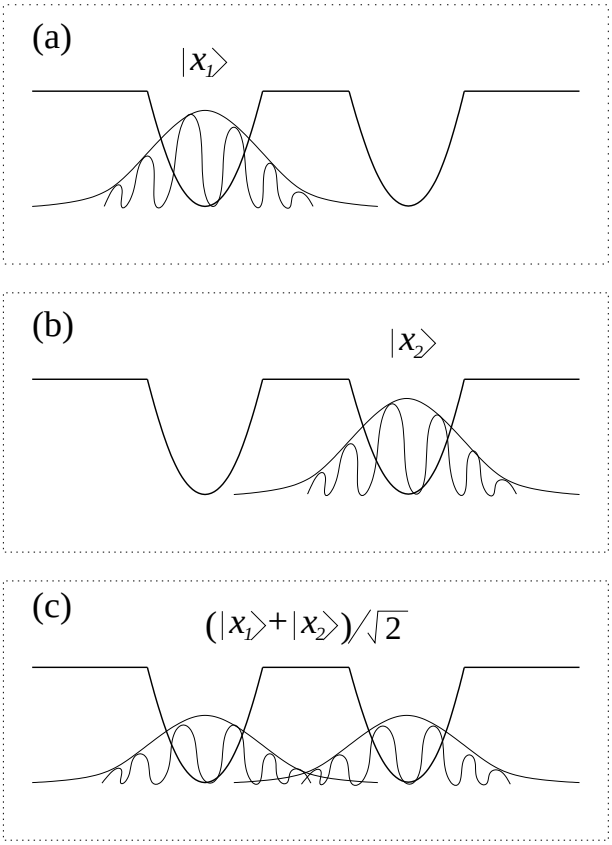

Figure 2.1: A schematic of a linear superposition of two Gaussian wave packets in a double potential well. A classical particle should be in one of the two potential wells at a certain point, but a quantum particle can be in a superposition of two different states like (c).

deavours to close these controversies [38, 39]. However, it is beyond the scope of this dissertation to discuss the debates around these problems in further detail.

This crucial principle of quantum physics forces one to introduce a new concept of the bit for quantum information. A quantum bit (qubit), the basic element for quantum information, is defined as an arbitrary superposition of the two truth value states, one for logical 0 and the other for logical 1. As we have already mentioned, it represents neither a case of a statistical mixture of 0 and 1 nor a value between those two. The qubit is defined in a two-dimensional Hilbert space $\mathcal{H}$ spanned by orthonormal basis vectors:

$$\{|0_L\rangle, |1_L\rangle\}. \tag{2.2}$$

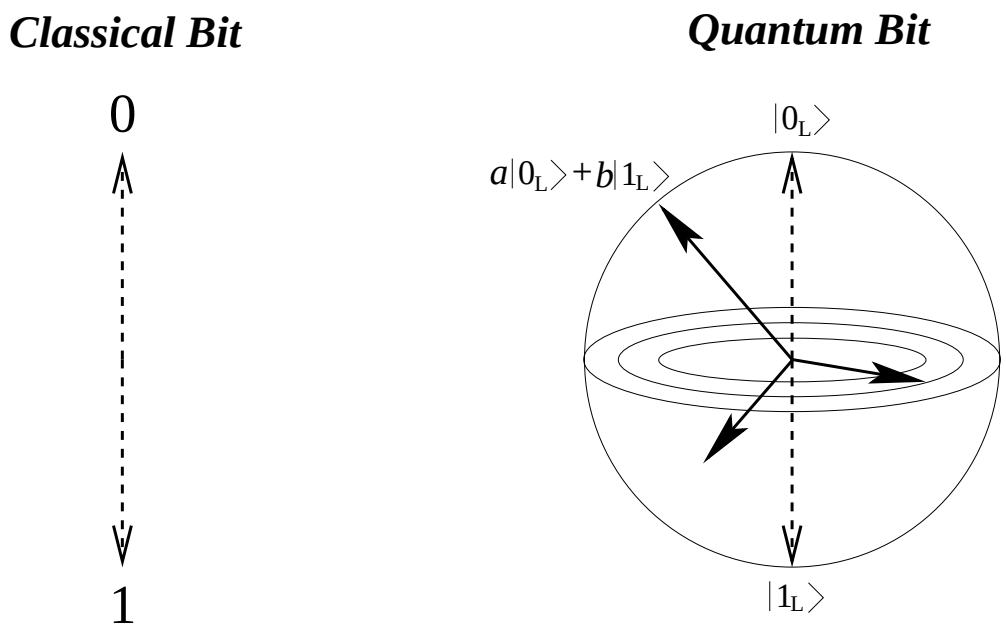

Figure 2.2: A schematic of classical and quantum bits. While a classical bit should occupy one of the two poles corresponding to 0 and 1, a quantum bit can be on any point of the Bloch sphere for it can be in various superposition states. In general, a qubit can be placed *inside* the sphere as it can be in a mixed state.

Then, a qubit state $|\psi\rangle$ is

$$|\psi\rangle = a|0_L\rangle + b|1_L\rangle, \tag{2.3}$$

which is a linear superposition of the two basis states with arbitrary complex numbers a and b. The normalisation condition, $|a|^2 + |b|^2 = 1$, should be met for a and b since $|a|^2$ ($|b|^2$) corresponds to the probability that the qubit is measured as $|0_L\rangle$ ($|1_L\rangle$). Note that the computational basis states can be arbitrarily chosen. For example, $(|0_L\rangle + |1_L\rangle)/\sqrt{2}$ and $(|0_L\rangle - |1_L\rangle)/\sqrt{2}$ can be another orthonormal basis set. The most general form of a density matrix for a qubit is

$$\rho_{qubit} = \frac{1}{2}(\mathbb{1} + \vec{r}\cdot\vec{\sigma}), \tag{2.4}$$

where $\vec{r}$ is a real vector and $\vec{\sigma}$ is the Pauli operator. The positivity condition of the density operator, $\langle\rho_{qubit}\rangle \geq 0$, imposes an inequality $|\vec{r}| \leq 1$. Then, a qubit is represented by $\vec{r}$ in an imaginary ball with a unit radius as shown in Fig. 2.2. This ball is called Bloch sphere. If a qubit is in a pure state, the corresponding

point will always be *on* the sphere.

One may naturally wonder if he or she can get more information from a qubit than from a classical bit as a qubit can exist as an infinite number of different superpositions. Actually, no more information can be gained from a qubit because the qubit readout is a quantum mechanical measurement process. Quantum mechanics does not allow one to measure a quantum state without disturbing it. Therefore, in general, a qubit cannot be read without disturbance while a classical bit can: A readout process for a qubit $|\psi\rangle$ will make the qubit state reduced to $|0_L\rangle$ or $|1_L\rangle$. For the same reason, an unknown qubit cannot be perfectly cloned, which is known as the *no cloning theorem* [40].

The quantum determinism postulate states that a pure quantum state evolves into a pure state in a perfectly *reproducible*[3] environment [41]. In the case of a reproducible environment, the dynamic evolution of a quantum system $|\Psi\rangle$ is governed by a unitary evolution U as $|\Psi\rangle \rightarrow U|\Psi\rangle$. However, the quantum determinism postulate assumes a situation without entanglement between the system and its environment due to their interactions. If we consider the environment a macroscopic *quantum* system and trace the system under consideration only, the system will somehow evolve into a mixed state by these interactions. (Note that the total system including the environment will still be in a pure state regardless of the interactions.) Zurek explained the appearance of a classical world from the quantum mechanical laws in terms of interactions of the system with its environment [42]. In the matrix representation of the quantum system, the off-diagonal terms get smaller by these interactions until the density matrix becomes diagonal. For the case of a qubit, it will cause the loss of information of the local phase. This process, called decoherence, is more conspicuous when the scale of the quantum system is macroscopic. Zurek showed that the decoherence time for a typical macroscopic system may be as short as 10^{-23}s [42]. This provides a persuasive argument of why we do not experience typical quantum effects in a macroscopic world. The Schrödinger's cat paradox

[3]When an environment is not controllable and thus it is not reproducible, the dynamic evolution is described with respective probabilities p_n's as

$$|\Psi\rangle\langle\Psi| \rightarrow \sum_n p_n U_n |\Psi\rangle\langle\Psi| U_n^\dagger. \tag{2.5}$$

In general, the resulting state in Eq. (2.5) is a mixed state, *i.e.*, it can no longer be represented by a state vector but by a density matrix.

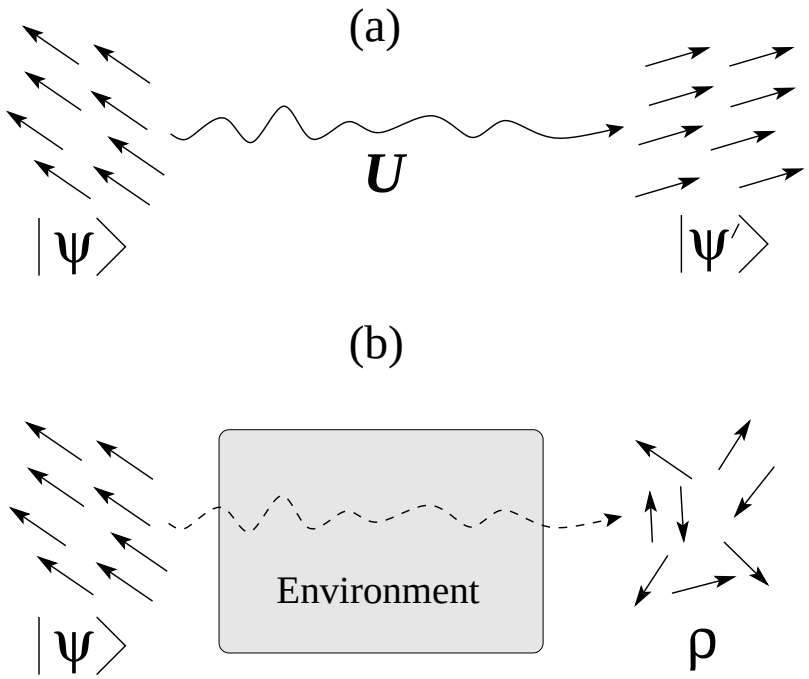

Figure 2.3: A schematic of (a) a deterministic evolution of a quantum system under the quantum determinism postulate and (b) a decoherence process in an environment. As a result of interactions with its environment, a quantum system loses its coherence and becomes a mixed state.

is argued away on this line. The decoherence effect has been pointed out to be the most formidable obstacle to efficient quantum information processing. Unfortunately, it is impossible to perfectly isolate a quantum system from its environment. Quantum error correcting codes [14, 15] and entanglement purification protocols [15, 43, 44] have been studied to overcome decoherence effects on qubits and entangled quantum channels for quantum information processing.

There have been several suggestions to realise qubits for quantum information processing in physical systems like atomic, optical and condensed matter systems. In principle, any two-dimensional quantum system can be considered a qubit system. A spin-1/2 particle, a two-level atom, and a photon polarisation state are typical examples: One can assume that a photon carries single-qubit information in its polarisation degree of freedom. However, it is another story to find out suitable qubit systems for quantum information processing, which should be initialisable, controllable, scalable, and readable with a long coherence time.

Optical qubits have some remarkable advantages as a candidate for the implementation of quantum information processing. For example, most of the operations may be performed at room temperature, and the coherence time of photons is long compared with the operation time typically required. Photons are especially suited for quantum communication as they travel at the speed of light and mostly immune from the effects of decoherence. Recent studies on quantum computation using linear optics have opened the possibilities for an implementation of an optical quantum computer [27].

2.2 Quantum entanglement

Quantum entanglement is one of the most profound features of quantum mechanics. It was first introduced by Schrödinger as follows [45]:

"When two systems, of which we know the states by their respective representatives, enter into temporary physical interaction due to known forces between them, and when after a time of mutual influence the systems separate again, then they can no longer be described in the same way as before, viz. by endowing each of them with a representative of its own. I would not call that one but rather the characteristic trait of quantum mechanics, the one that enforces its entire departure from classical lines of thought. By the interaction the two representatives have become entangled."

Recently, the quantum paradoxes discussed in the previous Section have been revisited and attributed to entanglement of physical systems [37, 38] rather than the traditional explanation based on Heisenberg's uncertainty principle. As was explained by Schrödinger, entangled states may arise as a result of interactions between quantum systems such as when a pair of particles are created simultaneously under the requirement that some attribute like total spin or momentum be conserved. At the same time, an entangled state easily loses its entanglement as it interacts with an environment. Entanglement plays a crucial role as resource in quantum information processing including quantum teleportation [7, 8, 9], quantum cryptography [11], and quantum computation [6].

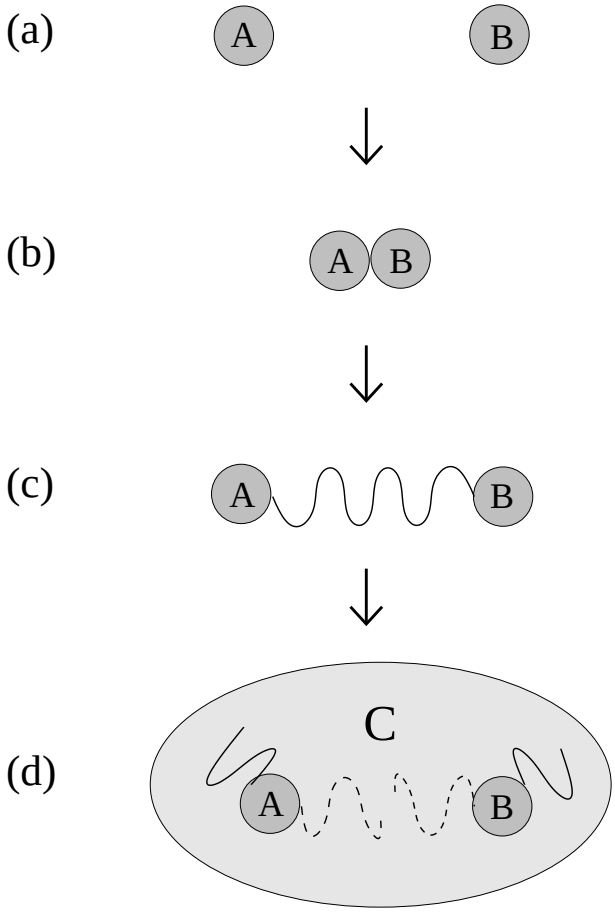

Figure 2.4: How do two physical systems get entangled and disentangled? (a) There are two separated physical systems A and B which are not entangled. (b) A and B interact with each other. (c) A and B become entangled. (d) A and B interact with the environment C and lose their entanglement.

Suppose a two-mode state defined in a Hilbert space $\mathcal{H}_1 \otimes \mathcal{H}_2$

$$|\Psi_-^B\rangle_{12} = \frac{1}{\sqrt{2}}(|0_L\rangle_1|1_L\rangle_2 - |1_L\rangle_1|0_L\rangle_2). \tag{2.6}$$

One can simply recognise that this state cannot be represented as a direct product of any two states $|\psi\rangle_1$ and $|\psi'\rangle_2$. In general, we say that a quantum state $|\Psi\rangle_{12}$ is entangled in $\mathcal{H}_1 \otimes \mathcal{H}_2$ when it cannot be represented as a direct product of two arbitrary states as

$$|\Psi\rangle_{12} = |\psi\rangle_1|\psi'\rangle_2, \tag{2.7}$$

where $|\psi\rangle_1$ ($|\psi'\rangle_2$) is a state vector defined in $\mathcal{H}_1$ ($\mathcal{H}_2$). This definition can be generalised to mixed states: Any state ρ_{12} is entangled (or inseparable) when it cannot be written in a convex combination[4] of direct products of density operators ρ_{r1}^A and ρ_{r2}^B as

$$\rho_{12} = \sum_r p_r \rho_{r1}^A \otimes \rho_{r2}^B. \tag{2.8}$$

Maximally entangled pure states are ideal as quantum channels for quantum information processing. For example, if a quantum channel for teleportation is not maximally entangled, the fidelity of teleportation will be lower than unity, the perfect one. It is generally very demanding to generate highly entangled quantum states. However, protocols have been developed to distil maximally or highly entangled states from non-maximally or lowly entangled ones using only local operations and classical communications [15]. These schemes, called entanglement purification (or distillation), will be studied in Chapter 9.

There have been many discussions and studies on how to define and quantify quantum entanglement. In general, quantum entanglement of a high-dimensional quantum state is not a tractable subject. For a bipartite state, the Peres-Horodecki criterion is a well known and useful sufficient condition for entanglement: A density matrix ρ is inseparable if its partial transpose[5] ρ^{T_2} has any negative eigenvalue(s) [46]. It has been shown that the Peres-Horodecki criterion is a necessary and sufficient condition for $2 \otimes 2$ and $2 \otimes 3$ systems [46]. For higher dimensional cases, it is no longer a necessary condition since there are entangled states for which their partial transposes are positive [47, 48].

A measure of entanglement $E(\rho)$ for a state ρ should satisfy the following conditions [49]: First, $E(\rho) = 0$ if and only if ρ is separable. Second, $E(\rho)$ is invariant under local unitary operations. Third, the expected entanglement cannot increase by local measurements and classical communications. For a pure state $|\psi\rangle_{12}$, the degree of entanglement can be defined by von Neumann entropy of the partial density operator as

$$E(|\psi\rangle_{12}) = -\mathrm{Tr}\rho_1 \ln \rho_1 = -\mathrm{Tr}\rho_2 \ln \rho_2 \tag{2.9}$$

[4] If $\sum_r p_r = 1$ and $0 \leq p_r \leq 1$ for each p_r, ρ_{12} is called a convex combination of $\rho_{r1}^A \otimes \rho_{r2}^B$.
[5] The partial transpose ρ^{T_2} of the density matrix ρ is specified as $\langle ij|\rho^{T_2}|kl\rangle = \langle il|\rho|kj\rangle$.

where ρ_1 and ρ_2 are partial density operators of the density operator $\rho_{12} = |\psi\rangle_{12}\langle\psi|$. We can find that the state (2.6) is maximally entangled which has 1 ebit of entanglement. For a mixed state, the degree of entanglement are defined in a few different ways. The entanglement of formation is intended to quantify the amount of quantum communication required to a given state. The entanglement of formation E_F is defined as [15]

$$E_F(\rho) = \min \Big[\sum_i p_i E(|\psi_i\rangle)|\rho = \sum_i p_i |\psi_i\rangle\langle\psi_i| \Big], \tag{2.10}$$

which is the least expected entanglement of any ensemble of pure states. The calculation of entanglement of formation is nontrivial for most cases. It becomes numerically intractable very rapidly as the dimensions of the Hilbert spaces increase. Analytical expressions of the entanglement of formation exist for a 2×2 system [50] and highly symmetrical states [51, 52]. The entanglement of distillation is defined based upon the entanglement distillation protocol [15]. Suppose that two parties share N pairs of qubits such that each pair is nonmaximally entangled but an identical mixed state ρ. Entanglement distillation protocols enable us to obtain $M(< N)$ maximally entangled states using only local operations and classical communications [15]. In the limit $N \to \infty$, the fidelity of the singlets (maximally entangled states) approaches 1 and the fraction M/N a fixed limit, called the asymptotic yield. Entanglement of distillation E_D is the maximum asymptotic yield of singlet states that can be produced from the given mixed state by local operation and classical communication. The distillable entanglement is important in terms of quantum information processing because maximally entangled states are preferred for quantum channels. Note that E_D is the *maximal* number of singlets that can be produced by local operations and classical communication while E_F corresponds to the *minimal* number under the same condition [53]. Horodecki *et al.* showed that any ensemble entanglement measure E suitable for the regime of high number of identically prepared entangled pairs satisfies $E_D \leq E \leq E_F$ [53].

The entanglement of relative entropy $E_R(\rho)$ is defined by [49]

$$E_R(\rho) = \min_{\rho' \in \mathcal{D}} S(\rho||\rho') \tag{2.11}$$

where $\mathcal{D}$ denotes the set of unentangled mixed states and $S(\rho||\rho') = \mathrm{Tr}\rho[\ln \rho -$

$\ln \rho']$ is the quantum relative entropy. The quantum relative entropy $S(\rho||\rho')$ tells us how difficult it is to distinguish the states ρ and ρ'. Negative eigenvalues of the partial trace of the density matrix are also used for quantification of entanglement [46, 54]. According to the Peres-Horodecki condition, a density matrix ρ is inseparable if ρ^{T_2} has any negative eigenvalue(s) [46] and the measure of entanglement E_N for ρ in terms of the negative eigenvalues of ρ^{T_2} [54]

$$E_N(\rho) = -2 \sum_i \lambda_i^- \tag{2.12}$$

where λ_i^- are the negative eigenvalue(s) of ρ^{T_2} and the factor 2 is introduced to have $0 \leq E_N(\rho) \leq 1$. Werner *et al.* introduced a more computable measure of entanglement, the negativity $\mathcal{N}(\rho)$ defined as [55]

$$\mathcal{N}(\rho) \equiv \frac{\|\rho^{T_2}\|_1 - 1}{2}, \tag{2.13}$$

which corresponds to the absolute value of the sum of negative eigenvalues of ρ^{T_2}. The negativity $\mathcal{N}(\rho)$ measures by how much ρ^{T_2} fails to be positive definite. For continuous-variable states, entanglement criteria for Gaussian states have been found [56, 57, 58] based on the Peres-Horodecki criterion. Recently, Giedke *et al.* calculated the entanglement of formation for symmetric Gaussian states [59]. All the entanglement measures mentioned above are reduced to the von Neumann entropy of entanglement for pure states.

It is another important problem how to experimentally detect entanglement of a quantum state in a laboratory. An experimental detection of entanglement was first addressed for pure states [60]. Procedures based on the use of collective measurements were proposed by Horodecki and Ekert [61]. A general method to detect entanglement with few local measurements was presented and optimal schemes were designed for two-dimensional systems, bound entangled states and entangled states of three qubits [62]. A protocol for this purpose has been found for Gaussian continuous-variable states [63] .

2.3 Coherent state

A coherent state can be defined as [64]

$$|\alpha\rangle = e^{-|\alpha|^2/2} \sum_{n=0}^{\infty} \frac{\alpha^n}{\sqrt{n!}} |n\rangle, \tag{2.14}$$

where $|n\rangle$ is a number state and $\alpha = \alpha_r + i\alpha_i$ is[6] a complex number. The coherent state has a few notable characteristics. Firstly, it is the eigenstate of an annihilation operator a with its eigenvalue α:

$$a|\alpha\rangle = \alpha|\alpha\rangle. \tag{2.15}$$

The coherent states form an overcomplete set in the infinite dimensional Hilbert space:

$$\frac{1}{\pi} \int_{-\infty}^{\infty} d^2\alpha |\alpha\rangle\langle\alpha| = \mathbb{1} \tag{2.16}$$

where $\mathbb{1}$ is the identity operator and $d^2\alpha = d\alpha_r d\alpha_i$. Therefore, any state can be represented by a combination of coherent states. The coherent state is a minimum uncertainty state and has the same quadrature variance about any direction in the phase space:

$$\Delta X \Delta P = 1, \quad \Delta X = \Delta P \tag{2.17}$$

where $\hat{X} = (a + a^\dagger)$, $\hat{P} = (a - a^\dagger)/i$, $(\Delta X)^2 = \langle \hat{X}^2 \rangle - \langle \hat{X} \rangle^2$ and $(\Delta P)^2 = \langle \hat{P}^2 \rangle - \langle \hat{P} \rangle^2$. The coherent state is a quantum mechanical analogy of a classical particle in the phase space. A classical particle is represented as a point in the phase space of the position and momentum variables. In quantum mechanics, this is prohibited by the uncertainty principle. The uncertainty relation for the two quadrature variables of light is $\Delta X \Delta P \geq 1$. The coherent state is the minimum point-like state in the quantum phase space. The coherent state is a very useful tool in quantum optics and a laser field is considered a good approximation of it.

There have been controversies on laser fields as resource of quantum infor-

[6]Here, α_r is the real part of α and α_i is the imaginary part of α. This notation will be used throughout this dissertation.

mation processing. Rudolph and Sanders argued that unconditional continuous-variable teleportation cannot be achieved with conventional laser sources thus the experiment performed in Ref. [31] cannot be readily considered unconditional teleportation [65]. Their argument is based on the fact that laser field is not a real coherent state. In quantum optics, it is often assumed that an ideal single-mode laser is given by a coherent state. However, it is well known that the phase ϕ of the laser field for the amplitude $|\alpha|e^{i\phi}$ is completely unknown. Therefore, a laser field should be represented by a mixed state

$$\rho_L = \int_0^{2\pi} \frac{d\phi}{2\pi} ||\alpha|e^{i\phi}\rangle\langle|\alpha|e^{i\phi}| = e^{-\alpha^2} \sum_0^\infty \frac{\alpha^{2n}}{n!} |n\rangle\langle n| \tag{2.18}$$

which is obviously not a coherent superposition of number states as it is diagonal in the energy eigenstate (Fock) basis. One cannot say "it is a coherent state even though its phase is unknown" based on the first decomposition in Eq. (2.18) because exactly the same statement could be made for a number state based on the second decomposition. The choice of a basis is simply arbitrary and one should not misuse any particular decomposition to interpret an experiment in a preferred way [66]. The same analysis for a two-mode squeezed state makes it fail to be an entangled state [65]. The argument on the existence of optical quantum coherence goes way back to Mϕlmer's analysis [67]. He conjectured that optical coherence does not exist in optics experiments and showed that quantum optics experiments can be explained without quantum coherence. Van Enk and Fuchs, on the contrary to Rudolph and Sanders in Ref. [65], claimed that coherent states play a privileged role in the description of laser light [68]. Wiseman also argued against Rudolph and Sanders in a different way that their claim is "baseless because true coherence is always illusory as the concept of absolute time on a scale beyond direct human experience is meaningless" [69].

2.4 Coherent state qubit

We now introduce qubit systems using coherent states. Let us consider two coherent states $|\alpha\rangle$ and $|-\alpha\rangle$. The two coherent states are not orthogonal to each other but their overlap $|\langle\alpha|-\alpha\rangle|^2 = e^{-4|\alpha|^2}$ decreases exponentially with $|\alpha|$. For example, when $|\alpha|$ is as small as 2, the overlap is $\approx 10^{-7}$, *i.e.*,

$|\langle\alpha| - \alpha\rangle|^2 \approx 0$. We identify the two coherent states of α as basis states for a logical qubit:

$$|\alpha\rangle \to |0_L\rangle, \quad |-\alpha\rangle \to |1_L\rangle. \tag{2.19}$$

A qubit state is then represented by

$$|\phi\rangle = \mathcal{A}|0_L\rangle + \mathcal{B}|1_L\rangle = \mathcal{A}|\alpha\rangle + \mathcal{B}|-\alpha\rangle \tag{2.20}$$

where the normalisation condition is

$$1 = \langle\phi|\phi\rangle = |\mathcal{A}|^2 + |\mathcal{B}|^2 + (\mathcal{A}\mathcal{B}^* + \mathcal{A}^*\mathcal{B})\langle\alpha| - \alpha\rangle \approx |\mathcal{A}|^2 + |\mathcal{B}|^2. \tag{2.21}$$

A coherent state qubit (2.20) has a couple of remarkable merits. As we will see, its readout can be easily performed. It is possible to realise non-trivial Bell-measurements only with linear optical elements. As a coherent state is a quantum analogy of a classical state (it becomes more classical as α gets larger), the coherent state qubit (2.20) is considered an example of the realisation of the Schrödinger's cat, and it is actually called "Schrödinger's cat state" or simply "cat state" in the case of $|\mathcal{A}| = |\mathcal{B}|$. It is interesting to explore the possibility of quantum information processing with macroscopic or mesoscopic quantum states. However, according to the decoherence theory, macroscopic quantum states decohere and lose their quantum characteristics faster than microscopic quantum states. As it was already pointed out in Section 2.1, this is one of the possible explanations why we cannot perform an experiment to demonstrate the quantum nature of macroscopic systems like real cats. We will study its examples in Chapters 3 and 4. Therefore, it is obvious that the coherent amplitude α for a coherent state qubit should not be too large during quantum information processing.

It is possible to construct an orthogonal qubit basis with two linear independent coherent states $|\alpha\rangle$ and $|-\alpha\rangle$. Consider the basis states

$$|e\rangle = M_+(|\alpha\rangle + |-\alpha\rangle) \to |0_L\rangle, \tag{2.22}$$

$$|d\rangle = M_-(|\alpha\rangle - |-\alpha\rangle) \to |1_L\rangle, \tag{2.23}$$

where M_+ and M_- are normalisation factors

$$M_\pm = \frac{1}{\sqrt{2(1 \pm \exp[-2|\alpha|^2])}}. \tag{2.24}$$

It can be simply shown that they form an orthonormal basis as

$$\langle e|d\rangle = \langle d|e\rangle = 0, \tag{2.25}$$

$$\langle e|e\rangle = \langle d|d\rangle = 1. \tag{2.26}$$

We can then define a 2-dimensional Hilbert space $\mathcal{H}_\alpha$ spanned by $|e\rangle$ and $|d\rangle$. The even cat state $|e\rangle$ contains only even number of photons while the odd cat state $|d\rangle$ contains only odd number of photons as

$$|e\rangle = M_+ e^{-\frac{|\alpha|^2}{2}} \sum_{n=0}^{\infty} \frac{1 + (-1)^n \alpha^n}{\sqrt{n!}} |n\rangle \tag{2.27}$$

$$= 2M_+ e^{-\frac{|\alpha|^2}{2}} \sum_{n=0}^{\infty} \frac{\alpha^{2n}}{\sqrt{(2n)!}} |2n\rangle, \tag{2.28}$$

$$|d\rangle = M_- e^{-\frac{|\alpha|^2}{2}} \sum_{n=0}^{\infty} \frac{1 - (-1)^n \alpha^n}{\sqrt{n!}} |n\rangle \tag{2.29}$$

$$= 2M_- e^{-\frac{|\alpha|^2}{2}} \sum_{n=0}^{\infty} \frac{\alpha^{(2n+1)}}{\sqrt{(2n+1)!}} |2n+1\rangle, \tag{2.30}$$

which means these two states can be discriminated by a photon parity measurement

$$O_\Pi = \sum_{n=0}^{\infty} (|2n\rangle\langle 2n| - |2n+1\rangle\langle 2n+1|). \tag{2.31}$$

The average photon number for $|e\rangle$ and $|d\rangle$ are

$$P_e = \langle e|\hat{n}|e\rangle = |\alpha|^2 \frac{1 - e^{-2|\alpha^2|}}{1 + e^{-2|\alpha^2|}}, \tag{2.32}$$

$$P_d = \langle d|\hat{n}|d\rangle = |\alpha|^2 \frac{1 + e^{-2|\alpha^2|}}{1 - e^{-2|\alpha^2|}}, \tag{2.33}$$

where $\hat{n} = a^\dagger a$ is the number operator. As α goes to zero, the odd cat state $|d\rangle$ approaches a single photon state $|1\rangle$ while the even cat state $|e\rangle$ approaches $|0\rangle$. No matter how small α is, there is no possibility that no photon will be detected from the state $|d\rangle$ at an ideal photodetector.

2.5 Entangled coherent states

We define entangled coherent states [70]

$$|ECS_1\rangle_{12} = \mathcal{N}'_\varphi(|\beta\rangle_1|\beta\rangle_2 + e^{i\varphi}|\gamma\rangle_1|\gamma\rangle_2), \tag{2.34}$$

$$|ECS_2\rangle_{12} = \mathcal{N}_\varphi(|\beta\rangle_1|\gamma\rangle_2 + e^{i\varphi}|\gamma\rangle_1|\beta\rangle_2), \tag{2.35}$$

where $|\beta\rangle$ and $|\gamma\rangle$ are coherent states with coherent amplitudes β and γ, φ is a relative phase factor, and $\mathcal{N}'_\varphi$ and $\mathcal{N}_\varphi$ are normalisation factors:

$$\mathcal{N}'_\varphi = \frac{1}{\sqrt{2 + \exp[-|\beta|^2 - |\gamma|^2]\Big(\exp[i\varphi + 2\beta^*\gamma] + \exp[-i\varphi + 2\beta\gamma^*]\Big)}}, \tag{2.36}$$

$$\mathcal{N}_\varphi = \frac{1}{\sqrt{2 + 2\cos\varphi \exp|\beta - \gamma|^2}}. \tag{2.37}$$

The entangled coherent states have been found to be very useful as quantum channels for quantum information processing. An entangled coherent state can be generated using coherent light propagating through a nonlinear medium [71] and a 50-50 beam splitter. Suppose a coherent superposition state

$$M'_-(|\sqrt{2}\alpha\rangle - |-\sqrt{2}\alpha\rangle), \tag{2.38}$$

where M'_- is a normalisation factor, is superposed on a vacuum $|0\rangle$ by a lossless 50:50 beam. It can be shown that the output state is

$$|\Psi_-\rangle_{12} = N_-(|\alpha\rangle_1|-\alpha\rangle_2 - |-\alpha\rangle_1|\alpha\rangle_2), \tag{2.39}$$

where N_- is the normalisation factor. A superposition of the two coherent states $|\sqrt{2}\alpha\rangle$ and $|-\sqrt{2}\alpha\rangle$ can be generated from a coherent state $|\sqrt{2}\alpha\rangle$ propagating through a nonlinear medium [71]. However, the nonlinear effect is typically very small to produce a coherent superposition state of the form (2.38). There have also been proposals to entangle fields in two spatially separated cavities [72]. The entangled coherent state and its usage for quantum teleportation [73, 74, 75], quantum computation [76, 77], and entanglement purification [75, 78] have all been recently studied. We will investigate, in further detail, how to generate an optical entangled coherent state in Chapter 11.

Let us consider two kinds of entangled coherent states which have symmetry in phase space:

$$|\Phi_\varphi\rangle_{12} = N_\varphi(|\alpha\rangle_1|\alpha\rangle_2 + e^{i\varphi}|-\alpha\rangle_1|-\alpha\rangle_2), \quad (2.40)$$

$$|\Psi_\varphi\rangle_{12} = N_\varphi(|\alpha\rangle_1|-\alpha\rangle_2 + e^{i\varphi}|-\alpha\rangle_1|\alpha\rangle_2). \quad (2.41)$$

where $N_\varphi = \{2(1+\cos\varphi e^{-4|\alpha|^2})\}^{-1/2}$ is the normalisation factor. It can be verified that any entangled coherent states in the form of $|ECS_1\rangle$ and $|ECS_2\rangle$ can be converted respectively to $|\Phi_\varphi\rangle$ or $|\Psi_\varphi\rangle$ by applying local unitary operations. By applying local unitary transformations, any state in the form of $|ECS_2\rangle$ with arbitrary amplitudes β and γ can be transformed to a form like that of Eqs. (2.40) and (2.41) and up to a global phase factor. Applying displacement operators $D_1(x)D_2(x)$, where $x = x_r + ix_i$ is complex, the entangled coherent state $|ECS_2\rangle$ becomes $|\Psi_\varphi\rangle$ up to a global phase ϕ:

$$|\Psi_\varphi\rangle = e^{-i\phi}D_1(x)D_2(x)|ECS_2\rangle_{12}, \quad (2.42)$$

where $x = -\frac{1}{2}(\beta+\gamma)$, $\alpha = \beta + x = -(\gamma + x)$, $\phi = x_i\beta_r - x_r\beta_i + x_i\alpha_r - x_r\alpha_i$, and the displacement operator is defined as $D(x) = \exp(xa^\dagger + x^*a)$. It is clear that N_φ is the same as $\mathcal{N}_\varphi$ neglecting the irrelevant global phase. A similar analysis can be made for $|ECS_1\rangle$ and $|\Phi_\varphi\rangle$. Note that $|\Phi_\varphi\rangle$ and $|\Psi_\varphi\rangle$ can be converted to each other simply by applying phase shifter $\hat{P}(\pi)$ on one of the two modes as

$$|\Psi_\varphi\rangle = P_2(\pi)|\Phi_\varphi\rangle \quad (2.43)$$

where $P(\varphi') = e^{i\hat{n}\varphi'}$ also is a local unitary operation. We thus can study either $|\Phi_\varphi\rangle$ or $|\Psi_\varphi\rangle$ without losing generality.

Using the orthogonal basis $\{|e\rangle, |d\rangle\}$, we can study entangled coherent states in the 2×2-dimensional Hilbert space. Entangled coherent states are represented in the orthogonal basis as

$$|\Phi_\varphi\rangle = \frac{N_\varphi}{4}\Big\{\frac{1+e^{i\varphi}}{M_+^2}|e\rangle|e\rangle + \frac{1+e^{i\varphi}}{M_-^2}|d\rangle|d\rangle + \frac{1-e^{i\varphi}}{M_+M_-}(|e\rangle|d\rangle + |d\rangle|e\rangle)\Big\}, \quad (2.44)$$

$$|\Psi_\varphi\rangle = \frac{N_\varphi}{4}\Big\{\frac{1+e^{i\varphi}}{M_+^2}|e\rangle|e\rangle - \frac{1+e^{i\varphi}}{M_-^2}|d\rangle|d\rangle - \frac{1-e^{i\varphi}}{M_+M_-}(|e\rangle|d\rangle - |d\rangle|e\rangle)\Big\}. \quad (2.45)$$

For $\varphi = 0$ and $\varphi = \pi$, $|\Phi_\varphi\rangle$ and $|\Psi_\varphi\rangle$ can be represented as

$$|\Phi_{\varphi=0}\rangle = \frac{N_{\varphi=0}}{2M_+^2}\Big(|e\rangle|e\rangle + \frac{M_+^2}{M_-^2}|d\rangle|d\rangle\Big), \tag{2.46}$$

$$|\Phi_{\varphi=\pi}\rangle = \frac{1}{\sqrt{2}}\Big(|e\rangle|d\rangle + |d\rangle|e\rangle\Big), \tag{2.47}$$

$$|\Psi_{\varphi=0}\rangle = \frac{N_{\varphi=0}}{2M_+^2}\Big(|e\rangle|e\rangle - \frac{M_+^2}{M_-^2}|d\rangle|d\rangle\Big), \tag{2.48}$$

$$|\Psi_{\varphi=\pi}\rangle = \frac{1}{\sqrt{2}}\Big(-|e\rangle|d\rangle + |d\rangle|e\rangle\Big), \tag{2.49}$$

where we can find that $|\Phi_{\varphi=\pi}\rangle$ and $|\Psi_{\varphi=\pi}\rangle$ are maximally entangled states regardless of α in the 2×2 Hilbert space $\mathcal{H}_\alpha^{(1)} \otimes \mathcal{H}_\alpha^{(2)}$. This characteristic of entangled coherent states has been pointed out by some authors [79, 80]. The entanglement of $|\Phi_\varphi\rangle$ and $|\Psi_\varphi\rangle$ can be obtained from Eqs. (2.44) and (2.45) by the von Neumann entropy of their reduced density matrices. The reduced density matrix ρ_1 is

$$\rho_1 = \mathrm{Tr}_2|\Phi_\varphi\rangle\langle\Phi_\varphi| = \frac{N_\varphi^2}{2}\begin{pmatrix} \frac{1+\cos\varphi e^{-2|\alpha|^2}}{M_+^2} & -i\frac{\sin\varphi e^{-2|\alpha|^2}}{M_+M_-} \\ i\frac{\sin\varphi e^{-2|\alpha|^2}}{M_+M_-} & \frac{1-\cos\varphi e^{-2|\alpha|^2}}{M_-^2} \end{pmatrix}. \tag{2.50}$$

We find that the degree of entanglement $E(|\alpha|, \varphi)$ for $|\Phi_\varphi\rangle$ is

$$\begin{aligned} E(|\alpha|, \varphi) &= -\mathrm{Tr}[\rho_1 \ln \rho_1] \\ &= -\lambda_1 \ln \lambda_1 - \lambda_2 \ln \lambda_2 \end{aligned} \tag{2.51}$$

where λ_1 and λ_2 are eigenvalues of the matrix ρ_1:

$$\lambda_1 = \frac{1}{4}\Big(2 - \sqrt{\frac{e^{-2i\varphi}(1+e^{i\varphi})^2(1+4e^{4|\alpha|^2+i\varphi}-2e^{i\varphi}+e^{2i\varphi})}{(e^{4|\alpha|^2}+\cos\varphi)^2}}\Big), \tag{2.52}$$

$$\lambda_2 = \frac{1}{4}\Big(2 + \sqrt{\frac{e^{-2i\varphi}(1+e^{i\varphi})^2(1+4e^{4|\alpha|^2+i\varphi}-2e^{i\varphi}+e^{2i\varphi})}{(e^{4|\alpha|^2}+\cos\varphi)^2}}\Big). \tag{2.53}$$

It is easily recognised that $|\Psi_\varphi\rangle$ also has the same degree of entanglement $E(|\alpha|, \varphi)$ as $|\Psi_\varphi\rangle$ is converted to $|\Phi_\varphi\rangle$ by a simple local unitary operation (2.43). The degree of entanglement $E(|\alpha|, \varphi)$ for an entangled coherent state has been so simply found because it was dealt with in the 2×2 space $\mathcal{H}_\alpha^{(1)} \otimes \mathcal{H}_\alpha^{(2)}$. Parker

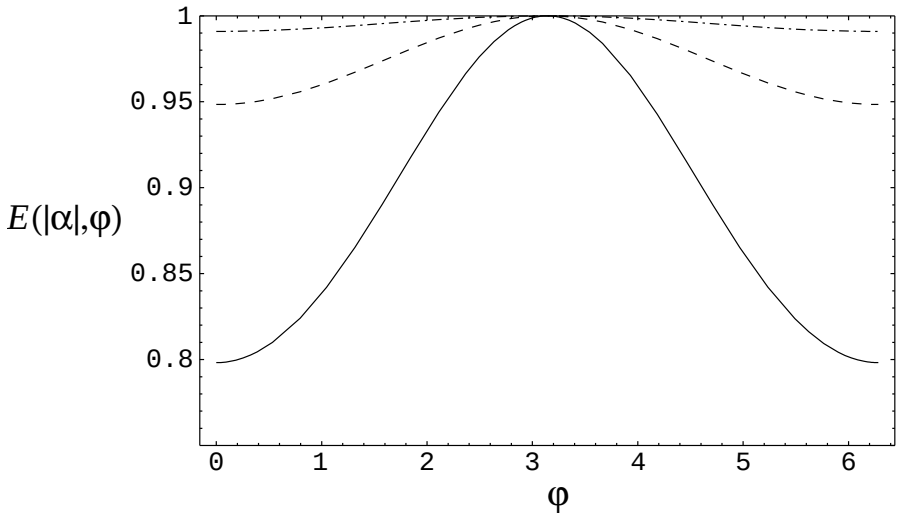

Figure 2.5: Measure of entanglement $E(|\alpha|, \varphi)$, quantified by the von Neumann entropy of the reduced density matrix, against the relative phase φ of the entangled coherent state. $|\alpha| = 0.8$ (solid line), $|\alpha| = 1$ (dashed line), $|\alpha| = 1.2$ (dot-dashed line), and $0 \leq \varphi < 2\pi$. This figure shows that when $|\alpha|$ is large, the quasi-Bell states are good approximations to maximally entangled Bell states.

considered an entangled coherent state in a continuous-variable basis and numerically calculated a degree of entanglement [81]. The degree $E(|\alpha|, \varphi)$ varies not only by the coherent amplitude α but also by the relative phase φ. When $\varphi = \pi$, as we have shown, both the entangled coherent states $|\Phi_\varphi\rangle$ and $|\Psi_\varphi\rangle$ are maximally entangled regardless of α, *i.e.*, $E(|\alpha|, \pi) = 1$. When $\varphi = 0$, on the other hand, $E(|\alpha|, \varphi)$ is minimised for a given coherent amplitude α. In Fig. 2.5, we also show that the entanglement $E(|\alpha|, \varphi)$ drastically approaches to 1 as $|\alpha|$ increases. We calculate $E(1, 0) \simeq 0.948$, $E(2, 0) \simeq 0.9999997$ and $E(3, 0) \simeq 1 - 6.7 \times 10^{-16}$.

The Bell basis is composed of four orthogonal Bell states

$$|\Phi^B_\pm\rangle_{12} = \frac{1}{\sqrt{2}}(|0_L\rangle_1|0_L\rangle_2 \pm |1_L\rangle_1|1_L\rangle_2), \tag{2.54}$$

$$|\Psi^B_\pm\rangle_{12} = \frac{1}{\sqrt{2}}(|0_L\rangle_1|1_L\rangle_2 \pm |1_L\rangle_1|0_L\rangle_2), \tag{2.55}$$

which are maximally entangled states of modes 1 and 2. We define quasi-Bell

states with coherent states as [79]

$$|\Phi_{\pm}\rangle_{12} = N_{\pm}(|\alpha\rangle_1|\alpha\rangle_2 \pm |-\alpha\rangle_1|-\alpha\rangle_2), \tag{2.56}$$

$$|\Psi_{\pm}\rangle_{12} = N_{\pm}(|\alpha\rangle_1|-\alpha\rangle_2 \pm |-\alpha\rangle_1|\alpha\rangle_2), \tag{2.57}$$

where $N_{\pm}$ is normalisation factors. One can immediately notice that the quasi-Bell states have already been dealt with in Eqs. (2.46) to (2.49). The four quasi-Bell states do not form a complete measurement set by themselves because they do not satisfy orthogonality and completeness. However, this set is a very good approximation of the Bell basis. These states are orthogonal to each other except

$$\langle\Psi_+|\Phi_+\rangle = \frac{1}{\cosh 2|\alpha|^2}, \tag{2.58}$$

and we immediately see that $|\Psi_+\rangle$ and $|\Phi_+\rangle$ rapidly become orthogonal as $|\alpha|$ grows.

2.6 Implementation of Bell-state measurement with linear optical elements

A Bell-state measurement, or simply Bell measurement, is very useful in quantum information processing. An efficient Bell measurement protocol is necessary to implement quantum teleportation. It is also used to construct quantum gates in quantum computation. There has been an experimental demonstration of a complete Bell measurement, which was used for teleportation, using nonlinear optical elements [82, 83]. It was shown that a complete Bell-state measurement on a product Hilbert space of two two-level systems is not possible using linear elements [84]. A Bell measurement scheme using linear optical elements [85] has been used to distinguish only up to two of the Bell states for teleportation [8] and dense coding [86]. However, a remarkable feature of quasi-Bell states is that each one of them can be unambiguously discriminated using only simple linear elements.

Suppose that each mode of the entangled state is incident on a 50-50

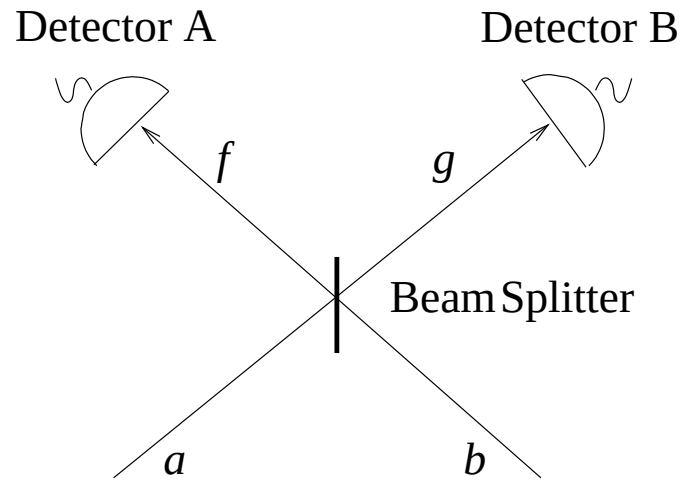

Figure 2.6: Scheme to discriminate all four Bell states using a 50:50 beam splitter and two photo-detectors. If an odd number of photons is detected at detector A for mode f then we know that the entangled state incident on the measurement set up was $|\Phi_-\rangle$. On the other hand, if an odd number of photons is detected at detector B for mode g then the incident entangled state was $|\Psi_-\rangle$. If a non-zero even number of photons is detected for mode f, the incident state was $|\Phi_+\rangle$ and if a non-zero even number is detected for mode g, it was $|\Psi_+\rangle$.

beam splitter. After passing the beam splitter, the quasi-Bell states become

$$\begin{aligned} |\Phi_+\rangle_{ab} &\longrightarrow |E\rangle_f|0\rangle_g, \\ |\Phi_-\rangle_{ab} &\longrightarrow |D\rangle_f|0\rangle_g, \\ |\Psi_+\rangle_{ab} &\longrightarrow |0\rangle_f|E\rangle_g, \\ |\Psi_-\rangle_{ab} &\longrightarrow |0\rangle_f|D\rangle_g, \end{aligned} \tag{2.59}$$

where the even cat state $|E\rangle = M'_+(|\sqrt{2}\alpha\rangle + |-\sqrt{2}\alpha\rangle)$ with the normalisation factor M'_+ contains only even numbers of photons, while the odd cat state $|D\rangle = M'_-(|\sqrt{2}\alpha\rangle - |-\sqrt{2}\alpha\rangle)$ with the normalisation factor M'_- contains only odd numbers of photons. By setting two photodetectors for the output modes f and g respectively to perform number parity measurement, the quasi-Bell measurement can be simply achieved. For example, if an odd number of photons is detected for mode f, the state $|\Phi_-\rangle$ is measured, and if an odd number of photons is detected for mode g, then $|\Psi_-\rangle$ is measured. Even though there is non-zero probability of failure in which both of the detectors do not register a photon due to the non-zero overlap of $|\langle 0|E\rangle|^2 = 2e^{-2|\alpha|^2}/(1+e^{-4|\alpha|^2})$, the

failure probability P_f is small for an appropriate choice of α and the failure is known from the result whenever it occurs. For example, the failure probability P_f is $\sim$28% for $\alpha = 0.8$, $\sim$14% for $\alpha = 1$ and only $\sim 10^{-4}$ for $\alpha = 2$.

We pointed out that α for a coherent state qubit should be small for a long decoherence time. However, if it is too small the success probability for the Bell-measurement will become low as we have seen. There is a trade-off between the coherence time and success probability. We will see $\alpha \simeq 3$ may be a good choice for quantum computation in Chapter 8.

One of the key requirements of this Bell-measurement scheme is to discern even and odd cat states. Ideally, photodetectors distinguishing $|n\rangle$ from $|n+1\rangle$ for any n, called discriminating photodetectors, are required, which do not yet exist [87]. In current technology, there are threshold photodetectors which can distinguish no photon and at least one photon with high efficiency [88, 89]. However, it is possible to distinguish up to any arbitrary number of photons by using ideal threshold photodetectors and beam splitters. One can use an array of beam splitters to distribute photons to be detected to as many threshold detectors as possible. The probability of undercounting photons is at most $k(k-1)/2N$, where k is the number of photons and N is the number of ideal threshold detectors [90]. The visible-light photon counter has been constructed to efficiently discriminate between one and two photons [89, 91]. In short, it does not seem to be difficult to discern a couple of photons with current technology. If we set $\alpha = 0.8$, $\sim$ 28% of the cases will be found to be zero photon, $\sim$ 35% of the cases will be found to be 1 photon, and $\sim$ 23% of the cases will be found to be 2 photons in our Bell-measurement scheme. In other word $\sim$ 63% of the cases will be found to be 0 or 1 photon, and $\sim$ 86% of the cases will be found to be equal to or less than 2 photons. The failure probability of $\sim$ 28% in which neither of the detectors register a photon should be excluded because one cannot exactly know the measured state in this case. Assuming that a photo-detecting scheme discriminates between 0, 1, and more than 1 photons, quantum teleportation with the total success probability $\sim$ 35% can be performed. If a photo-detecting scheme discriminates between 2 and more than 2 photons, quantum teleportation with the total success probability $\sim$ 58% can be performed.

The key ideas of discriminating four quasi-Bell states are as follows: (1)

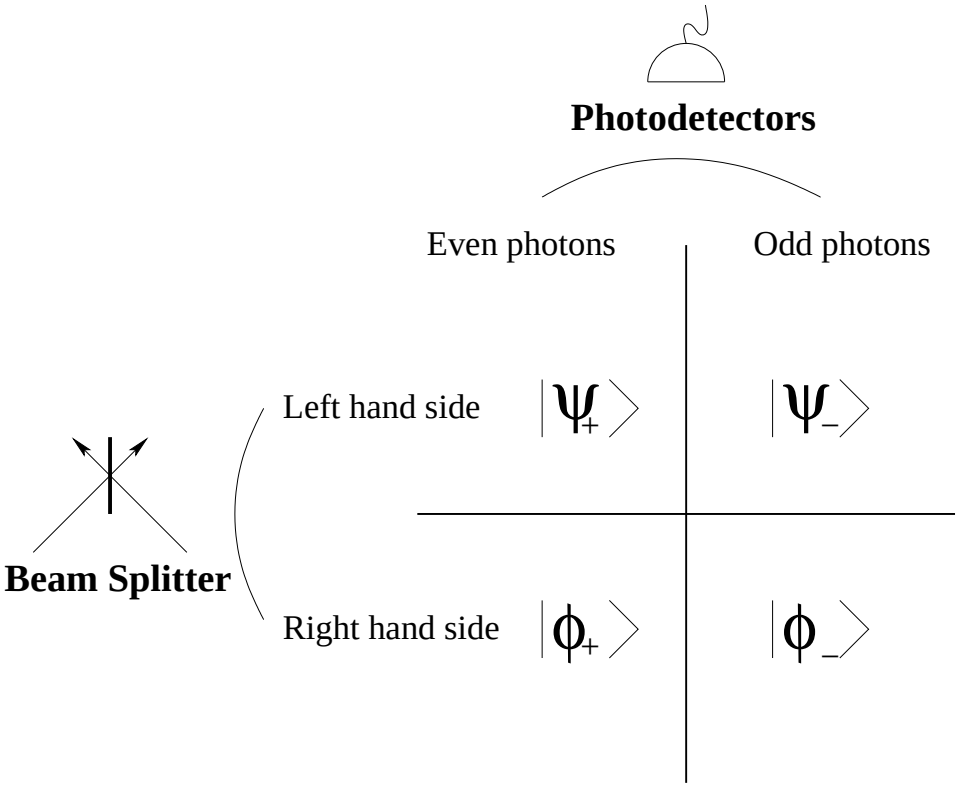

Figure 2.7: The key ideas of unambiguously discriminating four Bell states with a photodetector and a beam splitter.

The states $|\Phi_+\rangle$ and $|\Psi_+\rangle$ have only even number of photons while $|\Phi_-\rangle$ and $|\Psi_-\rangle$ have only odd number of photons; They can be discriminated by photon parity measurements. (2) Using a 50-50 beam splitter, we can move every photon of $|\Phi_+\rangle$ and $|\Phi_-\rangle$ to the one side of the beam splitter while moving every photon of $|\Psi_-\rangle$ and $|\Psi_-\rangle$ to the other side. This quasi-Bell measurement scheme can be used for concentration of pure entangled coherent states [75, 78], teleportation [75] and quantum computation with coherent state qubits [76].

Chapter 3

Quantum Nonlocality for An Entangled Coherent State

In quantum information processing, the most important ingredient is the nonlocal properties of the channel which can be easily destroyed in nature. In this Chapter, we study nonlocality of an entangled coherent state using photon parity measurement. We first investigate the nonlocality of a pure entangled coherent state, and move on to the dynamic behaviour of nonlocality for a decohered entangled coherent state in a vacuum (zero temperature) environment. The dynamic behaviour is also investigated in the framework of a 2×2 Hilbert space and the results are compared. It is found that nonlocality of a decohered entangled coherent sate persists longer when it is considered in a 2×2 space.

3.1 Quantum nonlocality

The paradox suggested by Einstein, Podolsky and Rosen (EPR) aroused a controversy over nonlocality of quantum mechanics [1]. Their question was "Can quantum mechanical description of physical reality be considered complete?" They suggested an entangled state, the EPR state, as a counter example against the completeness of quantum mechanics. The kernel of their argument can be reformulated as follows. To be a complete physical theory, every element of the physical reality must have a counterpart in the theory. From the noncommutativity of two different quantum observables, they argued that (1) the

quantum mechanical description of reality given by the wave function (or the state vector) is not complete or (2) when the operators corresponding to two physical quantities do not commute the two quantities cannot have simultaneous reality. Let us now suppose two distant parties, say Alice and Bob, each of whom has a spin-1/2 particle labelled by 1 and 2 respectively. The total system of the two particles can be in an EPR state[1],

$$|\psi_{EPR}\rangle = \frac{1}{\sqrt{2}}(|\uparrow\rangle_1|\downarrow\rangle_2 - |\downarrow\rangle_1|\uparrow\rangle_2), \tag{3.1}$$

where $|\uparrow\rangle$ and $|\downarrow\rangle$ are eigenstates of the spin operator S_z along z-axis. The EPR state $|\psi_{EPR}\rangle$ can be generated as a result of an interaction between particles 1 and 2 when the total spin of the two particles is conserved. The state $|\psi_{EPR}\rangle$ can also be represented in another basis as

$$|\psi_{EPR}\rangle = \frac{1}{\sqrt{2}}(|-\rangle_1|+\rangle_2 - |+\rangle_1|-\rangle_2), \tag{3.2}$$

where $|+\rangle = (|\uparrow\rangle + |\downarrow\rangle)/\sqrt{2}$ and $|-\rangle = (|\uparrow\rangle - |\downarrow\rangle)/\sqrt{2}$ denote eigenstates of the spin operator S_x along x-axis. Note that the spin operators S_z and S_x do not commute thus the spins along z- and x-axes cannot be determined simultaneously. Now suppose that Alice performs a measurement on the spin of particle 1 along z- and x-axes. If Alice measures the spin of particle 1 along z-axis and its outcome was $|\uparrow\rangle$, the state of Bob's particle 2 is reduced to $|\downarrow\rangle$. However, for example, if Alice performs the same measurement along the z-axis and the outcome was $|+\rangle$, the state of particle 2 is reduced to $|-\rangle$. In short, the state vector of particle 2 changes according to the kind of measurement performed on particle 1 and its outcome. Here, EPR argued that 'no real change can take place in the system 2 in consequence of anything that may be done to the first system', *i.e.*, the physical reality of particle 2 must not have changed regardless of any operation on particle 1. According the above argument, the state vector of a system can change while the physical reality of the system remains the same: Quantum mechanics makes it possible to assign different states to the same physical reality. Then the two physical quantities

[1]The original EPR state is a continuous-variable entangled state in which the position (or momentum) degrees of freedom of two distant systems are entangled. The original EPR state is not a normalisable physical state. We here discuss an EPR-Bohm state (spin singlet) for simplicity and completeness of the argument.

corresponding to S_z and S_x, respectively, may have the simultaneous reality with the definite eigenvalues. Therefore, the statement (2)[2] is not true and we are forced to admit the alternative (1).

It is important to note that EPR's argument assumed *locality*, which is not changed by any remote operations, to argue for reality. If EPR's implicit assumption of locality is not true, the above argument should go in the opposite direction: In this case, quantum mechanics can be a 'complete' theory. At this point, we can ask such a question: "Is there any theory, based on a local model, which can admit every entangled state like an EPR state?" As a trial to answer this question, one can assume the existence of a shared random variable between Alice and Bob: The local hidden variable model was expected to enable classical local theory to describe any 'nonlocal' states. The shared variable is used to locally generate a measurement outcome depending only on the choice of the local measurement. We can change the question to "Is there any *nonlocal* state that cannot be accepted by any local hidden variable theory?"

It was Bell who proposed the remarkable inequality that any local hidden variable theory should obey [2]. Various versions of Bell's inequality [92, 93] followed the original one [2]. Bell's inequality enables an experimental test on quantum nonlocality in a real laboratory. Experimental evidences have demonstrated the existence of nonlocal states which violate Bell's inequality [20], *i.e.*, the idea of local realism should be abandoned. Numerous theoretical studies and experimental demonstrations have been performed to understand nonlocal properties of quantum states.

Even though good experiments have been performed, it has been pointed out that there remain two possible loopholes. One is called the lightcone loophole that might allow local realistic interpretation. Some experiments have been performed with strict relativistic separation between measurements to close this loophole [94]. The other is the detection loophole due to detection inefficiency. According to this loophole, there is a possibility that the detected subensemble violates Bell's inequality even though the whole ensemble satisfies it. Some authors generalised Bell's inequality to the case of inefficient detection [93, 95, 96] and other proposals have been made [97] to close the detection loophole. Re-

[2]It is well known that Einstein's aesthetic sense could not tolerate such a statement like (2).

cently, an experiment on nonlocality has been performed with an efficient detection [98].

Quantum nonlocality of an entangled continuous-variable state has been discussed using the Schmidt form for entangled nonorthogonal states [99] and the quadrature-phase homodyne measurement [100]. A given state is nonlocal when it violates any Bell's inequalities. In fact, a state does not have to violate all the possible Bell's inequalities to be considered quantum nonlocal. A state is quantum nonlocal for the given Bell's inequality which is violated by the measurement of the state. Banaszek and Wódkiewicz (BW) defined a Bell's inequality based on the parity measurement and they found that the two-mode squeezed state violates Bell's inequality [101, 102].

It is important to choose the type of measurement variables when testing nonlocality for a given state. In the original EPR *gedanken* experiment [1], EPR considered the positions (or the momenta) of two particles as the measurement variables to discuss the two-body correlation. Bell [2] argued that the EPR wave function does not exhibit nonlocality because its Wigner function $W(x_1, p_1; x_2, p_2)$ is positive everywhere, allowing the description by a local hidden variable theory. Munro showed that various types of Bell's inequalities are not violated in terms of the homodyne measurements of two particles [100, 103]. To the contrary, Banaszek and Wódkiewicz [101, 102] examined even and odd parities as the measurement variables and showed that the EPR state and the two-mode squeezed state are nonlocal in the sense that they violate Bell's inequalities such as Clauser and Horne inequality and Clauser-Horne-Shimony-Holt inequality.

3.2 Bell-CHSH inequality

Probably the most well known version of Bell's inequalities is that of Clauser, Horne, Shimony and Holt (CHSH) [92]. The Bell-CHSH inequality and its violation in quantum mechanics can be introduced as follows. Let us first consider the case for classical observables. Suppose two distant particles 1 and 2, and physical observables A and A' (B and B') which can take on the values ± 1

corresponding to local measurements on particle 1 (2). It is easy to see that

$$AB + AB' + A'B - A'B' = \pm 2. \tag{3.3}$$

Let $p(A, A', B, B')$ be the probability that $A = a$, $A' = a'$, $B = b$ and $B' = b'$ for particle 1 and 2. The average value E of $AB + AB' + A'B - A'B'$ is

$$\begin{aligned} & E(AB + AB' + A'B - A'B') \\ & \quad = \sum_{A,A',B,B'} p(A, A', B, B')(AB + AB' + A'B - A'B') \\ & \quad = \sum_{A,A',B,B'} p(A, A', B, B')AB + p(A, A', B, B')AB' \\ & \qquad\qquad + (A, A', B, B')A'B + p(A, A', B, B')A'B' \\ & \quad = E(AB) + E(AB') + E(A'B) - E(A'B') \end{aligned} \tag{3.4}$$

and it is simple from Eqs. (3.3) and (3.4) to drive an inequality

$$-2 \leq E(AB) + E(AB') + E(A'B) - E(A'B') \leq 2. \tag{3.5}$$

The inequality (3.5) must hold in any theory in which local variables of particle 1 (2) determine the results of the experiments on particle 1 (2). We can apply the inequality (3.5) to a quantum state with appropriate quantum observables to test if it is a quantum nonlocal state which cannot exist in a local theory. Recall the EPR-Bohm state

$$|\psi_{EPR}\rangle = \frac{1}{\sqrt{2}}(|\uparrow\rangle_1|\downarrow\rangle_2 - |\downarrow\rangle_1|\uparrow\rangle_2), \tag{3.6}$$

shared by Alice and Bob. To find a combination which violates the inequality (3.5), Alice and Bob can construct their set of measurements $\mathbf{S}_1 \cdot \mathbf{a}$ and $\mathbf{S}_1 \cdot \mathbf{a}'$ for Alice, and $\mathbf{S}_2 \cdot \mathbf{b}$ and $\mathbf{S} \cdot \mathbf{b}'_2$ for Bob, varying the unit vectors $\mathbf{a}$, $\mathbf{a}'$, $\mathbf{b}$ and $\mathbf{b}'$, where $\mathbf{S} = (S_x, S_y, S_z)$ is the spin operator. The average value can be calculated to obtain the Bell-CHSH inequality as

$$-2 \leq B_{CHSH} \leq 2 \tag{3.7}$$

where the Bell function B_{CHSH} is defined as the average value, $B_{CHSH} \equiv \langle \mathcal{B}_{CHSH} \rangle$, with the Bell operator $\mathcal{B}_{CHSH}$

$$\mathcal{B}_{CHSH} \equiv \mathbf{S}_1 \cdot \mathbf{a} \otimes \mathbf{S}_2 \cdot \mathbf{b} + \mathbf{S}_1 \cdot \mathbf{a} \otimes \mathbf{S}_2 \cdot \mathbf{b}' + \mathbf{S} \cdot \mathbf{a}_1' \otimes \mathbf{S}_2 \cdot \mathbf{b} - \mathbf{S} \cdot \mathbf{a}_1' \otimes \mathbf{S}_2 \cdot \mathbf{b}'. \quad (3.8)$$

It is now obvious that the Bell-CHSH inequality is violated for the EPR singlet state $|\psi_{EPR}\rangle$. For example, if Alice and Bob set their set of the measurements as $\mathbf{S}_1 \cdot \mathbf{a} = s_z$, $\mathbf{S}_1 \cdot \mathbf{a}' = (s_z + s_x)/\sqrt{2}$, $\mathbf{S}_2 \cdot \mathbf{b} = \cos[\pi/8] s_z + \sin[\pi/8] s_x$, $\mathbf{S}_2 \cdot \mathbf{b}' = \cos[\pi/8] s_z + \sin[\pi/8] s_x$, we can find $B_{CHSH} = 2\sqrt{2}$ which violates the Bell-CHSH inequality. It is straightforward to find the upper and lower bounds of the Bell-CHSH inequality as [104, 105]

$$\begin{aligned} \langle \mathcal{B}_{CHSH} \rangle &= \langle 4 I_{2\times 2} + 4[\mathbf{S}_1 \cdot (\mathbf{a} \times \mathbf{a}')] \otimes [\mathbf{S}_2 \cdot (\mathbf{b} \times \mathbf{b}')] \rangle \leq 8, & (3.9) \\ |B_{CHSH}| &\leq 2\sqrt{2}. & (3.10) \end{aligned}$$

The inequality (3.10) is known as Cirel'son's bound [106].

3.3 Wigner representation of the Bell-CHSH inequality - Generalised Banaszek-Wódkiewicz inequality

We have pointed out that the type of quantum observable to be measured is a crucial factor in the nonlocality test. Banaszek and Wódkiewicz developed a Wigner function representation of Bell-CHSH inequality using a two-mode parity operator $\Pi(\zeta_1, \zeta_2)$ as a quantum observable [101, 102]. The two-mode parity operator $\Pi(\zeta_1, \zeta_2)$ is defined as

$$\Pi(\zeta_1, \zeta_2) = D_1(\zeta_1) D_2(\zeta_2) \Pi D_1^\dagger(\zeta_1) D_2^\dagger(\zeta_2), \quad (3.11)$$

where $D(\zeta_1)$ is the displacement operator $D(\zeta_1) = \exp[\zeta_1 \hat{a}^\dagger - \zeta_1^* \hat{a}]$ and

$$\begin{aligned} \Pi &= (\Pi_e - \Pi_o)_1 \otimes (\Pi_e - \Pi_o)_2 \\ &= \Pi_{e1} \otimes \Pi_{e2} - \Pi_{e1} \otimes \Pi_{o2} - \Pi_{o1} \otimes \Pi_{e2} + \Pi_{o1} \otimes \Pi_{o2}, & (3.12) \\ & & (3.13) \end{aligned}$$

with

$$\Pi_e = \sum_n^{\infty} |2n\rangle\langle 2n|, \quad \Pi_o = \sum_n^{\infty} |2n+1\rangle\langle 2n+1|. \tag{3.14}$$

The even and odd parity operators, $\hat{\Pi}_e$ and $\hat{\Pi}_o$, are the projection operators to measure the probabilities of the field having even and odd numbers of photons, respectively. We define the Bell operator $\mathcal{B}$ as

$$\mathcal{B} = \Pi(\zeta_1, \zeta_2) + \Pi(\zeta_1', \zeta_2) + \Pi(\zeta_1, \zeta_2') - \Pi(\zeta_1', \zeta_2') \tag{3.15}$$

and the Bell function as $B \equiv \langle \mathcal{B} \rangle$. The Bell-CHSH inequality is then

$$|B| = |\langle \Pi(\zeta_1, \zeta_2) + \Pi(\zeta_1, \zeta_2') + \Pi(\zeta_1', \zeta_2) - \Pi(\zeta_1', \zeta_2') \rangle| \leq 2. \tag{3.16}$$

We say the field is quantum-mechanically nonlocal as $|B|_{max}$ is larger than 2 and the nonlocality is stronger as $|B|_{max}$ gets larger. The displacement operation can be effectively performed using a beam splitter with the transmission coefficient close to one and a strong coherent state being injected into the other input port [102]. The two-mode Wigner function at a given phase point described by ζ_1 and ζ_2 is [107]

$$W(\zeta_1, \zeta_2) = \frac{4}{\pi^2} \mathrm{Tr}[\rho \Pi(\zeta_1, \zeta_2)], \tag{3.17}$$

where ρ is the density operator of the field. From Eqs.(3.16) and (3.17), we obtain the Wigner representation of Bell's inequality

$$|B| = \frac{\pi^2}{4} |W(\zeta_1, \zeta_2) + W(\zeta_1, \zeta_2') + W(\zeta_1', \zeta_2) - W(\zeta_1', \zeta_2')| \leq 2. \tag{3.18}$$

The Wigner function of a quantum state is obtained from the Fourier transform of its characteristic function

$$C(\eta_1, \eta_2) = \mathrm{Tr}[\rho D_1(\eta_1) D_2(\eta_2)]. \tag{3.19}$$

Banaszek and Wódkiewicz used their Bell function based on Wigner representation with $\zeta_1 = \zeta_2 = 0$. We consider all four variables $\zeta_1, \zeta_2, \zeta_1'$ and ζ_2' in our investigation of the Bell function as shown in Eq. (3.18) to test nonlocality more generally. In this Chapter and Chapters 4 and 5, we will see that the generalised BW inequality enables us to find deeper nonlocality for continuous-variable states.

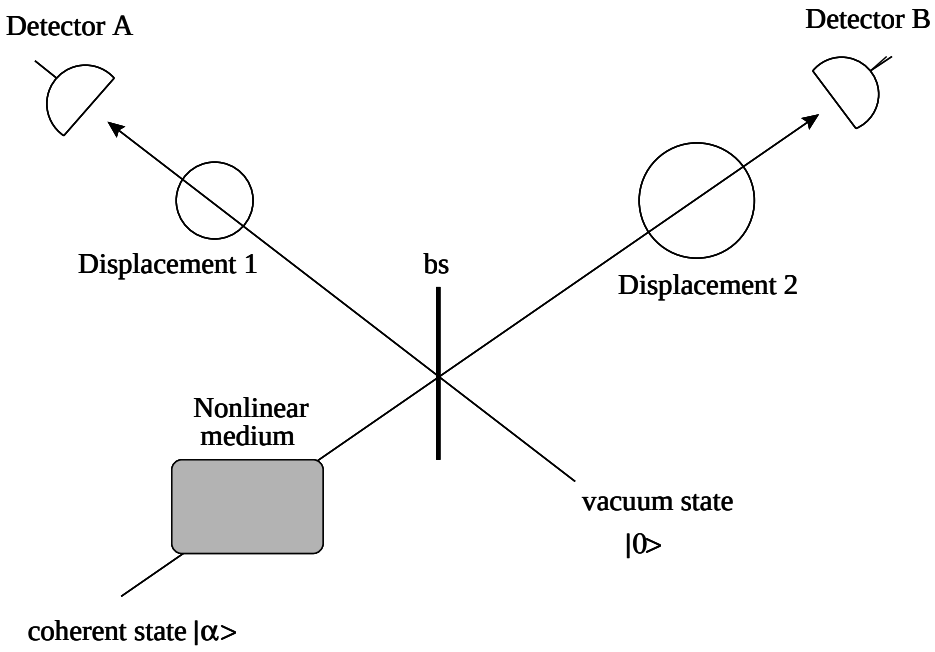

Figure 3.1: Nonlocality test for an entangled coherent state. A coherent state, nonlinear medium, and 50-50 beam splitter are used to generate an entangled coherent state.

3.4 Nonlocality for an entangled coherent state

We now consider the nonlocality of an entangled coherent state

$$|C_{\pm}\rangle = \frac{1}{\sqrt{N_{\pm}}}(|\alpha\rangle|-\alpha\rangle \pm |-\alpha\rangle|\alpha\rangle) \tag{3.20}$$

where $N_{\pm}$ are normalisation factors and α is assumed to be real for simplicity. The Wigner function of the entangled coherent state is

$$\begin{aligned} W_{ECS}(\zeta_1,\zeta_2) = 4\mathcal{N}^2\Big\{ & \exp[-2|\zeta_1-\alpha|^2 - 2|\zeta_2+\alpha|^2] \\ & + \exp[-2|\zeta_1+\alpha|^2 - 2|\zeta_2-\alpha|^2] \\ & - \exp[-2(\zeta_1-\alpha)(\zeta_1^*+\alpha) - 2(\zeta_2+\alpha)(\zeta_2^*-\alpha) - 4\alpha^2] \\ & - \exp[-2(\zeta_1^*-\alpha)(\zeta_1+\alpha) - 2(\zeta_2^*+\alpha)(\zeta_2-\alpha) - 4\alpha^2]\Big\}, \end{aligned} \tag{3.21}$$

from which the Bell function is simply obtained. The steepest descent method [108] was used to gain the maximum value for the absolute Bell function in Fig. 3.1. The maximum Bell-CHSH violation using Banaszek and Wódkiewicz's

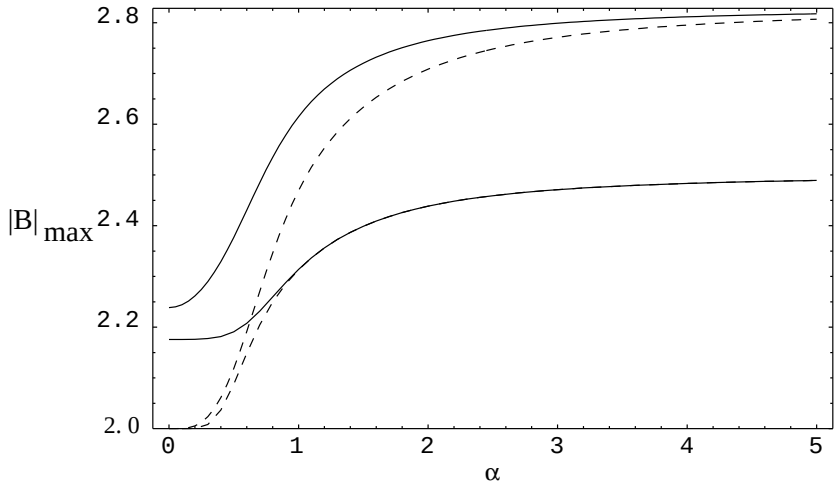

Figure 3.2: The maximum value of the absolute Bell function $|B|_{max}$ against amplitude α (> 0), of $|C_-\rangle$ (solid lines) and $|C_+\rangle$ (dashed lines) entangled coherent states. The higher valued solid and dashed lines are for the generalised BW inequality while the lower valued solid and dashed lines are for the case taking $\alpha = \zeta_2 = 0$.

version is approximately 2.19 for two-mode squeezed states as we will show in the following Chapter [101, 109] and 2.5 for entangled coherent states as shown in Fig. 3.2. However, for the generalised BW inequality in Eq. (3.18), both two-mode squeezed states [106] and entangled coherent states have a maximal Bell-CHSH violation of $2\sqrt{2}$ (as shown in Fig. 3.2). The entangled coherent states $|C_-\rangle$ and $|C_+\rangle$ violate the Bell inequality regardless of the size of the amplitude, $\alpha > 0$. As the amplitude α increases the maximal Bell function $|B|_{max}$ tends towards a maximum of $2\sqrt{2}$.

It is interesting to note that $|B|_{max}$ for the $|C_-\rangle$ state takes a higher value than for the $|C_+\rangle$ state. If the number state representation of the coherent state is [64]

$$|\alpha\rangle = \sum_n \frac{e^{-|\alpha|^2/2}\alpha^n}{\sqrt{n!}}|n\rangle \tag{3.22}$$

which means that, in the limit of small coherent amplitude α,

$$|\pm\alpha\rangle \approx e^{-|\alpha|^2/2}[|0\rangle \pm \alpha|1\rangle]. \tag{3.23}$$

Substituting this into the entangled coherent states $|C_+\rangle$ and $|C_-\rangle$ we find

$$\begin{aligned} |C_+\rangle &\propto |0\rangle|0\rangle - \alpha^2|1\rangle|1\rangle \\ |C_-\rangle &\propto \alpha(|1\rangle|0\rangle - |0\rangle|1\rangle) \end{aligned} \tag{3.24}$$

When α is small $|C_+\rangle \to |0\rangle|0\rangle$. As the weights of $|0\rangle|0\rangle$ and $|1\rangle|1\rangle$ are radically different $|C_+\rangle$ is only minimally entangled. However the two component states $|0\rangle|1\rangle$ and $|1\rangle|0\rangle$ are equally weighted for $|C_-\rangle$ which gives optimal entanglement. A pure entangled state always violates nonlocality [110]. Any entangled coherent state in a form as given in Eq. (3.20) is found to be nonlocal. We conjecture that any entangled coherent state as given in Eq. (2.34) also has nonlocality except when $\beta = \gamma$, *i.e.*, when the state is a product state.

The results shown in Fig. 3.2 were obtained from a numerical consideration of $|B|_{max}$ (3.18). In analogy with the work carried out in [109] we imposed the condition $B(|\zeta_1|, |\zeta_2|, |\zeta_1'|, |\zeta_2'|) = B(|\zeta_2|, |\zeta_1|, |\zeta_2'|, |\zeta_1'|)$. The method of steepest descent [108] was used to find the absolute maximum of the Bell function under our assumptions.

3.5 Dynamics of Nonlocality

A quantum system loses its quantum characteristics if it is open to the world. We modelled an entangled coherent state interacting with a dissipative environment (two independent vacuum reservoirs). To study the dynamics of nonlocality of continuous variable entangled coherent states it is necessary to find an expression of the time-dependent Bell-CHSH inequality. This in turn means finding an expression for the time-dependent decohered Wigner function.

The quantum channel decoheres when it interacts with its environment and becomes a mixed state of its density operator $\rho(\tau)$, where τ is the decoherence time. To know the time dependence of $\rho(\tau)$, we have to solve the master equation [111]

$$\frac{\partial \rho}{\partial \tau} = \hat{J}\rho + \hat{L}\rho \; ; \; \hat{J}\rho = \gamma \sum_i a_i \rho a_i^\dagger, \quad \hat{L}\rho = -\frac{\gamma}{2}\sum_i (a_i^\dagger a_i \rho + \rho a_i^\dagger a_i) \tag{3.25}$$

where a_i and $a_i^\dagger$ are the annihilation and creation operators for the field mode i and γ is the decay constant. We have assumed that each field mode is coupled to its environment at the same coupling rate γ. The formal solution of the master equation (3.25) can be written as

$$\rho(t) = \exp[(\hat{J} + \hat{L})\tau]\rho(0). \tag{3.26}$$

which leads to the solution for the initial single-mode dyadic $|\alpha\rangle\langle\beta|$

$$\exp[(\hat{J} + \hat{L})\tau]|\alpha\rangle\langle\beta| = \langle\beta|\alpha\rangle^{1-t^2}|\alpha t\rangle\langle\beta t| \tag{3.27}$$

where $t = e^{-\frac{1}{2}\gamma\tau}$. In this Chapter, we introduce a dimensionless normalised interaction time r which is related to t by the expression $r = \sqrt{1-t^2}$. When $\tau = 0, t = 1$ and $r = 0$. As $\tau \to \infty, t \to 0$ and $r \to 1$.

After solving the master equation (3.25) for the initial entangled coherent state, the time-dependent density operator $\rho(\tau)$ is obtained. Substituting $\rho(\tau)$ into Eq.(3.19), we calculate the characteristic function and its Fourier transform to obtain the Wigner function for the decohered entangled coherent state. Once again the results shown in Figs. 3.3-3.4 were obtained using the method of steepest descent to find the maximum value of the Bell function under our assumptions. The same symmetrical consideration as before (namely $B(|\alpha|, |\beta|, |\alpha'|, |\beta'|) = B(|\beta|, |\alpha|, |\beta'|, |\alpha'|)$) was imposed.

From Figs. 3.3-3.4 it is obvious that as the entangled coherent state interacts with its environment it fails the nonlocality test. From Fig. 3.3 it can be seen that as the coherent amplitude α increases the initial nonlocality increases and the rate of loss of nonlocality increases. The larger the initial amplitude, *i.e.*, the larger the initial nonlocality, the more rapid the loss of nonlocality occurs, *i.e.*, the shorter the duration of the nonlocality. This characteristic is due to the rapid destruction of a macroscopic quantum state and will be discussed in the following Chapter with two-mode squeezed states. As $r \to 1$, in Fig. 3.3, ρ becomes a product of two vacuum states and $|B|_{max}$ approaches the value 2.

We can see in Fig. 3.4 that the $|C_+\rangle$ state of the coherent amplitude $\alpha = 0.1$ has a long duration of nonlocality ($r \approx 0.375$). The duration of the nonlocality can be increased by decreasing the coherent amplitude.

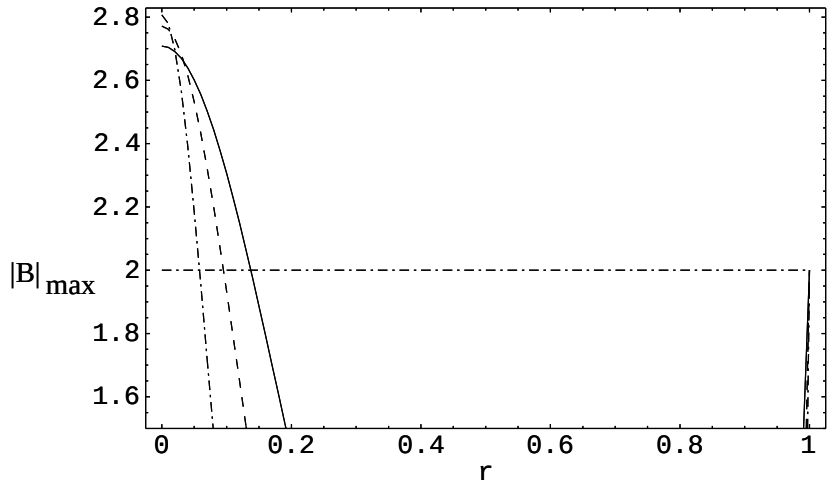

Figure 3.3: Nonlocality as a function of the dimensionless normalised time r for the $|C_-\rangle$ state in the vacuum. $\alpha = 2$ (solid line), $\alpha = 3$ (dashed line) and $\alpha = 5$ (dot-dashed line).

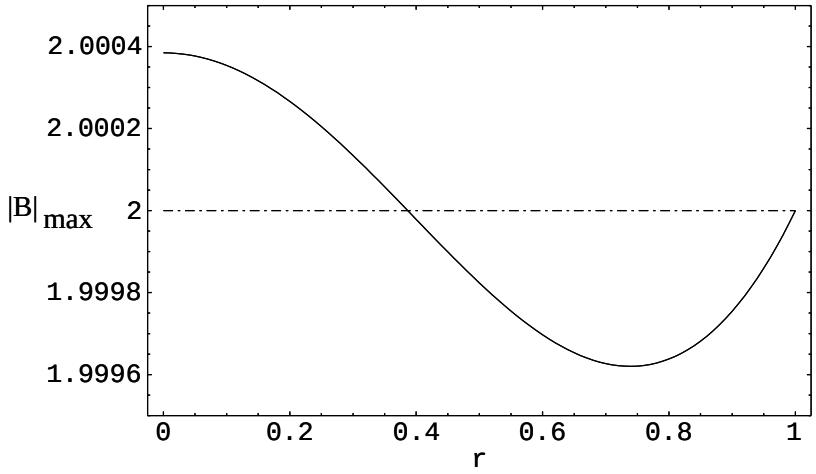

Figure 3.4: The $|C_+\rangle$ state for the coherent amplitude $\alpha = 0.1$, coupled to the vacuum environment, produces a prolonged nonlocal state.

3.6 Nonlocality test in 2×2 dimensional Hilbert space

Entangled coherent states can be considered in a 2×2 dimensional Hilbert space [75], where $|C_-\rangle$ shows maximal entanglement regardless of the value of α [79]. In this section, we will investigate nonlocality and the dynamics of the

entangled coherent state $|C_-\rangle$ in a vacuum environment within the framework of 2×2 Hilbert space (see also the discussions in Ref. [112]).

We consider two orthogonal states

$$|e\rangle = \frac{1}{\sqrt{\mathcal{N}_+}}\Big(|\alpha\rangle + |-\alpha\rangle\Big), \tag{3.28}$$

$$|d\rangle = \frac{1}{\sqrt{\mathcal{N}_-}}\Big(|\alpha\rangle - |-\alpha\rangle\Big) \tag{3.29}$$

where $\mathcal{N}_+ = 2 + 2e^{-2\alpha^2}$ and $\mathcal{N}_- = 2 - 2e^{-2\alpha^2}$ are normalisation factors. A two-dimensional Hilbert space can be spanned using these states as orthonormal bases. The entangled coherent state $|C_-\rangle$ can be represented in 2×2 dimensional Hilbert space as

$$|C_-\rangle_{12} = \frac{1}{\sqrt{2}}\Big(|e\rangle_1|d\rangle_2 - |d\rangle_1|e\rangle_2\Big), \tag{3.30}$$

where we recognise that $|C_-\rangle$ is maximally entangled.

The Bell-CHSH inequality for a bipartite spin-$\frac{1}{2}$ state $|\psi\rangle$ is $|B| \leq 2$, where

$$B = \langle\psi|\vec{a}\cdot\vec{\sigma}_1 \otimes \vec{b}\cdot\vec{\sigma}_2 + \vec{a}\cdot\vec{\sigma}_1 \otimes \vec{b}'\cdot\vec{\sigma}_2 + \vec{a}'\cdot\vec{\sigma}_1 \otimes \vec{b}\cdot\vec{\sigma}_2 - \vec{a}'\cdot\vec{\sigma}_1 \otimes \vec{b}'\cdot\vec{\sigma}_2|\psi\rangle \tag{3.31}$$

and $\vec{a}$, $\vec{a}'$, $\vec{b}$ and $\vec{b}'$ are three-dimensional unit vectors and σ's are Pauli matrices [104]. The unit vectors determine the directions of σ-operators which are measurement observables. They are usually realised by rotating the measurement apparatuses at both sides. The effect of these unit vectors can also be realised by local unitary operations on both particles of the pair independently, fixing the direction of the measurement apparatuses so that the measurement operator becomes $\sigma_{z1} \otimes \sigma_{z2}$.

We first consider ideal conditions for the nonlocality test. Assume $|e\rangle$ and $|d\rangle$ can be perfectly discriminated with eigenvalues 1 and -1 by an ideal measurement operator $O_s = |e\rangle\langle e| - |d\rangle\langle d|$, where the operator O_s is an analogy to σ_z in a spin-$\frac{1}{2}$ system. If an ideal rotation such as $R_x(\theta)$ around an axis,

$$\begin{aligned} R_x(\theta)|e\rangle &= \cos\theta|e\rangle + i\sin\theta|d\rangle, \\ R_x(\theta)|d\rangle &= i\sin\theta|e\rangle + \cos\theta|d\rangle, \end{aligned} \tag{3.32}$$

can be performed on the particles of both sides by two local measurements O_{s1} and O_{s2}, it can be proved that the entangled coherent state $|C_-\rangle$ maximally violates the Bell-CHSH inequality regardless of the value of α, *i.e.*, $|B|_{max} = 2\sqrt{2}$.

The dynamic change of nonlocality for the entangled coherent state can be obtained from its time-dependent density matrix. Assuming vacuum environment, it is possible to restrict our discussion in a 2×2 dimensional Hilbert space even for the mixed case. The basis vectors in Eqs. (3.28) and (3.29) now should be

$$|e(\tau)\rangle = \frac{1}{\sqrt{\mathcal{N}_+(\tau)}}(|t\alpha\rangle + |-t\alpha\rangle), \tag{3.33}$$

$$|d(\tau)\rangle = \frac{1}{\sqrt{\mathcal{N}_-(\tau)}}(|t\alpha\rangle - |-t\alpha\rangle), \tag{3.34}$$

where $\mathcal{N}_+(\tau) = 2 + 2e^{-2t^2\alpha^2}$ and $\mathcal{N}_-(\tau) = 2 - 2e^{-2t^2\alpha^2}$. Although $|e(\tau)\rangle$ and $|d(\tau)\rangle$ are time-dependent, they always remain orthogonal until $\tau \to \infty$.

With use of the master equation (3.25) we find the mixed density matrix $\rho_-(\tau)$ as follows

$$\rho_-(\tau) = \frac{1}{4\mathcal{N}_+\mathcal{N}_-}\begin{pmatrix} A & 0 & 0 & D \\ 0 & C & -C & 0 \\ 0 & -C & C & 0 \\ D & 0 & 0 & E \end{pmatrix}, \tag{3.35}$$

where A, C, D and E are defined as

$$A = (1-\Gamma)\mathcal{N}_+^2(\tau), \tag{3.36}$$

$$C = (1+\Gamma)\mathcal{N}_+(\tau)\mathcal{N}_-(\tau), \tag{3.37}$$

$$D = -(1-\Gamma)\mathcal{N}_+(\tau)\mathcal{N}_-(\tau), \tag{3.38}$$

$$E = (1-\Gamma)\mathcal{N}_-^2(\tau), \tag{3.39}$$

$$\Gamma = \exp\{-4(1-t^2)\alpha^2\}. \tag{3.40}$$

The maximal Bell-CHSH violation for a 2×2 dimensional state ρ is given

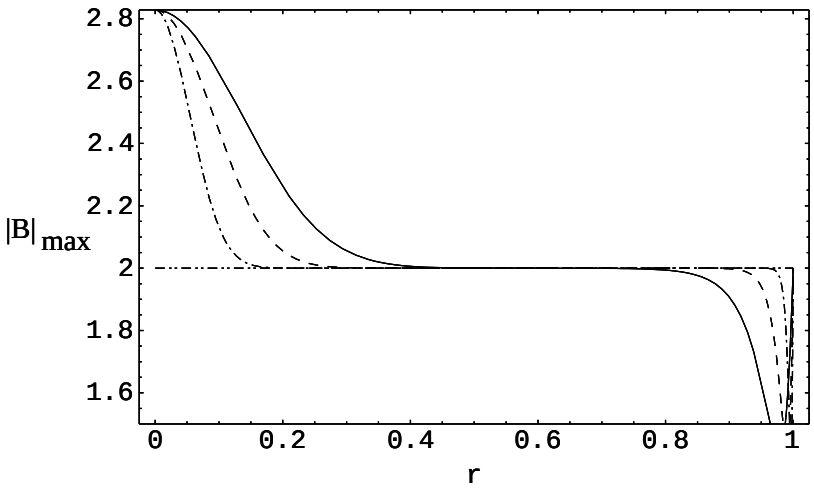

Figure 3.5: Bell measure for an entangled coherent state against normalised time r in 2×2 Hilbert space under perfect rotations. Nonlocality persists longer in 2×2 space than in continuous Hilbert space. $\alpha = 2$ (solid line), $\alpha = 3$ (dashed line) and $\alpha = 5$ (dot-dashed line).

in [113]

$$|B|_{max} = 2\sqrt{M(\rho)}, \tag{3.41}$$

where $M(\rho)$ is the sum of the two larger eigenvalues of $TT^{\dagger}$ and T is a 3×3 matrix whose elements are defined as $t_{nm} = \mathrm{T}r(\rho\sigma_m \otimes \sigma_n)$ with Pauli matrices represented by $\sigma' s$. Ideal measurement and rotation ability should be assumed again here to use this formula. The three eigenvalues of $TT^{\dagger}$ for the mixed entangled coherent state ρ_- are

$$\frac{(C+D)^2}{4\mathcal{N}_+^2\mathcal{N}_-^2}, \ \frac{(C-D)^2}{4\mathcal{N}_+^2\mathcal{N}_-^2}, \ \frac{(A-2C+E)^2}{16\mathcal{N}_+^2\mathcal{N}_-^2}, \tag{3.42}$$

from which $M(\rho_-)$ is obtained by calculating the sum of the two larger eigenvalues.

Fig. 3.5 shows $|B|_{max}$ versus the dimensionless time $r(\tau)$. Initially, $\rho_-(\tau = 0)$ is maximally entangled regardless of α, and $|B|_{max}$ has the maximal value $2\sqrt{2}$. As interaction time increases, nonlocality decreases. For $\tau \to \infty$, ρ_- becomes a direct product of two coherent states, which is a pure state, and $|B|_{max}$ becomes 2. It is clear from Fig. 3.5 that the nonlocality persists longer in 2×2 Hilbert space than in continuous-variable space, which is due to the

change of the observable in the different Hibert space. We can see that the nonlocality of a given state varies according to the Hilbert space in which the state is considered, as does entanglement also [75].

It has already been found that the decohered state $\rho_-(\tau)$ always remains entangled in 2×2 Hilbert space [75]. This indicates that the mixed state $\rho_-(\tau)$ retains some amount of entanglement even after it loses its nonlocality. For pure states, it is true that any entangled state violates Bell's inequality [110]. On the other hand, it was shown that there are mixed states which are entangled but do not violate Bell's inequality [114]. Our model in 2×2 space is one example of that case.

Because the state $|e\rangle$ contains only even numbers of photons and $|d\rangle$ contains only odd numbers of photons, these two states are eigenstates of the operator $O_r = \Pi_e - \Pi_o$ which is known as the pseudo-spin operator [115], *i.e.*,

$$O_r|x_n\rangle = \lambda_n|x_n\rangle; \quad n = 1, 2 \tag{3.43}$$

$$\lambda_{1,2} = \pm 1; \quad |x_{1,2}\rangle = |e\rangle, |d\rangle, \tag{3.44}$$

by which $|e\rangle$ and $|d\rangle$ can be perfectly discriminated. The parameters $\lambda_{1,2}$ are eigenvalues of the pseudo-spin operator O_r and $|x_{1,2}\rangle$ are eigenvectors of the operator. The measurement for the nonlocality test is now $\Pi = O_{r1} \otimes O_{r2}$, which is in fact the same as the Π defined in Eqs. (3.12) and (3.14). Therefore, the nonlocality test in 2×2 space can be performed by the same parity measurement as in Eqs. (3.12) and (3.14). Note that there is no way to distinguish between O_r and O_s in our restricted Hilbert space.

If an ideal rotation R_x is possible for $|e\rangle$ and $|d\rangle$, the same structure as $\vec{a} \cdot \vec{\sigma}_1 \otimes \vec{b} \cdot \vec{\sigma}_2$ can be perfectly made by Π. Cochrane *et al.* [116] showed[3] that rotation $R_x(\theta)$ can be approximately realised for $\alpha \gg 1$ by a displacement operator which can change the parity of the even state $|e\rangle$ and the odd state $|d\rangle$ [116, 117]. When a displacement operator $D(i\epsilon)$, where ϵ is real, is applied to a given parity eigenstate it shows oscillations between $|e\rangle$ and $|d\rangle$.

[3]See Appendix A where we point out a nontrivial mistake in their approximation and correct it.

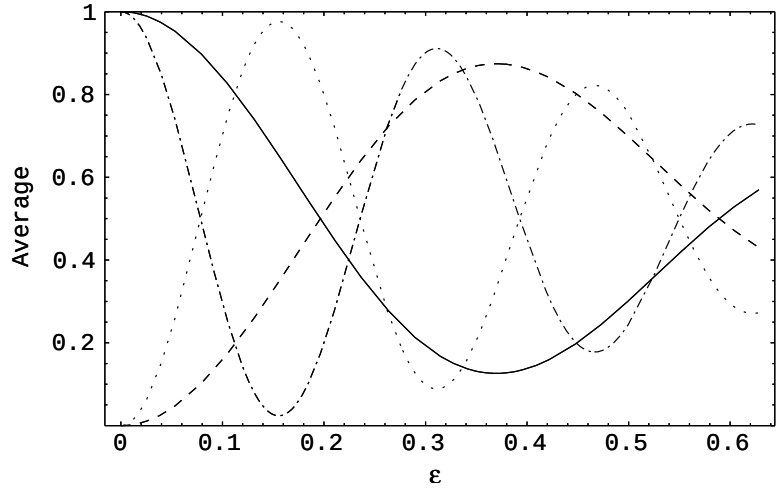

Figure 3.6: Oscillations in even and odd states by the displacement operator $D(i\epsilon)$. For $\alpha \gg 1$, the displacement operator acts as a sinusoidal rotation. For $\alpha = 2$, $\langle e'|\Pi_e|e'\rangle$ (solid line) and $\langle d'|\Pi_e|d'\rangle$ (dashed line). For $\alpha = 5$, $\langle e'|\Pi_e|e'\rangle$ (dot-dashed line) and $\langle d'|\Pi_e|d'\rangle$ (dotted line).

To obtain the Bell function, we can calculate

$$P_e(\epsilon) = \langle e'|\Pi_e|e'\rangle = \frac{e^{2i\alpha\epsilon}\cosh[(\alpha+i\epsilon)^2] + e^{-2i\alpha\epsilon}\cosh[(\alpha-i\epsilon)^2] + 2\cosh[\alpha^2+\epsilon^2]}{2e^{\epsilon^2}(e^{\alpha^2}+e^{-\alpha^2})}, \tag{3.45}$$

$$\widetilde{P}_e(\epsilon) = \langle d'|\Pi_e|d'\rangle = \frac{e^{2i\alpha\epsilon}\cosh[(\alpha+i\epsilon)^2] + e^{-2i\alpha\epsilon}\cosh[(\alpha-i\epsilon)^2] - 2\cosh[\alpha^2+\epsilon^2]}{2e^{\epsilon^2}(e^{\alpha^2}-e^{-\alpha^2})}, \tag{3.46}$$

$$I_e(\epsilon) = \langle e'|\Pi_e|d'\rangle = \frac{e^{2i\alpha\epsilon}\cosh[(\alpha+i\epsilon)^2] - e^{-2i\alpha\epsilon}\cosh[(\alpha-i\epsilon)^2]}{2e^{-\alpha^2+\epsilon^2}\sqrt{1-e^{-4\alpha^2}}}, \tag{3.47}$$

$$P_o(\epsilon) = \langle e'|\Pi_o|e'\rangle = 1 - P_e(\epsilon), \tag{3.48}$$

$$\widetilde{P}_o(\epsilon) = \langle d'|\Pi_o|d'\rangle = 1 - \widetilde{P}_e(\epsilon), \tag{3.49}$$

$$I_o(\epsilon) = \langle d'|\Pi_o|e'\rangle = -I_o(\epsilon), \tag{3.50}$$

where $|e'\rangle = D(i\epsilon)|e\rangle$ and $|d'\rangle = D(i\epsilon)|d\rangle$.

From the average values $P_e(\epsilon) = \langle e'|\Pi_e|e'\rangle$ and $\widetilde{P}_e(\epsilon) = \langle d'|\Pi_e|d'\rangle$ shown in Fig. 3.6, which represent the probabilities for the measured state to have even parity, we can see oscillations due to $D(i\epsilon)$ in the even and odd states.

The Bell-CHSH inequality is then obtained using Eqs. (3.45) to (3.50),

$$\begin{aligned}\mathcal{B} &= \langle C_-(\epsilon_1,\epsilon_2)|\Pi|C_-(\epsilon_1,\epsilon_2)\rangle + \langle C_-(\epsilon_1,\epsilon_2')|\Pi|C_-(\epsilon_1,\epsilon_2')\rangle \\ &\quad + \langle C_-(\epsilon_1',\epsilon_2)|\Pi|C_-(\epsilon_1',\epsilon_2)\rangle - \langle C_-(\epsilon_1',\epsilon_2')|\Pi|C_-(\epsilon_1',\epsilon_2')\rangle \qquad (3.51)\\ &= \Big(2P_e(\epsilon_1)-1\Big)\Big(\widetilde{P}_e(\epsilon_2)+\widetilde{P}_e(\epsilon_2')-1\Big) \\ &\quad + \Big(2\widetilde{P}_e(\epsilon_1)-1\Big)\Big(P_e(\epsilon_2)+P_e(\epsilon_2')-1\Big) \\ &\quad + \Big(2P_e(\epsilon_1')-1\Big)\Big(\widetilde{P}_e(\epsilon_2)-\widetilde{P}_e(\epsilon_2')\Big) + \Big(2\widetilde{P}_e(\epsilon_1')-1\Big)\Big(P_e(\epsilon_2)-P_e(\epsilon_2')\Big) \\ &\quad + 4I_e(\epsilon_1)\Big(I_e(\epsilon_2)+I_e(\epsilon_2')\Big) + 4I_e(\epsilon_1')\Big(I_e(\epsilon_2)-I_e(\epsilon_2')\Big), \qquad (3.52)\end{aligned}$$

where $|C_-(\epsilon_1,\epsilon_2)\rangle = D_1(i\epsilon_1)\otimes D_2(i\epsilon_2)|C_-\rangle_{12}$. The nonlocality of this pure entangled coherent state is the same as the nonlocality of the four variable consideration shown in Fig. 3.2 (higher valued solid line).

For a mixed state, $\rho_-(\tau)$ is used to obtain the Bell function,

$$\begin{aligned}\mathcal{B} &= \mathrm{Tr}\{\rho_-(\tau;\epsilon_1,\epsilon_2)\Pi\} + \mathrm{Tr}\{\rho_-(\tau;\epsilon_1,\epsilon_2')\Pi\} \\ &\quad + \mathrm{Tr}\{\rho_-(\tau;\epsilon_1',\epsilon_2)\Pi\} - \mathrm{Tr}\{\rho_-(\tau;\epsilon_1',\epsilon_2')\Pi\}, \qquad (3.53)\\ \rho_-(\tau;\epsilon_1,\epsilon_2) &= D_1(i\epsilon_1)\otimes D_2(i\epsilon_2)\rho_-(\tau)D_1^\dagger(i\epsilon_1)\otimes D_2^\dagger(i\epsilon_2). \qquad (3.54)\end{aligned}$$

To calculate $\mathrm{Tr}\{\rho_-(\tau;\epsilon_1,\epsilon_2)\Pi\}$, we need to use the redefined identity in the restricted Hilbert space,

$$\begin{aligned}\mathbb{1}_r &= |e(\tau)\rangle_1|e(\tau)\rangle_{22}\langle e(\tau)|_1\langle e(\tau)| + |e(\tau)\rangle_1|d(\tau)\rangle_{22}\langle d(\tau)|_1\langle e(\tau)| \\ &\quad + |d(\tau)\rangle_1|e(\tau)\rangle_{22}\langle e(\tau)|_1\langle d(\tau)| + |d(\tau)\rangle_1|d(\tau)\rangle_{22}\langle d(\tau)|_1\langle d(\tau)| \\ &\equiv \sum_{n=1}^{4}|X_n\rangle\langle X_n|, \qquad (3.55)\end{aligned}$$

which is not equal to the identity $\mathbb{1} = \frac{1}{\pi}\int d^2\alpha d^2\beta|\alpha\rangle|\beta\rangle\langle\beta|\langle\alpha|$ in the continuous-variable basis. Using

$$\begin{aligned}\mathrm{Tr}\{\rho_-(\tau;\epsilon_1,\epsilon_2)\Pi\} &= \sum_{n,m}\langle X_n|\rho_-(\tau)|X_m\rangle\langle X_m|D_1^\dagger(i\epsilon_1) \\ &\quad \otimes D_2^\dagger(i\epsilon_2)\Pi D_1(i\epsilon_1)\otimes D_2(i\epsilon_2)|X_n\rangle, \qquad (3.56)\end{aligned}$$

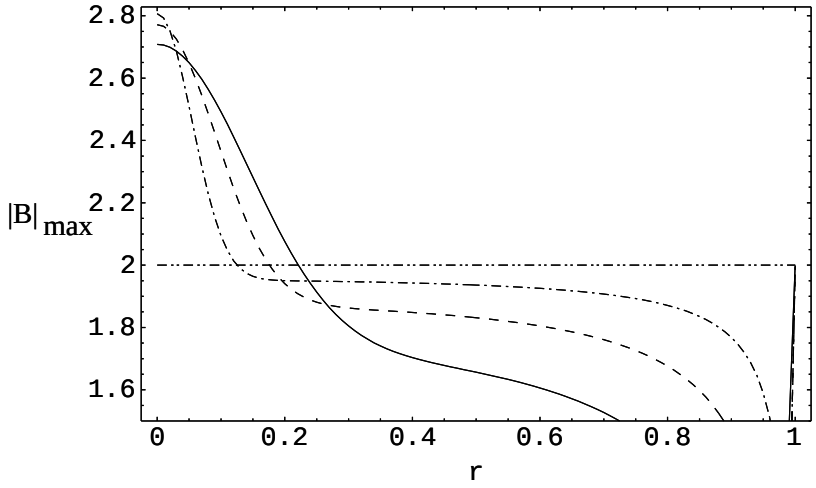

Figure 3.7: The absolute maximum of the Bell function $|B|_{max}$ against normalised time for a mixed entangled coherent state in 2×2 Hilbert space. For $\alpha \gg 1$, rotation needed for the nonlocality test in the 2-qubit state is ideally realised as shown in Fig. 3.6, and the Bell function approaches the ideal case shown in Fig. 3.5. $\alpha = 2$ (solid line), $\alpha = 3$ (dashed line) and $\alpha = 5$ (dot-dashed line).

B is obtained by a straightforward calculation as

$$
\begin{aligned}
B &= Ave(\epsilon_1, \epsilon_2) + Ave(\epsilon_1, \epsilon_2') + Ave(\epsilon_1', \epsilon_2) - Ave(\epsilon_1', \epsilon_2'), && (3.57)\\
Ave(\epsilon_1, \epsilon_2) &= g(\epsilon_1, \epsilon_2)A + l(\epsilon_1, \epsilon_2)E + 2h(\epsilon_1, \epsilon_2)(C - D) \\
&\qquad + \Big(j(\epsilon_1, \epsilon_2) + k(\epsilon_1, \epsilon_2)\Big)C, && (3.58)\\
g(\epsilon_1, \epsilon_2) &= (2\mathbf{P}_e(\epsilon_1) - 1)(2\widetilde{\mathbf{P}}_e(\epsilon_2) - 1), && (3.59)\\
h(\epsilon_1, \epsilon_2) &= 8\mathbf{I}_e(\epsilon_1)\mathbf{I}_e(\epsilon_2), && (3.60)\\
j(\epsilon_1, \epsilon_2) &= (2\mathbf{P}_e(\epsilon_1) - 1)(2\widetilde{\mathbf{P}}_e(\epsilon_2) - 1), && (3.61)\\
k(\epsilon_1, \epsilon_2) &= (2\mathbf{P}_e(\epsilon_1) - 1)(2\widetilde{\mathbf{P}}_e(\epsilon_2) - 1), && (3.62)\\
l(\epsilon_1, \epsilon_2) &= (2\mathbf{P}_e(\epsilon_1) - 1)(2\widetilde{\mathbf{P}}_e(\epsilon_2) - 1), && (3.63)
\end{aligned}
$$

where $\mathbf{P}_e(\epsilon) = \langle e'(\tau)|\Pi_e|e'(\tau)\rangle$, $\widetilde{\mathbf{P}}_e(\epsilon) = \langle d'(\tau)|\Pi_e|d'(\tau)\rangle$, $\mathbf{I}_e(\epsilon) = \langle e'(\tau)|\Pi_e|d'(\tau)\rangle$, $\mathbf{P}_o(\epsilon) = \langle e'(\tau)|\Pi_o|e'(\tau)\rangle = 1 - \mathbf{P}_e(\epsilon)$, $\widetilde{\mathbf{P}}_o(\epsilon) = \langle d'(\tau)|\Pi_o|d'(\tau)\rangle = 1 - \widetilde{\mathbf{P}}_e(\epsilon)$, $\mathbf{I}_o(\epsilon) = \langle d'(\tau)|\Pi_o|e'(\tau)\rangle = -\mathbf{I}_o(\epsilon)$. These are modified versions of Eqs. (3.45) to (3.50) with $|e'(\tau)\rangle = D(i\epsilon)|e(\tau)\rangle$ and $|d'(\tau)\rangle = D(i\epsilon)|d(\tau)\rangle$. As α increases, it is expected that the result in 2×2 space under the $D(i\epsilon)$ operation approaches to the ideal case shown in Fig. 3.5.

Fig. 3.7 shows the largest Bell violation $|B|_{max}$ for $\rho_-(\tau)$ against the normalised time. It is different from the former case of the continuous-variable entangled coherent state for $\tau \neq 0$, because the concerned identities are different from each other. The nonlocality of a given state can differ according to the Hilbert space concerned even though the same kind of measurement observable is used. For $\alpha \gg 1$, the rotation needed for the nonlocality test in the 2-qubit state is ideally realised, and the time variance of the nonlocality approaches to the ideal case in Fig. 3.5 as was expected. For $\alpha \ll 1$, required rotation deviates from the ideal case.

3.7 Remarks

In this Chapter, we have studied the dynamic behaviour of nonlocality for an entangled coherent state in a dissipative environment. The nonlocality test for an entangled coherent state can be realised with photon number measurement and displacement operations. The entangled coherent state is found to be nonlocal regardless of its amplitude. The higher the amplitude, the larger the nonlocality is. When the state interacts with its environment, the nonlocality is lost. The rapidity of the loss of nonlocality depends on the initial amplitude of the state. The larger the initial amplitude, *i.e.*, the larger the initial nonlocality, the more rapid the loss of nonlocality occurs. This is due to the rapid destruction of quantum coherence of a macroscopic quantum state. We will discuss this problem in further detail with two-mode squeezed states in the following Chapter. An entangled coherent state can be studied in 2×2 Hilbert space assuming a vacuum environment, where the nonlocality of the same state persists for longer in the dissipative environment. This is due to the change of the observable in the different Hibert space.

Chapter 4

Quantum Nonlocality for A Two-Mode Squeezed State

In this Chapter, we are interested in how the thermal environment affects the quantum nonlocality of the two-mode squeezed field. We study the dynamic behaviour of the quantum nonlocality based on the parity measurement for the two-mode squeezed state in the thermal environment. The nonlocality is stronger for the squeezed state with a larger degree of squeezing. It is found that the nonlocality disappears more rapidly in the thermal environment as the initial state is squeezed more.

4.1 The two-mode squeezed state

The squeezed light field is a very useful tool for quantum information processing over continuous variables. The recent experimental demonstration [31] of the quantum teleportation via the two-mode squeezed state [32] aroused great interest in continuous-variable quantum information processing among researchers in this field. Squeezed states can also be used for quantum cryptography [28], quantum computation [118] and precision measurement [119].

In Chapter 2, we introduced a coherent state and pointed out that the coherent state is a quantum analogy of a classical particle as it is the minimum point-like state in quantum mechanics. Even though one cannot make a smaller point-like state than a coherent state, it is possible to 'squeeze' it by applying

a unitary transformation on a coherent state. For example, one can imagine a squeezed state which shows the minimum uncertainty, *i.e.,* $\Delta X \Delta P = 1$, but squeezed as $\Delta X > \Delta P$. In this case, if ΔX approaches to infinity while ΔP approaches to zero, the state becomes an eigenstate of the operator $\hat{P}$. A squeezed state is obtained as

$$|\psi(\sigma)\rangle = \exp\left[\frac{1}{2}(\sigma^* \hat{a}^2 - \sigma \hat{a}^{\dagger 2})\right]|0\rangle, \tag{4.1}$$

where $\sigma = s\exp(-i\varphi)$, $|0\rangle$ is a vacuum state, and $\hat{a}$ is the annihilation operator. It is possible to generate a squeezed state for a two-mode system. The two-mode squeezed state is a correlated state of two field modes a and b that can be generated by a nonlinear $\chi^{(2)}$ medium [120, 121]. In this system, there exists the two-mode squeezing property, $\Delta(X_1 + X_2) > \Delta(P_1 + P_2)$ $\Big(\Delta(X_1 + X_2) < \Delta(P_1 + P_2)\Big)$, when $\Delta(P_1 + P_2)^2 < 2$ $\Big(\Delta(X_1 + X_2)^2 < 2\Big)$ [121]. The two-mode pure squeezed state is obtained by applying the unitary operator on the two-mode vacuum

$$|\Psi(\sigma)\rangle_{ab} = \exp\left(-\sigma \hat{a}\hat{b} + \sigma^* \hat{b}^\dagger \hat{a}^\dagger\right)|0\rangle_a |0\rangle_b \tag{4.2}$$

where $\hat{a}$ ($\hat{b}$) is an annihilation operator for the mode a (b). The value of the squeezing parameter s determines the degree of squeezing. The larger s is, the more the state is squeezed. Note that a two-mode squeezed state is generated by passing a single-mode squeezed state through a 50-50 beam splitter. The two-mode squeezed state is an optical realisation of the original EPR state and becomes identical to it as the squeezing parameter s goes to infinity. However, the mean photon number, which is $2\sinh^2 s_{sq}$, becomes infinity in this limit and such a state cannot be produced as it requires infinite energy.

4.2 Time evolution of two-mode squeezed states in a thermal environment

In the previous Chapter, we have studied the Bell function can then be written in terms of the Wigner functions at different phase-space points,

$$B(\zeta_1,\zeta_2)=\frac{\pi^2}{4}\left[W(0,0)+W(\zeta_1,0)+W(0,\zeta_2)-W(\zeta_1,\zeta_2)\right]. \tag{4.3}$$

The Wigner function corresponding to the squeezed state is the Fourier transform of its characteristic function $C_W(\eta_1,\eta_2)$ [121],

$$C_W(\eta_1,\eta_2)=\mathrm{Tr}\left\{\hat{\rho}\exp(\eta_1\hat{a}^\dagger-\eta_1^*\hat{a})\exp(\eta_2\hat{b}^\dagger-\eta_2^*\hat{b})\right\}. \tag{4.4}$$

For the two-mode squeezed state of the density matrix $\hat{\rho}=|\Psi_{ab}(\sigma)\rangle\langle\Psi_{ab}(\sigma)|$, the Wigner function is written as

$$W_{ab}(\zeta_1,\zeta_2)=\frac{4}{\pi^2}\exp\Big[-2\cosh(2s)\left(|\zeta_1|^2+|\zeta_2|^2\right)+2\sinh(2s)\left(\zeta_1\zeta_2+\zeta_1^*\zeta_2^*\right)\Big]. \tag{4.5}$$

The correlated nature of the two-mode squeezed state is exhibited by the $\zeta_1\zeta_2$ cross-term which vanishes when $s=0$.

The dynamics of a quantum system ρ coupled to a thermal environment is described by the master equation. The master equation of a single-mode state ρ in the interaction picture can be obtained by modelling the thermal reservoir as a large number of harmonic oscillators [122]:

$$\frac{d\rho}{dt}=\frac{\gamma}{2}(\bar{n}+1)(2a\rho a^\dagger-a^\dagger a\rho-\rho a^\dagger a)+\frac{\gamma}{2}\bar{n}(2a^\dagger\rho a-aa^\dagger\rho-\rho aa^\dagger), \tag{4.6}$$

where γ denotes the energy decay rate and $\bar{n}$ is the average thermal photon number. The Fokker-Planck equation (in Born-Markov approximation) describing the time evolution of the Wigner function in the interaction picture can be obtained from the master equation (4.6) as [122]

$$\frac{\partial W_{ab}(\zeta_1,\zeta_2,\tau)}{\partial\tau}=\frac{\gamma}{2}\sum_{\zeta_{1_i}=\zeta_1,\zeta_2}\left[\frac{\partial}{\partial\zeta_{1_i}}\zeta_{1_i}+\frac{\partial}{\partial\zeta_{1_i}^*}\zeta_{1_i}^*+2\left(\frac{1}{2}+\bar{n}\right)\frac{\partial^2}{\partial\zeta_{1_i}\partial\zeta_{1_i}^*}\right]W_{ab}(\zeta_1,\zeta_2,\tau), \tag{4.7}$$

where we have assumed that the two modes of the environment are independent of each other and the energy decay rate of each mode is the same to γ. The two modes are supposed to have the same average thermal photon number $\bar{n}$. By solving the Fokker-Planck equation (4.7), we get the time evolution of the Wigner function at time τ to be given by the convolution of the original function and the thermal environment [123],

$$W_{ab}(\zeta_1,\zeta_2,\tau)=\frac{1}{t(\tau)^4}\int d^2\zeta d^2\eta W_a^{th}(\zeta)W_b^{th}(\eta)W_{ab}\left(\frac{\zeta_1-r(\tau)\zeta}{t(\tau)},\frac{\zeta_2-r(\tau)\eta}{t(\tau)},\tau=0\right), \tag{4.8}$$

where the parameters $r(\tau)=\sqrt{1-e^{-\gamma\tau}}$ and $t(\tau)=\sqrt{e^{-\gamma\tau}}$. $W^{th}(\zeta)$ is the Wigner function for the thermal state of the average thermal photon number $\bar{n}$:

$$W^{th}(\zeta)=\frac{2}{\pi(1+2\bar{n})}\exp\left(-\frac{2|\zeta|^2}{1+2\bar{n}}\right). \tag{4.9}$$

Performing the integration in Eq. (4.8), the Wigner function for the initial two-mode squeezed state evolving in the thermal environment is obtained as

$$W_{ab}(\zeta_1,\zeta_2,\tau)=\mathcal{N}\exp\Big[-E(\tau)(|\zeta_1|^2+|\zeta_2|^2)+F(\tau)(\zeta_1\zeta_2+\zeta_1^*\zeta_2^*)\Big] \tag{4.10}$$

where

$$\begin{aligned}
E(\tau) &= \frac{2r(\tau)^2(1+2\bar{n})+2t(\tau)^2\cosh 2s}{D(\tau)}\\
F(\tau) &= \frac{2t(\tau)^2\sinh 2s}{D(\tau)}\\
D(\tau) &= t(\tau)^4+2r(\tau)^2t(\tau)^2(1+2\bar{n})\cosh 2s+r(\tau)^4(1+2\bar{n})^2
\end{aligned} \tag{4.11}$$

and $\mathcal{N}$ is the normalisation factor. In the limit of $s=0$, the $\zeta_1\zeta_2$ cross-term vanishes and the state can be represented by the direct product of each mode states such that $W_{ab}(\zeta_1,\zeta_2,\tau)=W_a(\zeta_1,\tau)W_b(\zeta_2,\tau)$. It is obvious that the Wigner function (4.10) exhibits the local characteristics in this limit.

The system will eventually assimilate with the environment which can be seen in the Wigner function, at the limit of $\tau\to\infty$,

$$W_{ab}(\zeta_1,\zeta_2)=\frac{4}{\pi^2(1+\bar{n})^2}\exp[-\frac{2}{(1+2\bar{n})}(|\zeta_1|^2+|\zeta_2|^2)]. \tag{4.12}$$

This is the direct product of two thermal states in modes a and b.

4.3 Evolution of quantum nonlocality

Substituting Eq. (4.10) into Eq. (4.3), we find the evolution of the nonlocality for the initial two-mode squeezed state in the thermal environment. The Bell function B at time τ is written by

$$B(\zeta_1,\zeta_2,\tau)=\frac{\pi^2\mathcal{N}}{4}\exp\Big\{1+\exp\left[-E(\tau)|\zeta_1|^2\right]+\exp\left[-E(\tau)|\zeta_2|^2\right] \\ -\exp\left[-E(\tau)(|\zeta_1|^2+|\zeta_2|^2)+2F(\tau)|\zeta_1\zeta_2|\cos\theta\right]\Big\} \quad (4.13)$$

where θ_{ζ_1} and θ_{ζ_2} are the phases of ζ_1 and ζ_2 and $\theta=\theta_{\zeta_1}+\theta_{\zeta_2}$. When $\cos\theta=-1$, the Bell function $B_m(|\zeta_1|,|\zeta_2|,\tau)$ is described by the absolute values $|\zeta_1|$ and $|\zeta_2|$. B_m is symmetric in exchanging ζ_1 and ζ_2 such that $B_m(|\zeta_1|,|\zeta_2|,\tau)=B_m(|\zeta_2|,|\zeta_1|,\tau)$. It is straightforward to show that $B\leq B_m$ at any instance of time τ. In order to find the evolution of the nonlocality, the maximal value $|B|_{max}$ of the Bell function B is calculated by the steepest descent method [108] and using the properties of $B_m(|\zeta_1|,|\zeta_2|,\tau)$. Recall that the field is quantum-mechanically nonlocal as $|B|_{max}$ is larger than 2 and the nonlocality is stronger as $|B|_{max}$ gets larger.

The initial two-mode squeezed state is always nonlocal as $|B|_{max}>2$ for $s>0$. $|B|_{max}$ increases monotonically as the degree s of squeezing increases. The state becomes maximally nonlocal with $|B|_{max}\sim 2.19055$ as $s\to\infty$ [101]. In an intermediate time $0<\tau<\infty$, the pure squeezed state evolves to a two-mode mixed squeezed state and nonlocality is lost at a certain evolution time. Figs. 4.1 and 4.2 show $|B|_{max}$ versus the dimensionless time $r(\tau)$ defined in Eq. (4.8). We find that the nonlocality initially prepared persists until the characteristic time $\tau_c(s,\bar{n})$ depending on the temperature of the thermal environment and the initial squeezing. In Fig. 4.1 it is found that, when the environment is the vacuum, $|B|_{max}$ decreases as time proceeds. After reaching at the minimum value, $|B|_{max}$ increases to 2 which is the value of $|B|_{max}$ for the vacuum. Even though it is not clearly seen in the figure due to the scale of the figure, for any $\bar{n}\neq 0$ thermal environment, $|B|_{max}$ increases to its value for

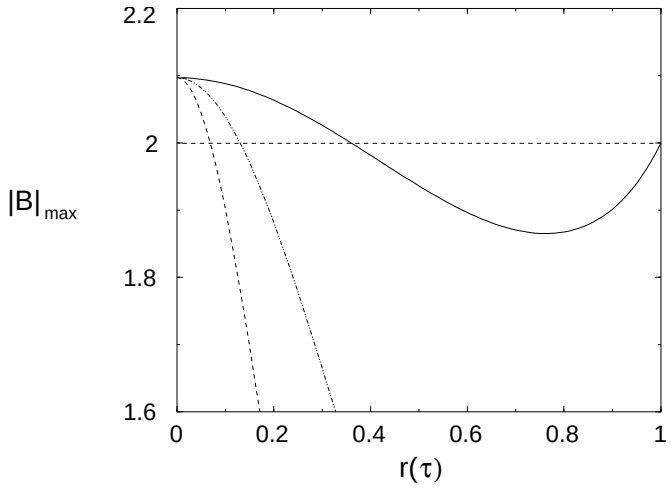

Figure 4.1: The time evolution of the maximal value $|B|_{max}$ of the Bell function versus the dimensionless time $r(\tau) \equiv \sqrt{1-\exp(-\gamma\tau)}$ which is 0 at $\tau = 0$ and 1 at $\tau = \infty$. The initial degree of squeezing $s = 0.3$ and the average photon number $\bar{n}$ of the thermal environment is $\bar{n} = 0$ (solid line), $\bar{n} = 0.5$ (dotted line), and $\bar{n} = 2$ (dashed line). The larger $\bar{n}$ is, the more rapidly the nonlocality is lost.

the thermal field after it decreases to a minimum. In Fig. 4.1, as $\bar{n}$ gets larger $|B|_{max}$ decreases much faster and further.

In Figs. 4.2, we identify an interesting phenomenon that the larger the initial degree of squeezing the more rapidly $|B|_{max}$ decreases. We analyse the reason why $|B|_{max}$ decreases more rapidly as the initial squeezing is larger as follows.

The two-mode squeezed state (4.2) can be represented by the continuous superposition of two-mode coherent states (A similar analysis was done for a single-mode squeezed state [124])

$$|\Psi_{ab}(\sigma)\rangle = \int d^2\alpha G(\alpha,\sigma)|\alpha,\alpha^* e^{i\varphi}\rangle \tag{4.14}$$

where the Gaussian weight function

$$G(\alpha,\sigma) = (\pi \sinh s)^{-1} \exp\left[-\left(\frac{1-\tanh s}{\tanh s}\right)|\alpha|^2\right]. \tag{4.15}$$

As s gets larger, the weight of a large α state is greater so that the contribution of $|\alpha,\alpha^* e^{i\varphi}\rangle$ of a large α becomes more important in the continuous superposition (4.14).

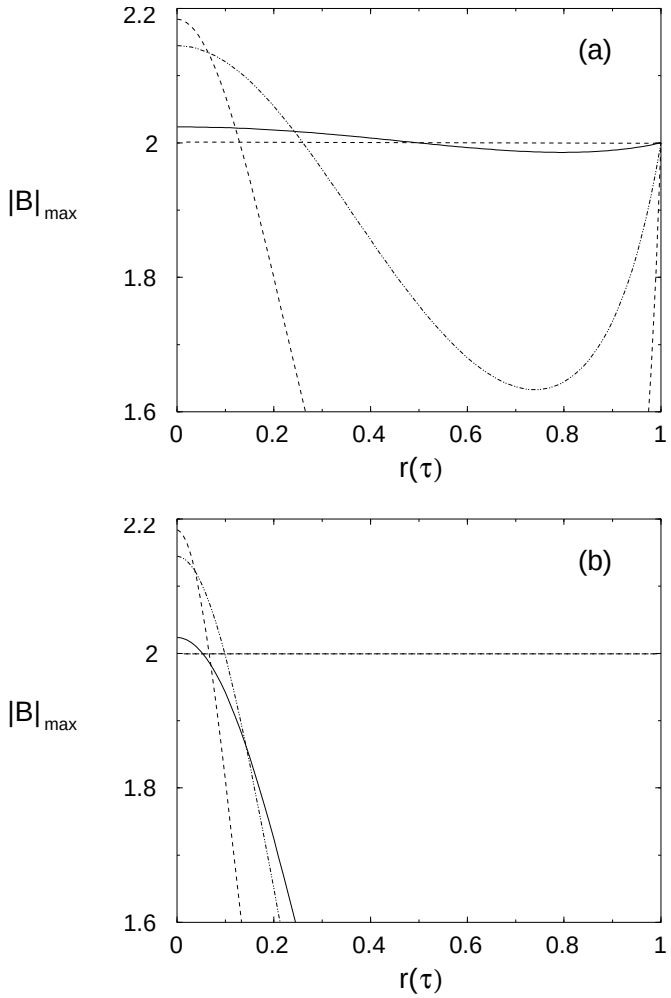

Figure 4.2: The time evolution of $|B|_{max}$ versus $r(\tau) \equiv \sqrt{1-\exp(-\gamma\tau)}$ when the squeezed state is prepared with the initial degree of squeezing $s = 0.1$(solid line), $s = 0.5$(dotted line), and $s = 1.0$(dashed line). The two-mode squeezed state is coupled with the $\bar{n} = 0$ vacuum (a) and the $\bar{n} = 1$ thermal environment (b). In the vacuum, the larger the degree of squeezing, the more rapidly the nonlocality is lost. In the $\bar{n} = 1$ thermal environment, we find that the nonlocality persists longer when the squeezing is $s \sim 0.5$.

The quantum interference between coherent component states is the key of quantum nature of the field. The quantum interference is destroyed by the environment. The speed of destruction depends on the distance between the coherent component states and the average thermal energy of the environment [125]. This is a reason why the macroscopic quantum superposition state is not easily seen in nature. In the continuous superposition (4.14) we find that as the degree of squeezing is larger, the superposition extends further so that the quantum interference can be destroyed more easily. The quantum nonlocality

in the two-mode squeezed state is also originated from the quantum interference between the coherent component states which can be destroyed easily as the contribution of the large amplitude coherent state becomes important.

In fact the uncertainty increases to its maximum and decreases to the value of the environment when a single-mode squeezed state is influenced by the thermal environment [122]. The uncertainty increases faster as the degree of squeezing is larger. This can be explained using the same argument as the loss of quantum nonlocality.

In Fig. 4.2(a), when the environment is in the vacuum, it is found that the characteristic time $\tau_c(s, \bar{n})$ to lose the quantum nonlocality is shorter as the initial degree of squeezing is larger. In Fig. 4.2(b), when the non-zero temperature thermal environment ($\bar{n} \neq 0$) is concerned, we find that the larger degree of squeezing does not necessarily result in the shorter characteristic time $\tau_c(s, \bar{n})$. This clearly shows that the characteristic time is a function of the average number of thermal photons as well as the degree of squeezing. However, it is still true that $|B|_{max}$ decreases faster (the slope of its curve is steeper) when s is larger. It is also found that $|B|_{max}$ decreases faster for $\bar{n} \neq 0$ than for $\bar{n} = 0$.

4.4 Remarks

We have studied the dynamic behaviour of the nonlocality for the two-mode squeezed state in the thermal environment. The two-mode squeezed state can be used for the quantum channel in quantum teleportation of a continuous variable state. The two-mode squeezed state is found to be a nonlocal state regardless of its degree of squeezing and the higher degree of squeezing brings about the larger quantum nonlocality. As the squeezed state is influenced by the thermal environment the nonlocality is lost. The rapidity of the loss of nonlocality depends on the initial degree of squeezing and the average thermal energy of the environment. The more strongly the initial field is squeezed, the more rapidly the maximum nonlocality decreases. These are in agreement with the results of the previous Chapter and have been analysed extensively.

Chapter 5

Quantum Nonlocality Test for Continuous-Variable States With Dichotomic Observables

Gisin and Peres found pairs of observables whose correlations violate Bell's inequality for a discrete N-dimensional entangled state [126]. Banaszek and Wódkiewicz (BW) studied Bell's inequality for continuous-variable states, in terms of Wigner representation in phase space based upon parity measurement and displacement operation [101, 102]. This is useful because of its experimental relevance but does not lead to maximal violation for the original Einstein-Podolsky-Rosen (EPR) state [127]. Recently, Chen *et al.* studied Bell's inequality of continuous-variable states [115] using their newly defined Bell operator [115, 128]. In contrast to the operators in BW formalism, the pseudo-spin operators are not experimentally easy to realise but the EPR state can maximally violate Bell's inequality in their framework [115].

In this Chapter, we relate Chen *et al.*'s "pseudo-spin" Bell operator to one of Gisin and Peres for a finite-dimensional state to bridge the gap between the discussions for the nonlocality of finite and infinite dimensional (or continuous-variable) systems. The origin of the pseudospin operator is attributed to the limiting case of the Gisin-Peres observable [126]. We investigate various versions of Clauser, Horne, Shimony and Holt (CHSH)'s inequality for continuous-variable states. It is pointed out that the BW formalism can be generalised to obtain a larger Bell violation [129], but it cannot give the maximal violation for

the EPR state even in the generalised version. We analyse the reason why the EPR state cannot maximally violate Bell's inequality in the generalised BW formalism. We compare the EPR state with an entangled state of two coherent states [70]. In contrast to the EPR state, the entangled coherent state shows the maximal Bell violation for certain limit both for the generalised BW and Chen *et al.*'s formalism. We also investigate Clauser and Horne (CH)'s version of Bell's inequality. We find the upper and lower bounds for the Bell-CH inequality and test whether the values for continuous-variable states reach these bounds.

5.1 Origin of pseudospin operator

Chen *et al.* introduced a pseudospin operator $\mathbf{s} = (s_x, s_y, s_z)$ for a nonlocality test of continuous variables as a direct analogy of a spin-1/2 system [115, 128]:

$$s_z = \sum_{n=0}^{\infty} \big(|2n+1\rangle\langle 2n+1| - |2n\rangle\langle 2n|\big), \tag{5.1}$$

$$s_x \pm s_y = 2s_{\pm}, \tag{5.2}$$

$$\mathbf{a}\cdot\mathbf{s} = s_z\cos\theta + \sin\theta(e^{i\varphi}s_- + e^{-i\varphi}s_+), \tag{5.3}$$

where $s_- = \sum_{n=0}^{\infty}|2n\rangle\langle 2n+1| = (s_+)^\dagger$ and $\mathbf{a}$ is a unit vector. The Bell-CHSH operator based upon the pseudospin operator is then defined as [92, 115]

$$\begin{aligned}\mathcal{B} = {} & (\mathbf{a}\cdot\mathbf{s}_1)\otimes(\mathbf{b}\cdot\mathbf{s}_2) + (\mathbf{a}\cdot\mathbf{s}_1)\otimes(\mathbf{b}'\cdot\mathbf{s}_2) \\ & + (\mathbf{a}'\cdot\mathbf{s}_1)\otimes(\mathbf{b}\cdot\mathbf{s}_2) - (\mathbf{a}'\cdot\mathbf{s}_1)\otimes(\mathbf{b}'\cdot\mathbf{s}_2),\end{aligned} \tag{5.4}$$

where 1 and 2 denote two different modes and $\mathbf{a}'$, $\mathbf{b}$ and $\mathbf{b}'$ are unit vectors.

Bell's inequality imposed by local hidden variable theory is then $|\langle\mathcal{B}\rangle| \leq 2$. In this formalism, the violation of the inequality is limited by Cirel'son bound $|\langle\mathcal{B}\rangle| \leq 2\sqrt{2}$ [115, 106] as we studied in Chapter 3. It was found that a two-mode squeezed state [121]

$$|\mathrm{TMSS}\rangle = \sum_{n=0}^{\infty}\frac{(\tanh r)^n}{\cosh r}|n\rangle|n\rangle, \tag{5.5}$$

where $|n\rangle$ is a number state and r is the squeezing parameter, maximally violates Bell's inequality, *i.e.* $|\langle\mathcal{B}\rangle|_{max} \to 2\sqrt{2}$ when r becomes infinity [115]. Note that the two-mode squeezed state (5.5) becomes the original EPR state when $r \to \infty$ [32].

Gisin and Peres found pairs of observables whose correlations violate Bell's inequality for an N-dimensional entangled state [126]

$$|\Psi\rangle = \sum_{n=0}^{N-1} c_n |\phi_n\rangle|\psi_n\rangle, \tag{5.6}$$

where $\{|\phi_n\rangle\}$ and $\{|\psi_n\rangle\}$ are any orthonormal bases. Further they showed that the violation of Bell's inequality is maximal in the case of a spin-j singlet state for an even j. The Gisin-Peres observable is

$$A(\theta) = \alpha_x \sin\theta + \alpha_z \cos\theta + \mathcal{E}, \tag{5.7}$$

where α_x and α_z are block-diagonal matrices in which each block is an ordinary Pauli matrix, σ_x and σ_z, respectively. $\mathcal{E}$ is a matrix whose only non-vanishing element is $\mathcal{E}_{N-1,N-1} = 1$ when N is odd and $\mathcal{E}$ is zero when N is even. The Bell operator is then defined as

$$\begin{aligned}\mathcal{B}_{GP} = &(\mathbf{a}\cdot A_1)\otimes(\mathbf{b}\cdot A_2) + (\mathbf{a}\cdot A_1)\otimes(\mathbf{b}'\cdot A_2) \\ &+ (\mathbf{a}'\cdot A_1)\otimes(\mathbf{b}\cdot A_2) - (\mathbf{a}'\cdot A_1)\otimes(\mathbf{b}'\cdot A_2),\end{aligned} \tag{5.8}$$

where A represents the Gisin-Peres observable $A(\theta)$. It was Gisin [130] who showed any entangled pure state violates a Bell's inequality. Later, Gisin and Peres [126] found the observable (5.7) to give the violation of Bell's inequality for any N-dimensional entangled pure state.

In the limit $N \to \infty$, we find that α_x and α_z become pseudospin operators s_x and s_z in Eq. (5.2) and $A(\theta)$ becomes $\mathbf{a}\cdot\mathbf{s}$ (with $\varphi = 0$) in Eq. (5.3). Note that the effect of $\mathcal{E}$ vanishes for $N \to \infty$. Understanding Chen *et al.*'s observables as a limiting case of a Gisin-Peres observable defined for a finite discrete system, it is now straightforward to show that the EPR state maximally violates Bell's inequality as the EPR state $\sum_{n=0}^{\infty}|n\rangle|n\rangle$ is the *infinite-dimensional singlet state*. Extending the Gisin and Peres' argument, we can make a remark:

Any bipartite pure infinite-dimensional entangled state violates Bell's inequality for observables based on the pseudospin observables.

5.2 The Bell-CHSH inequalities for continuous variables

5.2.1 The two-mode squeezed state

In the previous chapters, we introduced generalised BW inequality using parity operators in terms of the Wigner function:

$$\mathcal{B}_{BW} = \Pi_1(\zeta_1)\Pi_2(\zeta_2) + \Pi_1(\zeta_1')\Pi_2(\zeta_2) + \Pi_1(\zeta_1)\Pi_2(\zeta_2') - \Pi_1(\zeta_1')\Pi_2(\zeta_2'), \quad (5.9)$$

$$|\langle\mathcal{B}_{BW}\rangle| = \frac{\pi^2}{4}|W(\zeta_1,\zeta_2) + W(\zeta_1,\zeta_2') + W(\zeta_1',\zeta_2) - W(\zeta_1',\zeta_2')| \leq 2, \quad (5.10)$$

where $W(\zeta_1,\zeta_2)$ represents the Wigner function of a given state. Using $\Pi_1(\zeta_1)\Pi_1(\zeta_1) = \Pi_2(\zeta_1)\Pi_2(\zeta_1) = \mathbb{1}$, it is straightforward to check the Cirel'son bound $|\langle\mathcal{B}_{BW}\rangle| \leq 2\sqrt{2}$ in the generalised BW formalism. Recall the Wigner function of the two-mode squeezed state [131]

$$W_{TMSS}(\zeta_1,\zeta_2) = \frac{4}{\pi^2}\exp[-2\cosh 2r(|\zeta_1|^2+|\zeta_2|^2)+2\sinh 2r(\zeta_1\zeta_2+\zeta_1^*\zeta_2^*)], \quad (5.11)$$

with which the Bell function $B_{BW} \equiv \langle\mathcal{B}_{BW}\rangle$ can be calculated. In the infinite squeezing limit, the absolute Bell function maximises as $|B_{BW}|_{max} \to 8/3^{9/8} \simeq 2.32$ at $\zeta_1 = -\zeta_1' = \zeta_2'/2 = \sqrt{(\ln 3)/16\cosh 2r}$ and $\zeta_2 = 0$. This shows that the EPR state does not maximally violate Bell's inequality in the generalised BW formalism. In Fig. 5.1(a), using the generalised BW formalism, the maximised value $|B_{BW}|_{max}$ is plotted for the two-mode squeezed state and compared with the violation of Bell's inequality based on other formalisms. (The method of steepest descent [108] is used in Fig. 5.1(a) and other figures in the paper to get the maximised value of violation within the formalism.)

The reason why the generalised BW formalism does not give the maximum violation for the EPR state can be explained as follows. The operator s_z in Eq. (5.1) is equivalent to BW's observable $\Pi(\zeta_1)$ when $\zeta_1 = 0$ except a

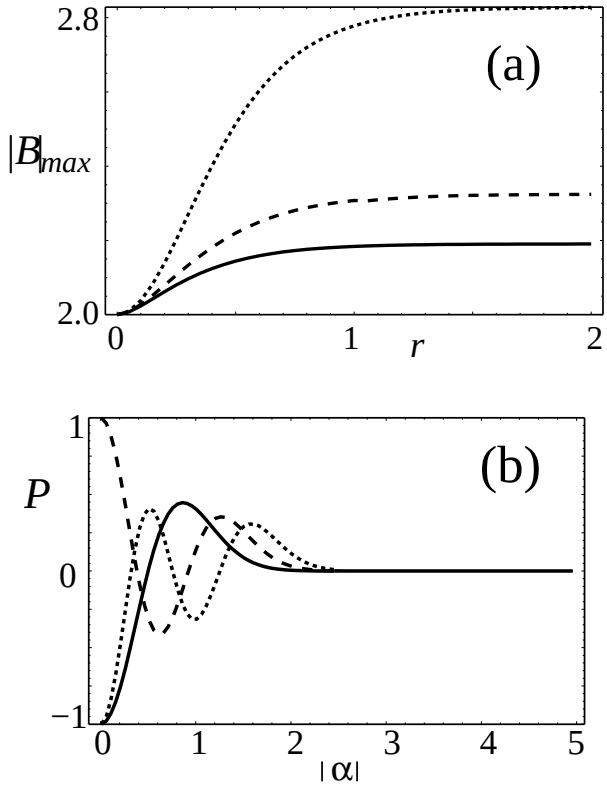

Figure 5.1: (a) The maximised value of absolute Bell function $|B|_{max}$ for a two-mode squeezed state vs the squeezing parameter r in the BW (solid line), the generalised BW (dashed), and Chen *et al.*'s (dotted) formalisms. It is shown that the EPR state does not maximally violate Bell's inequality in the generalised BW formalism. (b) The expectation value P of BW's observable for number states of $n = 1$ (solid), $n = 2$ (dashed), and $n = 3$ (dotted) is plotted against the absolute displacement parameter $|\zeta_1|$.

trivial sign change. The main difference is that BW use the displacement operator while Chen *et al.* use the direct analogy of the rotation of spin operators. When the Gisin-Peres observable $A(\theta)$ (or equivalently pseudospin observable $\mathbf{a}\cdot\mathbf{s}$ with $\varphi = 0$) is applied on an arbitrary state $\sum_{n=0}^{\infty} f(n)|n\rangle$, where $f(n)$ is an arbitrary function, we obtain

$$A(\theta)\sum_{n=0}^{\infty} f(n)|n\rangle = \sqrt{2}\cos(\theta-\pi/4)\sum_{n=0}^{\infty} f(2n)|2n\rangle + \sqrt{2}\sin(\theta-\pi/4)\sum_{n=0}^{\infty} f(2n+1)|2n+1\rangle. \quad (5.12)$$

The operator $A(\theta)$ rotates $\sum f(n)|n\rangle$ into even and odd parity states; the pseu-

dospin observable (5.3) can completely flip the parity of any given state by changing the angle. Note that the only measurement applied to the nonlocality test here is the parity measurement. Differently from the pseudospin operator, BW's observable $\Pi(\zeta_1)$ does not assure the complete parity change, which makes it impossible to find the maximal Bell violation of the two-mode squeezed state. In the two-mode squeezed state, orthogonal number states, which have well defined parity, are the entangled elements. The expectation value of BW's observable for a number state is obtained as [132]

$$\begin{aligned} P(n,|\zeta|) &= \langle n|\Pi(\zeta)|n\rangle \\ &= \frac{e^{-|\zeta|^2}|\zeta|^{2n}}{n!}\sum_{k=0}^{\infty}\left\{\frac{(2k)!}{|\zeta|^{4k}}\left(L_{2k}^{(n-2k)}(|\zeta|^2)\right)^2\frac{(2k+1)!}{|\zeta|^{4k+2}}\left(L_{2k+2}^{(n-2k-1)}(|\zeta|^2)\right)^2\right\}, \end{aligned} \tag{5.13}$$

where $L_q^{(p)}(x)$ is an associated Laguerre polynomial. We numerically assess $P(n,|\zeta|)$ for some different numbers and check that the parity of the number states cannot be perfectly flipped by changing the parameter ζ of the displacement operator $D(\zeta)$ as shown in Fig. 5.1(b).

5.2.2 The entangled coherent state

The entangled coherent state [70] is another important continuous-variable entangled state. Many possible applications to quantum information processing have been studied utilising entangled coherent states [75, 76, 78]. The entangled coherent state $|\mathrm{ECS}\rangle$ can be defined as

$$|\mathrm{ECS}\rangle = \mathcal{N}(|\alpha\rangle|-\alpha\rangle - |-\alpha\rangle|\alpha\rangle), \tag{5.14}$$

where $\mathcal{N}$ is a normalisation factor and $|\alpha\rangle$ is a coherent state with $\alpha \neq 0$. For the case of the entangled coherent state, the Bell function in the generalised

BW formalism (5.10) can be calculated from its Wigner function:

$$\begin{aligned} W_{ECS}(\zeta_1,\zeta_2) = 4\mathcal{N}^2\Big\{ & \exp[-2|\zeta_1-\alpha|^2-2|\zeta_2+\alpha|^2] \\ & + \exp[-2|\zeta_1+\alpha|^2-2|\zeta_2-\alpha|^2] \\ & - \exp[-2(\zeta_1-\alpha)(\zeta_1^*+\alpha)-2(\zeta_2+\alpha)(\zeta_2^*-\alpha)-4\alpha^2] \\ & - \exp[-2(\zeta_1^*-\alpha)(\zeta_1+\alpha)-2(\zeta_2^*+\alpha)(\zeta_2-\alpha)-4\alpha^2]\Big\}, \end{aligned} \tag{5.15}$$

where α is assumed to be real for simplicity. We find that the Bell function approaches $2\sqrt{2}$ for $\alpha \to \infty$ [129] at $\zeta_1 = 0$, $\zeta_2 = 5\pi/16\alpha$, $\zeta_1' = \pi/8\alpha$ and $\zeta_2' = 3\pi/16\alpha$ as shown in Fig. 5.2(a).

The entangled coherent state can be represented in the 2×2-Hilbert space as

$$|\mathrm{ECS}\rangle = \frac{1}{\sqrt{2}}(|e\rangle|d\rangle - |d\rangle|e\rangle), \tag{5.16}$$

where $|e\rangle = \mathcal{N}_+(|\alpha\rangle + |-\alpha\rangle)$ and $|d\rangle = \mathcal{N}_-(|\alpha\rangle - |-\alpha\rangle)$ are even and odd cat states with normalisation factors $\mathcal{N}_+$ and $\mathcal{N}_-$. Note that these states form an orthogonal basis, regardless of the value of α, which span the two-dimensional Hilbert space. Suppose that an ideal rotation $R_x(\theta)$ around the x axis,

$$\begin{aligned} R_x(\theta)|e\rangle &= \cos\theta|e\rangle + i\sin\theta|d\rangle, \\ R_x(\theta)|d\rangle &= i\sin\theta|e\rangle + \cos\theta|d\rangle, \end{aligned} \tag{5.17}$$

can be performed on the both sides of the entangled coherent state (5.16). Because the state (5.16) is the same as the EPR-Bohm state of a two-qubit system, it can be easily proved that it maximally violates the Bell's inequality, *i.e.*, the maximised Bell function is $2\sqrt{2}$. Remarkably, it is known that the displacement operator acts like the rotation $R_x(\theta)$ on the even and odd cat states for $\alpha \gg 1$ [129, 116]. The fidelity can be checked that $|\langle e|D^\dagger(i\zeta_{1_i})R_x(\theta)|e\rangle|^2 = |\langle d|D^\dagger(i\zeta_{1_i})R_x(\theta)|d\rangle|^2 \to 1$ for $\alpha \to \infty$, where $\theta = 2\alpha\zeta_{1_i}$ and ζ_{1_i} is real. As a result, the parity of the even and odd cat states, which are the orthogonal entangled elements in the entangled coherent state, can be perfectly flipped by the displacement operator for $\alpha \to \infty$ as is implied in Fig. 5.2(b) [129]. This property permits the maximal Bell violation of the entangled coherent state for a large coherent amplitude.

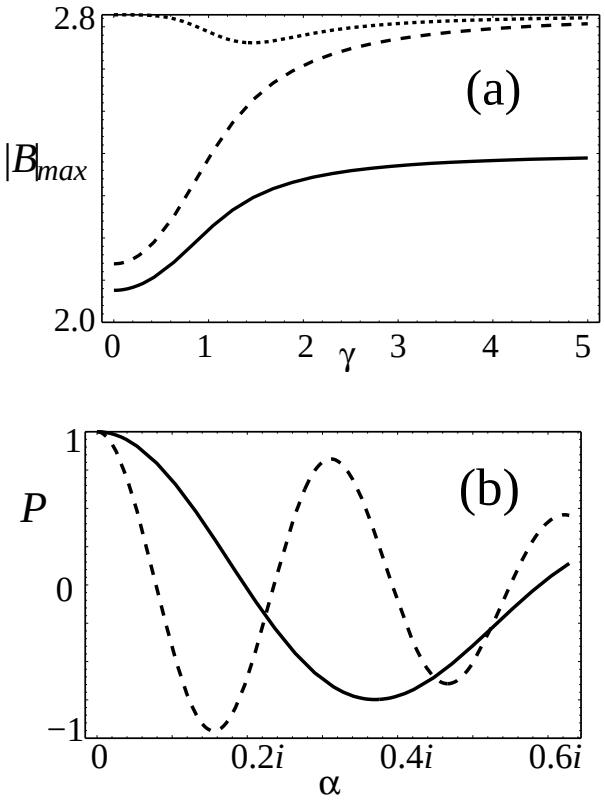

Figure 5.2: (a) The maximised value of absolute Bell function $|B|_{max}$ for an entangled coherent state is plotted against its coherent amplitude α using the BW (solid), the generalised BW (dashed), and Chen *et al.*'s (dotted) formalisms. The entangled coherent state maximally violates Bell's inequality in the generalised BW formalism for $\alpha \to \infty$ and in the Chen *et al.*'s formalism both for $\alpha \to 0$ (but $\alpha \neq 0$) and for $\alpha \to \infty$. (b) The expectation value P of BW's observable for the even cat state is plotted against ζ_1 for $\alpha = 2$ (solid) and $\alpha = 5$ (dashed). For $\alpha \gg 1$, the displacement operator acts like a rotation so that the parity of the even and odd cat states may be well flipped.

In the pseudospin formalism, the correlation function $E(\theta_1, \varphi_1, \theta_2, \varphi_2) = \langle \mathrm{ECS}|s_1(\theta_1, \varphi_1) \otimes s_2(\theta_2, \varphi_2)|\mathrm{ECS}\rangle$ of the entangled coherent state is

$$E(\theta_1, \varphi_1, \theta_2, \varphi_2) = -\cos\theta_1 \cos\theta_2 - K(\alpha)\cos(\varphi_1 - \varphi_2)\sin\theta_1 \sin\theta_2,$$
$$K(\alpha) = \frac{\cosh\alpha^2 \sinh\alpha^2}{(\sum_{n=0}^{\infty} \frac{\alpha^{4n+1}}{\sqrt{(2n)!(2n+1)!}})^2}, \tag{5.18}$$

where $0 < K(\alpha) < 1$, and $K(\alpha)$ approaches to 1 when $\alpha \to 0$ (but $\alpha \neq 0$) and $\alpha \to \infty$. The maximised value of the Bell function $B = \langle \mathcal{B} \rangle$ is obtained from

Eq. (5.18) as

$$|B|_{max} = 2\sqrt{1 + K(\alpha)^2} \tag{5.19}$$

by setting $\theta_1 = 0$, $\theta_1' = \pi/2$, $\theta_2 = -\theta_2'$ and $\varphi_1 = \varphi_2 = 0$. Then, the maximal violation is found for the two extreme cases, $\alpha \to 0$ and $\alpha \to \infty$. When α is small, the entangled coherent state is not maximally entangled in an infinite-dimensional Hilbert space, as tracing the state over one mode variables the von Neumann entropy is not infinite. It is interesting to note that the non-maximally entangled state maximally violates Bell's inequality. We attribute this mismatch to the dichotomic nature of the test of quantum nonlocality for an infinite-dimensional system. However, the entangled coherent state is maximally entangled in the 2×2 Hilbert space but it does not always maximally violate the Bell-CHSH inequality as shown in Fig. 5.2(a). This shows that the pseudospin formalism is not a 'perfect' analogy of a two-qubit system when a qubit is composed of two orthogonal even and odd cat states. The pseudospin operator $\mathbf{a} \cdot \mathbf{s}$ (with $\varphi = 0$) in Eq. (5.3) can be written as $\mathbf{a} \cdot \mathbf{s} = U(\theta) s_z$ where a unitary rotation $U(\theta)$ is

$$U(\theta)|2n+1\rangle = \cos\theta|2n+1\rangle + \sin\theta|2n\rangle, \tag{5.20}$$

$$U(\theta)|2n\rangle = -\sin\theta|2n+1\rangle + \cos\theta|2n\rangle. \tag{5.21}$$

The even (odd) cat state does not flip into the odd (even) cat state by $U(\theta)$; it is only the parity of the given state which changes. The fidelity between the 'rotated' odd cat state and the even cat state is obtained as

$$|\langle d|U(\pi/2)|e\rangle|^2 = K(\alpha) \tag{5.22}$$

which is smaller than 1. It is clear that $|e\rangle$ and $|d\rangle$ are well flipped to each other only for the limiting cases of $\alpha \to 0$ and $\alpha \to \infty$. In other words, the rotation may get the given states out of the 2×2 space spanned by $|e\rangle$ and $|d\rangle$. Note, for example, that $U(\pi/2)|e\rangle$ cannot be represented by a linear superposition of $|e\rangle$ and $|d\rangle$.

5.3 The Clauser-Horne inequality

We have studied quantum nonlocality of continuous-variable states using the Bell-CHSH inequality [92] and all the arguments have been based upon the parity measurement. The Clauser and Horne's version of the Bell's inequality [93] can also be considered to test the nonlocality of continuous-variable states with photon number measurement [101, 102]. We will investigate the Bell-CH inequality in this section.

5.3.1 The bound values for Bell-CH inequality

The bound values for the Bell-CHSH inequality $\pm 2\sqrt{2}$ are well known as Cirel'son bound [106]. The upper bound $(-1+\sqrt{2})/2$ of the Bell-CH inequality was proved by comparing the CH and CHSH inequalities [133]. The bound values for the Bell-CH inequality can also be simply found as follows. The Bell-CH operator for a two-qubit system is defined as [93, 101, 102]

$$\begin{aligned}\mathcal{B}_{CH} = {} & \xi_1(\theta_1)\otimes\xi_2(\theta_2) + \xi_1(\theta_1)\otimes\xi_2(\theta_2') + \xi_1(\theta_1')\otimes\xi_2(\theta_2) \\ & - \xi_1(\theta_1')\otimes\xi_2(\theta_2') - \xi_1(\theta_1)\otimes\mathbb{1}_2 - \mathbb{1}_1\otimes\xi_2(\theta_2),\end{aligned} \tag{5.23}$$

where $\xi(\theta) = |\theta\rangle\langle\theta|$ and $|\theta\rangle = \cos\theta|0\rangle + \sin\theta|1\rangle$. then the local theory imposes the inequality $-1 \le \langle\mathcal{B}_{CH}\rangle \le 0$. Note here that we investigate a simple 2×2 system without loss of generality. One can prove by direct calculation

$$\mathcal{B}_{CH}^2 = -\mathcal{B}_{CH} - \Delta, \tag{5.24}$$

where

$$\Delta = \langle\theta_1|\theta_1'\rangle\Big(|\theta_1\rangle\langle\theta_1'| - |\theta_1'\rangle\langle\theta_1|\Big)_1 \otimes \langle\theta_2|\theta_2'\rangle\Big(|\theta_2\rangle\langle\theta_2'| - |\theta_2'\rangle\langle\theta_2|\Big)_2. \tag{5.25}$$

Using $\langle\mathcal{B}_{CH}\rangle^2 \le \langle\mathcal{B}_{CH}^2\rangle$, the average of Eq. (5.24) becomes

$$\langle\mathcal{B}_{CH}\rangle^2 + \langle\mathcal{B}_{CH}\rangle + \langle\Delta\rangle \le 0, \tag{5.26}$$

and the Bell-CH function $B_{CH} \equiv \langle \mathcal{B}_{CH} \rangle$ is

$$\frac{-1-\sqrt{1-4\langle\Delta\rangle}}{2} \leq B_{CH} \leq \frac{-1+\sqrt{1-4\langle\Delta\rangle}}{2}. \tag{5.27}$$

The maximal and minimal values of $\langle\Delta\rangle$ can be obtained from the eigenvalues of Δ [104], which are $\pm\sin[2(\theta_1-\theta_1')]\sin[2(\theta_2-\theta_2')]/4$. The inequality $-1/4 \leq \langle\Delta\rangle \leq 1/4$ is then obtained. Finally, the maximum and minimum of the Bell-CH function are found at $\langle\Delta\rangle = -1/4$ as

$$\frac{-1-\sqrt{2}}{2} \leq B_{CH} \leq \frac{-1+\sqrt{2}}{2} \tag{5.28}$$

in which the upper and lower bounds of the Bell-CH function are given. For example, the Bell-CH function for a single-photon entangled state

$$|\psi\rangle = \frac{1}{\sqrt{2}}(|0\rangle|1\rangle - |1\rangle|0\rangle) \tag{5.29}$$

is calculated to be

$$B_{CH} = \frac{1}{4}\Big\{ \cos[2(\theta_1'-\theta_2')) - \cos[2(\theta_1-\theta_2') - \cos[2(\theta_1'-\theta_2) - \cos[2(\theta_1-\theta_2)] - 2\Big\}. \tag{5.30}$$

This maximises to $(\sqrt{2}-1)/2 \simeq 0.21$ at $\theta_1 = 0$, $\theta_2 = -3\pi/8$, $\theta_1' = \pi/4$ and $\theta_2' = -5\pi/8$ [134] and minimises to $-(\sqrt{2}+1)/2 \simeq -1.21$ at $\theta_1 = 0$, $\theta_1' = \pi/4$ and $\theta_2 = -\theta_2' = \pi/8$.

5.3.2 Bell-CH inequalities for continuous variables

BW used the Q function for the test of the Bell-CH inequality violation of the simple single-photon entangled state (5.29) [101, 102]. The Q function for a two-mode state ρ_{12} is defined as

$$Q_{12}(\zeta_1,\zeta_2) = \frac{{}_2\langle\zeta_2|_1\langle\zeta_1|\rho_{12}|\zeta_1\rangle_1|\zeta_2\rangle_2}{\pi^2}, \tag{5.31}$$

where $|\zeta_1\rangle$ and $|\zeta_2\rangle$ are coherent states. The Bell-CH function in terms of Q representation is

$$\begin{aligned} B_{CH-BW} &= \langle \upsilon_1(\zeta_1)\otimes\upsilon_2(\zeta_2) + \upsilon_1(\zeta_1)\otimes\upsilon_2(\zeta_2') \\ &\quad +\upsilon_1(\zeta_1')\otimes\upsilon_2(\zeta_2) - \upsilon_1(\zeta_1')\otimes\upsilon_2(\zeta_2') \\ &\quad -\upsilon_1(\zeta_1)\otimes\mathbb{1}_2 - \mathbb{1}_1\otimes\upsilon_2(\zeta_2)\rangle \\ &= \pi^2[Q_{12}(\zeta_1,\zeta_2) + Q_{12}(\zeta_1,\zeta_2') + Q_{12}(\zeta_1',\zeta_2) \\ &\quad -Q_{12}(\zeta_1',\zeta_2')] - \pi[Q_1(\zeta_1) + Q_2(\zeta_2)], \end{aligned} \tag{5.32}$$

where $Q_1(\zeta_1)$ and $Q_2(\zeta_2)$ are the marginal Q functions of modes 1 and 2, and $\upsilon(\zeta_1) = D(\zeta_1)|0\rangle\langle 0|D^\dagger(\zeta_1)$. Eq. (5.32) is a generalised version of the BW's formalism as BW considered $\zeta_1 = \zeta_2 = 0$ [101, 102]. In this case the measurement results are distinguished according to the presence of photons, in other words, the dichotomic outcomes are no photon and the presence of photons. This is more realistic because the parity of photon numbers is difficult to measure with currently developed photodetectors.

The Q function for the two-mode squeezed state is [131]

$$Q_{TMSS}(\zeta_1,\zeta_2) = \frac{1}{\pi^2\cosh^2 r}\exp[-|\zeta_1|^2 - |\zeta_2|^2 + \tanh r(\zeta_1\zeta_2 + \zeta_1^*\zeta_2^*)] \tag{5.33}$$

and the Q function for the entangled coherent state

$$\begin{aligned} Q_{ECS}(\zeta_1,\zeta_2) = \mathcal{N}^2\Big\{ &\exp[-|\zeta_1-\alpha|^2 - |\zeta_2+\alpha|^2] \\ &+ \exp[-|\zeta_1+\alpha|^2 - |\zeta_2-\alpha|^2] \\ &- \exp[-(\zeta_1-\alpha)(\zeta_1^*+\alpha) - (\zeta_2+\alpha)(\zeta_2^*-\alpha) - 4\alpha^2] \\ &- \exp[-(\zeta_1^*-\alpha)(\zeta_1+\alpha) - (\zeta_2^*+\alpha)(\zeta_2-\alpha) - 4\alpha^2]\Big\}. \end{aligned} \tag{5.34}$$

The marginal Q function of each state can also be simply obtained from Eqs. (5.33) and (5.34). One can investigate the violation of the Bell-CH inequality for the two different states from Eqs. (5.32), (5.33) and (5.34). The results are plotted in Figs. 5.3(a) and (b).

For the two-mode squeezed state, the degree of the violation of the Bell-CH inequality increases as generalising the BW formalism. However, it increases

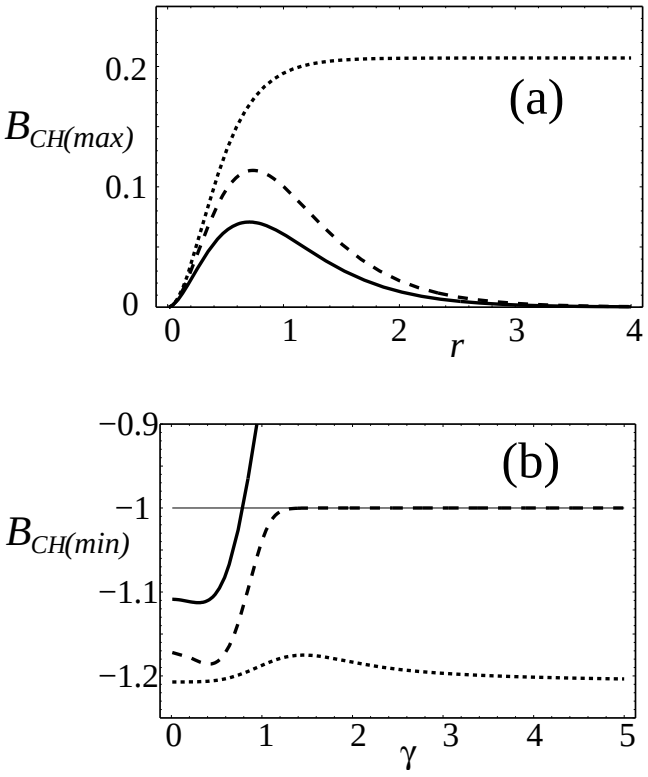

Figure 5.3: (a) The maximised Bell-CH function $B_{CH(max)}$ for a two-mode squeezed state is plotted against the degree of squeezing r using the BW (solid line) and the generalised BW (dashed) formalisms. The maximised function $B_{CH(max)}$ of the same state based upon parity measurement for the same state is given (dotted line). (b) The minimised Bell-CH function $B_{CH(min)}$ for an entangled coherent state is plotted against its coherent amplitude α using the BW (solid line) and the generalised BW (dashed) formalisms. The minimised function $B_{CH(min)}$ based upon the parity measurement is plotted for the same state (dotted line).

up to a peak and decreases as increasing the squeezing r, which is shown in Fig. 5.3(a). The two-mode squeezed state is a separable pure state when r is zero, where no violation of the Bell's inequality is found. As r increases, entanglement becomes to exist, which causes the violation of the Bell's inequality. However, as r increases, the average photon number increases and the weight of $|0\rangle|0\rangle$ decreases as seen in Eq. (5.5). As the BW formalism of the Bell-CH violation is based on the nonlocality of no photon and presence of photons, its violation diminishes when r is large.

The even and odd cat states become the no-photon and single-photon

number states respectively, *i.e.* $|e\rangle \to |0\rangle$ and $|d\rangle \to |1\rangle$, when $\alpha \to 0$. Therefore, the entangled coherent state approaches to the single-photon entangled state (5.29) in this limit. It can be simply shown that the degree of the Bell-CH violation in the generalised BW formalism for the entangled coherent state for $\alpha \to 0$ ($B_{CH-BW} \simeq -1.17$) is the same as the one for the single photon entangled state (5.29). It is larger than the maximised value found by BW ($B_{CH-BW} \simeq -1.11$) [101, 102] which is also shown in Fig. 5.3(b). However, it still does not reach the maximal violation $-(1+\sqrt{2})/2 \simeq -1.21$, which the single-photon entangled state (5.29) shows with perfect rotations. It does not maximally violate the Bell-CH inequality because of the imperfect rotations by the displacement operator used in the BW formalism (5.32). Note that the displacement operator does not flip $|0\rangle$ to $|1\rangle$ and *vice versa* (see Fig. 5.1(b)). As α becomes large, one can observe qualitatively the same phenomenon as for the two-mode squeezed state. The Bell violation approaches to zero as $\alpha \to \infty$ because of the decrease of the weight of the term $|0\rangle|0\rangle$.

Instead of the measurement of the presence of photons, the parity measurement can be used with the unitary rotation $U(\theta)$ to investigate the Bell-CH inequality. The Bell-CH function is defined as

$$\begin{aligned} B_{CH}^{(\Pi)} = \langle & \chi_1(\theta_1) \otimes \chi_2(\theta_2) + \chi_1(\theta_1) \otimes \chi_2(\theta_2') \\ & + \chi_1(\theta_1') \otimes \chi_2(\theta_2) - \chi_1(\theta_1') \otimes \chi_2(\theta_2') \\ & - \chi_1(\theta_1) \otimes \mathbb{1}_2 - \mathbb{1}_1 \otimes \chi_2(\theta_2) \rangle, \end{aligned} \tag{5.35}$$

$$\chi(\theta) = \sum_{n=0}^{\infty} U(\theta)|2n\rangle\langle 2n|U^{\dagger}(\theta). \tag{5.36}$$

For the two-mode squeezed state,

$$\langle \chi_1(\theta_1) \otimes \chi_2(\theta_2) \rangle = \sin\theta_1 \cos\theta_1 \sin\theta_2 \cos\theta_2 \tanh 2r, \tag{5.37}$$

$$\langle \chi_1(\theta_1) \otimes \mathbb{1} \rangle = \frac{(\cos^2\theta_1 \cosh^2 r + \sin^2\theta_1^2 \sinh^2 r)}{\cosh 2r}, \tag{5.38}$$

and for the entangled coherent state,

$$\langle \chi_1(\theta_1) \otimes \chi_2(\theta_2) \rangle = \frac{1}{2}(\sin^2\theta_1 \cos^2\theta_2 + \sin^2\theta_1 \cos^2\theta_2) - K(\alpha) \sin\theta_1 \cos\theta_1 \sin\theta_2 \cos\theta_2, \tag{5.39}$$

$$\langle \chi_1(\theta_1) \otimes \mathbb{1} \rangle = \frac{1}{2}(\cos^2\theta_1 + \sin^2\theta_1), \tag{5.40}$$

from which the Bell-CH function $B_{CH}^{(\Pi)}$ can be obtained. In both cases, we find that the Bell-CH function approaches to the maximal violation $B_{CH}^{(\Pi)} \to -(1 \pm \sqrt{2})/2$. For the two-mode squeezed state, $B_{CH}^{(\Pi)}$ reaches the maximal violation for $r \to \infty$ as shown in Fig. 5.3(a). The upper bound is found at $\theta_1 = 0$, $\theta_2 = -3\pi/8$, $\theta_1' = \pi/4$ and $\theta_2' = -5\pi/8$, and the lower bound at $\theta_1 = 0$, $\theta_2 = -\theta_2' = \pi/8$ and $\theta_1' = \pi/4$. As shown in Fig. 5.3(b), for the entangled coherent state, $B_{CH}^{(\Pi)}$ reaches the maximal violation for $\alpha \to 0$ and $\alpha \to \infty$ at the same angles.

5.4 Remarks

We have studied the violation of Bell's inequalities using various formalisms. We have been able to discuss the link between the discussions for the quantum nonlocality of finite and infinite dimensional systems. The pseudospin operator [115] can be understood as the limiting case of a Gisin-Peres observable [126]. The BW formalism [101, 102] can be generalised to obtain a larger Bell violation [129]. However, the original EPR state cannot maximally violate Bell's inequality even in the the generalised version of the BW formalism. We discussed the reason compared with the case of the entangled coherent state which shows maximal violation of Bell's inequality in the generalised BW formalism. Our result is in agreement with the recent study of nonlocality of a two-mode squeezed state in absorbing optical fibers [135]. In [135], the authors found that nonlocality of the two-mode squeezed state is more robust against a dissipative environment in the pseudospin approach than in the previous study [109] based on the BW formalism. It was shown that the dichotomic measurement for the presence of photons is not so effective in finding the nonlocality of two-mode squeezed states and entangled coherent states.

However, it should be pointed out that the nonlocality based on the Wigner and Q functions is very useful because the measurement of W and Q functions is experimentally possible [136] while the implementation of other operations which we have discussed here have difficulties in their experimental realisation. Note also that Banaszek *et al.* studied the Bell-CH inequality for a single-photon entangled state and a two-mode squeezed state in terms of Q representation [137]. They took imperfect detection efficiency into consideration. Recently, a paper generalising the work of Chen *et al.* where different qubit states are assigned to a continuous variable system has also appeared [138].

Chapter 6

Quantum Teleportation with An Entangled Coherent State

This Chapter contains a detailed analysis of quantum teleportation via an entangled coherent state as the quantum channel. In quantum information processing, the entangled coherent state is normally categorised into a two-mode continuous-variable state. However, it has already been shown in Chapter 2 that it is possible to study entangled coherent states within the framework of a 2×2 dimensional Hilbert space. We assess the entanglement of an evolved entangled coherent state in a vacuum environment and how useful it can be to transfer the quantum information.

We first construct an orthogonal Bell basis set from non-orthogonal coherent states to reformulate the problem to 2×2 dimensional Hilbert space. We then investigate the Bell-state measurement scheme that works perfectly in the large amplitude limit. The Bell measurement scheme composed of linear devices is proposed for use in entanglement concentration and quantum teleportation. Van Enk and Hirota's teleportation scheme [73] is re-illustrated in our framework. When the quantum system is open to the outside world, the initially prepared system decoheres and becomes mixed. Assuming the vacuum environment, we find how an entangled coherent state loses its initial entanglement as interacting with the environment. We use the measure of entanglement [54] based on the partial transposition condition of entanglement [46]. We then consider optimal quantum teleportation via the mixed quantum channel. We find that even though the channel is always entangled under the influence of

the vacuum environment, it becomes useless for teleportation at some point.

6.1 Quantum teleportation

The nonlocal property of quantum mechanics enables a striking phenomenon called quantum teleportation. By quantum teleportation, an unknown quantum state is disentangled in a sending place and its perfect replica appears at a distant place via dual quantum and classical channels. Quantum teleportation is an interesting example to demonstrate a quantum property and is useful for quantum information processing. The key ingredients of quantum teleportation are a quantum channel, which is an entangled state, and Bell-type measurement.

Let us begin with a simple problem: Is it possible to realise a disembodied transport of an *unknown* quantum state $|\phi\rangle$ between two distant parties? Until recently, physicists thought that the answer would be negative because of the implication of the no cloning theorem which prohibits producing a perfect copy of an unknown quantum state. However, in 1993, Bennett *et al.* suggested an intriguing Gedanken experiment [7]. According to their suggestion, it is possible to teleport an unknown quantum state utilising a pre-arranged entangled state. Bennett *et al.*'s suggestion was to teleport a simple 2-dimensional system as follows. Suppose that Alice wants to send an unknown quantum state

$$|\phi\rangle_1 = a|\uparrow\rangle_1 + b|\downarrow\rangle_1. \tag{6.1}$$

The first procedure that Alice and Bob should perform is to prepare the EPR singlet state

$$|\psi_{EPR}\rangle_{23} = \frac{1}{\sqrt{2}}(|\uparrow\rangle_2|\downarrow\rangle_3 - |\downarrow\rangle_2|\uparrow\rangle_3), \tag{6.2}$$

and share the pair between two, so that Alice has the particle 2 and Bob has particle 3. The total system $|\Phi\rangle_{123}$ of the three particles is in a direct product state $|\Phi\rangle_{123} = |\phi\rangle_1|\psi_{EPR}\rangle_{23}$ and can be represented by the Bell basis of particles 1 and 2 as

$$\begin{aligned}|\Phi\rangle_{123} = \frac{1}{2}[&|\Psi_-\rangle_{12}(-a|\uparrow\rangle_3 - b|\downarrow\rangle_3) + |\Psi_+\rangle_{12}(-a|\uparrow\rangle_3 + b|\downarrow\rangle_3) \\ &+ |\Phi_-\rangle_{12}(a|\uparrow\rangle_3 + b|\downarrow\rangle_3) + |\Phi_-\rangle_{12}(a|\uparrow\rangle_3 - b|\downarrow\rangle_3)].\end{aligned} \tag{6.3}$$

If Alice performs a Bell measurement on particles 1 and 2 at her side, Bob's state will be reduced to one of the four components corresponding to particle 3 in Eq. (6.3). After the measurement, Alice sends Bob the result of her measurement which corresponds to 2 classical-bit information so that Bob can reconstruct the original unknown state by performing the corresponding unitary operation on particle 3. For example, if the outcome of Alice's measurement is $|\Phi_+\rangle_{12}$, Bob will operate with σ_z to finish the teleportation procedure.

The quantum teleportation of a 2-dimensional system has been experimentally demonstrated with the polarisation of light [8, 9]. It is possible to extend quantum teleportation of a two-dimensional system to an arbitrary N-dimensional or a continuous-variable system. Vaidman first pointed out how an original EPR state, which is a maximally entangled state, can be employed with nonlocal measurements for teleportation of continuous variables [139]. He suggested two different methods in the framework of nonlocal measurements. One is teleportation via "crossed" space-time nonlocal measurements and the other is a generalisation of Bennett *el al.*'s scheme [7] by nonlocal measurements. In the second method, the original EPR state with perfect correlations in both position and momentum is generated by nonlocal measurements. Even though Vaidman's ideas are creative applications of nonlocal measurements to quantum teleportation, it is difficult to realise in real experiments. Braunstein and Kimble suggested a protocol for an experimentally realisable teleportation of a continuous-variable system [32]. Their scheme utilises a two-mode squeezed state to teleport quadrature variables of light. The squeezing parameter determines the fidelity, which is a measure of how the input and output states are close, of teleportation. A successful experiment was performed by Furusawa *et al.* to demonstrate teleportation of continuous variables [31], though there has been controversy on the requirement of optical coherence for continuous-variable teleportation and the success of Furusawa *et al.*'s experiment [140, 141].

Teleportation protocols can be used for quantum computation where storage of information is required. There was an experiment for teleportation of nuclear-qubit states, where a quantum state of a carbon nucleus was teleported to a hydrogen nucleus over interatomic distances using nuclear magnetic resonance [142]. While light fields are ideal for quantum communication, atoms are advantageous for the long-term storage of quantum information. Atoms are

not ideal for quantum communication and information transfer as they move slowly and interact strongly with an environment. There was a proposal to combine the advantages of using both photons for transfer and atoms for storage of quantum information to teleport atomic states over macroscopic distances [143].

6.2 Construction of Bell basis with entangled coherent states

We have considered two kinds of entangled coherent states which have symmetry in phase space:

$$|C_1\rangle = \frac{1}{\sqrt{N}}(|\alpha\rangle|\alpha\rangle + e^{i\varphi}|-\alpha\rangle|-\alpha\rangle), \tag{6.4}$$

$$|C_2\rangle = \frac{1}{\sqrt{N'}}(|\alpha\rangle|-\alpha\rangle + e^{i\varphi'}|-\alpha\rangle|\alpha\rangle), \tag{6.5}$$

where $|\alpha\rangle$ and $|-\alpha\rangle$ are coherent states of amplitudes α and $-\alpha$, N and N' are normalisation factors, and φ and φ' are relative phase factors. In Chapter 2, it was verified that any entangled coherent states in the form of $(|\beta\rangle|\beta\rangle + e^{i\varphi}|\gamma\rangle|\gamma\rangle)/\sqrt{\mathcal{N}}$ or $(|\beta\rangle|\gamma\rangle + e^{i\varphi'}|\gamma\rangle|\beta\rangle)/\sqrt{\mathcal{N}'}$, where β and γ are any complex amplitudes, can be converted respectively to $|C_1\rangle$ or $|C_2\rangle$ by applying local unitary operations. As we have also pointed in Chapter 2, it is possible to consider an entangled coherent state in $C^2 \otimes C^2$ Hilbert space. It makes the problem simpler because two-qubit entangled states have the simplest mathematical structure among entangled states. In Chapter 2, we introduced odd and even cat states as the basis states for the reduced two-dimensional Hilbert space. However, the basis states can be arbitrarily chosen from the linear independent vectors $|\alpha\rangle$ and $|-\alpha\rangle$. Suppose new orthonormal bases by superposing non-orthogonal and linear independent two coherent states $|\alpha\rangle$ and $|-\alpha\rangle$:

$$|\psi_+\rangle = \frac{1}{\sqrt{N_\theta}}(\cos\theta e^{-\frac{1}{2}i\phi}|\alpha\rangle - \sin\theta e^{\frac{1}{2}i\phi}|-\alpha\rangle), \tag{6.6}$$

$$|\psi_-\rangle = \frac{1}{\sqrt{N_\theta}}(-\sin\theta e^{-\frac{1}{2}i\phi}|\alpha\rangle + \cos\theta e^{\frac{1}{2}i\phi}|-\alpha\rangle), \tag{6.7}$$

where $N_\theta = \cos^2 2\theta$ is a normalisation factor and real parameters θ and ϕ are defined as

$$\sin 2\theta e^{-i\phi} = \langle \alpha | -\alpha \rangle = \exp[-2|\alpha|^2]. \tag{6.8}$$

We define four maximally entangled Bell states using the orthonormal bases in (6.6) and (6.7):

$$|B_{1,2}\rangle = \frac{1}{\sqrt{2}}(|\psi_+\rangle|\psi_+\rangle \pm |\psi_-\rangle|\psi_-\rangle), \tag{6.9}$$

$$|B_{3,4}\rangle = \frac{1}{\sqrt{2}}(|\psi_+\rangle|\psi_-\rangle \pm |\psi_-\rangle|\psi_+\rangle). \tag{6.10}$$

They can be represented by $|\alpha\rangle$ and $|-\alpha^*\rangle$ as

$$\begin{aligned} |B_1\rangle &= \frac{1}{\sqrt{2}N_\theta}\Big\{ e^{-i\phi}|\alpha\rangle|\alpha\rangle + e^{i\phi}|-\alpha\rangle|-\alpha\rangle \\ &\qquad - \sin 2\theta\Big(|\alpha\rangle|-\alpha\rangle + |-\alpha\rangle|\alpha\rangle\Big)\Big\}, \end{aligned} \tag{6.11}$$

$$|B_2\rangle = \frac{1}{\sqrt{2N_\theta}}\Big(e^{-i\phi}|\alpha\rangle|\alpha\rangle - e^{i\phi}|-\alpha\rangle|-\alpha\rangle\Big), \tag{6.12}$$

$$\begin{aligned} |B_3\rangle &= \frac{1}{\sqrt{2}N_\theta}\Big\{ |\alpha\rangle|-\alpha\rangle + |-\alpha\rangle|\alpha\rangle \\ &\qquad - \sin 2\theta\Big(e^{-i\phi}|\alpha\rangle|\alpha\rangle + e^{i\phi}|-\alpha\rangle|-\alpha\rangle\Big)\Big\}, \end{aligned} \tag{6.13}$$

$$|B_4\rangle = \frac{1}{\sqrt{2N_\theta}}\Big(|\alpha\rangle|-\alpha\rangle - |-\alpha\rangle|\alpha\rangle\Big), \tag{6.14}$$

where we immediately recognise that $|B_2\rangle$ and $|B_4\rangle$ are in the form of entangled coherent states $|C_1\rangle$ and $|C_2\rangle$ while $|B_1\rangle$ and $|B_3\rangle$ become so as $|\alpha| \to \infty$.

Now we are ready to consider decoherence and teleportation with mixed entangled coherent states. For simplicity we assume $\phi = 0$, *i.e.*, α is real, in the rest of the Chapter.

6.3 Teleportation via a pure channel

There have been studies on the quantum teleportation of a coherent superposition state via an entangled coherent channel $|B_2\rangle$ [73]. Here, we suggest a

scheme for the same purpose with the use of Bell bases (6.11), (6.12), (6.13), and (6.14). The scheme includes direct realisation of Bell-state measurements. We also show that the Bell-state measurement method enables the entanglement concentration of partially entangled coherent states.

6.3.1 Teleportation and Bell-state measurement

Let us assume that Alice wants to teleport a coherent superposition state

$$|\psi\rangle_a = \mathcal{A}|\alpha\rangle_a + \mathcal{B}|-\alpha\rangle_a \tag{6.15}$$

via the pure entangled coherent channel $|B_4\rangle_{bc}$, where the amplitudes $\mathcal{A}$ and $\mathcal{B}$ are unknown. The state (6.15) can be represented as

$$|\psi\rangle_a = \mathcal{A}'|\psi_+\rangle_a + \mathcal{B}'|\psi_-\rangle_a \tag{6.16}$$

with $\mathcal{A}' = \mathcal{A}\cos\theta + \mathcal{B}\sin\theta$ and $\mathcal{B}' = \mathcal{A}\sin\theta + \mathcal{B}\cos\theta$. After sharing the quantum channel $|B_4\rangle_{bc}$, Alice performs a Bell-state measurement on her part of the quantum channel and the state (6.15) and sends the outcome to Bob. Bob accordingly chooses one of the unitary transformations $\{i\sigma_y, \sigma_x, -\sigma_z, \mathbb{1}\}$ to perform on his part of the quantum channel. Here σ's are Pauli operators and $\mathbb{1}$ is the identity operator and the correspondence between the measurement outcomes and the unitary operations are $B_1 \Rightarrow i\sigma_y$, $B_2 \Rightarrow \sigma_x$, $B_3 \Rightarrow -\sigma_z$, $B_4 \Rightarrow \mathbb{1}$. Acting of these operators on $|\alpha\rangle$ and$|-\alpha\rangle$ gives effects as follows:

$$|\ \alpha\rangle \xrightarrow{i\sigma_y} \frac{1}{N_\theta}\big(\sin 2\theta|\alpha\rangle - |-\alpha\rangle\big), \tag{6.17}$$

$$|\ -\alpha\rangle \xrightarrow{i\sigma_y} \frac{1}{N_\theta}\big(|\alpha\rangle - \sin 2\theta|-\alpha\rangle\big), \tag{6.18}$$

$$|\ \alpha\rangle \xleftrightarrow{\sigma_x} |-\alpha\rangle, \tag{6.19}$$

$$|\ \alpha\rangle \xrightarrow{-\sigma_z} \frac{1}{N_\theta}\big(|\alpha\rangle - \sin 2\theta|-\alpha\rangle\big), \tag{6.20}$$

$$|\ -\alpha\rangle \xrightarrow{-\sigma_z} \frac{1}{N_\theta}\big(\sin 2\theta|\alpha\rangle - |-\alpha\rangle\big). \tag{6.21}$$

It is not a trivial problem to discriminate all four Bell states. In fact it was shown that complete Bell-state measurements on a product Hilbert space of two

two-level systems are not possible using linear elements [84]. We here employ the Bell-state measurement scheme studied in Chapter 2, according the basis state in this Chapter, to discriminate Bell states constructed from entangled coherent states. Although perfect discrimination is not possible, arbitrarily high precision can be achieved when the amplitude of the coherent states becomes large. For simplicity, we shall assume that the 50:50 beam splitter imparts equal phase shifts to reflected and transmitted fields.

Suppose that each mode of the entangled state is incident on the beam splitter. After passing the beam splitter (bs), the Bell states become

$$\begin{aligned}
|B_1\rangle_{ab} &\xrightarrow{bs} \frac{1}{\sqrt{2N_\theta}}(|even\rangle_f|0\rangle_g - \sin 2\theta|0\rangle_f|even\rangle_g), \\
|B_2\rangle_{ab} &\xrightarrow{bs} \frac{1}{\sqrt{2N_\theta}}|odd\rangle_f|0\rangle_g, \\
|B_3\rangle_{ab} &\xrightarrow{bs} \frac{1}{\sqrt{2N_\theta}}(|0\rangle_f|even\rangle_g, -\sin 2\theta|even\rangle_f|0\rangle_g), \\
|B_4\rangle_{ab} &\xrightarrow{bs} \frac{1}{\sqrt{2N_\theta}}|0\rangle_f|odd\rangle_g,
\end{aligned} \tag{6.22}$$

where $|even\rangle = |\sqrt{2}\alpha\rangle + |-\sqrt{2}\alpha\rangle$ has non-zero photon-number probabilities only for even numbers of photons and $|odd\rangle = |\sqrt{2}\alpha\rangle - |-\sqrt{2}\alpha\rangle$ has non-zero photon-number probabilities only for odd numbers of photons. Note that $|even\rangle$ and $|odd\rangle$ are not normalised. If an odd number of photons is detected at detector A for mode f then we know that the entangled state incident on the measurement set up was $|B_2\rangle$. On the other hand, if an odd number of photons is detected at detector B for mode g then the incident entangled state was $|B_4\rangle$. When even numbers of photons are measured, we cannot in general tell if the incident state was $|B_1\rangle$ or $|B_3\rangle$. However, for $\sin 2\theta$ $(= \langle\alpha| - \alpha\rangle) \simeq 0$, *i.e.* $\alpha \gg 1$, if a non-zero even number of photons is detected for mode f, the incident state was $|B_1\rangle$, and if a non-zero even number is detected for mode g, it was $|B_3\rangle$. When $\sin 2\theta$ is not negligible, the probability of wrong estimation is

$$P_i(\alpha) = \frac{1}{2(1 + e^{4\alpha^2})}. \tag{6.23}$$

For the limit of $\alpha \gg 1$, this probability approaches to zero and all the Bell states can be discriminated with arbitrarily high precision.

When the measurement outcome is $|B_2\rangle$, the receiver performs $|\alpha\rangle \leftrightarrow |-\alpha\rangle$ on c. Such a phase shift by π can be done using a phase shifter whose action is described by $R(\varphi) = \mathrm{e}^{i\varphi a^\dagger a}$:

$$R(\varphi) a R^\dagger(\varphi) = a\mathrm{e}^{-i\varphi}, \tag{6.24}$$

where a and $a^\dagger$ are the annihilation and creation operators. When the measurement outcome is $|B_4\rangle$, the receiver does nothing on c as the required unitary transformation is only the identity operation $\mathbb{1}$. When the outcome is $|B_3\rangle$, an operator $\frac{1}{N_\theta}(|\alpha\rangle\langle\alpha| - |-\alpha\rangle\langle-\alpha|)$ plays the corresponding role, which becomes a unitary operator for $\alpha \gg 1$. This transformation can be obtained by displacement operator $D(i\pi/4\alpha)$ and be simply realised by a beam splitter and a strong coherent field as explained in Chapter 3[1]. When the outcome is $|B_1\rangle$, σ_x and σ_z should be successively applied.

6.3.2 Concentration of partial entanglement via entanglement swapping

If the initially prepared quantum channel is in a pure but not maximally entangled state, the channel may be distilled to a maximally entangled state before using it for quantum information processing including teleportation. This process is known as the entanglement concentration protocol [144, 43]. For an entangled coherent channel, it can be simply realised via entanglement swapping [145, 146] using the Bell measurement proposed in Sec. 6.3.1.

Suppose an ensemble of a partially entangled pure state

$$|D_4\rangle = \frac{1}{\sqrt{N_\eta}}(\cos\eta|\alpha\rangle|-\alpha\rangle - \sin\eta|-\alpha\rangle|\alpha\rangle) \tag{6.25}$$

from which we want to distil a sub-ensemble of a maximally entangled state. N_η is a normalisation factor and the real phase factor η, $0 < \eta < \pi/2$, determines the degree of entanglement for $|D_4\rangle$. The state $|D_4\rangle$ in (6.25) is written in the

[1]There are more detailed discussions on this transformation in Chapter 8 and Appendix A.

orthonormal bases (6.6) and (6.7) as follows:

$$|D_4\rangle = \frac{1}{\sqrt{N_\eta}} \left\{ \begin{array}{l} \frac{1}{2}\sin 2\theta(\cos\eta - \sin\eta)\big(|\psi_+\rangle|\psi_+\rangle + |\psi_-\rangle|\psi_-\rangle\big) \\ +\big(\cos^2\theta\cos\eta - \sin^2\theta\sin\eta\big)|\psi_+\rangle|\psi_-\rangle \\ +\big(\sin^2\theta\cos\eta - \cos^2\theta\sin\eta\big)|\psi_-\rangle|\psi_+\rangle \end{array} \right\}. \quad (6.26)$$

First, we consider the case when α is large. In this case, state $|D_4\rangle \simeq |E_4\rangle$ where

$$|E_4\rangle = \cos\eta|\psi_+\rangle|\psi_-\rangle - \sin\eta|\psi_-\rangle|\psi_+\rangle. \quad (6.27)$$

After sharing a quantum channel between Alice and Bob, Alice prepares a pair of particles which are in the same entangled state as the quantum channel. Alice then performs Bell-state measurement on her pair of the quantum channel. If the measurement outcome is B_1 or B_2, the other particle of Alice's and Bob's quantum channel is, respectively, in maximally entangled state $|B_1\rangle_{b'c}$ or $|B_2\rangle_{b'c}$ where Alice's particle is denoted by b'. Otherwise, Alice's particle and Bob's quantum channel are not in a maximally entangled state:

$$|B_3'\rangle_{b'c} = \frac{1}{\sqrt{N_\eta'}}(\cos^2\eta|\psi_+\rangle_{b'}|\psi_-\rangle_c + \sin^2\eta|\psi_-\rangle_{b'}|\psi_+\rangle_c), \quad (6.28)$$

$$|B_4'\rangle_{b'c} = \frac{1}{\sqrt{N_\eta'}}(\cos^2\eta|\psi_+\rangle_{b'}|\psi_-\rangle_c - \sin^2\eta|\psi_-\rangle_{b'}|\psi_+\rangle_c), \quad (6.29)$$

respectively for measurement outcome of B_3 or B_4. N_η' is a normalisation factor. The probability P_1 and P_2 to obtain the maximally entangled state $|B_1\rangle_{b'c}$ and $|B_2\rangle_{b'c}$ are $P_1 = P_2 = \cos^2\eta\sin^2\eta$. In this way, no matter how small the initial entanglement is, it is possible to distil some maximally entangled coherent channels from partially entangled pure channels.

We now consider the concentration protocol when α is not large enough to neglect $\sin 2\theta$. In this case, only two Bell-states $|B_2\rangle$ and $|B_4\rangle$ can be precisely measured. Extending the previous argument leading to (6.29), when the measurement outcome is $|B_4\rangle$, the resulting state for particles b' and c is not maximally entangled. However, we can find that, for the measurement outcome of $|B_2\rangle$, the resulting state is $|B_2\rangle_{b'c}$ even for the case of α small. The success

probability $\mathcal{P}_2$ for this case is

$$\mathcal{P}_2(\theta,\eta) = \frac{\cos^4 2\theta \sin^2 2\eta}{4(1-\sin^2 2\theta \sin 2\eta)} \tag{6.30}$$

where $\mathcal{P}_2 \to 0$ for $\alpha \simeq 0$ and $\mathcal{P}_2 \to \cos^2\eta \sin^2\eta$ for $\alpha \gg 1$.

6.4 Decay of the entangled coherent channel: measure of entanglement

When the entangled coherent channel $|B_4\rangle$ is embedded in a vacuum environment, the channel decoheres and becomes a mixed state of its density operator $\rho_4(\tau)$, where τ stands for the decoherence time. To know the time dependence of $\rho_4(\tau)$, we have to solve the master equation (3.25). In Chapter 3, we have studied its formal solution and found the solution for single-mode dyadic

$$\exp[(\hat{J}+\hat{L})\tau]|\alpha\rangle\langle\beta| = \langle\beta|\alpha\rangle^{1-t^2}|\alpha t\rangle\langle\beta t| \tag{6.31}$$

where $t = e^{-\frac{1}{2}\gamma\tau}$. For later use, we introduce a normalised interaction time r which is related to t: $r = \sqrt{1-t^2}$.

To restrict our discussion in a 2×2 dimensional Hilbert space even for the mixed case, the orthonormal basis vectors (6.6) and (6.7) are now τ-dependent:

$$|\Psi_+(\tau)\rangle = \frac{1}{\sqrt{N_\Theta}}(\cos\Theta|t\alpha\rangle - \sin\Theta|-t\alpha\rangle), \tag{6.32}$$

$$|\Psi_-(\tau)\rangle = \frac{1}{\sqrt{N_\Theta}}(-\sin\Theta|t\alpha\rangle + \cos\Theta|-t\alpha\rangle), \tag{6.33}$$

where $\sin 2\Theta = \exp(-2t^2\alpha^2)$. The unknown state to teleport and the Bell-state bases are newly defined according to the new basis vectors Eqs. (6.32) and (6.33).

Any two dimensional bipartite state can be written as

$$\rho = \frac{1}{4}\left(\mathbb{1}\otimes\mathbb{1} + \vec{v}\cdot\vec{\sigma}\otimes\mathbb{1} + \mathbb{1}\otimes\vec{s}\cdot\vec{\sigma} + \sum_{m,n=1}^{3} t_{nm}\sigma_n\otimes\sigma_m\right), \tag{6.34}$$

where coefficients $t_{nm} = \mathrm{Tr}(\rho\sigma_m \otimes \sigma_n)$ form a real matrix T. Vectors $\vec{v}$ and $\vec{s}$ are local parameters which determine the reduced density operator of each mode

$$\rho_b = \mathrm{Tr}_c\rho = \frac{1}{2}(\mathbb{1} + \vec{v}\cdot\vec{\sigma}), \tag{6.35}$$

$$\rho_c = \mathrm{Tr}_b\rho = \frac{1}{2}(\mathbb{1} + \vec{s}\cdot\vec{\sigma}), \tag{6.36}$$

while the matrix T is responsible for correlation[147]

$$\mathcal{E}(a,b) = \mathrm{Tr}(\rho\,\vec{a}\cdot\vec{\sigma}\otimes\vec{b}\cdot\vec{\sigma}) = (\vec{a}, T\vec{b}). \tag{6.37}$$

With use of Eqs. (6.14) and (6.31), we find $\vec{v}$, $\vec{s}$, and T for the mixed channel $\rho_4(\tau)$ as follows

$$\vec{v} = \vec{s} = \left(\frac{B}{N_\theta},\ 0,\ 0\right), \tag{6.38}$$

$$T = \frac{1}{2N_\theta}\begin{pmatrix} A+D & 0 & 0 \\ 0 & -A+D & 0 \\ 0 & 0 & A-C \end{pmatrix}, \tag{6.39}$$

where A, B, C and D are defined as

$$\begin{aligned} A &= (1-\Gamma)\exp(-4t^2\alpha^2), \\ B &= (1-\Gamma)\exp(-2t^2\alpha^2), \\ C &= 2-(1+\Gamma)\exp(-4t^2\alpha^2), \\ D &= -2\Gamma+(1+\Gamma)\exp(-4t^2\alpha^2), \\ \Gamma &= \exp[-4(1-t^2)\alpha^2]. \end{aligned} \tag{6.40}$$

Note that N_θ is a time-independent normalisation factor and $\rho_4(\tau \neq 0)$ can not be represented by a Bell-diagonal matrix.

The necessary and sufficient condition for separability of a two dimensional bipartite system is the positivity of the partial transposition of its density matrix [46]. Consider a density matrix ρ for a 2×2 system and its partial transposition ρ^{T_2}. The density matrix ρ is inseparable iff ρ^{T_2} has any negative eigenvalue(s). We define the measure of entanglement E for ρ in terms of the negative eigenvalues of ρ^{T_2} [54]. The measure of entanglement E is then defined

as

$$E = -2\sum_i \lambda_i^- \tag{6.41}$$

where λ_i^- are the negative eigenvalue(s) of ρ^{T_2} and the factor 2 is introduced to have $0 \leq E \leq 1$.

For $\rho_4(\tau)$ we find the time evolution of the measure of entanglement

$$E(\tau) = \frac{\sqrt{16B^2 + (C-D)^2} - (2A + C + D)}{4N_\theta}. \tag{6.42}$$

Initially, the state $|B_4\rangle$ is maximally entangled, *i.e.*, $E(\tau = 0) = 1$, regardless of α. It is seen in Fig. 6.1(a) that the mixed state $\rho_4(\tau)$ is never separable at the interaction time $\tau < \infty$. It should be noted that the larger the initial amplitude α, the more rapidly the entanglement is degraded. It is known that the speed of destruction of quantum interference depends on the distance between the coherent component states[125]. When the amplitudes of coherent component states are larger, the entanglement due to their quantum interference is more fragile.

6.5 Teleportation via a mixed channel

The optimal fidelity of teleportation in any general scheme by means of trace-preserving local quantum operations and classical communication (LQCC) via a single channel can be obtained from the maximal singlet fraction of the channel[148]. The relation is

$$f(\rho) = \frac{F(\rho)N + 1}{N + 1}, \tag{6.43}$$

where $f(\rho)$ is the optimal fidelity for the given quantum channel ρ, $F(\rho)$ is the maximal singlet fraction of the channel, and N is the dimension of the related Hilbert space $C^N \otimes C^N$. $F(\rho)$ is defined as $\max\langle\Phi|\rho|\Phi\rangle$ where the maximum is taken over all the $N \times N$ maximally entangled states.

Any 2×2 channel becomes useless for quantum teleportation when the optimal fidelity $f(\rho)$ is less than the classical limit 2/3. In other words, when

$F(\rho) \leq 1/2$, the channel is useless for quantum teleportation. To find the maximally entangled basis in which a given channel has the highest fraction of a maximally entangled state, it suffices to find rotations which diagonalise T [149]. In the case of ρ_4, T in (6.39) is always a diagonal matrix. This means that the Bell bases constructed from Eqs. (6.32) and (6.33) give the maximal singlet fraction at any decay time. The optimal fidelity $f(\rho_4)$ obtained by Eq. (6.43) and the definition of the maximal singlet fraction is

$$f(\rho_4) = \frac{1}{3}\max\left\{1 + \frac{e^{4\alpha^2} - e^{4t^2\alpha^2}}{e^{4\alpha^2} - 1}, \frac{e^{4t^2\alpha^2} - e^{4r^2\alpha^2} + 2e^{4\alpha^2} - 2}{e^{4\alpha^2} - 1}\right\}. \tag{6.44}$$

Because the initially defined Bell bases always give the maximal singlet fraction, the optimal fidelity is obtained by the standard teleportation scheme with Bell measurement and unitary operations. This means that the experimental proposal in Sec. 6.3 for a pure channel can also be used for a mixed channel to obtain the optimal fidelity. The optimal fidelity for the standard teleportation scheme is

$$f_s(\rho_4) = \max\left[\frac{1}{2}(1 - \frac{1}{3}\mathrm{Tr}TO)\right] = f(\rho_4), \tag{6.45}$$

where the maximum is taken over all possible rotations $O = O^+(3)$[147]. As the interaction time varies, parameters $\vec{v}$, $\vec{s}$ and T are changed. For the decoherence model we consider in this Chapter, T alone affects the fidelity of teleportation.

Fig. 6.1(b) shows the optimal fidelity at the normalised decay time r. The channel is always entangled as shown in Fig. 6.1(a). However, after the characteristic time $r_c = 1/\sqrt{2}$ the channel becomes useless for teleportation. It is worth noting that the characteristic time does not depend on the initial α value. This is confirmed by the fact that the only real solution of the equation $f(\rho_4) = 2/3$ is $r = 1/\sqrt{2}$ regardless of α. Bennett *et al.* [15] have pointed out that some states with nonzero entanglement do not have the maximal singlet fractions higher than 1/2. The decohered entangled coherent channel $\rho_4(r \geq r_c)$ is an example of such a case.

As the interaction time varies, all of matrix T and local parameters $\vec{v}$ and $\vec{s}$ are changed. For the decoherence model we consider in this Chapter, T alone affects the fidelity of teleportation as shown in Eq. (6.45) while the local parameters $\vec{v}$ and $\vec{s}$ do not. We investigate how T, $\vec{v}$ and $\vec{s}$ affect the entanglement of the decohered channel in the following.

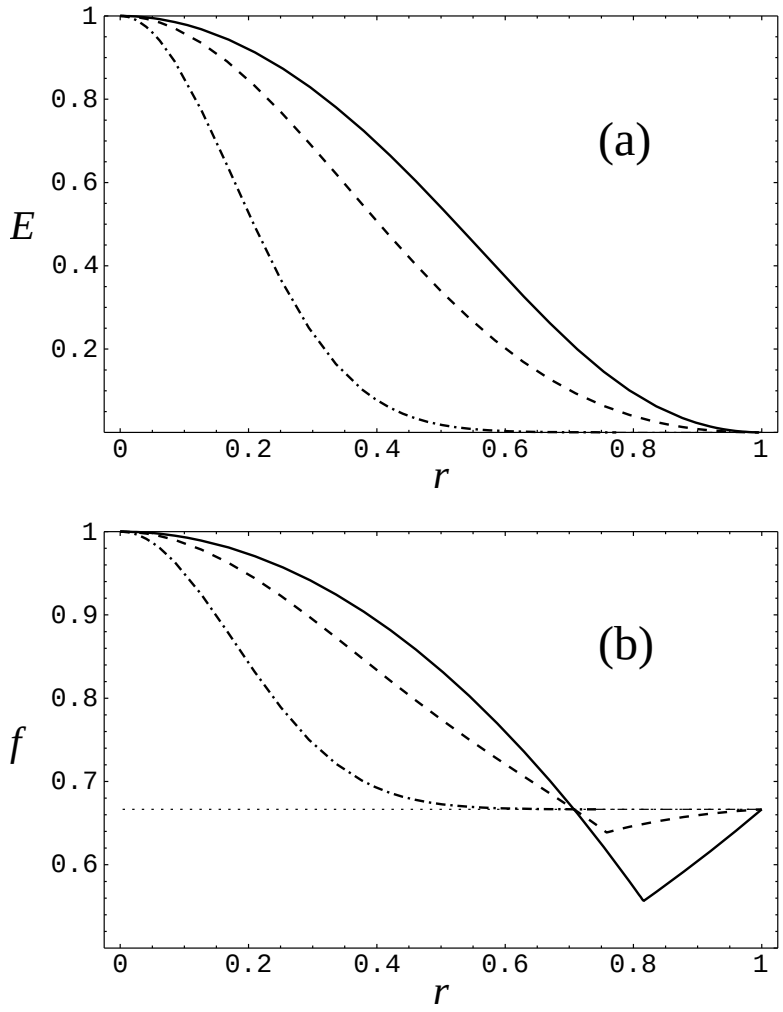

Figure 6.1: (a) Entanglement E for the mixed entangled coherent channel against the normalised decoherence time $r = \sqrt{1 - e^{-\gamma\tau}}$. (b) Optimal fidelity f of quantum teleportation with the mixed entangled coherent channel. The maximum fidelity 2/3 obtained by classical teleportation is plotted by a dotted line. We can clearly see that the mixed channel is not useful in quantum teleportation from $r = 1/\sqrt{2}$ even though it is always entangled. $\alpha = 0.1$ (solid line), $\alpha = 1$ (long dashed) and $\alpha = 2$ (dot dashed).

In Eqs. (6.38) and (6.42), it is clear that all T, $\vec{v}$, and $\vec{s}$ affect entanglement of the channel. The change of T with the decay time decreases the entanglement of the channel. On the other hand, the change of the local states represented by the change of $\vec{v}$ and $\vec{s}$ partially recovers the entanglement. It becomes clear by the following analysis. Suppose a τ-dependent quantum channel whose T changes as in (6.39) but local parameters $\vec{v}$ and $\vec{s}$ remain zero. The

density matrix of the mixed channel at τ is

$$\rho_T(\tau) = \frac{1}{4}\left(\mathbb{1}\otimes\mathbb{1} + \sum_{m,n=1}^{3} t_{nm}\sigma_n \otimes \sigma_m\right) \tag{6.46}$$

and the degree of entanglement is

$$E_T(\tau) = \max\Big\{ -\frac{A+D}{2N_\theta},\ 0\Big\}, \tag{6.47}$$

where $E_T(\tau)$ decreases faster than $E(\tau)$ in Eq. (6.42). Note that this channel is not directly related to the decoherence model concerned here.

For this assumption, teleportation fidelity is not changed from Eq. (6.45) due to the same T and linearly dependent on the entanglement $E_T(\tau)$ while $E_T(\tau)$ has a nonzero value. The mixed channel $\rho_T(\tau)$ is useful for teleportation iff it is entangled, as for any entangled channel with diagonal T and $\vec{v} = \vec{s} = 0$ [147].

Comparing $E(\tau)$ with $E_T(\tau)$, it is clear that some amount of entanglement is added to $E(\tau)$ by the increase of B/N_θ of $\vec{v}$ and $\vec{s}$. We can thus say that the environmental effects on the local states contribute towards entanglement but this "additive entanglement" is not useful for teleportation at all. Therefore, teleportation fidelity is lower than 2/3 even when the channel is entangled.

Bose and Vedral [150] found that not only entanglement but also mixedness of quantum channels affect the fidelity of teleportation. We may conjecture that the higher entanglement and the lower mixedness (higher purity) result in the better fidelity. In this case, it is shown to be true only when the channel is useful for teleportation. The mixedness of a given state ρ can be quantified by its linear entropy $S(\rho) = 1 - \mathrm{Tr}(\rho^2)$. For the decohered entangled coherent channel, the linear entropy is

$$S(\rho_4) = \frac{(e^{8r^2\alpha^2}-1)(e^{8t^2\alpha^2}-1)}{2(e^{4\alpha^2}-1)^2}, \tag{6.48}$$

which increases to the maximal value and then decreases to zero as shown in Fig. 6.5 because the channel interacts with the vacuum and the state for $\tau \to \infty$ approaches to the two-mode vacuum which is a pure state. We found that

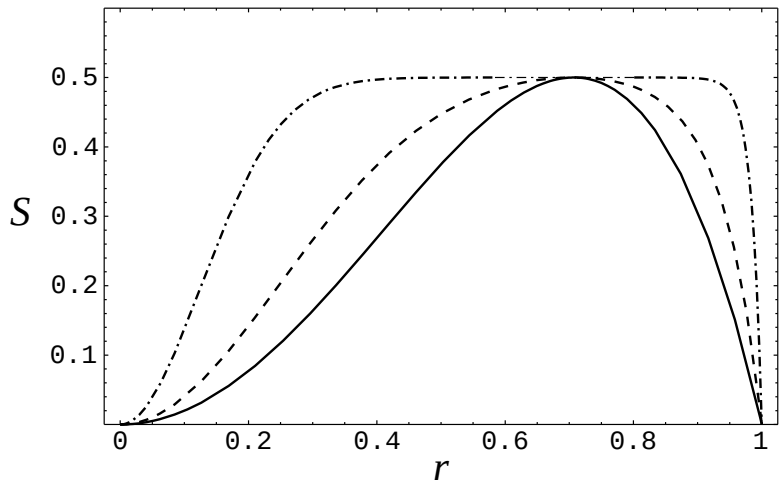

Figure 6.2: Mixedness S quantified by the linear entropy for the mixed entangled coherent state against the normalised decoherence time r. The mixedness becomes maximised at the characteristic time r_c after which the channel is no longer useful for teleportation. $\alpha = 0.1$ (solid line), $\alpha = 1$ (long dashed) and $\alpha = 2$ (dot dashed).

mixedness becomes maximised at the characteristic time r_c. It is confirmed by solving the equation $\partial S(\rho_4)/\partial r = 0$ which yields a unique real solution $r = 1/\sqrt{2} = r_c$ again regardless of α. It is easily checked that von Neumann entropy as a measurement of mixedness gives exactly the same result.

Horodecki *et al.* [149] showed that any entangled 2×2 density matrix can be distilled to a singlet form by local filtering [43, 151] and an entanglement concentration protocol [144]. If sufficiently many entangled 2×2 channels are given, no matter how small the entanglement of the channels is, some maximally entangled channels can be obtained from the original pairs. Because the decohered channel ρ_4 is entangled at any decay time, the ensemble represented by $\rho_4(\tau)$ can be purified to obtain some maximally entangled channels. We have seen that the singlet fraction $F(\rho_4)$ becomes smaller than $1/2$ after r_c, meanwhile the purification protocol in [144] can be applied when the singlet fraction of a given density matrix is larger than $1/2$. Therefore, if the decay time is longer than r_c, a local filtering or a generalised measurement [149] should be first performed on ρ_4 for purification. It has been pointed out that the filtering process allows one to transfer the entanglement hidden in the relation between $\vec{v}$, $\vec{s}$ and T (the entanglement added by change of the local states) to T [149].

6.6 Usefulness for continuous-variable teleportation

We have studied entangled coherent states in a 2×2 Hilbert space. However, entangled coherent states are in fact continuous-variable states in infinite dimensional Hilbert space. If $|B_2\rangle$ and $|B_4\rangle$ are considered in infinite dimensional Hilbert space, they are not maximally entangled any more[152]. It is thus natural to ask such a question: how useful are the entangled coherent states for teleportation of continuous-variable states?

In the protocol proposed in [32] and demonstrated experimentally in [31] for continuous-variable teleportation, a two-mode squeezed state is used as the quantum channel and a joint homodyne measurement as Alice's measurement. An unknown quantum state in Eq. (6.15) can be teleported by a two-mode squeezed state, and the fidelity becomes unity for the limit of infinite squeezing.

Assume that a coherent state of an unknown amplitude is the state to teleport via an entangled coherent state, $|C_2\rangle$ in Eq. (6.5) with $\varphi' = 0$. After a straightforward calculation, the fidelity is obtained [153]

$$f(\alpha) = \frac{1 + \exp(-2\alpha_r^2)}{2\big[1 + \exp(-4\alpha_r^2)\big]}. \tag{6.49}$$

Note that $f(\alpha)$ is independent from the amplitude of the unknown coherent state to teleport. It depends only on the real part of coherent amplitude α of the quantum channel. We find from Eq. (6.49) that the fidelity is always better than $1/2$. The maximal value is about 0.6 when $\alpha_r \simeq \pm 0.7$.

6.7 Remarks

We have studied a mixed entangled coherent channel in 2×2 Hilbert space. We constructed orthogonal Bell bases with entangled coherent states to consider their entanglement and usefulness for teleportation in a dissipative environment. A pure entangled coherent channel is shown to teleport perfectly some quantum information. We investigated an experimental scheme for teleportation and

entanglement concentration with a realisable Bell-measurement method.

It is found that a mixed entangled coherent state is always entangled regardless of the decay time. The larger initial amplitude α, the more rapidly entanglement is degraded. This is in agreement with the fact that macroscopic quantum effects are not easily seen because it is more fragile.

Because a decohered entangled coherent channel is entangled at any decay time, its ensemble can be purified by an entanglement purification protocol [144] and used for reliable teleportation. On the other hand, it is shown that the optimal fidelity of teleportation attainable using a single pair is better than the classical limit 2/3 only until a certain characteristic time r_c, at which the mixedness of the channel becomes maximised. The maximal singlet fraction of the state is not more than 1/2 after r_c, even though it is still entangled.

Entanglement and mixedness [150] of quantum channels are important factors which affect teleportation. Until the characteristic time, both entanglement and purity decrease, which causes the decrease of teleportation fidelity. After the time r_c, the purity of the channel is recovered back even though entanglement decreases further. The experimental realisation of purification for the mixed channels deserves further investigation.

Chapter 7

Quantum Teleportation with A Two-Mode Squeezed State

A continuous variable state can be teleported with use of a two-mode squeezed vacuum for a quantum channel [32]. In this Chapter, we investigate the teleportation via a mixed two-mode squeezed channel to consider the influence of a thermal environment. We are interested in the transfer of non-classical properties of quantum states. It is assumed that the thermal environment gives the same effect on each mode of the quantum channel and the original state is prepared in a pure state.

7.1 Quasiprobability functions

Before considering quantum teleportation, we briefly review the quasiprobability functions. The family of quasiprobability functions are obtained by the following convolution relation [154]

$$R_\sigma(\zeta) = \int d^2\xi \left[\frac{2}{\pi(1-\sigma)} \exp\left(-\frac{2\left|\zeta-\xi\right|^2}{1-\sigma}\right)\right] P(\xi) \tag{7.1}$$

where the σ-parameterised $R_\sigma(\zeta)$ function becomes Q function for $\sigma = -1$, Wigner (W) function for $\sigma = 0$, and P function for $\sigma = 1$. By the Fourier

transform, we find the relation between their characteristic functions

$$C_\sigma^R(\eta) = \exp\left[-\frac{(1-\sigma)|\eta|^2}{2}\right] C^P(\eta) \tag{7.2}$$

where $C_\sigma^R(\eta)$ and $C_\sigma^P(\eta)$ are the characteristic functions for the R and P functions, respectively. The family of two-mode quasiprobability functions can be analogously defined as

$$R_\sigma(\zeta_a,\zeta_b) = \frac{4}{\pi^2(1-\sigma)^2}\int d^2\eta_a d^2\eta_b \exp\left(-\frac{2\left|\zeta_a-\eta_a\right|^2}{1-\sigma} - \frac{2\left|\zeta_b-\eta_b\right|^2}{1-\sigma}\right) P(\eta_a,\eta_b). \tag{7.3}$$

7.2 Teleportation using a two-mode vacuum

Suppose that Alice at the sending station wants to teleport an unknown state to Bob at a distant receiving station via a two-mode squeezed vacuum. Two modes b and c of the squeezed state are distributed separately to the sending and receiving stations. Recall the Wigner function of the two-mode squeezed vacuum,

$$W_{qc}(\zeta_b,\zeta_c) = \frac{4}{\pi^2}\exp\left[-2\left(|\zeta_b|^2+|\zeta_c|^2\right)\cosh 2s_{qc} + 2\left(\zeta_b\zeta_c+\zeta_b^*\zeta_c^*\right)\sinh 2s_{qc}\right], \tag{7.4}$$

where s_{qc} is the degree of squeezing and the complex quadrature phase variable $\zeta_{b,c} = \zeta_{b,c}^r + i\zeta_{b,c}^i$. When $s_{qc}\to\infty$ the state (7.4) manifests the maximum entanglement and becomes an original EPR state.

At the sending station, the original unknown state of mode a is mixed with a mode b of the quantum channel by a 50/50 beam splitter. Before the action of the beam splitter, the total state is a product of the original state and the state of the quantum channel, which is represented by the total Wigner function $W_t(\zeta_a,\zeta_b,\zeta_c) = W_o(\zeta_a)W_{qc}(\zeta_b,\zeta_c)$ where $W_o(\zeta_a)$ is the Wigner function of the original state $\hat{\rho}_o$. The product state of the original field and quantum channel becomes entangled at the beam splitter. Considering the unitary action of the beam splitter, the quadrature variables $\zeta_{d,e}$ of the output fields are related to those of the input fields: $\zeta_{d,e} = (\zeta_b \pm \zeta_a)/\sqrt{2}$. The Wigner function

$W_t^B(\zeta_d, \zeta_e, \zeta_c)$ for the total field after the beam splitter is

$$W_t^B(\zeta_d, \zeta_e, \zeta_c) = W_t\left(\frac{\zeta_e + \zeta_d}{\sqrt{2}}, \frac{\zeta_e - \zeta_d}{\sqrt{2}}, \zeta_c\right) \tag{7.5}$$

which exhibits entanglement between the modes a and b.

Setting homodyne detectors at the output ports of the beam splitter, the imaginary part of ζ_d and the real part of ζ_e are simultaneously measured by appropriately choosing the phases of reference fields for the homodyne detectors. Each measurement result is transmitted to the receiving station to displace the quadrature variables of the field mode c. We have to make sure that the displacement operation is done on the photon of mode c entangled with the photon measured at the sending station. After the displacement $\Delta(\zeta_d^i, \zeta_e^r)$ the field of mode c becomes to be represented by the Wigner function $W_r(\zeta_c)$;

$$W_r(\zeta_c) = \int d^2\zeta_d \; d^2\zeta_e W_t^B(\zeta_d, \zeta_e, \zeta_c - \Delta(\zeta_d^i, \zeta_e^r)). \tag{7.6}$$

Braunstein and Kimble [32] found that the displacement of $\Delta(\zeta_d^i, \zeta_e^r) = -\sqrt{2}(\zeta_e^r - i\zeta_d^i)$ maximises the fidelity when the channel is a pure two-mode squeezed state. The probability $P(\zeta_d^i, \zeta_e^r)$ of measuring ζ_d^i and ζ_e^r at the sending station is the same as the marginal Wigner function

$$P(\zeta_d^i, \zeta_e^r) \;\; = \;\; \int d\zeta_d^r \; d\zeta_e^i d^2\zeta_c W_t^B(\zeta_d, \zeta_e, \zeta_c). \tag{7.7}$$

7.3 Two-mode squeezed vacuum in thermal environments

The quantum channel initially in the two-mode squeezed vacuum results in a mixed state by the interaction with the thermal environment. Assuming that two thermal modes are independently coupled with the quantum channel the dynamics of the squeezed field is described by a Fokker-Planck equation (4.7) studied in Chapter 4. The two thermal modes are assumed to have the same average energy and coupled with the channel in the same strength. This assumption is reasonable as the two modes of the squeezed state are in the same

frequency and the temperature of the environment is normally the same. The time-dependent Wigner function (4.10) obtained in Chapter 4 is represented as

$$W_{qc}(\zeta_b,\zeta_c;T)=\mathcal{N}\exp\left[-\frac{2\Gamma}{\Gamma^2-\Lambda^2}\left(|\zeta_b|^2+|\zeta_c|^2\right)+\frac{2\Lambda}{\Gamma^2-\Lambda^2}\left(\zeta_b\zeta_c+\zeta_b^*\zeta_c^*\right)\right] \tag{7.8}$$

where $\mathcal{N}$ is the normalisation factor and two parameters, $\Gamma=T(1+2\bar{n})+(1-T)\cosh 2s_{qc}$, $\Lambda=(1-T)\sinh 2s_{qc}$. The renormalised time $T(t)=1-\exp(-\gamma t)$. The relative strength of Λ to Γ determines how much the mixed channel is entangled. When Λ is zero for $T\to 1$, the channel loses any correlation so to have neither classical nor quantum correlation. At $T=0$ the mixed squeezed state (7.8) is simply the squeezed vacuum (7.4).

When the quantum channel is embedded in thermal environments, the teleported state is still represented by the Wigner function (7.6) with the quantum channel (7.8). However, a question remains on the unitary operation at the receiving station when the channel is a mixed state. According to the philosophy of the faithful teleportation, the displacement has to be determined to maximise the fidelity of teleportation. The fidelity $\mathcal{F}$, which measures how close the teleported state is to the original state, is the projection of the original pure state $|\Psi_o\rangle$ onto the teleported state of the density operator $\hat{\rho}_r$: $\mathcal{F}=\langle\Psi_o|\hat{\rho}_r|\Psi_o\rangle$. The fidelity is also represented by the overlap between the Wigner functions for the original and teleported states [155];

$$\mathcal{F}=\pi\int d^2\zeta W_o(\zeta)W_r(\zeta). \tag{7.9}$$

For a maximally entangled quantum channel, the original pure state is reproduced at the receiving station and the fidelity is unity. For an impure or partially entangled channel, the unitary operation at the receiving station may depend on original states to maximise the fidelity, which has been shown for the teleportation of a two-level state [156, 54]. For the infinite dimensional Hilbert space, a formal study is very much complicated. However, we have found that even when the channel is mixed, the displacement of $\Delta(\zeta_d^i,\zeta_e^r)=-\sqrt{2}(\zeta_e^r-i\zeta_d^i)$ maximises the fidelity for an initial coherent state.

7.4 Separability of the quantum channel

A discrete bipartite system of modes b and c is separable when its density operator is represented by $\hat{\rho} = \sum_r P_r \hat{\rho}_{b,r} \otimes \hat{\rho}_{c,r}$. Separability and measures of entanglement for continuous variable states has been studied [152, 157]. In particular, Duan *et al.* found a criterion to determine the separability of a two-mode Gaussian state. Lee *et al.* employed a somewhat different approach to find when a two-mode squeezed vacuum in thermal environments is separable and not quantum-mechanically entangled [154]. This analysis is described for any two-mode Gaussian state in Appendix B.

As shown in Appendix B, the mixed two-mode squeezed vacuum in the thermal environment is separable when a positive definite P function can be assigned to it. The mixed two-mode squeezed vacuum serving the quantum channel can then be written by a statistical mixture of the direct-product states;

$$\hat{\rho}_{qc} = \int d^2\xi \mathcal{P}(\xi) \hat{\rho}_b(\xi) \otimes \hat{\rho}_c(\xi) \tag{7.10}$$

where $\mathcal{P}(\xi)$ is a probability density function.

With use of Eqs. (7.3) and (7.8), we find that the mixed two-mode squeezed vacuum is separable when $n_\tau = 1$ where n_τ is defined as

$$n_\tau(\bar{n}, s_{qc}, T) \equiv \Gamma - \Lambda = (2\bar{n} + 1)\, T + (1 - T) \exp(-2s_{qc}) \tag{7.11}$$

according to the condition (B.10). This is in agreement with Duan *et al.*'s separation criterion [157]. The pure two-mode squeezed vacuum for $T = 0$, is never separable unless $s_{qc} = 0$. For the zero temperature environment, i.e., $\bar{n} = 0$, the two-mode squeezed state stays quantum-mechanically entangled at any time. For the reasons given in Sec. IV, we call n_τ as the noise factor.

If $n_\tau < 1$, the quantum channel state is entangled and the teleportation is performed at the quantum level. When $n_\tau \geq 1$, the quantum channel is no longer quantum-mechanically entangled. However the inter-mode correlation is still there as $\Lambda \neq 0$ in Eq. (7.8). Questions then arise: Does this classical correlation influence the teleportation? Can any nonclassical properties imposed in an original state be teleported by the classically-correlated channel? Braunstein

and Kimble found that when a pure two-mode squeezed state is separable, i.e., $s_{sq} = 0$, observation of any nonclassical features in the teleported state is precluded. However, when a pure state is separable there is no classical correlation either.

7.5 Transfer of nonclassical features

An imperfect replica state is reproduced at the receiving station when the quantum channel is not maximally entangled. It is well known that any linear noise-addition process, for example linear dissipation and amplification, can be described by the convolution relation of the quasiprobability functions [123]. With use of the Wigner functions for an arbitrary original state and for an impure quantum channel (7.8), we find that the equation (7.6) leads to the following convolution relation

$$W_r(\zeta) = \int d^2\xi P_\tau(\zeta - \xi) W_o(\xi) \tag{7.12}$$

where the function P_τ characterises the teleportation process;

$$P_\tau(\zeta - \xi) = \frac{1}{\pi n_\tau} \exp\left(-\frac{1}{n_\tau} |\zeta - \xi|^2\right) \tag{7.13}$$

and the noise factor n_τ, defined in Eq. (7.11), is completely determined by the characteristics of the quantum channel. The noise factor increases monotonously as the interaction time T increases. The larger the initial squeezing, the less vulnerable the quantum channel is.

The noise factor n_τ is related to the fidelity. With use of Eqs. (7.9) and (7.12) the fidelity can be written as

$$\mathcal{F} = \pi \int d^2\zeta d^2\xi W_o(\zeta) P_\tau(\zeta - \xi) W_o(\xi). \tag{7.14}$$

In the limit of $n_\tau \to 0$, the function $P_\tau(\zeta - \xi)$ in Eq. (7.13) becomes a delta function and the fidelity becomes unity. The teleportation loses the original information completely with $\mathcal{F} = 0$ in the limit of $n_\tau \to \infty$.

The properties of the nonclassical states have been calculated and illustrated by quasiprobability functions. The nonclassical features are associated especially with negative values and singularity of the quasiprobability P function [158, 159, 160]. Suppose an original state whose P function is not positive everywhere in phase space. When this state is teleported, its nonclassical features are certainly transferred to the teleported state if the teleportation is perfect. If the teleportation is poor, the teleported state may have its P function positive definite and lose the nonclassical features.

By the Fourier transform of Eq. (7.12), the convolution relation is represented in terms of the characteristic functions as

$$C_r^W(\eta) = \exp(-\bar{n}_\tau|\eta|^2)C_o^W(\eta). \tag{7.15}$$

Using the relation (7.2) between characteristic functions, Eq.(7.15) is written as

$$C_r^P(\eta) = \exp[-(n_\tau - 1)|\eta|^2]C_o^Q(\eta), \tag{7.16}$$

where $C_o^Q(\eta)$ is the characteristic function for $R_{\sigma=-1}(\zeta)$ of the original state. The P function is not semi-positive definite if its characteristic function $C_r^P(\eta)$ is not inverse-Fourier-transformable. Even when it is inverse-Fourier-transformable, there is a chance for the P function to become negative at some points of phase space. Lütkenhaus and Barnett found that only when $\sigma \leq -1$ the quasiprobability $R_\sigma(\zeta)$ for any state is semi-positive definite. We are sure that, for any original state, the left-hand side of Eq. (7.16) is inverse-Fourier transformed to a P function semi-positive definite only when $n_\tau \geq 1$. This condition is the same as the separability condition (7.11) for the quantum channel. We conclude that when a quantum channel is separable, i.e., not quantum-mechanically entangled, no nonclassical features implicit in an original state is transferred by teleportation. In other words, nonclassical features are not teleported via a classically-correlated channel.

As an example, we examine the transfer of quadrature squeezing which an unknown original state may have. The quadrature-phase operator is defined as

$$\hat{X}(\phi) = e^{-i\phi}\hat{a} + e^{i\phi}\hat{a}^\dagger \tag{7.17}$$

where $\hat{a}$ ($\hat{a}^\dagger$) is an annihilation (creation) operator and ϕ related to the angle

in phase space. A state is said to be squeezed if the quadrature-phase variance $[\Delta X(\phi)]^2 < 1$ for an angle ϕ. The expectation value of an observable for a state can be obtained by use of the characteristic function $C^P(\eta)$ for its P function [161];

$$\langle (\hat{a}^\dagger)^m \hat{a}^n \rangle = \frac{\partial^m}{\partial \eta^m} \frac{\partial^n}{\partial (-\eta^*)^n} C^P(\eta) \Big|_{\eta=\eta^*=0}. \tag{7.18}$$

Substituting Eq. (7.16) into Eq. (7.18), the mean quadrature phase $\bar{X}_r(\phi)$ and variance $[\Delta X_r(\phi)]^2$ for the teleported state can be calculated

$$\bar{X}_r(\phi) = \bar{X}_o(\phi); \quad [\Delta X_r(\phi)]^2 = [\Delta X_o(\phi)]^2 + 2n_\tau, \tag{7.19}$$

where $\bar{X}_o(\phi)$ and $[\Delta X_o(\phi)]^2$ are the mean quadrature phase and variance for the original state. It is interesting to realise that the mean quadrature phase does not change at all during teleportation. From Eq. (7.19), we can simply notice that squeezing properties cannot be teleported when $n_r \geq 1/2$; the quantum channel should be entangled enough as $n_\tau < 1/2$ to transfer squeezing properties.

A squeezed vacuum with the degree of squeezing s_o is written in the Wigner representation as

$$W_o(\zeta) = \frac{2}{\pi} \exp\left[-2\exp(2s_o)\zeta_r^2 - 2\exp(-2s_o)\zeta_i^2\right] \tag{7.20}$$

where ζ_r and ζ_i are real and imaginary parts of ζ. Its teleported state is represented by the Wigner function

$$W_r(\zeta) = \frac{2}{\pi\sqrt{A(s_o)A(-s_o)}} \exp\left[-\frac{2}{A(s_o)}\zeta_r^2 - \frac{2}{A(-s_o)}\zeta_i^2\right] \tag{7.21}$$

where the parameter $A(s_o) = 2n_\tau + \exp(-2s_o)$. The fidelity is given by

$$\mathcal{F}(s_o) = \left(n_\tau^2 + 2n_\tau \cosh 2s_o + 1\right)^{-1/2}. \tag{7.22}$$

When the teleportation is classical with $n_\tau = 1$, $\mathcal{F}(s_o) = (2 + 2\cosh 2s_o)^{-1/2}$.

7.6 Remarks

Quantum teleportation can be made more reliable by sophisticated schemes such as purification of the impure or partially entangled quantum channel [152, 162], detection with perfect efficiency, and well-defined unitary operation. However, in the real world, the influence of noise cannot easily be disregarded. We have been interested in the influence of noise on the transfer of nonclassicalities which may be imposed in an original unknown state. To make the problem simple while honouring the real experimental situation, we assumed that the same amount of noise affects the two modes of the quantum channel. We found that when the quantum channel is separable the transfer of any nonclassicality is impossible: Nonclassical features can not be teleported via a classically-correlated channel. The separability of a two-mode Gaussian state is considered using the possibility of assigning a positive well-defined P function to the state after some local unitary operations. As an example, we have analysed the transfer of the squeezing property.

Chapter 8

Quantum Computation using Coherent States

The theory of quantum computation promises to revolutionise the future of computer technology with merits in factoring large integers [4] and combinational searches [5]. In recent years, the physical implementation of a quantum computer has been intensively studied. Quantum computing using optical systems has been studied as one of several plausible models. Recently, it was found that universal quantum computation may be realised only with single photon sources, single photon detectors and simple linear optical elements without nonlinear interactions [27]. While this result is extremely striking, it has some obstacles such as inefficiency of the single photon source and photo-detection to its experimental realisation. Another problem is that the optical networks are too complex to realise near-deterministic scalable quantum computation.

A coherent field is a fundamental tool in quantum optics and linear superposition of two coherent states is considered one of the realisable mesoscopic quantum systems [71]. In particular, Cochrane *et al.* [116] showed how logical qubits can be implemented using even and odd coherent superposition states which are defined as $|\alpha\rangle \pm |-\alpha\rangle$ with $|\alpha\rangle$ and $|-\alpha\rangle$ representing coherent states of π phase difference. The two superposition states form orthogonal bases in two-dimensional Hilbert space and they can be discriminated by photon number measurement. There were some proposals to entangle such logical qubits with atomic states [163]. One drawback of using even and odd cat states as a logical qubit basis for quantum computation is that they are extremely sensitive to

photon loss and detection inefficiency as was explained in Chapter 2.

In this Chapter, we present a method to implement universal quantum computation using coherent states. This proposal makes it possible to realise universal quantum computation based on quantum teleportation [7] which was shown to be a useful tool in controlled gate operation [164]. It is also found that this scheme may be robust to detection inefficiency.

8.1 Quantum computer

To begin this Chapter, let us try to briefly answer the following basic questions: First, what is a quantum computer? Second, how is quantum computation performed? Third, why do we need a quantum computer or what are advantages of quantum computation compared with classical computation? Fourth, how can we implement a physical quantum computer?

A quantum computer is a collection of l qubit systems [165], which can be represented as

$$|\psi_{QC}\rangle = \sum_{x=0}^{2^l-1} c_x|x\rangle, \tag{8.1}$$

where $|x\rangle$ denotes a direct product state of l basis states (each of those is $|0_L\rangle$ or $|1_L\rangle$) and the normalisation condition is $\sum_x |c_x|^2 = 1$. To perform quantum computation, a quantum computer makes a sequence of unitary operations. Each of the unitary operations, called a quantum gate, is applied to a qubit or to more than one qubit in a combined way. After a computation process, all the qubits are finally measured for a readout and the measurement result will produce a set of l binary numbers.

If any computation can be performed by a set of gates, the set is called universal. For example, the NAND gate is a universal gate in classical computation. Classical computation is based upon Boolean logic, where NAND and NOT gates are basic gates used to construct various circuits for any computation. For quantum computation, the C-NOT gate and 1-bit unitary gate are a well known universal set of quantum gates [166]. There are universal

quantum gates which satisfy universality by themselves as a single gate[1]. The NAND gate, which is a basic gate in classical computation, is an irreversible gate because the amount of output information is less than the input information. The irreversible characteristic of computation means that a computer always dissipates some amount of heat during a computation process and it can be a nontrivial obstacle to building a computer on a small scale [167]. On the contrary, quantum gates are in definition reversible because they are unitary transformations of which unique inverse unitary transformations always exist. In fact, one may in theory have reversibility (quantum or classical) of gate operations without losing information during computational process. Irreversibility results from erasure [167] and it is at re-setting where irreversibility comes in.

In classical computation, parallel processing is a strong solution to decrease the time required for a certain computation. Parallel computing enables the linear decrease of the computation time by the increase of the number of processors, *i.e.*, the increase of the size of the physical system. In quantum computing, one can gain an exponential increase of the amount of parallelism under the same condition: There is a possibility for an exponential decrease of the computation time by a linear increase of the size of the physical system.

Suppose a function $f(y)$

$$f : (0, 1, \cdots, 2^{m-1}) \rightarrow (0, 1, \cdots, 2^{n-1}), \tag{8.2}$$

where n and m are positive integers. It is possible to construct a quantum circuit performing the following unitary transformation U_f:

$$U_f|y\rangle_a|0\rangle_b = |y\rangle_a|f(y)\rangle_b, \tag{8.3}$$

where the register a keeps the input value while the result $f(y)$ is in the register b. Here, it is indispensable to use both the registers, a and b, to ensure the reversibility of quantum computation. If we use a single register such as $U_f|y\rangle = |f(y)\rangle$, the final state may lose some information about the input state in case y and $f(y)$ do not have one-to-one correspondence: Such a process does not

[1]It has been found that many of 2-qubit quantum gates are universal [168].

correspond to a quantum unitary transformation. If a superposed state,

$$\frac{1}{2^{m/2}} \sum_{y=0}^{2^{m-1}} |y\rangle, \tag{8.4}$$

is given for the input state instead of $|y\rangle$ in Eq. (8.3), the final state becomes

$$U_f\Big(\frac{1}{2^{m/2}} \sum_{y=0}^{2^{m-1}} |y\rangle\Big)|0\rangle = \frac{1}{2^{m/2}} \sum_{y=0}^{2^{m-1}} |y\rangle|f(y)\rangle. \tag{8.5}$$

Note that the state (8.5) contains information about $f(0)$ to $f(2^{m-1})$. This means a quantum computer computes $f(y)$ for more than two input values by a single process. It is obvious that the total number of qubits including both registers a and b is $2m$ and such a quantum system can compute $f(y)$ for 2^m input values by the single process U_f: We gain the exponential increase of parallelism by linear increase of the physical system. This characteristic, called quantum parallelism, is a fundamental feature of many quantum algorithms.

However, quantum parallelism is not directly applicable to a faster computation. The final stage of quantum computation to measure each qubit will reduce the quantum state (8.5) to one of $|y\rangle|f(y)\rangle$'s and only one of the many results will remain. It is a separate problem to find out useful algorithms which make use of quantum parallelism. Deutsch presented a simple problem showing how quantum computation can outperform classical computation in testing whether a function $f : (0, 1) \to (0, 1)$ is constant or balanced [169]. Deutsch and Josza generalised this algorithm to a general n-qubit case [170]. Shor's polynomial time algorithms for factorisation and computation of discrete logarithms are the most important algorithms showing the power of quantum computing [4]. Grover discovered a fast quantum algorithm for a search problem, which is also a significant breakthrough [5].

To physically realise a quantum computer, there are a few major requirements. First, one should decide a physical system for qubit encoding. This system should be initialisable, scalable, and measurable with universal gate operations. An efficient error correcting scheme should exist to overcome decoherence and imperfect operations. DiVincenzo discussed 'five plus two' basic requirements for the physical implementation of quantum computation with the

following subtitles [171]: (1) A scalable physical system with well characterised qubits, (2) the ability to initialise the state of the qubits to a simple fiducial state, (3) the relevant decoherence time much longer than the gate operation time, (4) universal set of quantum gates, (5) a qubit specific measurement capability, (6) the ability to inter-convert stationary and flying qubits, and (7) the ability to faithfully transmit flying qubits between specified locations.

There have been various approaches for implementation of quantum computation including nuclear magnetic resonance (NMR) [172], ion trap [173], neutral atom [174], optical [175, 27] and solid state [176] quantum computers. Each of them has its own strengths as well as limitations according to DiVincenzo's criteria. The optical approach is one of the strongest candidates for the physical implementation of a quantum computer with some remarkable advantages [26]. It is relatively easy to observe quantum interference in optical systems and coherence time is generally much longer than operation time. Most of the operations can be done at room temperature. The requirement of nonlinearity has been pointed out as an obstacle to realise an optical quantum computer. Unfortunately, nonlinear effects in existing materials, required for the indispensable photon-photon coupling, are extremely small. The Giant Kerr effect has been observed in some experiments reporting light speed reduction [177]. It has been found by Knill *et al.* that requirement of nonlinearity can be circumvented by a probabilistic way [27]. Linear optics quantum computing is a scheme using linear optical devices, a single photon source and photodetectors [27, 178]. Knill *et al.* employed dual rail logic in which a qubit is represented by a single photon occupation of one mode of a pair of optical modes [27]. Even though the linear optics quantum computation is basically a probabilistic scheme, it is possible to build a near-deterministic scheme by successive applications of conditional measurements [27]. In this case, the increase of resources and complexity of circuits are a heavy cost to be paid for a higher success probability. The inefficiency of the single photon source and detection inefficiency are other serious problems. Recently, there have been some remarkable advances in single photon generating and efficient photodetecting. Single photon detectors with efficiency of $\sim 90\%$ have been demonstrated [89]. There have been experimental reports for the generation of single photons using single quantum dots [179] and single atoms in a cavity [180]. However, their efficiency is still not satisfactory, only $\sim 8\%$.

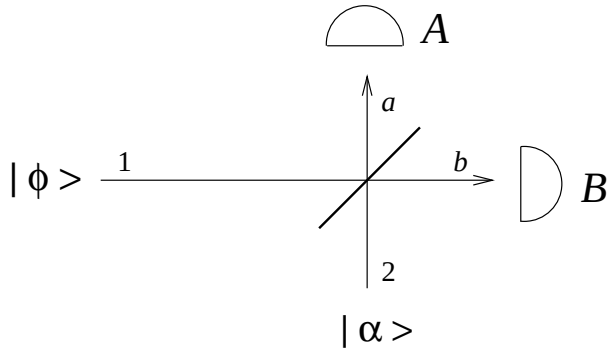

Figure 8.1: Measurement scheme for $|\phi\rangle_1 = \mathcal{A}|\alpha\rangle_1 + \mathcal{B}|-\alpha\rangle_1$ with a 50-50 beam splitter and auxiliary state $|\alpha\rangle_2$. If detector A registers any photon(s) while detector B does not, the measurement outcome is $|\alpha\rangle$, i.e. $|0_L\rangle$. On the contrary, A does not click while B does, the measurement outcome is $|-\alpha\rangle$, i.e. $|1_L\rangle$.

8.2 Readout scheme and universal gate operations for coherent state qubits

Let us consider the readout of a coherent state qubit, which was defined in Chapter 2,

$$|\phi\rangle = \mathcal{A}|\alpha\rangle + \mathcal{B}|-\alpha\rangle, \tag{8.6}$$

where $|\alpha\rangle$ and $|-\alpha\rangle$ form a logical qubit basis. The basis states, $|\alpha\rangle$ and $|-\alpha\rangle$, can be discriminated by a simple measurement scheme with a 50-50 beam splitter, an auxiliary coherent field of amplitude α and two photodetectors as shown in Fig. 8.1. At the beam splitter, the input state $|\phi\rangle_1$ is superposed with the auxiliary state $|\alpha\rangle_2$ and gives the output

$$|\phi_R\rangle_{ab} = \mathcal{A}|\sqrt{2}\alpha\rangle_a|0\rangle_b + \mathcal{B}|0\rangle_a|-\sqrt{2}\alpha\rangle_b. \tag{8.7}$$

If detector A registers any photon(s) while detector B does not, we know that $|\alpha\rangle$ was measured. On the contrary, if A does not click while B does, the measurement outcome was $|-\alpha\rangle$. Even though there is non-zero probability of failure $P_f(\phi_R) = |\langle 00|\phi_R\rangle|^2 = |\mathcal{A}+\mathcal{B}|^2 e^{-2\alpha^2}$ in which both of the detectors do not register a photon, the failure is known from the result whenever it occurs, and P_f approaches to zero exponentially as α increases.

An arbitrary 1-bit rotation and a controlled-NOT (CNOT) gate for two-

qubit states form a set which satisfies all the requirements for a universal gate operation. For any SU(2) unitary operation, there is a unique rotation $R(\theta, \phi, \eta)$ around the x, y and z axes. Cochrane *et al.* showed that the rotation around x axis for even and odd coherent superposition states can be realised using a interaction Hamiltonian $H_D = \hbar(\beta a^\dagger + \beta^* a)$, where β is the complex amplitude of the classical driving force [116]. The evolution by this Hamiltonian corresponds to the displacement operator, $D(\delta) = \exp(\delta a^\dagger - \delta^* a)$, where a and $a^\dagger$ are respectively annihilation and creation operators. In a similar way, z-rotation

$$U_z(\theta/2) = \begin{pmatrix} e^{i\theta/2} & 0 \\ 0 & e^{-i\theta/2} \end{pmatrix} \tag{8.8}$$

for a logical qubit $|\phi\rangle$ can be obtained. A coherent state is a displaced vacuum $|\alpha\rangle = D(\alpha)|0\rangle$. We know that two displacement operators $D(\alpha)$ and $D(\delta)$ do not commute but the product $D(\alpha)D(\delta)$ is simply $D(\alpha + \delta)$ multiplied by a phase factor, $\exp[(\alpha\delta^* - \alpha^*\delta)/2]$. This phase factor plays a role to rotate the logical qubit. The action of displacement operator $D(i\epsilon)$, where ϵ ($\ll 1$) is real, on the qubit $|\phi\rangle$ is the same as z-rotation of the qubit by $U_z(2\alpha\epsilon)$. We can easily check their similarity by calculating the fidelity:

$$\begin{aligned} |\langle\phi|U_z^\dagger(2\alpha\epsilon)D(i\epsilon)|\phi\rangle|^2 &= e^{-\epsilon^2}\left\{|\mathcal{A}|^2 + |\mathcal{B}|^2 + e^{-2\alpha^2}(\mathcal{A}\mathcal{B}^* e^{-2i\alpha\epsilon} + \mathcal{A}^*\mathcal{B}e^{2i\alpha\epsilon})\right\}^2 \\ &\approx \exp[-\epsilon^2] \approx 1. \end{aligned} \tag{8.9}$$

Thus the rotation angle θ depends on α and ϵ: $\theta = 4\alpha\epsilon$. A small amount of ϵ suffices to make one cycle of rotation as α is relatively large. The displacement operation $D(i\epsilon)$ can be effectively performed using a beam splitter with the transmission coefficient T close to unity and a high-intensity coherent field of amplitude $i\mathcal{E}$, where $\mathcal{E}$ is real, as shown in Fig. 8.2(a). It is known that the effect of the beam splitter is described by $D(i\mathcal{E}\sqrt{1-T})$ in the limit of $T \to 1$ and $\mathcal{E} \gg 1$. (More rigorously the output state becomes mixed but in the limit it can well be approximated to a pure state as shown in [129].)

To achieve any arbitrary 1-bit rotation, we need to operate $U_x(\pi/4)$ and $U_x(-\pi/4)$ which are rotations by $\pi/2$ and $-\pi/2$, respectively, around the x axis. We find that $U_x(\pi/4)$ can be realised using a nonlinear medium. Even though the efficiency of nonlinear interaction can be a problem, there was an experimental report of a successful measurement of giant Kerr nonlinearity [177].

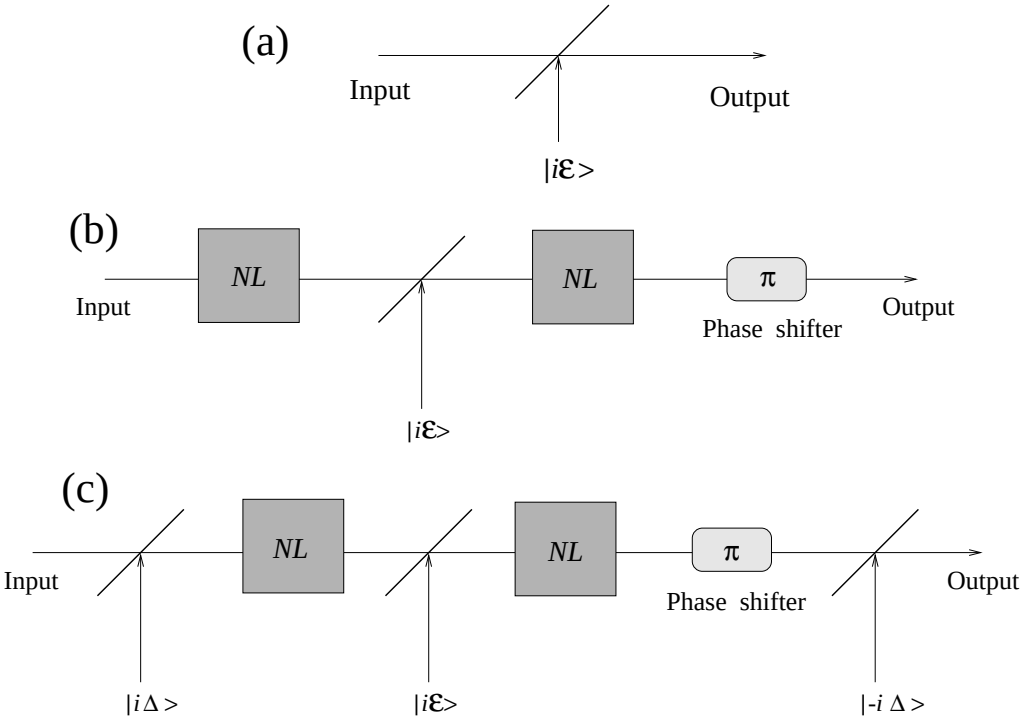

Figure 8.2: 1-bit rotation around the z (a), y (b), and x axes (c) for a qubit state of coherent fields. NL represents a nonlinear medium. The transmission coefficient T of the beam splitters is assumed to be close to unity. $\mathcal{E}$ corresponds to $\frac{\theta}{4\alpha\sqrt{1-T}}$, where θ is the required degree for a rotation and α is the coherent amplitude of the qubit state $|\phi\rangle$. $\Delta = \frac{\pi}{8\alpha\sqrt{1-T}}$. Starting from a coherent state, an arbitrary qubit can be prepared up to a global phase using the above operations.

The anharmonic-oscillator Hamiltonian of an amplitude-dispersive medium is [71]

$$\mathcal{H}_{NL} = \omega a^\dagger a + \lambda (a^\dagger a)^2, \tag{8.10}$$

where ω is the frequency of the coherent field and λ is the strength of the anharmonic term. When the interaction time t in the medium is π/λ, coherent states $|\alpha\rangle$ and $|-\alpha\rangle$ evolve as follows:

$$|\alpha\rangle \longrightarrow \frac{e^{-i\pi/4}}{\sqrt{2}}(|\alpha\rangle + i|-\alpha\rangle)\ ; \quad |-\alpha\rangle \longrightarrow \frac{e^{-i\pi/4}}{\sqrt{2}}(i|\alpha\rangle + |-\alpha\rangle), \tag{8.11}$$

which corresponds to $U_x(\pi/4)$ up to a global phase shift. The other rotation $U_x(-\pi/4)$ can be realised by applying a phase shifter $P(\pi)$, which acts $|\alpha\rangle \leftrightarrow |-\alpha\rangle$, after or before $U_x(\pi/4)$ operation. Note that $P(\pi)$ corresponds to π-rotation around the x axis, *i.e.* a 1-bit NOT gate. The other two required

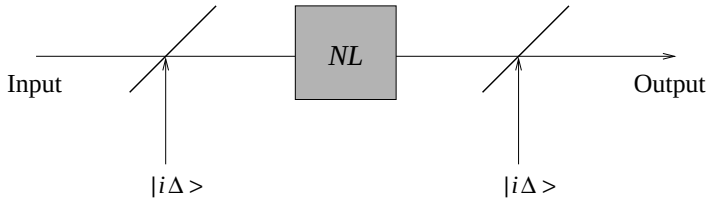

Figure 8.3: Hadamard gate for a qubit state $|\phi\rangle = \mathcal{A}|\alpha\rangle + \mathcal{B}|-\alpha\rangle$. The coherent field amplitude $i\Delta$ is $i\frac{\pi}{8\alpha\sqrt{1-T}}$ and the transmission coefficient T of the beam splitters is close to unity. The irrelevant global phase is neglected.

unitary operations $U_y(\phi/2)$ and $U_z(\eta/2)$ which correspond to rotations around the y and x axes can be realised using the following identities [181]

$$U_y(\phi/2) = U_x(-\pi/4)U_z(\phi/2)U_x(\pi/4)\ ;\quad U_x(\eta/2) = U_z(-\pi/4)U_y(\eta/2)U_z(\pi/4). \tag{8.12}$$

Therefore, any 1-bit rotation can be performed up to a global phase with beam splitters, nonlinear media, phase shifters and auxiliary coherent light fields as shown in Fig. 8.2. As an example, we can construct the Hadamard gate H as

$$H = -U_z(\pi/4)U_x(\pi/4)U_z(\pi/4), \tag{8.13}$$

which is shown in Fig 8.3. Using these operations, any 1-qubit state $|\phi\rangle = \mathcal{A}|\alpha\rangle + \mathcal{B}|-\alpha\rangle$ with arbitrary $\mathcal{A}$ and $\mathcal{B}$ can be prepared up to a global phase from a coherent state.

For a universal gate operation, a CNOT gate is required besides 1-bit rotation. It was found that the CNOT operation can be realised using a teleportation protocol [164]. For a superposition of coherent states, quantum teleportation protocols have been suggested by utilising an entangled coherent state [73, 75] including an entanglement purification scheme [75]. However, the success probability of this teleportation scheme is limited to less than 1/2 in practise and the required photon parity measurement is very sensitive to detection inefficiency and photon loss as the parity alternates by missing one photon. We suggest a teleportation protocol as follows to circumvent those problems.

For any ideal teleportation scheme, a maximally entangled pair, Bell measurement and unitary operations are required [7]. In our case, necessary unitary operations σ_x and σ_z correspond to a phase shift $P(\pi)$ and dis-

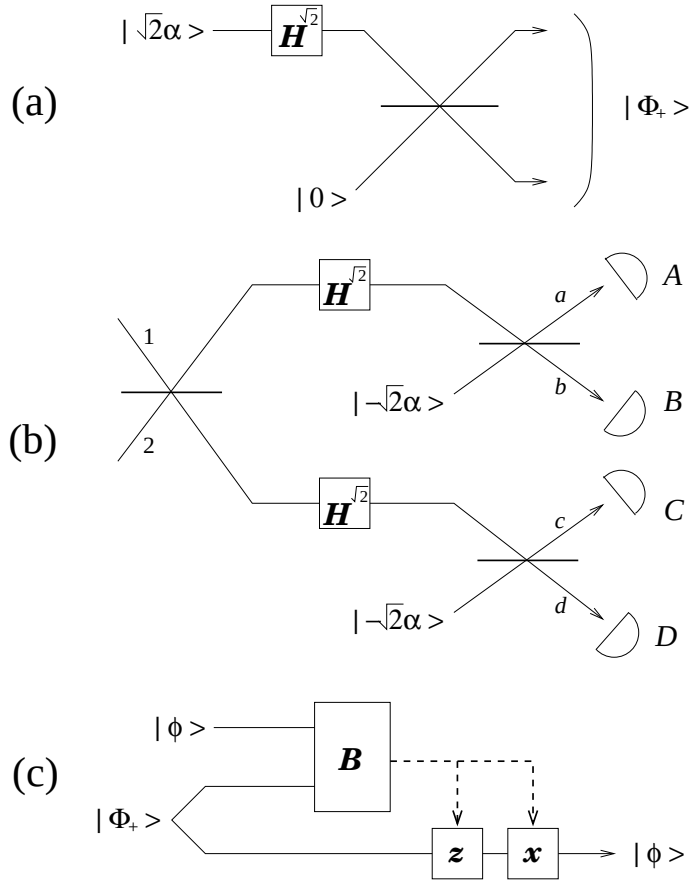

Figure 8.4: Teleportation process for an unknown state $|\phi\rangle = \mathcal{A}|\alpha\rangle + \mathcal{B}|-\alpha\rangle$. $H^{\sqrt{2}}$ represent the Hadamard gate with an incident qubit state of coherent amplitudes $\pm\sqrt{2}\alpha$. B represents the Bell measurement. x and z represent π rotation around the x and z axes. (a) Generation of the quantum channel $|\Phi_+\rangle$. (b) Bell-state measurement with arbitrarily high precision. If detector A does not click, the measurement outcome is $|\Phi_+\rangle$, and so on. Only one of the four detectors does not detect any photon at a measurement event for $\alpha \gg 1$. (c) Scheme to teleport $|\phi\rangle$ via the entangled quantum channel $|\Phi_+\rangle$. The Pauli operations represented by x and z are performed according to the result of Bell measurement B.

placement operation $D(\frac{i\pi}{4\alpha\sqrt{1-T}})$ respectively. An entangled coherent channel $|\Phi_+\rangle = \mathcal{N}_+(|\alpha\rangle|\alpha\rangle + |-\alpha\rangle|-\alpha\rangle)$, where $\mathcal{N}_+$ is a normalisation factor, can be generated from a coherent state passing through a $H^{\sqrt{2}}$ gate and a 50-50 beam splitter as shown in Fig. 8.4(a). The subscript $\sqrt{2}$ in $H^{\sqrt{2}}$ stands for the amplitude of the incident field being $\sqrt{2}\alpha$. Note that the coherent amplitude $i\Delta$ for a unitary operation shown in Fig. 8.3 should be $i\pi/[8\alpha\sqrt{2(1-T)}]$ for the $H^{\sqrt{2}}$-gate operation. The Bell measurement shown in Fig. 8.4(b) is to distinguish

four quasi-Bell states [79],

$$|\Phi_\pm\rangle = \mathcal{N}_\pm(|\alpha,\alpha\rangle \pm |-\alpha,-\alpha\rangle), \tag{8.14}$$

$$|\Psi_\pm\rangle = \mathcal{N}_\pm(|\alpha,-\alpha\rangle \pm |-\alpha,\alpha\rangle), \tag{8.15}$$

where $|\pm\alpha,\pm\alpha\rangle = |\pm\alpha\rangle \otimes |\pm\alpha\rangle$ and $\mathcal{N}_\pm$ are normalisation factors for α as large as 3. Note that the quasi-Bell states become maximally entangled Bell states when $\alpha \gg 1$. If the incident field to the first beam splitter in Fig. 8.4 (b) is $|\Phi_+\rangle_{12}$, it becomes $|0, 2\alpha, -\sqrt{2}\alpha, \sqrt{2}\alpha\rangle_{abcd}$ at detectors A, B, C, and D. If detector A does not click while the others do, the measurement outcome is $|\Phi_+\rangle_{12}$. Likewise, only B does not click for the measurement outcome $|\Phi_-\rangle_{12}$, C for $|\Psi_+\rangle_{12}$, and D for $|\Psi_-\rangle_{12}$. The failure probability for which no photon is detected at more than one detector, which is due to the non-zero probability of $\langle 0|\pm 2\alpha\rangle$ and $\langle 0|\pm\sqrt{2}\alpha\rangle$, approaches to zero rapidly as α increases, and, moreover, the failure is always known when it occurs. The scheme to teleport $|\phi\rangle$ via the entangled channel $|\Phi_+\rangle$ is summarised in Fig. 8.4(c). When the Bell measurement outcome is $|\Phi_+\rangle$, the output state does not need any operation. When the Bell measurement outcomes is $|\Phi_-\rangle$ or $|\Psi_+\rangle$, σ_z or σ_x is required respectively. The unitary operations σ_z and σ_x should be successively applied for the outcome $|\Psi_-\rangle$.

Gottesman and Chuang showed that the teleportation protocol can be used to construct a CNOT gate [164]. To apply their suggestion in our scheme, we need to use two three-mode entangled states represented by

$$|\xi\rangle = \mathcal{N}\Big(|\sqrt{2}\alpha,\alpha,\alpha\rangle + |-\sqrt{2}\alpha,-\alpha,-\alpha\rangle\Big) \tag{8.16}$$

and the quantum teleportation protocol we just developed, where $\mathcal{N}$ is a normalisation factor. The entangled state $|\xi\rangle$ can be generated by passing a coherent field $|2\alpha\rangle$ through a H^2-gate, which is a Hadamard gate for a qubit with logical bases $|\pm 2\alpha\rangle$, and two 50-50 beam splitters as shown in Fig. 8.5(a). After generating $|\xi\rangle_{abc}$ and $|\xi\rangle_{def}$, Hadamard operations are applied to $|\xi\rangle_{def}$ as shown in

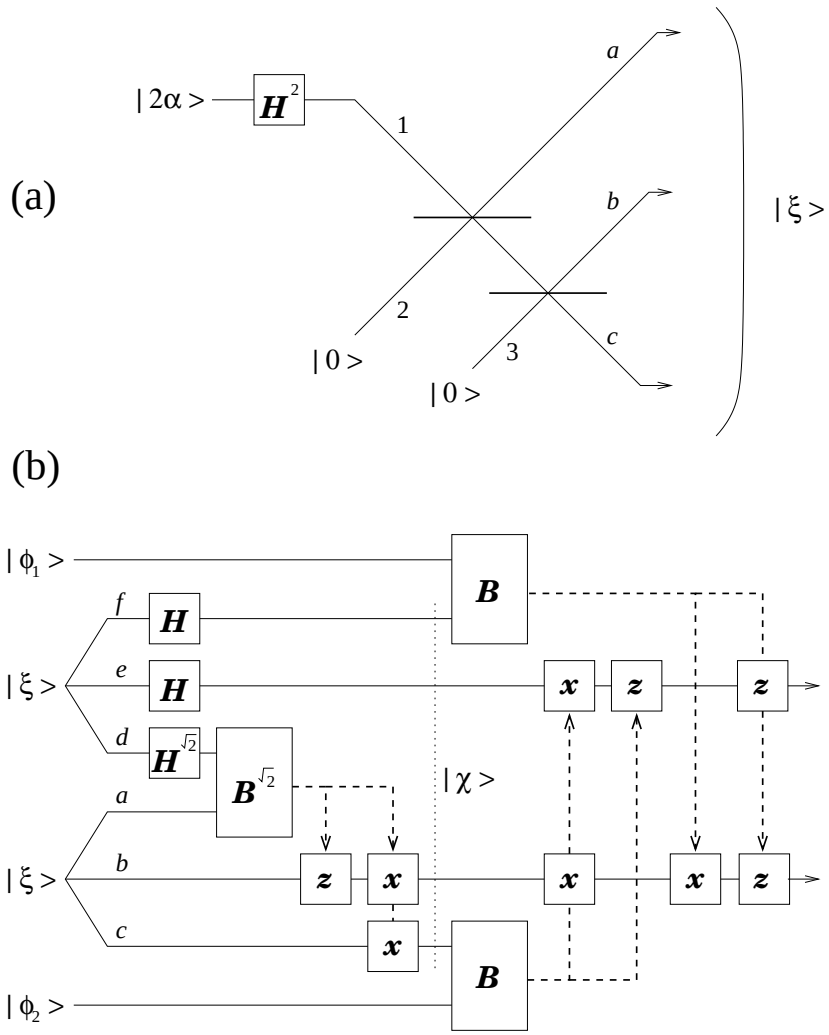

Figure 8.5: CNOT operation using teleportation protocol and three-mode entanglement. (a) Generation of a three-mode entangled state $|\xi\rangle = \mathcal{N}(|\sqrt{2}\alpha, \alpha, \alpha\rangle + |-\sqrt{2}\alpha, -\alpha, -\alpha\rangle$ with beam splitters. H^2-gate is the Hadamard gate with an incident qubit state of amplitudes $\pm 2\alpha$. (b) CNOT operation with the use of the coherent field $|\xi\rangle$ and the teleportation protocol. A four-mode entangled state $|\chi\rangle$ is generated for the operation at the left-hand side of the circuit. $|\phi_1\rangle$ is the target bit and $|\phi_2\rangle$ is the control bit here.

Fig. 8.5(a). This makes the given state $|\xi\rangle_{abc} \otimes |\xi\rangle_{def}$ to be

$$\begin{aligned}
\longrightarrow\ & |\Phi'_+\rangle_{ad}\Big\{|\alpha,\alpha\rangle\big(|\alpha,\alpha\rangle + |-\alpha,-\alpha\rangle\big) + |-\alpha,-\alpha\rangle\big(|\alpha,-\alpha\rangle + |-\alpha,\alpha\rangle\big)\Big\}_{bcef} \\
& + |\Phi'_-\rangle_{ad}\Big\{|\alpha,\alpha\rangle\big(|\alpha,\alpha\rangle + |-\alpha,-\alpha\rangle\big) - |-\alpha,-\alpha\rangle\big(|\alpha,-\alpha\rangle + |-\alpha,\alpha\rangle\big)\Big\}_{bcef} \\
& + |\Psi'_+\rangle_{ad}\Big\{|-\alpha,-\alpha\rangle\big(|\alpha,\alpha\rangle + |-\alpha,-\alpha\rangle\big) + |\alpha,\alpha\rangle\big(|\alpha,-\alpha\rangle + |-\alpha,\alpha\rangle\big)\Big\}_{bcef} \\
& + |\Psi'_-\rangle_{ad}\Big\{|-\alpha,-\alpha\rangle\big(|\alpha,\alpha\rangle + |-\alpha,-\alpha\rangle\big) - |\alpha,\alpha\rangle\big(|\alpha,-\alpha\rangle + |-\alpha,\alpha\rangle\big)\Big\}_{bcef},
\end{aligned} \tag{8.17}$$

where $|\Phi'_\pm\rangle$ and $|\Phi'_\pm\rangle$ are quasi-Bell states with the coherent amplitude $\pm\sqrt{2}\alpha$ and the normalisation factor is omitted. The Bell measurement $B^{\sqrt{2}}$ in the figure, must be performed on modes a and d. It can be easily shown from Eq. (8.17) that a four-mode entangled state

$$|\chi\rangle_{bcef} = \mathcal{N}'\Big[|\alpha,\alpha\rangle\big(|\alpha,\alpha\rangle + |-\alpha,-\alpha\rangle\big) + |-\alpha,-\alpha\rangle\big(|\alpha,-\alpha\rangle + |-\alpha,\alpha\rangle\big)\Big], \tag{8.18}$$

where $\mathcal{N}'$ is a normalisation factor, is generated after the appropriate unitary operation according to the Bell measurement result as shown in Fig. 8.5(b). The entangled state $|\chi\rangle_{bcef}$ is used to complete the CNOT gate on the right-hand side of the circuit in Fig. 8.5(b), which can be verified by a little algebra [164].

8.3 Estimation of possible errors

We have shown that universal quantum computation using coherent states can be realised even with limited detection efficiency. We already pointed out that the failure probability for the measurement which is of the order of $|\langle\sqrt{2}\alpha|0\rangle|^2$ is not only very small for a reasonably large α but also the failure is known whenever it occurs. If the detection efficiency of a photodetector is d, the failure probability P_f^d of the detector not to resister any photon, while the incident field is $|\phi_R\rangle_{ab}$ in Eq. (8.7), is

$$P_f^d = \sum_{n,m=0}^{\infty} |{}_a\langle n|{}_b\langle m|\phi_R\rangle_{ab}|^2 (1-d)^n (1-d)^m \approx \sum_{n=0}^{\infty} |\langle n|\sqrt{2}\alpha\rangle|^2 (1-d)^n, \tag{8.19}$$

where approximation (2.21) is used. For example, suppose that $\alpha = 3$ and the detection efficiency of the detectors is 90% which is a reasonable value for an avalanched photodetector [89], the failure probability P_f^d that the detector misses all the photons is $P_f^d \approx 9 \times 10^{-8}$.

If the effect of ϵ for the displacement operator is not negligible, a qubit state $|\phi'\rangle_1 = D(i\epsilon_1)\cdots D(i\epsilon_N)|\phi\rangle_1$ after N displacement operations may be

$$|\phi'\rangle_1 = \mathcal{A}'\Big|\alpha + i\sum_{n=1}^{N}\epsilon_n\Big\rangle_1 + \mathcal{B}'\Big| - \alpha + i\sum_{n=1}^{N}\epsilon_n\Big\rangle_b. \tag{8.20}$$

After passing a 50-50 beam splitter with an auxiliary state $|\alpha\rangle_2$ as shown in Fig. 8.1, the state $|\phi'\rangle_1$ becomes

$$|\phi'_R\rangle_{ab} = \mathcal{A}'\Big|\sqrt{2}\alpha+\frac{i}{\sqrt{2}}\sum_{n=1}^{N}\epsilon_n\Big\rangle_a\Big|\frac{i}{\sqrt{2}}\sum_{n=1}^{N}\epsilon_n\Big\rangle_b+\mathcal{B}'\Big|\frac{i}{\sqrt{2}}\sum_{n=1}^{N}\epsilon_n\Big\rangle_a\Big|-\sqrt{2}\alpha+\frac{i}{\sqrt{2}}\sum_{n=1}^{N}\epsilon_n\Big\rangle_b. \tag{8.21}$$

In this condition, there is non-zero probability $\widetilde{P}_f^d$ in principle for undetected errors in which detector $A(B)$ detects any photon and $B(A)$ does not while the incident state $|\phi'\rangle_1$ was $|1_L\rangle$ ($|0_L\rangle$) (see Fig. 8.1). For the worst case, all ϵ_n's may have the same sign with a large N. One useful trick to overcome this problem is to flip the sign of ϵ_n appropriately for each operation, noting that the rotation $R_z(\theta)$ can be performed both by positive and negative θ. By this way, we can keep $\sum_{n=1}^{N}\epsilon_n \sim \bar{\epsilon} = \pi/4\alpha$, regardless of N, then Eq. (8.21) can be represented as

$$|\phi'_R\rangle_{ab} = \mathcal{A}'\Big|\sqrt{2}\alpha + \frac{i\bar{\epsilon}}{\sqrt{2}}\Big\rangle_a\Big|\frac{i\bar{\epsilon}}{\sqrt{2}}\Big\rangle_b + \mathcal{B}'\Big|\frac{i\bar{\epsilon}}{\sqrt{2}}\Big\rangle_a\Big| - \sqrt{2}\alpha + \frac{i\bar{\epsilon}}{\sqrt{2}}\Big\rangle_b. \tag{8.22}$$

In this condition, the fidelity between the final state (8.20) and the ideal output is of oder $e^{-\epsilon^2}$ from Eq. (8.9). The fidelity of ≈ 0.93 is then obtained for $\alpha = 3$.

Differently from P_f^d, the undetected error probability $\widetilde{P}_f^d$ is a probability of making an error without being recognised. Considering the accumulated error as in Eq. (8.22), in order to minimise the undetected error $\widetilde{P}_f^d$ while keeping P_f^d low, we need to modify the criterion to discriminate $|\pm\sqrt{2}\alpha + i\bar{\epsilon}/\sqrt{2}\rangle$ and $|i\bar{\epsilon}/\sqrt{2}\rangle$. Ideally we took $\bar{\epsilon} = 0$ and discriminated the two states by detection of any photons and no photon. In this case, the probability of $|\pm\sqrt{2}\alpha + i\bar{\epsilon}/\sqrt{2}\rangle$

registering no photon is

$$p_A = \sum_{n=0}^{\infty} |\langle n| \pm \sqrt{2}\alpha + i\bar{\epsilon}/\sqrt{2}\rangle|^2 (1-d)^n \tag{8.23}$$

and the probability of the state $|i\bar{\epsilon}/\sqrt{2}\rangle$ registering one or more photons is

$$p_B = \sum_{m=1}^{\infty}\sum_{n=m}^{\infty} |\langle n|i\bar{\epsilon}/\sqrt{2}\rangle|^2 {}_nC_m d^m (1-d)^{n-m} \tag{8.24}$$

where ${}_nC_m = n!/m!(n-m)!$. Both p_A and p_B approach to zero as α increases. We then obtain undetected error probability $\widetilde{P}_f^d = p_A \times p_B$. On the other hand, the success probability P_s is the probability in that $|i\bar{\epsilon}/\sqrt{2}\rangle$ yields no photon and $|\pm\sqrt{2}\alpha + i\bar{\epsilon}/\sqrt{2}\rangle$ yields any photon(s) is

$$P_s = \sum_{n=0}^{\infty} |\langle n|i\epsilon/\sqrt{2}\rangle|^2 (1-d)^n \times \sum_{m=1}^{\infty}\sum_{n=m}^{\infty} |\langle n|\sqrt{2}\alpha + i\bar{\epsilon}/\sqrt{2}\rangle|^2 {}_nC_m d^m (1-d)^{n-m}. \tag{8.25}$$

The detected error probability is $P_f^d = 1 - P_s - \widetilde{P}_f^d$. Suppose that $\alpha = 3$ ($\bar{\epsilon}$ is then ≈ 0.26), and the detection efficiency is again 90% then, $p_A \approx 9 \times 10^{-8}$ and $p_B \approx 0.030$ are obtained. If we keep the criterion for the ideal case, we find $\widetilde{P}_f^d \approx 3 \times 10^{-9}$ and $P_f^d \approx 0.030$. However, if we take the registration of 0,1 and 2 photons as the measurement of $|i\bar{\epsilon}/\sqrt{2}\rangle$ then p_A, p_B and P_s should be re-defined as follows:

$$\begin{aligned} p_A = {} & \sum_{n=0}^{\infty} |\langle n|\sqrt{2}\alpha + i\bar{\epsilon}/\sqrt{2}\rangle|^2 (1-d)^n + \sum_{n=1}^{\infty} |\langle n|\sqrt{2}\alpha + i\bar{\epsilon}/\sqrt{2}\rangle|^2 d(1-d)^{n-1} \\ & + \sum_{n=2}^{\infty} |\langle n|\sqrt{2}\alpha + i\bar{\epsilon}/\sqrt{2}\rangle|^2 d^2 (1-d)^{n-2} \end{aligned} \tag{8.26}$$

$$p_B = \sum_{m=3}^{\infty}\sum_{n=m}^{\infty} |\langle n|i\bar{\epsilon}/\sqrt{2}\rangle|^2 {}_nC_m d^m (1-d)^{n-m} \tag{8.27}$$

$$\begin{aligned} P_s = {} & \left\{ \sum_{n=0}^{\infty} |\langle n|i\bar{\epsilon}/\sqrt{2}\rangle|^2 (1-d)^n + \sum_{n=1}^{\infty} |\langle n|i\bar{\epsilon}/\sqrt{2}\rangle|^2 d(1-d)^{n-1} \right. \\ & \left. + \sum_{n=2}^{\infty} |\langle n|i\bar{\epsilon}/\sqrt{2}\rangle|^2 d^2 (1-d)^{n-2} \right\} \\ & \times \sum_{m=3}^{\infty}\sum_{n=m}^{\infty} |\langle n|\sqrt{2}\alpha + i\bar{\epsilon}/\sqrt{2}\rangle|^2 {}_nC_m d^m (1-d)^{n-m}. \end{aligned} \tag{8.28}$$

We then find $\widetilde{P}_f^d \approx 6\times10^{-11}$ and $P_f^d \approx 2\times10^{-5}$ for $\alpha = 3$ and $d = 0.9$. Recently, Takeuchi *et al.* [89] developed an avalanched photodetector which can discern 0,1, and 2 photons with high efficiency.

Decoherence is considered one of the main obstacles in quantum computation. When a qubit state $|\phi\rangle$ is subject to a vacuum environment it evolves to [111]

$$\rho_M(\tau) = \mathcal{N}_\tau\Big\{|\mathcal{A}|^2|t\alpha\rangle\langle t\alpha| + |\mathcal{B}|^2|-t\alpha\rangle\langle -t\alpha| + \Gamma\Big(\mathcal{A}\mathcal{B}^*|t\alpha\rangle\langle -t\alpha| + \mathcal{A}^*\mathcal{B}|-t\alpha\rangle\langle t\alpha|\Big)\Big\}$$

where $t = e^{-\gamma\tau/2}$, $\Gamma = e^{-2(1-t^2)\alpha^2}$, γ is the energy decay rate, τ is the interaction time, and $\mathcal{N}_\tau$ is the normalisation factor. Considering decoherence, we need to change $|0_L\rangle$ and $|1_L\rangle$ to $|t\alpha\rangle$ and $|-t\alpha\rangle$. The auxiliary coherent fields for computation have to be changed likewise. The larger the initial coherent amplitude α is, the longer the condition that $\langle t\alpha|-t\alpha\rangle \approx 0$ is preserved, but the decoherence becomes more rapid as α increases because Γ decreases more rapidly for a larger α. The energy decay rate γ of the relevant system and number of required operations for computation may be the crucial factors to decide the value of α. However, decohered states can still be represented by combinations of 1-bit errors for time-dependent logical qubits $|t\alpha\rangle$ and $|-t\alpha\rangle$. It is known that an error correction circuit for an arbitrary 1-qubit error can be built using CNOT and 1-bit unitary operations [182].

8.4 Remarks

In this Chapter, we have found that near-deterministic universal quantum computation can be realised using coherent states. Efficient readout is possible using beam splitters and coherent light sources. Single-bit unitary transformation can be performed using beam splitters and nonlinear media, and CNOT gate can be constructed based on teleportation protocol. Teleportation of a coherent state qubit can be accomplished with a complete Bell measurement using nonlinear media, photodetectors, coherent light sources, and beam splitters. This scheme enables efficient quantum computation even with limited detection efficiency.

Alternatively, the universal gate operations developed in this Chapter

can be achieved by linear optical elements and pre-arranged quantum channels. Ralph *et al.* showed that universal gate operations are possible with linear optics and pre-arranged cat states for a qubit state $|\phi_P\rangle = \mathcal{A}|0\rangle + \mathcal{B}|\alpha\rangle$ [77] which is slightly different from the coherent state qubit $|\phi_R\rangle$ in Eq. (8.6) in our scheme. They showed that single qubit and CNOT operations can be approximately performed with beam splitters, phase shifters, displacement operations, photodetectors and pre-arranged cat states. Note that the CNOT gate in our scheme (see Fig. 8.5) can be performed by Bell measurements, linear optical operations $P(\pi)$ and $D(\frac{i\pi}{4\alpha\sqrt{1-T}})$ and the four-mode entangled state $|\xi\rangle$. As shown in Chapter 2, the Bell measurements can be performed by linear optical devices and photodetectors. Ralph *et al.*'s method for a single qubit operation can be directly applied to our qubit state $|\phi\rangle_R$ because $|\phi\rangle_R$ ($|\phi\rangle_P$) is simply converted to the form of $|\phi\rangle_P$ ($|\phi\rangle_R$) by a displacement operation. However, a large coherent amplitude ($\alpha > 20$) is required to obtain high fidelity ($F > 0.9$) for this appoximation [77]. In this case, the photo-counting ability to discriminate between odd and even numbers of photons is extremely hard, which may be a major obstacle to the physical implementation.

Decohered states can be represented by combinations of 1-bit errors for time-dependent coherent state qubits of reduced amplitude. A purification scheme for decohered entangled channels will be studied in the following Chapter. Detailed error correction methods for our scheme deserves further investigation. The nonlinear effect [71] used in this Chapter is typically too weak to generate required superposition states in current technology. The study of generating coherent superposition of optical states requires further study.

Chapter 9

Entanglement Purification for Entangled Coherent States

Highly entangled states play a key role in an efficient realisation of quantum information processing including quantum teleportation [7], cryptography [11] and computation [6]. When an entangled state prepared for quantum information processing is open to an environment, the pure entangled state becomes mixed one and the entanglement of the original state becomes inevitably degraded. To obtain highly entangled states from less entangled mixed ones, entanglement purification (or distillation) protocols [15, 43, 44] have been proposed. Entanglement purification protocols enable to obtain maximally entangled states from a large ensemble of non-maximally entangled states using only local operations and classical communications [15]. Bennett *et al.* first proposed the entanglement purification protocol, where the implementation of a nontrivial CNOT gate is required [15]. Pan *et al.* found a purification scheme using only linear optical devices, where a polarising beam splitter takes the role of the CNOT gate [44]. Entanglement purification was experimentally demonstrated for entanglement of photon-polarisation states [183]. Entanglement purification of continuous-variable states has also been studied [184, 185, 186, 187] but is more difficult than cases for two-qubit systems. It is known that Gaussian states cannot be distilled by Gaussian local operations and classical communication [188]. There exists a protocol to map *pure* non-Gaussian states onto approximately Gaussian states to distil highly entangled bipartite Gaussian states [186].

In the previous Chapters, we have studied entangled coherent states for

quantum information processing and quantum nonlocality tests. The entanglement concentration of pure entangled coherent states can be simply done using the quasi-Bell measurement scheme studied in Chapter 2 [75]. There is a need for a purification scheme not only for pure states but also for mixed entangled coherent states. Entangled coherent states are categorised into non-Gaussian continuous-variable states and their purification would be very hard if they are considered in an infinite-dimensional Hilbert space. In this Chapter, we suggest an entanglement purification scheme for mixed entangled coherent states in the framework of 2×2 Hilbert space introduced in Chapter 2. This scheme is based on the use of 50-50 beam splitters and photodetectors. We show that our scheme can be directly applied for entangled coherent states of the Werner form based on quasi-Bell states [79]. The scheme can also be useful for general mixed entangled coherent states using additional nonlinear interactions.

9.1 Entanglement purification for mixed states

In Chapter 2, we defined a 2-dimensional Hilbert space $\mathcal{H}_\alpha$ with two linear independent vectors $|\alpha\rangle$ and $|-\alpha\rangle$. The orthonormal basis for the Hilbert space $\mathcal{H}_\alpha$ has been constructed

$$|u\rangle = M_+(|\alpha\rangle + |-\alpha\rangle), \tag{9.1}$$

$$|v\rangle = M_-(|\alpha\rangle - |-\alpha\rangle), \tag{9.2}$$

where M_+ and M_- are normalisation factors. Substituting φ by 0 and π, we have also defined quasi-Bell states [79]

$$|\Phi_\pm\rangle_{ab} = N_\pm(|\alpha\rangle_a|\alpha\rangle_b \pm |-\alpha\rangle_a|-\alpha\rangle_b), \tag{9.3}$$

$$|\Psi_\pm\rangle_{ab} = N_\pm(|\alpha\rangle_a|-\alpha\rangle_b \pm |-\alpha\rangle_a|\alpha\rangle_b), \tag{9.4}$$

where $N_\pm$ are normalisation factors. These states are orthogonal to each other except $\langle\Psi_+|\Phi_+\rangle = 1/\cosh 2|\alpha|^2$, which is very small for $\alpha \gg 1$.

Suppose that Alice and Bob's ensemble to be purified is represented by

$$\rho_{ab} = F|\Phi_-\rangle\langle\Phi_-| + (1-F)|\Psi_-\rangle\langle\Psi_-|, \tag{9.5}$$

where F is the fidelity defined as $\langle\Phi_-|\rho_{ab}|\Phi_-\rangle$ and $0 < F < 1$. Note that $|\Phi_-\rangle$ and $|\Psi_-\rangle$ are maximally entangled and orthogonal to each other regardless of α. Alice and Bob choose two pairs from the ensemble which are represented by the following density operator

$$\begin{aligned}\rho_{ab}\rho_{a'b'} = {} & F^2|\Phi_-\rangle\langle\Phi_-| \otimes |\Phi_-\rangle\langle\Phi_-| + F(1-F)|\Phi_-\rangle\langle\Phi_-| \otimes |\Psi_-\rangle\langle\Psi_-| \\ & + F(1-F)|\Psi_-\rangle\langle\Psi_-| \otimes |\Phi_-\rangle\langle\Phi_-| + (1-F)^2|\Psi_-\rangle\langle\Psi_-| \otimes |\Psi_-\rangle\langle\Psi_-|.\end{aligned} \tag{9.6}$$

The fields of modes a and a' are in Alice's possession while b and b' in Bob's. In Fig. 9.1(a), we show that Alice's action to purify the mixed entangled state. The same is conducted by Bob on his fields of b and b'.

There are four possibilities for the fields of a and a' incident onto the beam splitter ($BS1$), which gives the output (In the following, only the cat part for a component of the mixed state is shown to describe the action of the apparatuses)

$$|\alpha\rangle_a|\alpha\rangle_{a'} \longrightarrow |\sqrt{2}\alpha\rangle_f|0\rangle_{f'}, \tag{9.7}$$

$$|\alpha\rangle_a|-\alpha\rangle_{a'} \longrightarrow |0\rangle_f|\sqrt{2}\alpha\rangle_{f'}, \tag{9.8}$$

$$|-\alpha\rangle_a|\alpha\rangle_{a'} \longrightarrow |0\rangle_f|-\sqrt{2}\alpha\rangle_{f'}, \tag{9.9}$$

$$|-\alpha\rangle_a|-\alpha\rangle_{a'} \longrightarrow |-\sqrt{2}\alpha\rangle_f|0\rangle_{f'}. \tag{9.10}$$

In the boxed apparatus P1, Alice checks if modes a and a' were in the same state by counting photons at the photodetectors $A1$ and $A2$. If both modes a and a' are in $|\alpha\rangle$ or $|-\alpha\rangle$, f' is in the vacuum, in which case the output field of the beam splitter $BS2$ is $|\alpha, -\alpha\rangle_{t1,t2}$. Otherwise, the output field is either $|2\alpha, 0\rangle_{t1,t2}$ or $|0, 2\alpha\rangle_{t1,t2}$. When both the photodetectors $A1$ and $A2$ register any photon(s), Alice and Bob are sure that the two modes a and a' were in the same state but when either $A1$ or $A2$ does not register a photon, a and a' were likely in different states. Of course, there is a probability not to register a photon even though the two modes were in the same state, which is due to the nonzero overlap of $|\langle 0|\sqrt{2}\alpha\rangle|^2$.

It can be simply shown that the second and third terms of Eq. (9.6) are always discarded by the action of P1 and Bob's apparatus same as P1. For example, at the output ports of $BS1$ and Bob's beam splitter corresponding to

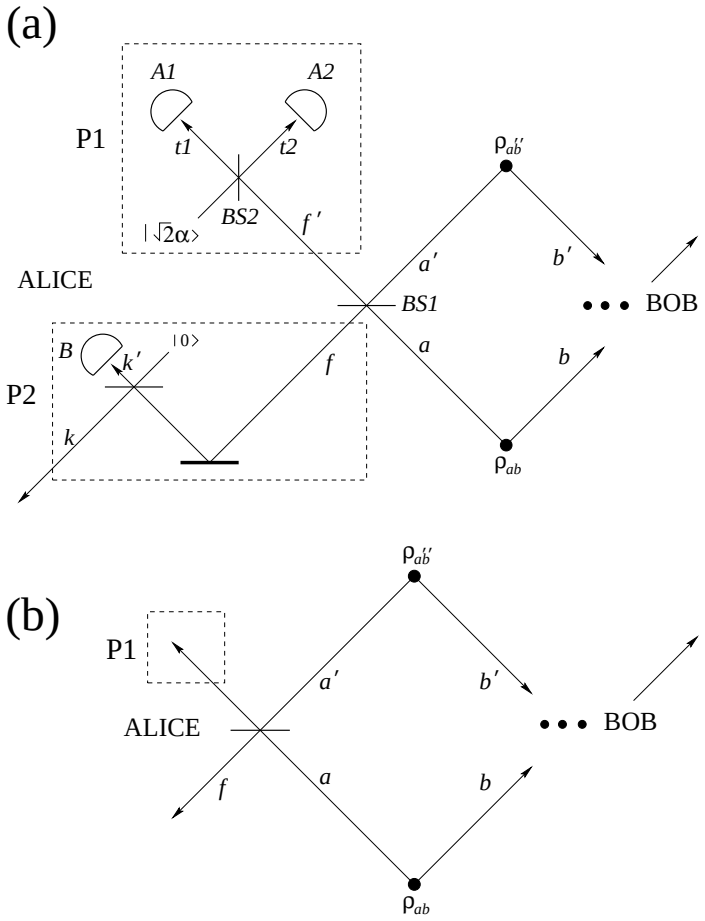

Figure 9.1: (a) Entanglement purification scheme for mixed entangled coherent states. P1 tests if the incident fields a and a' were in the same state by simultaneous clicks at $A1$ and $A2$. For P2, detector B is set for photon parity measurement. Bob performs the same on his field of modes b and b' as Alice. If Alice and Bob measure the same parity, the pair is selected. By iterating this process maximally entangled pairs can be obtained from a sufficiently large ensemble of mixed states. (b) Simpler purification scheme to increase the coherent amplitude of the purified state. The success probability of this scheme is more than twice as large as the scheme with P1 and P2 shown in (a).

$BS1$, $|\Phi_-\rangle_{ab}|\Psi_-\rangle_{a'b'}$ becomes

$$|\Phi_-\rangle_{ab}|\Psi_-\rangle_{a'b'} \longrightarrow N_-^2\big(|\sqrt{2}\alpha,0,0,\sqrt{2}\alpha\rangle - |0,\sqrt{2}\alpha,\sqrt{2}\alpha,0\rangle \\ - |0,-\sqrt{2}\alpha,-\sqrt{2}\alpha,0\rangle + |-\sqrt{2}\alpha,0,0,-\sqrt{2}\alpha\rangle\big)_{fgf'g'}, \tag{9.11}$$

where g and g' are the output field modes from Bob's beam splitter corresponding to $BS1$. The fields of modes f' and g' can never be in $|0\rangle$ at the same time; at least, one of the four detectors of Alice and Bob must not click. The third term of Eq. (9.6) can be shown to lead to the same result by the same analysis.

For the cases of the first and fourth terms in Eq. (9.6), all four detectors may register photon(s). After the beam splitter, the ket of $(|\Phi_-\rangle\langle\Phi_-|)_{ab} \otimes (|\Phi_-\rangle\langle\Phi_-|)_{a'b'}$ of Eq. (9.6) becomes

$$|\Phi_-\rangle_{ab}|\Phi_-\rangle_{a'b'} \longrightarrow |\Phi'_+\rangle_{fg}|0,0\rangle_{f'g'} - |0,0\rangle_{fg}|\Phi'_+\rangle_{f'g'}, \tag{9.12}$$

where $|\Phi'_+\rangle = N'_+(|\sqrt{2}\alpha,\sqrt{2}\alpha\rangle + |-\sqrt{2}\alpha,-\sqrt{2}\alpha\rangle)$ with the normalisation factor N'_+. The normalisation factor in the right hand side of Eq. (9.12) is omitted. The first term is reduced to $|\Phi'_+\rangle_{fg}\langle\Phi'_+|$ after $|0,0\rangle_{f'g'}\langle 0,0|$ is measured out by Alice and Bob's P1's. Similarly, the fourth term of Eq. (9.6) yields $|\Psi'_+\rangle_{fg}\langle\Psi'_+|$, where $|\Psi'_+\rangle$ is defined in the same way as $|\Phi'_+\rangle$, after $|0,0\rangle_{f'g'}\langle 0,0|$ is measured. Thus the density matrix for the field of modes f and g conditioned on simultaneous measurement of photons at all four photodetectors is

$$\rho_{fg} = F'|\Phi'_+\rangle\langle\Phi'_+| + (1-F')|\Psi'_+\rangle\langle\Psi'_+|, \tag{9.13}$$

where

$$F' = \frac{F^2}{F^2+(1-F)^2} \tag{9.14}$$

and F' is always larger than F for any $F > 1/2$.

If the pair is selected by Alice and Bob's P1's, each of them performs another process (P2) for the selected pair. The pair is incident onto a 50-50 beam splitter at each site of Alice and Bob shown in Fig. 9.1(a). If the selected

pair is $|\Phi'_+\rangle\langle\Phi'_+|$ of Eq. (9.13), then the beam splitter gives

$$|\Phi'_+\rangle_{fg} \longrightarrow |\Phi_+\rangle_{kl}\Big(\frac{M_-}{M_+}|u,u\rangle_{k'l'}+\frac{M_+}{M_-}|v,v\rangle_{k'l'}\Big)+|\Phi_-\rangle_{kl}\frac{N_+}{N_-}\Big(|u,v\rangle_{k'l'}+|v,u\rangle_{k'l'}\Big), \tag{9.15}$$

where l and l' are field modes at Bob's site corresponding to k and k'. The normalisation factor is omitted in Eq. (9.15). It is known that $|u\rangle$ contains only even numbers of photons and $|v\rangle$ contains only odd numbers of photons. The state is reduced to $|\Phi_-\rangle$ when different parities are measured at k' and l' by Alice and Bob respectively. The same analysis shows that $|\Psi_-\rangle$ remains by P2's for $|\Psi'_+\rangle_{fg}\langle\Psi'_+|$ of Eq. (9.13) which is originated from the fourth term of Eq. (9.6).

The total state after the full process becomes

$$\rho_{fg} = F'|\Phi_-\rangle\langle\Phi_-| + (1-F')|\Psi_-\rangle\langle\Psi_-|. \tag{9.16}$$

We already saw from Eq. (9.14) that F' is larger than F for any $F > 1/2$. Alice and Bob can perform as many iterations as they need for higher entanglement. The success probability P_s for one iteration is

$$P_s = \frac{F^2+(1-F)^2}{4}\Big(1-\frac{2e^{-4|\alpha|^2}}{1+e^{-8|\alpha|^2}}\Big)\Big(\frac{1-e^{-4|\alpha|^2}}{1+e^{-8|\alpha|^2}}\Big), \tag{9.17}$$

which approaches to $P_s = \frac{F^2+(1-F)^2}{4}$ and $1/8 \leq P_s \leq 1/4$ for $|\alpha| \gg 1$.

By reiterating this process including P1 and P2, Alice and Bob can distil some maximally entangled states $|\Phi_-\rangle$ asymptotically. Of course, a sufficiently large ensemble and initial fidelity $F > 1/2$ are required for successful purification [15]. P2 may be different depending on the type of entangled coherent states to be distilled. For example, if Alice and Bob need to distil $|\Phi_+\rangle$ instead of $|\Phi_-\rangle$, pairs should be selected when the measurement outcomes yield the same parity.

Let us now consider the roles of P1 and P2 by comparing our scheme with Refs. [15] and [44]. Pan *et al.* suggested a purification scheme for the entanglement of linearly polarised photons, where they use polarising beam splitters (PBS's) with photodetectors to test if the two photons are in the same polarisation [44]. From Eqs. (9.7) to (9.10), we pointed out that P1 is to test whether the two fields a and a' are in the same state. Hence P1 plays a similar

role in our scheme as PBS's in [44]. Next, consider P2 which enables to perform orthogonal measurement based on $|\alpha\rangle \pm |-\alpha\rangle$. This measurement is also necessary in the other schemes [15, 44]. (We will show later that this process (P2) is not always necessary in our scheme.) Pan *et al.* explained that a PBS in their scheme has the same effect as a controlled-NOT gate in the scheme suggested by Bennett *et al.* [15] except that the success probability is half as large as [15]. Both the schemes [15, 44] can be directly applied to any Werner states without additional bilateral rotations, thereby it is clear that our scheme is also applicable to any Werner-type states.

If Alice and Bob want to distil entangled coherent states $|\Phi_+\rangle$ or $|\Psi_+\rangle$ while increasing their coherent amplitudes, it can be simply accomplished by performing only P1 in Fig. 9.1(b). Suppose that Alice and Bob need to purify a type of ensemble

$$\rho_{ab} = G_1|\Phi_+\rangle\langle\Phi_+| + G_2|\Psi_+\rangle\langle\Psi_+|, \tag{9.18}$$

where $G_1 + G_2 \simeq 1$ for $|\alpha| \gg 1$. If P1 is successful, the selected pair becomes

$$\rho_{fg} = G_1'|\Phi_+'\rangle\langle\Phi_+'| + G_2'|\Psi_+'\rangle\langle\Psi_+'|, \tag{9.19}$$

where G_1' is larger than G_1 for any $G_1 > G_2$. After n iterations, they get a subensemble with higher fidelity of

$$|\Phi_+^F\rangle \;=\; \mathcal{N}_+(|2^{n/2}\alpha\rangle|2^{n/2}\alpha\rangle + |-2^{n/2}\alpha\rangle|-2^{n/2}\alpha\rangle), \tag{9.20}$$

where the coherent amplitude has increased. Here, $\mathcal{N}_+$ is a normalisation factor. For example, if G_1 is 2/3 and coherent amplitude α is 2, the fidelity and the amplitude will be ~ 0.99999 and 8 respectively after three times of iterations.

Note that the success probability P_s' of this simplified scheme is

$$P_s' = \frac{F^2 + (1-F)^2}{2}\Big(1 - \frac{2e^{-4|\alpha|^2}}{1 + e^{-8|\alpha|^2}}\Big), \tag{9.21}$$

which is more than twice as large as that of the scheme shown in Fig. 9.1(a) and approaches to $1/4 < P_s' < 1/2$ for $|\alpha| \gg 1$. This is due to the fact that the process P2 is not directly for entanglement purification differently from the

other two schemes [15, 44]. We separated P1 and P2 while the other schemes do both processes by one measurement. In our case, the process P1 purifies the mixed ensemble but the resulting state has a larger amplitude. It should be noted that even though the simplified scheme is applicable to any Werner-type states, (symmetric) entangled coherent states $|\Phi_+\rangle$ and $|\Psi_+\rangle$ can only be obtained by it.

9.2 Purification for general mixed states

We have shown that a mixed Werner state may be purified using beam splitters and photodetectors. A general mixed state may be transformed into a Werner state by random bilateral rotations [43, 189]. The Werner state can then be distilled purified. For the case of spin-1/2 systems, the required rotations are B_x, B_y and B_z which correspond to $\pi/2$ rotations around x, y and z axes.

In the previous Chapter, we have studied single-mode unitary transformations for a coherent state qubit. The B_x rotation can be realised using a nonlinear medium for the entangled coherent state as shown in Eqs (8.10) and (8.11). The B_z rotation can be obtained by displacement operator $D(\delta) = \exp(\delta a^\dagger - \delta^* a)$ as shown in Eqs. (8.8) and (8.9). We know that two displacement operators $D(\alpha)$ and $D(\delta)$ do not commute but the product $D(\alpha)D(\delta)$ is simply $D(\alpha+\delta)$ multiplied by a phase factor, $\exp[\frac{1}{2}(\alpha\delta^* - \alpha^*\delta)]$. This phase factor plays a role to rotate the logical qubit. The action of displacement operator $D(i\epsilon)$, where ϵ ($\ll 1$) is real, on a qubit $|\phi\rangle = a|\alpha\rangle + b|-\alpha\rangle$ is the same as z-rotation of the qubit by $U_z(\theta/2 = 2\alpha\epsilon)$. The displacement operation $D(i\epsilon)$ can be effectively performed using a beam splitter with the transmission coefficient T close to unity and a high-intensity coherent field of amplitude $i\mathcal{E}$, where $\mathcal{E}$ is real. It is known that the effect of the beam splitter is described by $D(i\mathcal{E}\sqrt{1-T})$ in the limit of $T \to 1$ and $\mathcal{E} \gg 1$. For the B_z rotation, ϵ should be taken to be $\pi/8\alpha$ so that the incident coherent field may be $|i\pi/(8\alpha\sqrt{1-T})\rangle$. The B_y rotation can be realised by applying B_x and B_z together with σ_z noting

$$B_y = -\sigma_z B_x B_z B_x, \tag{9.22}$$

where σ_z is π rotation around z axis. The coherent state $|i\pi/(4\alpha\sqrt{1-T})\rangle$ should be used to perform σ_z.

Alice and Bob can perform random bilateral rotations to transform the initial general mixed state into a Werner state. In this process, the efficiency of nonlinear interaction can affect the efficiency of the scheme.

9.3 Purification for decohered states in vacuum

We now apply our scheme to a physical example in a dissipative environment. When the entangled coherent channel $|\Phi_-\rangle$ is embedded in a vacuum, the channel decoheres and becomes a mixed state of its density operator $\rho_{ab}(\tau)$, where τ stands for the decoherence time. By solving the master equation (3.25) the mixed state $\rho_{ab}(\tau)$ can be straightforwardly obtained as

$$\begin{aligned}\rho_{ab}(\tau) = \widetilde{N}(\tau)\Big\{&|t\alpha, t\alpha\rangle\langle t\alpha, t\alpha| + |-t\alpha, -t\alpha\rangle\langle -t\alpha, -t\alpha| \\ &- \Gamma(|t\alpha, t\alpha\rangle\langle -t\alpha, -t\alpha| + |-t\alpha, -t\alpha\rangle\langle t\alpha, t\alpha|)\Big\},\end{aligned} \tag{9.23}$$

where $|\pm t\alpha, \pm t\alpha\rangle = |\pm t\alpha\rangle_a|\pm t\alpha\rangle_b$, $t = e^{-\gamma\tau/2}$, $\Gamma = \exp[-4(1-t^2)|\alpha|^2]$, and $\widetilde{N}(\tau)$ is the normalisation factor. The decohered state $\rho_{ab}(\tau)$ may be represented by the dynamic quasi-Bell states defined as follows:

$$|\widetilde{\Phi}_\pm\rangle_{ab} = \widetilde{N}_\pm(|t\alpha\rangle_a|t\alpha\rangle_b \pm |-t\alpha\rangle_a|-t\alpha\rangle_b), \tag{9.24}$$

$$|\widetilde{\Psi}_\pm\rangle_{ab} = \widetilde{N}_\pm(|t\alpha\rangle_a|-t\alpha\rangle_b \pm |-t\alpha\rangle_a|t\alpha\rangle_b), \tag{9.25}$$

where $\widetilde{N}_\pm = \{2(1 \pm e^{-4t^2|\alpha|^2})\}^{-1/2}$. The decohered state is then

$$\begin{aligned}\rho_{ab}(\tau) &= \widetilde{N}(\tau)\Big\{\frac{(1+\Gamma)}{\widetilde{N}_-^2}|\widetilde{\Phi}_-\rangle\langle\widetilde{\Phi}_-| + \frac{(1-\Gamma)}{\widetilde{N}_-^2}|\widetilde{\Phi}_+\rangle\langle\widetilde{\Phi}_+|\Big\} \\ &\equiv F(\tau)|\widetilde{\Phi}_-\rangle\langle\widetilde{\Phi}_-| + (1-F(\tau))|\widetilde{\Phi}_+\rangle\langle\widetilde{\Phi}_+|\end{aligned} \tag{9.26}$$

where, regardless of the decay time τ, $|\widetilde{\Phi}_-\rangle$ is maximally entangled and $|\widetilde{\Phi}_-\rangle$ and $|\widetilde{\Phi}_+\rangle$ are orthogonal to each other. The decohered state (9.26) is not in the

same form as Eq. (9.5) so that we need some bilateral unitary transformations before the purification scheme is applied. We find that unitary operation B_x on each side of Alice and Bob transforms the state into

$$B_{xa}B_{xb}\rho_{ab}(\tau)B_{xb}^{\dagger}B_{xa}^{\dagger} = F(\tau)|\widetilde{\Phi}_{-}\rangle\langle\widetilde{\Phi}_{-}| + (1-F(\tau))|\widetilde{\Psi}_{+}\rangle\langle\widetilde{\Psi}_{+}|, \tag{9.27}$$

which is obviously distillable form using the schemes explained in Sec. 3. A Hadamard gate H for coherent states [76, 77] can also be used to transform the state (9.26) into a distillable form

$$H_aH_b\rho_{ab}(\tau)H_b^{\dagger}H_a^{\dagger} = N_h\Big\{F(\tau)|\widetilde{\Psi}_{+}\rangle\langle\widetilde{\Psi}_{+}| + (1-F(\tau))|\widetilde{\Phi}_{+}\rangle\langle\widetilde{\Phi}_{+}|\Big\}, \tag{9.28}$$

where N_h is the normalisation factor due to the nonzero overlap between $|\widetilde{\Psi}_{+}\rangle$ and $|\widetilde{\Phi}_{+}\rangle$. Note that the Hadamard operation for coherent states can be approximately realised using linear elements if cat states are pre-arranged [77].

The ensemble of state (9.26) can be purified successfully only when $F(\tau)$ is larger than 1/2. Because

$$F(\tau) = \frac{N_{+}^2(1+\Gamma)}{N_{+}^2(1+\Gamma) - N_{-}^2(1-\Gamma)}, \tag{9.29}$$

it is found that purification is successful when the decoherence time $\gamma\tau < \ln 2$ regardless of α. This result is in agreement with the decay time until which teleportation can be successfully performed via an entangled coherent state shown in Ref. [75].

9.4 Multi-mode purification

Besides a two-mode entangled coherent state, a multi-mode entangled coherent state [190] can be used for quantum computation using coherent-state qubits [76]. There is a suggestion for multi-mode entanglement purification based on controlled-NOT operation [191]. In this subsection we investigate an example of application of our scheme to multi-mode entangled states.

Multi-mode entangled coherent states can be generated using a coherent

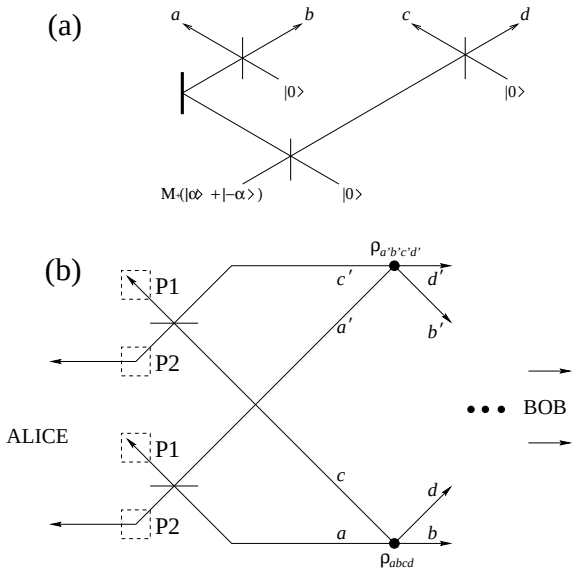

Figure 9.2: (a) Schematic for generation of a four-mode entangled coherent state using a nonlinear medium and 50-50 beam splitters. A coherent-superposition state $M_+(|\alpha\rangle+|-\alpha\rangle)$ can be prepared using a nonlinear medium before it passes through beam splitters. (b) Entanglement purification for four-mode entangled coherent states.

superposition state and 50-50 beam splitters. The number of required beam splitters is $N-1$, where N is the number of modes for the multi-mode entangled state. For example, a four-mode entangled state can be generated as shown in Fig. 9.2(a). After passing the three beam splitters, the four-mode entangled state $|B_1\rangle = \mathcal{N}_-(|\alpha,\alpha,\alpha,\alpha\rangle + |-\alpha,-\alpha,-\alpha,-\alpha\rangle)$ is generated. Suppose Alice and Bob's ensemble to be purified is represented by

$$\rho_{ab} = F|B_1\rangle\langle B_1| + G|B_2\rangle\langle B_2|, \tag{9.30}$$

where $|B_2\rangle = \mathcal{N}_-(|\alpha,-\alpha,\alpha,-\alpha\rangle + |-\alpha,\alpha,-\alpha,\alpha\rangle)$ and $|B_2\rangle$ can be generated in a similar way as $|B_1\rangle$. By extending the scheme studied above, the ensemble (9.30) can be purified as shown in Fig. 9.2(b). After one successful iteration of the purification process, the originally selected pairs become

$$\rho_{ab} = F'|B_1\rangle\langle B_1| + G'|B_2\rangle\langle B_2|, \tag{9.31}$$

where $F' = \frac{F^2}{F^2+(1-F^2)}$ is always larger than F for $F > G$. Alice and Bob can

iterate the process as many time as required for their use. Note that this scheme can be applied to any N-mode entangled states of the same type and so does the simpler scheme only with P1.

9.5 Remarks

We have suggested an entanglement purification scheme for mixed entangled coherent states. Our scheme is based on the use of 50-50 beam splitters and photodetectors. The scheme is directly applicable for mixed entangled coherent states of the Werner type, and can be useful for general two-mode mixed states using additional nonlinear interactions. We have also suggested a simplified variation of this scheme which, however, increases the coherent amplitude of the entangled coherent state. We applied our scheme to an entangled coherent state decohered in a vacuum environment.

Finally, we would like to address possible difficulties for experimental realisation of the purification scheme. We already pointed out that the nonlinear interaction required for the generation of cat states and for additional bilateral rotations to purify some non-Werner type states is extremely difficult, while the efforts to improve nonlinearity that additional noise is being continuously investigated. If the entangled coherent state is subject to a thermal environment, it is not straightforward to represent the decohered state in the simple basis of the quasi-Bell states (9.3) and (9.4). The purification of a decohered state due to thermal environment will be much more complicated and will deserve further studies. Laser phase drift can be another obstacle to realise quantum information processing with coherent states and phase stabilisation methods via mixing of laser beams can be used to reduce the drifts. Apart from the phase drift, There has been a controversy on whether conventional laser sources can be used for quantum communication with coherent states [140, 141]. Most recent study [141] shows that the conventional laser can be used for quantum teleportation and for generating continuous-variable entanglement because optical coherence is not necessary for the purpose.

For quantum information processing, an entangled coherent state is normally assumed to have a large coherent amplitude. Even though the success

probability of the purification scheme is better as the coherent amplitude, α, is larger, it does not change much. For example, the success rate is about 5% degraded for $\alpha = 1$ compared with the case for $\alpha \to \infty$. To use the first purification scheme described in Fig. 2(a), even and odd numbers of photons have to be discriminated. If the coherent amplitude is large, the efficiency to discriminate even and odd numbers of photons becomes low due to the dark current. However, when the coherent amplitude is small, a highly efficient avalanche photodiode can be used to discriminate even (0 and 2) photon numbers and odd (1) photon number [89] because, for example, taking $\alpha = 1$ the probability of photon number being 0 and 2 for an even cat state is about 97% and the probability of photon number being 1 is about 85%. Takeuchi *et al.* used threefold tight shielding and viewports that worked as infrared blocking filters to eliminate the dark count. On the other hand, the second purification scheme in Fig. 2(b) is robust against detection inefficiency when α is large because it is enough to discern a coherent state and a vacuum in this simplified scheme. By employing a distributed photon counter or a homodyne detector, we have even a higher detection efficiency to discern a coherent state and a vacuum.

Chapter 10

Simulation of Quantum Random Walks with Classical Light Field

Random walks are useful models for physicists to study statistical behaviours of nature such as Brownian motions of free particles [192]. They have also been studied for practical use such as algorithms in computer science [193] and risk management in finance [194]. Quantum versions of random walks have been recently studied both for fundamental interests and for the expectation of building new algorithms for quantum computation [195]. There have been several suggestions for a practical implementation of quantum random walks, using ions in linear traps, optical lattices and cavity-QED [196, 197]. Recently, proposals for the implementation of quantum random walks with linear optical elements have been suggested [198, 200] and the first search algorithm using quantum random walks has been reported [201]. Quantum random walks typically show very different patterns from the Gaussian distributions for classical random walks, which have some remarkable characteristics including an exponentially fast hitting time [195]. It has been pointed out that these differences are due to the existence of quantum coherence [196].

A scheme to simulate quantum random walks on a line using the wave nature of classical light fields is suggested in this Chapter. This is related to the fact that the idea of quantum coherence is originally borrowed from the interference of wave mechanics shown in Young's double-slit experiment. It is also possible to simulate decoherence processes using linear optical devices and input coherent states in our scheme. Note that Knight *et al.* also pointed

out the possibility of simulation of quantum random walks using classical fields [205].

10.1 Quantum random walk with linear optical elements

In uni-dimensional coined random walks, the walker is restricted to move along a line with a number of discrete integer points on it. The walker is supposed to be a classical particle on one of the integer points. A coin tossing determines whether the walker moves left or right for each step. In the quantum version of coined random walks, the classical coin is replaced by a quantum bit whose states $|L\rangle$ and $|R\rangle$ represent the logical values LEFT and RIGHT. The quantum coin can be embodied by an internal degree of freedom of the walker itself [195]. The walker, which is a quantum particle, moves conditioned to the result of the coin tossing operation which is realised by a Hadamard transform [196]. For example, the transformation for one step of the particle from an arbitrary point X is simply

$$\begin{aligned} |X,R\rangle &\longrightarrow \frac{1}{\sqrt{2}}(|X+1,R\rangle + |X-1,L\rangle), \\ |X,L\rangle &\longrightarrow \frac{1}{\sqrt{2}}(|X+1,R\rangle - |X-1,L\rangle). \end{aligned} \tag{10.1}$$

After n steps, the state of the system is $|\Psi_n\rangle$. Differently from the classical walks on a line, where the position of the particle is monitored at every step of the process, in the quantum version the walker remains in a superposition of many positions until the final measurement is performed. The probability for the particle being at X_k after n steps is $\mathcal{P}_n(X_k) = |\langle R|\langle X_k|\Psi_n\rangle|^2 + |\langle L|\langle X_k|\Psi_n\rangle|^2$. During the quantum random walk process, destructive as well as constructive interference may occur. The quantum correlation between two different positions on a line introduced at the first step may be kept by delaying the measurement step until the final iteration.

The probability distribution to find the particle at a given position is generally dependent on the initial state of the system [196] and exhibits a very structured pattern (See Fig. 10.1). This allows only numerical evaluations of its variance. It has been shown that, roughly, the standard deviation σ_{QRW} grows

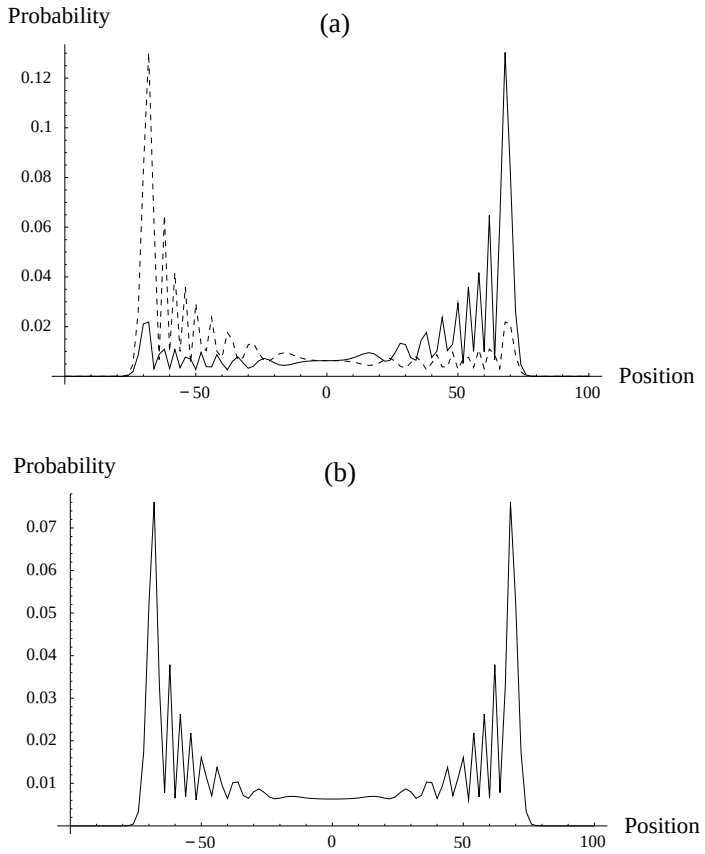

Figure 10.1: Probability distribution, as a function of the position of a walker on a line, in a quantum random walk process after $N = 100$ steps. **(a)** Comparison between the initial states $|R\rangle_c \otimes |0\rangle$ (dashed line) and $|L\rangle_c \otimes |0\rangle$. The bias in the probability distribution, due to the asymmetric action of the coin-tossing operator is evident. (**b**) The symmetry in the probabilities is restored if the initial state $|\Psi_0\rangle = 1/\sqrt{2}\,(i\,|R\rangle + |L\rangle)_c \otimes |0\rangle$ is taken. In these plots, just the probabilities for the even position of the walker on a line are represented. This is because only the probabilities relative to positions labelled by integers having the same parity as N are non-zero, in the quantum random walk algorithm.

linearly with N and is independent from the initial state of the coin [197]. Thus, the walker in quantum walks explores its possible configurations faster than in classical walks, where the standard deviation grows as $\sqrt{N}$. This motivates the conjecture that algorithms based on quantum random walks could beat their classical versions in terms of the time needed to solve a problem [201].

There have been a few suggestions for experimental implementations of quantum random walks [197]. Recently, it has been shown that quantum random walks can be realised using linear optical elements [198]. In this scheme,

polarisation beam splitters, half-wave plates and photodetectors are used. The walker is embodied in a single-photon state and the entire scheme is based on the quantum coherence of two polarisation states of the photon. This result is inspiring as a first proposal for an all-optical implementation of a quantum random walk, even if it requires a reliable single-photon state source, which is very demanding, and the apparatus is highly sensitive to variations in the photons polarisation.

First, we propose a scheme which uses ordinary 50:50 beam splitters, phase shifters and photodetectors. We formulate quantum random walks with the coin tossing operation embedded in the translation of the walker particle. In our scheme, the polarisation degree of freedom does not play a role and, thus, is not considered at all. A single-mode field, including a thermal field, may be used as an input to simulate the distribution of the quantum random walk. In fact, this may be apparent if we recall that Young used a thermal field for his double-slit experiment and showed interference.

Let us consider the experimental set-up, composed of 50:50 beam splitters, phase shifters, and photodetectors, shown in Fig. 10.2. For convenience, we denote the field modes propagating sidewards by s and downwards by d. As the beam splitters used here are polarisation insensitive, these modes do not refer to polarisation. Here, we consider a single-photon state $|1\rangle_s$ as the initial state of the walker and we show that, in this case, our scheme gives rise to coined quantum random walks on a line. At the first beam splitter, $\hat{B}_1(\theta,\phi)$, the input field is mixed with a field mode prepared in a vacuum state (Fig. 10.2(**a**)). The following transformation is realised

$$\hat{B}_1(\theta,\phi)|0,1\rangle_{ds} = \cos\frac{\theta}{2}|1,0\rangle_{ds} + e^{i\phi}\sin\frac{\theta}{2}|0,1\rangle_{ds}, \tag{10.2}$$

where $\hat{B}_1(\theta,\phi) = \exp\{\theta/2(e^{i\phi}\hat{a}_s^\dagger\hat{a}_d - e^{-i\phi}\hat{a}_d^\dagger\hat{a}_s)\}$ is the beam splitter operator and $\hat{a}_{s,d}$ ($\hat{a}_{s,d}^\dagger$) are the annihilation (creation) operators for a sideward and a downward field mode, respectively. We define the transformation in Eq. (10.2)

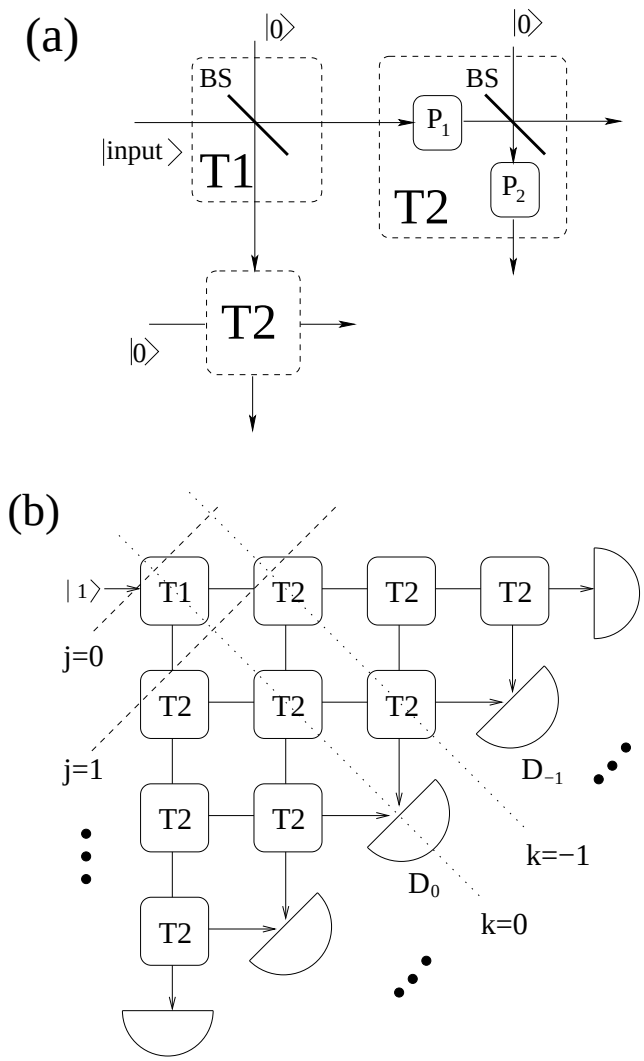

Figure 10.2: All-optical set-up for the simulation of quantum random walks on a line. (**a**) Two different kinds of operations are shown: T1 is an ordinary beam splitter $\hat{B}_1(\theta, \phi)$. T2 involves the cascade of the phase shifter $\hat{P}_1(\pi/2)$, of a 50:50 beam splitter $\hat{B}_2(\pi/2, \pi)$ and of the phase shifter $\hat{P}_2(-\pi/2)$. (**b**) Proposed set-up, shown up to the fourth dynamic line. Apart the input state, all the other modes are initially prepared in vacuum states.

as T1. We introduce the transformation T2

$$|1,0\rangle_{d,s} \rightarrow \frac{1}{\sqrt{2}}(|1,0\rangle + |0,1\rangle)_{d,s}, \tag{10.3}$$

$$|0,1\rangle_{d,s} \rightarrow \frac{1}{\sqrt{2}}(|1,0\rangle - |0,1\rangle)_{d,s}, \tag{10.4}$$

which can be realised with a 50:50 beam splitter, $\hat{B}_2(\pi/2, \pi)$, and two phase

shifters $\hat{P}_1(\pi/2) = e^{i\pi\hat{a}_s^\dagger\hat{a}_s/2}$ and $\hat{P}_2(-\pi/2) = e^{-i\pi\hat{a}_d^\dagger\hat{a}_d/2}$ as shown in Fig. 10.2(**a**).

The scheme can simply be illustrated as recursive applications of T2 after the initial transformation T1, as shown in Fig. 10.2(**b**). A dynamic line [198] is represented by a row of aligned optical elements (or photodetectors), labelled j in Fig. 10.2(**b**). On the other hand, a node is given by a point represented by k on a dynamic line. For example, the detector D_{-2} is on the fourth dynamic line and occupies the node $k = -2$. If a photon is incident downward (sideward) on a dynamic line j and node k, we represent its state as $|k,d\rangle_j$ ($|k,s\rangle_j$). The transition from a dynamic line j to $j+1$ by means of the operation T2 is synthesised by

$$\begin{aligned} |k,d\rangle_j &\to \frac{1}{\sqrt{2}}\left(|k+1,d\rangle + |k-1,s\rangle\right)_{j+1}, \\ |k,s\rangle_j &\to \frac{1}{\sqrt{2}}\left(|k+1,d\rangle - |k-1,s\rangle\right)_{j+1}. \end{aligned} \tag{10.5}$$

We notice that Eqs. (10.5) are equivalent to Eqs. (10.1). Thus, the actions of T1 and T2 on a single-photon state exactly corresponds to a coined quantum random walk. Any initial coin state, up to an irrelevant global phase, can be prepared changing θ and φ in T1. If $\theta = \pi/2$ and $\phi = -\pi/2$, we get the symmetric probability distribution that corresponds to the initial coin state $(|R\rangle + i|L\rangle)/\sqrt{2}$ in a coined quantum walk [197]. In our model, the difference between quantum and classical walks from a certain step is due to the interference of the walker's paths on the T2 processes[1].

A problem of the approach employing *dynamic lines* for quantum random walks is that the required number of resources grows quadratically with the number of steps. This imposes serious limitations to the scalability of such a proposal [199]. In the alternative proposal in Fig. 10.3, this problem is bypassed measuring all the even positions by the upper row of detectors, while the odd ones are detected by the lower row. Acousto-Optic Modulators (AOMs) [202] are used to guide a beam toward a mirror for further steps or toward a detector for the measurement. When the AOMs in the top row have to deflect the light beams toward the detectors, those in the bottom row should not be active. The beam splitters and phase shifters in Fig. 10.2 and in Fig. 10.3 are the same.

[1]Note that classical random walks can be easily obtained removing all the phase shifters. In this case, indeed, there can be no destructive interference that makes the quantum random walk different from its classical counterpart.

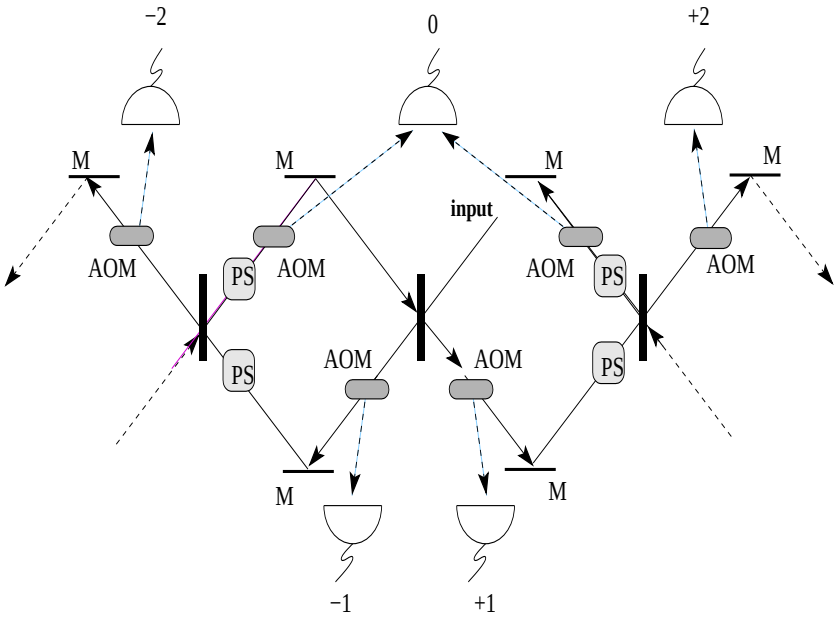

Figure 10.3: Alternative set-up for quantum random walk on a line. In this scheme, the number of required resources scales linearly with the number of steps N. Two rows of Acousto-Optic Modulators (AOM) direct the incoming beams of light to the perfect mirrors M or to the detectors row. This set-up is conceptually equivalent to that sketched in Fig. 10.2(**b**).

Even if the scheme is demanding, from the experimental point of view, the number of required resources increases only linearly with the number of steps.

10.2 Analysis with different states of the walker

In this Section we show that the scheme suggested in Fig. 10.2 exhibits the same interference pattern at the detectors regardless of the nature of the input state. We first address the case of an input coherent state and, then, we extend the analysis to any field.

10.2.1 Coherent states

A coherent state $|\alpha\rangle$ ($\alpha \in \mathbb{C}$) is generally assumed to be the best description of the state of a laser beam. We consider $|\alpha\rangle$ as the input state of the walker. The action of the beam splitter operator on two input coherent states does not lead

to any entanglement between the output modes [203]. Assuming $\theta = \pi/2$ and $\phi = -\pi/2$ for the T1 process, we can calculate the distribution of the average photon-number as a function of the position k on the chosen final dynamic line. For example, for $N = 4$ steps, we find the final state

$$\begin{aligned} |\Phi_4\rangle = &\left|\frac{-i\alpha}{4}, s\right\rangle_4^{-4} \left|\frac{-i\alpha}{4}, d\right\rangle_4^{-2} \left|\frac{1-2i}{4}\alpha, s\right\rangle_4^{-2} \left|\frac{\alpha}{4}, d\right\rangle_4^{0} \\ &\otimes \left|\frac{i\alpha}{4}, s\right\rangle_4^{0} \left|\frac{-2-i}{4}\alpha, d\right\rangle_4^{+2} \left|\frac{\alpha}{4}, s\right\rangle_4^{+2} \left|\frac{-\alpha}{4}, d\right\rangle_4^{+4}, \end{aligned} \tag{10.6}$$

with $|\alpha, s\rangle_j^k$ ($|\alpha, d\rangle_j^k$) that indicates a coherent state incident sideward (downward) on a dynamic line j and node k. The average photon-number $\mathcal{N}_p(N,k)$ for node k is $\mathcal{N}_p(4,k) = \mathcal{M}(4,k)\mathcal{N}_{in}(|\alpha\rangle)$, with

$$\mathcal{M}(4,\pm 4) = \frac{1}{16},\ \mathcal{M}(4,\pm 2) = \frac{3}{8},\ \mathcal{M}(4,0) = \frac{1}{8}. \tag{10.7}$$

Here, $\mathcal{N}_{in}(|\alpha\rangle) = |\alpha|^2$ is the average photon number for the input state $|\alpha\rangle$ and $\mathcal{M}(N,k)$ is the *normalised photon-number distribution* at step N and node k. It characterises the output photon-number distribution at the detectors. We find that the distribution $\mathcal{M}(4,k)$ for an input coherent state is the same as the one for the single photon input [197], *i.e.*, the two different inputs result in the same photon-number distribution. The average photon numbers for steps, $N = 4, 5, 6$ are shown in Fig. 10.4. The deviations of a quantum walk from its classical counterpart appears from the fourth step. This is due to the particular values of the parameters in the transformation T1: $\theta = \pi/2$ and $\phi = -\pi/2$. Since a coherent state input results in the same quantum random walk pattern of the single photon case for all the steps we have considered, we conjecture that the quantum walk pattern results even any initial state for a general number of steps N. In what follows, we prove the validity of this conjecture.

10.2.2 General case

With the proposed set-up, the quantum walk process can be represented as

$$|\Phi_N\rangle = \hat{U}_{T(j=N)} ... \hat{U}_{T(j=1)} \hat{T}_{1(j=0)} |\Phi_0\rangle \equiv \ \widehat{U}_{QW}^N |\Phi_0\rangle,$$

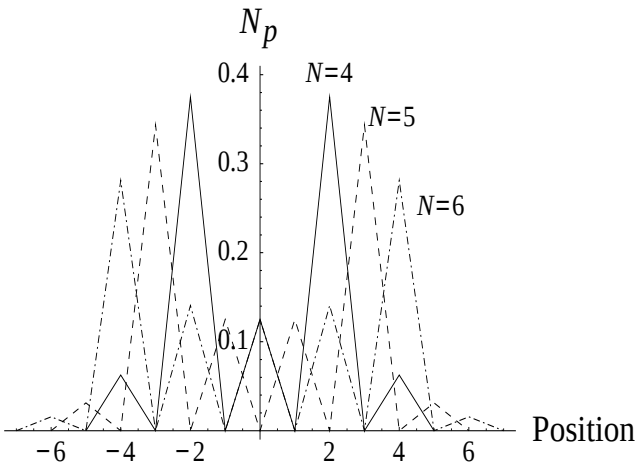

Figure 10.4: Average photon-number distribution for an input coherent state $|\alpha = 1\rangle$, as a function of the position along the final dynamic line. Three different cases are considered: the solid-line curve is relative to a number of steps $N = 4$; the dashed-line represents $N = 5$ while the dot-dashed one is for $N = 6$. The plots match perfectly the graphs expected for a coined quantum walk on a line. In the general case of $\alpha \neq 1$, N_p has to be normalised with respect to $|\alpha|^2$.

where $|\Phi_0\rangle$ is the input state, N is the number of steps, and $\hat{U}_T$ is an appropriate unitary transformation for each step. For a coherent state, the previous result can be summarised as

$$|\Phi_0\rangle = |\alpha\rangle \xrightarrow{\widehat{U}_{QW}^N} |\chi_1\alpha\rangle_1|\chi_2\alpha\rangle_2...|\chi_N\alpha\rangle_{2N} = |\Phi_N\rangle. \tag{10.8}$$

Eq. (10.6) is an explicit example. The average photon number for mode r ($0 \leq r \leq 2N$) is $n_r = |\chi_r|^2|\alpha|^2 = |\chi_r|^2\mathcal{N}_{in}(|\alpha\rangle)$, with $r = 0$ corresponding to the mode incident on the detector that occupies $j = N$, $k = -N$. It is easy to show that the average photon number for the k-th node and j-th step is given by $\mathcal{N}_p(j,k) = n_{j-k} + n_{j-k+1} = (|\chi_{j-k}|^2 + |\chi_{j-k+1}|^2)\mathcal{N}_{tot}(|\alpha\rangle)$, where $\chi_0 = \chi_{2N+1} \equiv 0$. This result also means that

$$\mathcal{M}(j,k) = |\chi_{j-k}|^2 + |\chi_{j-k+1}|^2. \tag{10.9}$$

Note that χ_r does not depend on the amplitude of the initial state but only on the structure of $\widehat{U}_{QW}^N$.

The initial state density operator in P representation can be generally

written as [192, 204]

$$\rho_0 = \int d^2\alpha P(\alpha)|\alpha\rangle\langle\alpha|, \tag{10.10}$$

where $P(\alpha)$ is the P representation of the initial state ρ_0. Provided that $P(\alpha)$ is a sufficiently singular generalised function, such a representation exists for any given operator ρ_0 [204]. After N steps, the density operator evolves as:

$$\rho_N = \hat{U}_{QW}^N \rho_0 \hat{U}_{QW}^{N\dagger} = \int d^2\alpha P(\alpha)|\chi_1\alpha\rangle_1\langle\chi_1\alpha| \otimes .. \otimes |\chi_{2N}\alpha\rangle_{2N}\langle\chi_{2N}\alpha| \tag{10.11}$$

where Eqs. (10.8) and (10.10) have been used. The P representation is particularly appropriate for our aim to find the average photon-number distribution since it can be shown that the moments of the P representation give the expectation values of normally-ordered products of bosonic operators [192, 204].

The marginal density matrix for mode r is simply obtained as

$$\rho_r = \int d^2\alpha P(\alpha)|\chi_r\alpha\rangle_r\langle\chi_r\alpha|. \tag{10.12}$$

The average photon number for the r-th mode is

$$n_r = \mathrm{Tr}_r[\rho_r \hat{a}^\dagger \hat{a}] = |\chi_r|^2 \int d^2\alpha P(\alpha)\,|\alpha|^2 = |\chi_r|^2 \mathcal{N}_{in}(\rho_0),$$

and the average photon number for the j-th step and k-th node is $\mathcal{N}_p(j,k) = \mathcal{M}(j,k)\mathcal{N}_{tot}(\rho_0) = (|\chi_{j-k}|^2 + |\chi_{j-k+1}|^2)\mathcal{N}_{tot}(\rho_0)$, from which Eq. (10.9) is found to hold for the case of any input field. The interference pattern determined by $\mathcal{M}(j,k)$ does not depend on the initial input state. For a given set of beam splitters and phase shifters, any input state will result in the same interference pattern. Only an overall factor will be changed, according to the total average photon-number of the initial state. For a classical light, in a pictorial way, the result is nothing but quantum random walks with many walkers simulated by interference between fields. For a weak field, the quantum random walks with a single walker can be probabilistically performed. For example, given a coherent state with $\alpha = 1$, a single photon is detected with 37% of the probability.

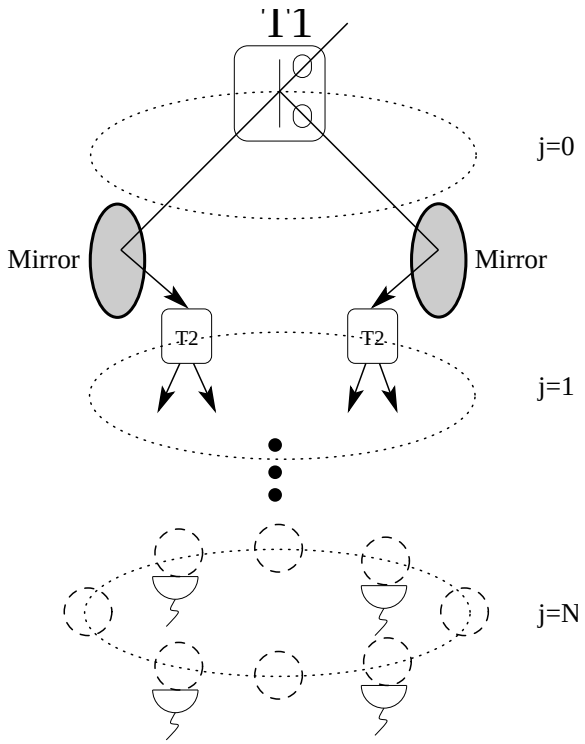

Figure 10.5: An implementation of a quantum random walk on a circle using 'dynamic circles'. Mirrors are used to change the paths of light fields.

10.3 Remarks

We have investigated an all-optical set-up to simulate a quantum random walk process using ordinary beam splitters, phase shifters, and photodetectors. For a single-photon state input, the process realised is shown to be equivalent to a coined quantum random walk. Starting from this result, we have investigated the case of an input coherent state. This class of states gives rise to exactly the same pattern with a single-photon case (and, thus, with a coined quantum walk on a line) with respect to the average photon-number distribution. We have proved how our set-up is sufficiently flexible to work for any initial state.

We have addressed the question of the number of resources needed to implement a given number of steps describing an alternative set-up. It turns out that a quantum walk on a line could be implemented, with input coherent states, using a number of resources that grows linearly with N.

It is possible to extend our scheme to quantum random walks on a circle

as shown in Fig. 10.5. One can use 'dynamic circles' and mirrors to change the paths of light fields. The transformation T1 is used only for the first dynamic circle and T2's are employed for further steps. This implementation is simply based on the simulation scheme of a quantum walk on a line studied in this Chapter. It is obvious that this modified version will simulate quantum walks on a circle with classical fields. It is an interesting open question how to simulate quantum random walks using the wave nature of classical fields in higher dimensions, general graphs and hypercubes. The possibility of classical simulation of quantum random walks does not mean that it can be used for a practical quantum algorithm. There remain important open questions for further studies such as 'what can we gain from the classical simulation of quantum walks in terms of speed-up of quantum computation?'

Chapter 11

Generating Optical Cat States

As we have studied, an optical cat state of a propagating field can be extremely useful both for the study of fundamental quantum physics and for application of quantum information processing. Once such cat states are generated, quantum teleportation [73, 74, 75], nonlocality test [129, 206], generation and purification [75, 78] of entangled coherent states and universal quantum computation [76, 77] may become realisable using current technology.

It has been known theoretically that the cat state can be generated from a coherent state by a nonlinear interaction in a Kerr medium [71]. However, the Kerr nonlinearity of currently available nonlinear medium is too small to generate the required coherent superposition state. It was pointed out that one needs an optical fibre of about 3,000km for an optical frequency of $\omega \approx 5 \times 10^{14}$rad/sec to generate a coherent superposition state with currently available Kerr nonlinearity using two-mode nonlinear interactions and a Mach-Zehnder interferometer [207, 208]. A nonlinear cell of about 1,500km is required when single-mode interactions are used [209]. Even though it is possible in principle to make such a long nonlinear optical fibre, the decoherence effect during the propagation will become too large. A signal loses half of its energy in about 15km of propagation through a typical commercial fibre used for telecommunication [210, 211]. This will make the required state lose its quantum characteristics and useless for quantum information processing. Proponents of photonic crystal fibre foresee fibres with losses of less than 0.01db/km for optical networks [212]. Experimental efforts are being made for optical fibres with small losses and losses as low as 0.01db/km have been reported for Flurozirconate (ZrF4) fibres [213]. Even in

such cases, a signal attenuates by half in about 300km, which is still not enough to generate a cat state with the currently available nonlinear strength.

Some alternative methods have been studied to generate a superposition of macroscopically distinguishable states using conditional measurements [214, 215]. One drawback of these schemes is that a highly efficient photon number measurement is required to obtain a coherent superposition state, which is difficult using current technology. Cavity quantum electrodynamics has been studied to enhance nonlinearity [216]. Even though there have been experimental demonstrations of generating cat states in a cavity and in a trap [217, 218], unfortunately, all the suggested schemes for quantum information processing with coherent states [73, 75, 74, 76, 77, 78] require *propagating* optical cat states. There were other suggestions to generate cat states with trapped ions [219] and with solitons [220].

Electromagnetically induced transparency (EIT) has been studied as a method to obtain a giant Kerr nonlinearity [221]. There has been an experimental report of an indirect measurement of a giant Kerr nonlinearity utilising EIT [177] and an inspiring suggestion to generate cat states with it [222]. However, this developing technology of EIT has not been exactly at hand to generate an optical cat state. In short, generating a propagating optical cat state is extremely demanding with currently available Kerr effect, and a developed scheme to generate a cat state with small nonlinear effect is required.

As we have pointed out, a signal in an optical fibre loses half of its energy in about 300km (or more) and this makes currently available noneliear media almost useless for our purpose. However, if we can reduce the required level of nonliearity by, e.g, 10 times (or 20 times), such a level of nonliear effect will be gained in an obtical fibre of 150km (or 75km). Then there will be a good possibility of producing a cat state using the nonlinear fibre. Our scheme, which will be studied in this Chapter, is an effort to considerably reduce the required nonlinear effect to generate a cat state using beam splitters and homodyne measurements which are efficient tools in quantum optics.

11.1 Generating a cat state with Kerr nonlinearity and its limitation

A cat state is defined as

$$|cat_{\alpha,\varphi}\rangle = \mathcal{N}(\alpha,\varphi)(|\alpha\rangle + e^{i\varphi}|-\alpha\rangle), \tag{11.1}$$

where $\mathcal{N}(\alpha,\varphi)$ is a normalisation factor, $|\alpha\rangle$ is a coherent state of its amplitude α, and φ is a real local phase factor. Note that the relative phase φ can be approximately controlled by the displacement operation for a given cat state with $\alpha \gg 1$ [76, 116]. Under the influence of the nonlinear interaction given by the Hamiltonian (8.10), the initial coherent state with the coherent amplitude α evolves to the following state at time τ:

$$|\psi(\tau)\rangle = e^{-|\alpha^2|/2}\sum_{n}^{\infty}\frac{\alpha^n e^{-i\phi_n}}{\sqrt{n!}}|n\rangle, \tag{11.2}$$

where $\phi_n = \lambda t n^2$ and λ is the strength of the nonlinearity. When the interaction time τ in the medium is $\pi/\lambda N$, coherent state $|\alpha\rangle$ evolves [209]

$$|\psi_N\rangle = \sum_{n=1}^{N} C_{n,N}|-\alpha e^{2in\pi/N}\rangle \tag{11.3}$$

where $C_{n,N} = e^{i\xi_n}/\sqrt{N}$. Comparing Eqs. (11.2) and (11.3) for an arbitrary N, we find an equation for the arguments ξ_n's

$$\frac{1}{\sqrt{N}}\sum_{n=1}^{N} e^{i\xi_n}(-e^{2in\pi/N})^k = \exp(-i\pi k^2/N), \tag{11.4}$$

where $k = 0, 1, ..., N-1$. By solving the N coupled equations given by Eq. (11.4), the values ξ_n's are obtained as [223]

$$C_{n,N} = \frac{e^{i\xi_n}}{\sqrt{N}} = \frac{1}{N}\sum_{k=0}^{N-1}(-1)^k \exp[-\frac{i\pi k}{N}(2n-k)]. \tag{11.5}$$

The length L of the nonlinear cell corresponding τ is $L = v\pi/2\lambda N$, where v is the velocity of light. For $N = 2$, we obtain a desired cat state of the

form (11.1) with $\varphi = \pi/2$ [71]. We pointed out that the nonlinear coupling λ is typically very small that $N = 2$ cannot be obtained in a length limit in which decoherence effect can be neglected. It can be shown that the required length L corresponding $N = 2$ to generate a cat state called Yurke-Stoler (Y-S) state is about 1,500km when a typical Kerr nonlinearity is used [207, 224, 209]. Furthermore, usually $\alpha \gg 1$ is required for quantum computation using cat states with small error [76, 77]. For example, $\alpha > 20$ is required in [77]. Such a large α may cause even a faster decoherence in a nonlinear medium [111, 125].

11.2 Generating a cat state with smaller nonlinearity

If λ is not large enough, instead of the state (11.1), a different type of coherent superposition state (11.3) with $N > 2$ can be obtained. From the state (11.3), it is necessary to remove all the other coherent component states except two coherent states of a π phase difference. First, we assume that the state (11.3) is incident to a 50-50 beam splitter with vacuum as shown in Fig. 11.2. The initial coherent amplitude α is supposed to be real for simplicity. The state (11.3), after passing through the beam splitter, becomes

$$|\psi_N\rangle = \sum_{n=1}^{N} C_{n,N}|-\alpha e^{2in\pi/N}/\sqrt{2}\rangle|-\alpha e^{2in\pi/N}/\sqrt{2}\rangle, \tag{11.6}$$

where all $|C_{n,N}|$'s have the same value. The imaginary part of the coherent amplitude in the state (11.6) is then measured by homodyne detection. By the measurement result, the state is reduced to

$$\begin{aligned} |\psi_N^{(1)}\rangle &= \mathcal{N}_\psi \sum_{n=1}^{N} C_{n,N}\langle P|-\alpha e^{2in\pi/N}/\sqrt{2}\rangle|-\alpha e^{2in\pi/N}/\sqrt{2}\rangle \\ &\equiv \sum_{n=1}^{N} C_{n,N}^{(1)}(\alpha)|-\alpha e^{2in\pi/N}/\sqrt{2}\rangle, \end{aligned} \tag{11.7}$$

where $\mathcal{N}_\psi$ is the normalisation factor and $|P\rangle$ is the eigenstate of $\hat{P} = (a - a^\dagger)/i$ and a and $a^\dagger$ are creation and annihilation operators respectively. After the

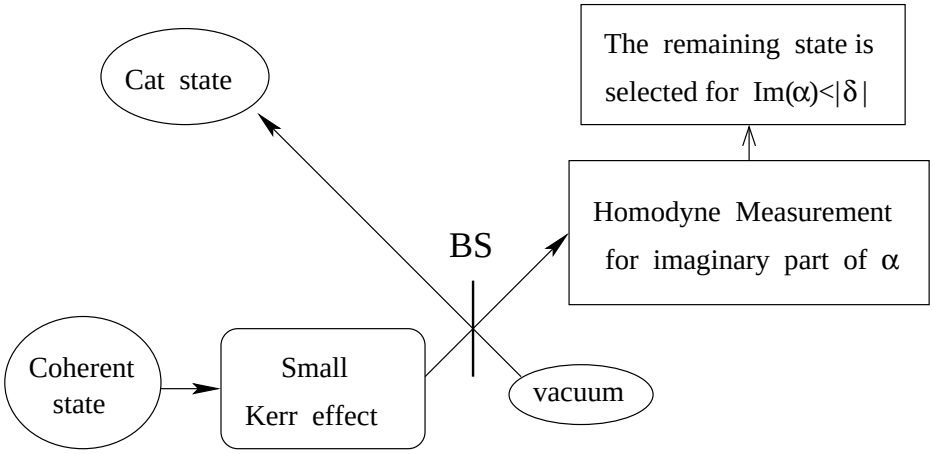

Figure 11.1: Scheme to generate a cat state using small Kerr nonlinearity, a beam splitter, and homodyne detection.

homodyne measurement, the state is selected when the measurement result has certain values. If $|C^{(1)}_{N/2,N}(\alpha)|$ and $|C^{(1)}_{N,N}(\alpha)|$ in Eq. (11.7) have the same nonzero value and all the other $|C^{(1)}_{n,N}(\alpha)|$'s are zero, then the state becomes a desired cat state. For example, if $P = 0$ is measured, the coefficients $|C^{(1)}_{n,N}(\alpha)|$'s are the largest when $n = N/2$ and $n = N$. The coefficients become smaller as n is far from the two points and can be close to zero for all the other n's for an appropriately large α. The resulting state becomes close to a cat state. If the fidelity of the obtained state is not satisfactory, another trial can be made in the same way.

The fidelity is a measure of how close two given states are. We first define a 'perfect' cat state as

$$|cat_{\alpha/\sqrt{2},\varphi_N}\rangle = \mathcal{N}_c\big(C^{(1)}_{N/2,N}|\alpha/\sqrt{2}\rangle + C^{(1)}_{N,N}|-\alpha/\sqrt{2}\rangle\big), \tag{11.8}$$

where $\mathcal{N}_c$ is the normalisation factor and the equality $|C^{(1)}_{N/2,N}(\alpha)| = |C^{(1)}_{N,N}(\alpha)|$ always holds. The fidelity between the state (11.7) obtained and the perfect cat

state (11.8) is then

$$f(\alpha,N,P) = |\langle cat_{\alpha/\sqrt{2},\varphi_N}|\psi_N^{(1)}\rangle|^2$$
$$= \mathcal{N}_c^2\mathcal{N}_\psi^2\Big|C_{N/2,N}^{(1)\,*}\sum_{n=1}^{N}C_{n,N}^{(1)}\exp[-\frac{\alpha^2}{2}(1+e^{2in\pi/N})]$$
$$+ C_{N,N}^{(1)\,*}\sum_{n=1}^{N}C_{n,N}^{(1)}\exp[-\frac{\alpha^2}{2}(1-e^{2in\pi/N})]\Big|^2. \quad (11.9)$$

The probability of getting this result is obtained as

$$\mathcal{P}(\alpha,N,\delta) = \int_\delta dP\mathrm{Tr}[\rho_1|P\rangle\langle P|]$$
$$= \int_\delta dP\sum_{nm}^{N}\langle -\alpha e^{2in\pi/N}/\sqrt{2}|P\rangle\langle P|-\alpha e^{2im\pi/N}/\sqrt{2}\rangle$$
$$\times\exp[-\frac{\alpha^2}{2}(1-e^{2i(m-n)\pi/N})] \quad (11.10)$$

where $\rho_1 = \mathrm{Tr}_2[|\psi_N\rangle_{12\ 12}\langle\psi_N|]$ and δ is the range in which the high fidelity is obtained. The range δ of P will be determined by the desired level of the fidelity. Note that the initial coherent amplitude α needs to be larger as N increases for better fidelity.

We first examine a case that the nonlinear strengh is 10 times weaker than the required value to produce a coherent superposition state of $N = 2$ for $\alpha = 20$. In this case, we get a superposition of 20 coherent states, *i.e.*, $N = 20$ instead of $N = 2$. After the nonlinear medium, the fidelity F between an ideal cat state and the obtained state is ~ 0.1. The probability distribution of X, which corresponds to the conjugate variable of P, is shown in Fig. 11.2(a). After beam splitting and the homodyne measurement, the state can be drastically reduced to a cat state, and the fidelity is $F = 0.999857$ when the measurement result is $P = 0$. Fig. 11.2(b) shows two well-separated peaks of the cat state for the case of $P = 0$. The range δ, where $F > 0.9$ is obtained, is shown in Fig 11.3. In order to calculate the total success probability, all the regions should be carefully integrated. The success probability for $F > 0.9$ is then $\sim 1.8\%$, which means that roughly 50 trials are required to obtain a cat state of $F > 0.9$.

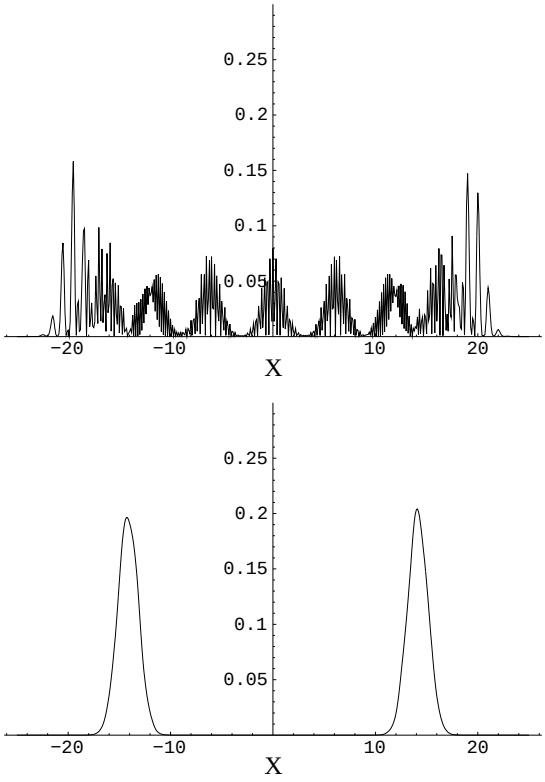

Figure 11.2: (a) The marginal quadrature probability of the state after passing a low efficient nonlinear medium and (b) the marginal quadrature probability of the obtained cat state after the beam splitter and homodyne detection. $N = 20$, $\alpha = 20$ and the horizontal axis represents the quadrature variable X. It is clear from the figures that a cat state with well separated peaks is obtained after the process.

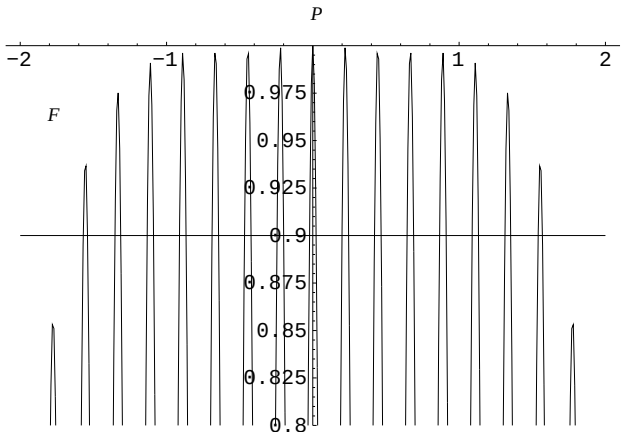

Figure 11.3: Fidelity F of the obtained cat state when $N = 20$ and $\alpha = 20$. $F > 0.9$ is obtained for the certain area of measurement result P.

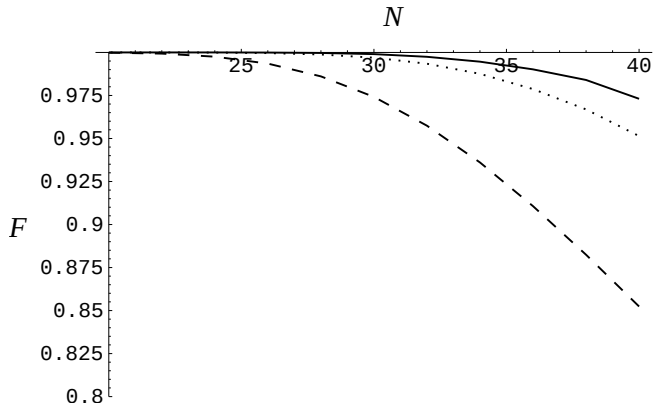

Figure 11.4: Maximal fidelity F obtained by a single application (dashed line) and iterative applications (dotted and solid lines for the second and the third iterations respectively) of the scheme. N is even.

For $N = 20$, we have assumed the Kerr nonlinearity weaker by 10 times. The fidelity is reduced as the nonlinearity decreases, which in effect increases N. If $N = 40$, *i.e.*, the nonlinearity is weaker than the required level by 20 times, the maximal fidelity is 0.852349. However, by iterating this process, a cat state with higher fidelity can be obtained. For example, if another beam splitter and homodyne measurement are applied to the state (11.7), the state obtained is

$$\begin{aligned} |\psi_N^{(2)}\rangle &= \mathcal{N}_\psi^{(1)} \sum_{n=1}^{N} C_{n,N}^{(1)} \langle P| - \alpha e^{2in\pi/N}/2\rangle| - \alpha e^{2in\pi/N}/2\rangle \\ &\equiv \sum_{n=1}^{N} C_{n,N}^{(2)}(\alpha)| - \alpha e^{2in\pi/N}/2\rangle. \end{aligned} \tag{11.11}$$

It can be easily seen that the resulting state (11.11) is closer to the 'perfect' cat state. After this second iteration, the maximal fidelity $F \simeq 0.95$ is obtained and another iteration can give $F \simeq 0.97$. More iteration can be applied for even better fidelity but it causes smaller coherent amplitude.

The success probability $p^{(2)}$ for the second trial can be obtained in the same way. It is clear that $p^{(2)}$ may be significantly larger than $p^{(1)}$ because $|\psi_N^{(1)}\rangle$ may be much closer to the perfect cat state than $|\psi_N\rangle$ is. However, the overall probability is the multiplication of those for all the iterations. The success probability becomes closer to unity as the homodyne measurement iterates.

11.3 Alternative scheme using a two-mode nonlinear interaction

Gerry [207] suggested a scheme to generate cat states using a two-mode nonlinear interaction, a Mach-Zehnder interferometer, beam splitters, a single photon state, threshold photodetectors, and a phase shifter. In his experimental setup, it is possible to generate a state

$$|\psi_{\kappa,\nu}(\beta)\rangle = N_{\kappa,\nu}(|\beta\rangle + e^{i\nu}|\beta e^{-i\kappa}\rangle), \tag{11.12}$$

where $\kappa = \lambda L/v$, L is the length of the Kerr medium, v is the velocity of light in the medium and $N_{\kappa,\nu}$ is a normalisation factor. The relative phase ν is determined by the phase shifter in Ref. [207]. The state (11.12) becomes the desired cat state when $\nu = \pi$. An optical fibre of about 3,000km for an optical frequency of $\omega \approx 5 \times 10^{14}$rad/sec is required to generate such a cat state [207, 208]. However, even when ν is small (*i.e.* $\nu < \pi$) due to a short length of the fibre, it is simply possible to transform the obtained state (11.12) to a cat state (11.1) using a displacement operation[1] up to an irrelevant global phase:

$$|cat_{\alpha,\varphi}\rangle = D(x)|\psi_{\kappa,\nu}(\beta)\rangle \tag{11.13}$$

where $x = -\beta(1 + e^{i\kappa})/2$, $\varphi = \nu + e^{i\kappa}$ and $\alpha = \beta + x$. The only problem here is that the coherent amplitude α may be too small enough because of the weak nonlinearity. However, it is also possible to increase the coherent amplitude probabilistically using beam splitters and threshold photodetectors. Let us assume that two 'small' cat states $|cat_{\alpha,\varphi}\rangle$ and $|cat_{\alpha,\varphi'}\rangle$ are obtained in this way. First, pass any two obtained cat states (not necessarily identical in their relative phases) through a 50-50 beam splitter (BS1) as

$$|cat_{\alpha,\varphi}\rangle_a|cat_{\alpha,\varphi'}\rangle_b \rightarrow \frac{|cat_{\sqrt{2}\alpha,\varphi+\varphi'}\rangle_f|0\rangle_g}{\mathcal{N}(\sqrt{2}\alpha,\varphi+\varphi')} + \frac{e^{i\varphi'}|0\rangle_f|cat_{\sqrt{2}\alpha,\varphi-\varphi'}\rangle_g}{\mathcal{N}(\sqrt{2}\alpha,\varphi-\varphi')}, \tag{11.14}$$

where the normalisation factor is omitted in the right-hand-side. After passing another 50-50 beam splitter (BS2) with a coherent state $|\sqrt{2}\alpha\rangle_f$, two photode-

[1] We studied that a displacement operation can be performed using a beam splitter and a strong coherent field in Chapter 8.

tectors detect photons as shown in Fig. 11.5. If both of the detectors A and B click simultaneously, a cat state $|cat_{\alpha,\varphi-\varphi'}\rangle_g$, with the coherent amplitude $\sqrt{2}\alpha$, is obtained for mode g. This scheme can be iteratively applied to gain an arbitrarily 'large' cat state. The weak nonlinear effects will only reduce the success probability which is $\simeq 1/2$ for $\alpha \gg 1$. Suppose that small even cat states, $|cat_{\alpha,0}\rangle$, are obtained by this scheme. The success probability P_s for increasing the coherent amplitude is obtained as

$$\begin{aligned} P_s &= {}_b\langle cat_{\alpha,0}|_a\langle cat_{\alpha,0}|_f\langle\sqrt{2}\alpha|\hat{B}_1^\dagger\hat{B}_2^\dagger\hat{N}_{t1}\hat{N}_{t2}\hat{B}_2\hat{B}_1|\sqrt{2}\alpha\rangle_f|cat_{\alpha,0}\rangle_a|cat_{\alpha,0}\rangle_b \\ &= \frac{(e^{2|\alpha|^2}+e^{-2|\alpha|^2})(1-e^{-|\alpha|^2})^2}{2(e^{2|\alpha|^2}+e^{-2|\alpha|^2}+2)}, \end{aligned} \tag{11.15}$$

where $\hat{B}_1$ is the first beam splitter operator for modes a and b, $\hat{B}_2$ is the second beam splitter operator for modes f and f', and $\hat{N}_{t1} = \sum_{n=1}^{\infty}|n\rangle_{t1}\langle n|$. When $\beta = 40$ and the nonlinear strength is 100 times weaker than the required value, one can gain a small cat state of the absolute value 0.628 of the coherent amplitude. This small cat state can be increased to 0.889 with the success probability 3.0%. Note that the success probability for each step increases as the amplitude increases. A cat state with $|\alpha| \simeq 1.33$ is obtained with the probability $\simeq 0.003$, *i.e.*, 300 to 400 times of trials are needed to generate such a cat state. We can see, from the argument in Chapter 2, that this value ($|\alpha| \simeq 1.33$) for a cat state is appropriate to generate an entangled coherent state for Bell-state measurements and teleportation. A value $|\alpha| \simeq 3.55$, which may be used for quantum computation, can be obtained with the probability $\simeq 10^{-4}$. Note that a *probabilistic* scheme for producing a cat state can be enough in our scheme for universal quantum computation as explained in Chapter 8. A cat state with a large amplitude, *e.g.*, $|\alpha| \simeq 28.43$, may be obtained with a very low probability $\simeq 1.7 \times 10^{-6}$ by iterative applications.

This scheme can also be used to recover the reduced coherent amplitude in our previous scheme presented in Section 11.2. A coherent amplitude is reduced as $\alpha \to \alpha/\sqrt{2}$ during the process of the previous scheme. The process P, boxed in Fig. 11.5, will probabilistically recover the coherent amplitude as $\alpha/\sqrt{2} \to \alpha$. Note that the scheme P can increase the quantum nature of a given cat state including entanglement. Suppose an even cat state which is given to generate an entangled coherent state [70]. An entangled coherent state can be

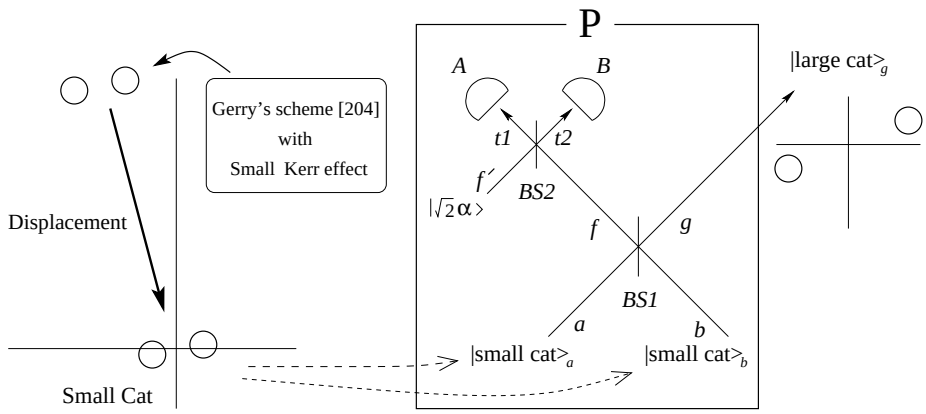

Figure 11.5: An alternative scheme to generate a cat state with a small Kerr effect.

simply generated with a cat state at a 50-50 beam splitter. When α is small, the entanglement of the generated entangled coherent state is also small [78]. However, it is possible to 'distil' some cat states with a larger α from a number of cat states with a small α by P processes. The obtained cat states can be used to generate highly entangled coherent states.

11.4 Remarks

The propagating cat state in an optical system is useful for various applications of quantum information processing. However, weak nonliear effects have been pointed out as a main obstacle to generate such a state. We have suggested a scheme to generate a cat state using relatively small nonlinearity compared with the currently required level using beam splitters and homodyne detection. It was found that the required nonlinear effect to generate a useful cat state with $\alpha \gtrsim 20$ and $F \gtrsim 0.9$ can be reduced by 20 times. An alternative scheme was suggested to reduce the required nonlinear effect based on the scheme [207] using a two-mode nonlinear interaction and a single photon state. We have found that the required nonlinear effect for a cat state generation with $\alpha \simeq 40$ can be reduced by 100 times but the success probability becomes low depending on the coherent amplitude of the desired state. A cat state with a coherent amplitude $\alpha \simeq 1.33$ ($\alpha \simeq 3.55$) may be obtained under the above conditions with the success probability $\simeq 0.003$ ($\simeq 0.0001$).

Chapter 12

Conclusion

We have studied quantum information processing using non-classical light in optical systems. Light fields are useful in quantum information processing and the optical approach is one of the strongest candidates for realisation of quantum computation and communication. There have been optical approaches based on single-photons and Gaussian continuous-variable states for quantum information processing. Our approach utilising optical coherent states and their entanglement is somehow different from those ones. Even though we considered quantum systems normally categorised into continuous-variable states, they were dealt with in a 2×2 dimensional Hilbert space. It has merits particularly in simplicity compared with the others for practical implementations of quantum information processing. We have also studied non-classical nature of various continuous-variable states which are used as quantum channels for quantum information processing. We have tried to understand nonlocal properties of the Gaussian and non-Gaussian continuous-variable states.

Quantum nonlocality is easily destroyed in an environment while it is a key ingredient in quantum information processing. We have been interested in environmental effects on quantum channels. Quantum non-locality has been tested for an entangled coherent state. When the entangled coherent state is embedded in a vacuum environment, its entanglement is degraded but not totally lost. A pure entangled coherent state violates Bell's inequality regardless of its coherent amplitude. The higher the initial nonlocality, the more rapidly quantum nonlocality is lost. *The quantum nonlocality persists longer when it is considered in a* 2×2 *Hilbert space.* It has been found that when it deco-

heres, the entangled coherent state fails the non-locality test, which contrasts with the fact that the decohered entangled state is always entangled. We have studied the dynamic behaviour of the nonlocality for the two-mode squeezed state in the thermal environment. The two-mode squeezed state is found to be a nonlocal state regardless of its degree of squeezing and the higher degree of squeezing brings about the larger quantum nonlocality. As the squeezed state is influenced by the thermal environment the nonlocality is lost. The rapidity of the loss of nonlocality depends on the initial degree of squeezing and the average thermal energy of the environment. The more strongly the initial field is squeezed, the more rapidly the maximum nonlocality decreases. This result is in agreement with the case of an entangled coherent state and due to the fact that a macroscopic quantum system is more fragile than a microscopic quantum system.

There have been theoretical and experimental studies on quantum nonlocality for continuous variables, based on dichotomic observables. In particular, we have been interested in two cases of dichotomic observables for the light field of continuous variables: One case is even and odd numbers of photons and the other case is no photon and the presence of photons. We have analysed various observables to give the maximum violation of Bell's inequalities for continuous-variable states. We have discussed an observable which gives the violation of Bell's inequality for any entangled pure continuous variable state. However, it does not have to be a maximally entangled state to give the maximal violation of the Bell's inequality. This is attributed to a generic problem of testing the quantum nonlocality of an infinite-dimensional state using a dichotomic observable.

A quantum teleportation scheme and an entanglement concentration protocol using entangled coherent states have been suggested. A complete Bell-state measurement, which enables quantum teleportation, computation and entanglement concentration, can be realised with an arbitrarily high precision using only linear elements. Teleportation of a coherent state qubit can be accomplished using an entangled coherent channel, photodetectors, coherent light sources, and beam splitters. A decohered entangled coherent state in a dissipative environment may be useless for quantum teleportation as it gives the optimal fidelity of teleportation less than the classical limit 2/3. The telepor-

tation scheme has been extended and applied to gate operations. It has been found that universal gate operations are possible for a coherent state qubit. Single-bit unitary transformations can be performed using beam splitters and nonlinear media, and a CNOT gate can be constructed based on teleportation protocol. Efficient readout is possible using beam splitters and coherent light sources. The quantum computation scheme has been shown to be robust to detection inefficiency. Alternatively, the universal gate operations can be achieved by linear optical elements and pre-arranged quantum channels. In this case, the photo-counting ability to discriminate between odd and even numbers of photons is required.

An entanglement purification scheme for mixed entangled coherent states has been suggested to overcome the decoherence of quantum channels. This scheme is directly applicable to mixed entangled coherent states of the Werner type, and can be useful for general mixed states using additional nonlinear interactions. We have applied it to entangled coherent states decohered in a vacuum environment and found the decay time until which they can be purified.

We have investigated an all-optical set-up to simulate a quantum random walk process using a classical light field. It was shown how to realise quantum random walks on a line by means of beam splitters, phase shifters, and photodetectors. We have analysed the proposed scheme for different kinds of input states. The process realised was shown to be equivalent to a coined quantum random walk for a single-photon state. We have found that any quantum or classical field gives rise to exactly the same pattern with a single-photon case with respect to the average photon number distribution. From this result, we have learned that a quantum random walk is understood in terms of the particle-wave duality of a quantum particle.

Finally, the generation of propagating optical cat states in optical systems was studied. The propagating cat state is useful for various application of quantum information processing. However, insufficient nonlinear strength has been pointed out as the main obstacle to generate such a state. We have suggested a scheme to generate a cat state using relatively small nonlinearity compared with the currently required level using beam splitters and homodyne detection. It was found that the required nonlinear effect to generate a useful cat state with $\alpha \gtrsim 20$ and $F \gtrsim 0.9$ may be reduced to less than $1/20$. An

alternative scheme was suggested to reduce the required nonlinear effect based on the scheme in Ref. [207] using a two-mode nonlinear interaction and a single photon state. We have found that the required nonlinear effect for the cat state generation with $\alpha \simeq 40$ may be reduced by 100 times but the success probability becomes low depending on the coherent amplitude of the desired state.

The approach to quantum information processing using coherent states and their entanglement is still being developed and refined. For example, Matsko *et al.* [225] and Paternostro *et al.* [222] made a meaningful progress in generating the cat state. Ralph *et al.* presented an improved and extended version of the coherent-state quantum computation including an error correcting scheme [226]. The teleportation scheme developed in the dissertation does not seem to be far from experimental realisation. As we have discussed, there are a few different approaches and a lot of suggestions for the implementation of quantum information processing. It is hard to predict which will eventually survive and which will perish. However, we have seen fruitful by-products out of each approach including deeper understanding of quantum physics itself. This dissertation might be understood as one of those endeavours.

Bibliography

[1] A. Einstein, B. Podolsky and N. Rosen, Phys. Rev. **47**, 777 (1935).

[2] J. S. Bell, Physics **1**, 195 (1964).

[3] R. Feynman, Physics **21** 6 & 7, 467.

[4] P. Shor, in *Proceedings of the 35th Annual Symposium on Foundation of Computer Science* (IEEE Computer Society Press, Santa Fe, NM, 1994).

[5] L. K. Grover, Phys. Rev. Lett. **79**, 325 (1997).

[6] A. Barenco, D. Deutsch, A. Ekert and R Jozsa, Phys. Rev. Lett. **74**, 4083 (1995).

[7] C. H. Bennett, G. Brassard, C. Crépeau, R. Jozsa, A. Peres and W. K. Wootters, Phys. Rev. Lett. **70**, 1895 (1993).

[8] D. Bouwmeester, J. W. Pan, K. Mattle, M. Eibl, H. Weinfurter and A. Zeilinger, Nature **390**, 575 (1997).

[9] D. Boschi, S. Branca, F. De Martini, L. Harcy and S. Popescu, Phys. Rev. Lett. **80**, 1121 (1998).

[10] C. H. Bennett and G. Brassard, *Proceedings of IEEE International Conference on Computers, System and Signal Processing*, 175 (December, 1984)

[11] A. Ekert, Phys. Rev. Lett. **67**, 661 (1991).

[12] G. E. Moore, Electronics, April 19 (1965).

[13] Lecture 1, David Deutsch lectures on quantum physics, available at http://camb.qubit.org.

[14] E. Knill and R. Laflamme, Phys. Rev. A **55**, 900 (1997); D. Gottesman, Phys. Rev. A **54** 1862 (1996); A. R. Calderbank, E. M. Rains, N. J. A. Sloane and P. W. Shor. Phys. Rev. Lett. **78** 405 (1997); A. M. Steane, *IEEE Transactions on Information Theory* **45**, 2492 (1999).

[15] C. H. Bennett, D. P. DiVincenzo, J. A. Smolin and W. K. Wootters, Phys. Rev. A **54**, 3824 (1996).

[16] I. L. Chuang, L. M. K. Vandersypen, X. Zhou, D. W. Leung and S. Lloyd, Nature *393*, 143-146 (1998).

[17] J. A. Jones and M. Mosca, J. Chem. Phys. **109** 1 (1998).

[18] L. M. K. Vandersypen, M. Steffen, G. Breyta, C. S. Yannoni, M. H. Sherwood and I. L. Chuang, Nature **414** 883 (2001).

[19] J. Hogan, Nature **424**, 484 (2003).

[20] S. J. Freedman and J. F. Clauser, Phys. Rev. Lett. **28**, 938 (1972); A. Aspect, P. Grangier and G. Roser, Phys. Rev. Lett. **47**, 460 (1981).

[21] Y. H. Shih and C. O. Alley, Phys. Rev. Lett. **61**, 2921 (1988); Z. Y. Ou and L. Mandel, Phys. Rev. Lett. **61**, 50 (1988); J. G. Rarity and P. R. Tapster, Phys. Rev. Lett. **64**, 2495 (1990).

[22] P. R. Tapster, J. G. Rarity and P. C. M. Owens, Phys. Rev. Lett. **73**, 1923 (1994); W. Tittel, J. Brendel, H. Zbinden and N. Gisin, Phys. Rev. Lett. **81**, 3563 (1998); G. Weihs, T. Jennewein, C. Simon, H. Weinfurter and A. Zeilinger, Phys. Rev. Lett. **81**, 5039 (1998).

[23] M. Aspelmeyer, H. R. Böhm, T. Gyatso, T. Jennewein, R. Kaltenbaek, M. Lindenthal, G. Molina-Terriza, A. Poppe, K. Resch, M. Taraba, R. Ursin, P. Walther and A. Zeilinger, Science **301** 621 (2003).

[24] C. H. Bennett, F. Bessette, G. Brassard, L. Salvail and J. Smolin, Journal of Cryptology **5**, 3 (1992).

[25] A. Shields *et al.*, Conference on Lasers and Electro-Optics (CLEO) in Baltimore, Maryland, US (2003).

[26] *Quantum Computing Roadmap Overview, Quantum Information Science and Technology Roadmap Project*, Quantum Information Science Technology Experts Panel, Los Alamos National Lab (available at http://qist.lanl.gov, 2002); *Optical Approaches to Quantum Information Processing and Quantum Computing, Quantum Information Science and Technology Roadmap Project*, Edited by T. Heinrichs, Compiled by G. Milburn and P. Kwiat, Los Alamos National Lab (available at http://qist.lanl.gov, 2002) and references therein.

[27] E. Knill, R. Laflamme and G. J. Milburn, Nature **409**, 46 (2001).

[28] T. C. Ralph, Phys. Rev. A **61**, 010303(R) (2000).

[29] F. Grosshans and P. Grangier, Phys. Rev. Lett. **88** 057902 (2002).

[30] Ch. Silberhorn, T. C. Ralph, N. Lütkenhaus, G. Leuchs Phys. Rev. Lett. **89**, 167901 (2002).

[31] A. Furusawa, J. L. Sørensen, S. L. Braunstein, C. A. Fuchs, H. J. Kimble and E. S. Polzik, Science **282**, 706 (1998).

[32] S. L. Braunstein and H. J. Kimble, Phys. Rev. Lett. , **80**, 869 (1998).

[33] C. E. Shannon, *Bell System Tech.* F.. 27 329, 623 (1948).

[34] R. Feynman, R. Leighton and M. Sands *The Feynman Lectures on Physics Vol. III*, Ch. 1, (Addison Wesley, Reading, 1965).

[35] L. Hardy, Phys. Rev. Lett. **68**, 2981 (1992).

[36] A. Whitaker, Einstein, Bohr and the Quantum Dilemma, Cambridge University Press (1996).

[37] P. L. Knight, Nature **395**, 12 (1998) and references therein.

[38] S. Dürr, T. Nonn and G. Rempe, Nature **395** 33 (1998).

[39] Y. Aharonov, A. Botero. S. Popescu, B. Reznik and J. Tollaksen, Physics Letters A **301**, 130 (2002).

[40] W. K. Wootters and W. H. Zurek, Nature **299**, 802 (1982).

[41] A. Peres, *Quantum Theory: Concepts and Methods*, Kluwer Academic Publishers (1993).

[42] W. H. Zurek, Physics Today **46**(4), 13, 81 (1993).

[43] C. Bennett, H. J. Bernstein, S. Popescu and B. Schumacher, Phys. Rev. A **53**, 2046 (1996).

[44] J. Pan, C. Simon, Č. Brukner and A. Zeilinger

[45] E. Schrödinger, Proceedings of the Cambridge Philosophical Society **31** (1935): 555-563; **32** (1936): 446-451.

[46] A. Peres, Phys. Rev. Lett. **77**, 1413 (1996); M. Horodecki, P. Horodecki and R Horodecki, Phys. Lett. A **223**, 1 (1996).

[47] P. Horodecki, Phys. Lett. A **232**, 233 (1997).

[48] C. H. Bennett, D. P. DiVincenzo, T. Mor, P. W. Shor, J. A. Smolin and B. M. Terhal, Phys. Rev. Lett. **82**, 5385 (1999).

[49] V. Vedral and M. B. Plenio, Phys. Rev. A **57**, 1619 (1998).

[50] W. K. Wooters, Phys. Rev. Lett. **80**,2245 (1998).

[51] B. M. Terhal and K. G. H. Vollbrecht, Phys. Rev. Lett. **85**, 2625 (2000).

[52] K. G. H. Vollbrecht and R. F. Werner, Phys. Rev. A **64**, 062307 (2000).

[53] M. Horodecki, P. Horodecki, R. Horodecki, Phys. Rev. Lett. **84** (2000) 2014.

[54] J. Lee and M. S. Kim, Phys. Rev. Lett. **84**, 4236 (2000); J. Lee, M. S. Kim, Y. -J. Park and S. Lee, J. Mod. Opt. **47**, 2151 (2000).

[55] G. Vidal and R. F. Werner, Phys. Rev. A **65**, 032314 (2002)

[56] L.-M. Duan, G. Giedke, J. I. Cirac and P. Zoller, Phys. Rev. Lett. **84**, 2722 (2000).

[57] R. Simon, Phys. Rev. Lett. **84**, 2726 (2000).

[58] G. Giedke, B. Kraus, M. Lewenstein and J. I. Cirac, Phys. Rev. Lett. **87**, 167904 (2001)

[59] G. Giedke, M. M. Wolf, O. Krügger, R. F. Werner and J. I. Cirac, to be published in Phys. Rev. Lett. , quan-ph/0304042 (2003)

[60] J. Sancho, S. Huelga, Phys. Rev. A **61**, 042303 (2000).

[61] P. Horodecki and A. Ekert, Phys. Rev. Lett. **89**, 127902 (2002).

[62] O. Gühne, P. Hyllus, D. Bruss, A. Ekert, M. Lewenstein, C. Macchiavello and A. Sanpera, Phys. Rev. A **66**, 062305 (2002).

[63] M. S. Kim, J. Lee and W. J. Munro, Phys. Rev. A **66**, R030301 (2002).

[64] K. E. Cahill and R. J. Glauber, Phys. Rev. **177**, 1857 (1969).

[65] T. Rudolph and B. C. Sanders, Phys. Rev. Lett. **87**, 077903 (2001).

[66] P. Kok and S. L. Braunstein, Phys. Rev. A **61**, 042304 (2000).

[67] K. Mϕlmer, J. Mod. Opt. **44** 1937 (1997); Phys. Rev. A **55** 3195 (1997).

[68] S. J. van Enk and C. A. Fuchs, Phys. Rev. Lett. **88**, 027902 (2002).

[69] H. M. Wiseman, J. Mod. Opt. **50**, 1797 (2003).

[70] B. C. Sanders, Phys. Rev. A **45**, 6811 (1992); B. C. Sanders, K. S. Lee and M. S. Kim, Phys. Rev. A **52**, 735 (1995).

[71] B. Yurke and D. Stoler, Phys. Rev. Lett. **57**, 13 (1986).

[72] L. Davidovich, A. Maali, M. Brune, J. M. Raimond and S. Haroche, Phys. Rev. Lett. **71**, 2360 (1993).

[73] S. J. van Enk and O. Hirota, Phys. Rev. A **64**, 022313 (2001).

[74] X. Wang, Phys. Rev. A **64**, 022302 (2001).

[75] H. Jeong, M. S. Kim and J. Lee, Phys. Rev. A **64**, 052308 (2001).

[76] H. Jeong and M. S. Kim, Phys. Rev. A **65**, 042305 (2002).

[77] T. C. Ralph, W. J. Munro and G. J. Milburn, e-print quant-ph/0110115.

[78] H. Jeong and M. S. Kim, Quantum Information and Computation **2**, 208 (2002).

[79] O. Hirota and M. Sasaki, e-print quant-ph/0101018;O. Hirota, S. J. van Enk, K. Nakamura, M. Sohma and K. Kato, e-print quant-ph/0101096.

[80] X. Wang (2001), J. Phys. A: Math. Gen. **35(1)**, 165 (2002).

[81] S. Parker, S. Bose and M.B. Plenio, Phys. Rev. A. 61, 32305 (1999).

[82] D. Vitali, M. Fortunato and P. Tombesi, Phys. Rev. Lett. **85** 445 (2000).

[83] Y. -H. Kim, S. P. Kulik and Y. Shih, Phys. Rev. Lett. **86**, 1370 (2001); J. Mod. Opt. **49**, 221 (2001).

[84] N. Lütkenhaus, J. Calsamiglia and K.-A. Suominen, Phys. Rev. A **59**, 3295 (1999).

[85] S. L. Braunstein and A. Mann, Phys. Rev. A **51**, R1727 (1995).

[86] K. Mattle, H. Weinfurter, P. G. Kwiat and A, Zeilinger, Phys. Rev. Lett. **76**, 4656 (1996).

[87] K. J. Resch, J. S. Lundeen and A. M. Steinberg, Phys. Rev. A **63** 020102(R) (2001).

[88] P. G. Kwiat, A. M. Steinberg and R. Y. Chiao, Phys. Rev. A **48**, R867 (1993).

[89] S. Takeuchi, Y. Yamamoto and H. H. Hogue (1999), Appl. Phys. Lett. **74**, 1063 (1999).

[90] P. Kok and S. L. Braunstein, Phys. Rev. A **63**, 033812 (2001).

[91] J. Kim, S Takeuchi, Y. Yamamoto and H. H. Hogue, Appl. Phys. Lett. **74**, 902 (1999).

[92] J. F. Clauser, M. A. Horne, A. Shimony and R. A. Holt, Phys. Rev. Lett. **23**, 880 (1969).

[93] J. F. Clauser and M. A. Horne, Phys. Rev. D **10**, 526 (1974).

[94] G. Weihs, T. Jennewin, C. Simon, H. Weinfurter, and A. Zeilinger, Phys. Rev. Lett. **81**, 5039 (1998); A. Aspect, Nature **398**, 189 (1999).

[95] A. Garg and N. D. Mermin, Phys. Rev. D **35**, 3831 (1987).

[96] J. Larsson, Phys. Rev. A **57**, 3304 (1998).

[97] A. Aspect, J. Dalibard and G. Roger, Phys. Rev. Lett. **49**, 1804-1807 (1982); P. R. Tapster, J. G. Rarity and P. C. M. Owens, Phys. Rev. Lett. **73**, 1923-1926 (1994); A. Aspect, Nature **398**, 189-190 (1999).

[98] M. A. Rowe, D. Kielpinski, V. Meyer, C. A. Sackett, W. M. Itano, C. Monroe and D. J. Wineland, Nature **409**, 791 (2001) and references therein.

[99] A. Mann, B. C. Sanders, and W. J. Munro, Phys. Rev. A **51**, 989 (1995).

[100] B. Yurke and D. Stoler, Phys. Rev. Lett. **79**, 4941 (1997); A. Gilchrist, P. Deuar and M. D. Reid, Phys. Rev. Lett. **80**, 3169 (1998); W. J. Munro, Phys. Rev. A **59**, 4197 (1999).

[101] K. Banaszek and K. Wódkiewicz, Phys. Rev. A **58**, 4345 (1998).

[102] K. Banaszek and K. Wódkiewicz, Phys. Rev. Lett. **99**, 2009 (1999).

[103] Z. Y. Ou, S. F. Pereira, H. J. Kimble, and K. C. Peng, Phys. Rev. Lett. **68**, 3663 (1992).

[104] S. L. Braunstein, A. Mann and M. Revzen, Phys. Rev. Lett. **68**, 3259 (1992).

[105] L. J. Landau, Phys. Lett. A **120**, 54 (1987).

[106] B. S. Cirel'son, Lett. Math. Phys. **4**, 93 (1980).

[107] H. Moya-Cessa and P. L. Knight, Phys. Rev. A **48**, 2479 (1993); B.-G. Englert, N. Sterpi, and H. Walther, Opt. Commun. **100**, 526 (1993).

[108] W. H. Press, B. P. Flannery, S. A. Teukolsky and W. T. Vetterling, *Numerical Recipes* (Cambridge University Press, Cambridge, 1988).

[109] H. Jeong, J. Lee and M. S. Kim, Phys. Rev. A **61**, 052101 (2000).

[110] N. Gisin, Phys. Lett. A **154**, 201 (1991).

[111] S. J. D. Phoenix, Phys. Rev. A **41**, 5132 (1990).

[112] W. J. Munro, G. J. Milburn and B. C. Sanders, Phys. Rev. A **62**, 052108 (2000); D. A. Rice, G. Jaegar and B. C. Sanders, Phys. Rev. A **62**, 012101 (2001).

[113] R. Horodecki, P. Horodecki and M. Horodecki, Phys. Lett. A **200**, 340 (1995).

[114] S. Popescu, Phys. Rev. Lett. **72**, 797 (1994); R. Horodecki, P. Horodecki and M. Horodecki, Phys. Lett. A **200**, 340 (1995).

[115] Z. Chen, J. Pan, G. Hou and Y. Zhang, Phys. Rev. Lett. , **88**, 040406 (2002).

[116] P. T. Cochrane, G. J. Milburn and W. J. Munro, Phys. Rev. A **59**, 2631 (1999).

[117] W. J. Munro, G. J. Milburn, and B. C. Sanders, Phys. Rev. A **62**, 052108 (2000).

[118] S. Lloyd and S. L. Braunstein, Phys. Rev. Lett. **82**, 1784 (1999).

[119] C. M. Caves, K. S. Thorne, R. W. P. Drever, V. D. Sandberg and M. Zimmermann, Rev. Mod. Phys. **52**. 341 (1980).

[120] C. Caves and B. L. Schumacher, Phys. Rev. A **31**, 3093 (1985).

[121] S. M. Barnett and P. L. Knight, J. Mod. Opt. **34**, 841 (1987).

[122] D. F. Walls and G. J. Milburn, *Quantum Optics* (Springer, Berlin, 1994).

[123] M. S. Kim and N. Imoto, Phys. Rev. A. **52**, 2401(1995).

[124] J. Janszky and A. V. Vinogradov, Phys. Rev. Lett. **64**, 2771 (1990); V. Bužek and P. L. Knight, Opt. Commun. **81**, 331 (1991).

[125] M. S. Kim and V. Bužek, Phys. Rev. A **46**, 4239 (1992).

[126] N. Gisin and A. Peres, Phys. Lett. A **162**, 15 (1992).

[127] A. Kuzmich, I. A. Walmsley and L. Mandel, Phys. Rev. Lett. **85**, 1349 (2000).

[128] H. Halvorson, Lett. Math. Phys. **53**, 321 (2000).

[129] D. Wilson, H. Jeong and M. S. Kim, J. Mod Opt **49** 851 (2002).

[130] N. Gisin, Phys. Lett A **154**, 201 (1991).

[131] S. M. Barnett and P. L. Knight, J. Mod. Opt. **34**, 841 (1987).

[132] K. E. Cahill and R. J. Glauber. Phys. Rev. **177**, 1875 (1969).

[133] A. Cabello, Phys. Rev. Lett. **88** 060403 (2002).

[134] P. H. Eberhard, Phys. Rev. A **47**, R747 (1993).

[135] R. Filip and L. Mišta Jr. eprint quan-ph/0201114, (2002).

[136] D. T. Smithey, M. Beck, M. G. Raymer and A. Faridani, Phys. Rev. Lett. **70**, 1244 (1993).

[137] K. Banaszek, A. Dragan, K. Wódkiewicz, and C. Radzewicz, Phys.Rev.A **66**, 043803 (2002).

[138] J. Larsson, preprint quant-ph/0208125, to be published in Phys.Rev.A.

[139] L. Vaidman, Phys. Rev. A. **49**, 1473(1994).

[140] T. Rudolph and B.C. Sanders, Phys. Rev. Lett. **87**, 077903 (2001).

[141] S.J. van Enk and C.A. Fuchs, Phys. Rev. Lett. **88**, 027902 (2002).

[142] M. A. Nielson, E. Knill and R. Laflamme, Nature **396**, 52 (1998).

[143] S. Bose, P. L. Knight, M. B. Plenio and V. Vedral, Phys. Rev. Lett. **83** 5158 (1999).

[144] C. H. Bennett, S. Popescu, B. Schumacher, J. A. Smolin and W. K. Wootters, Phys. Rev. Lett. **76**, 722 (1996).

[145] S. Bose, V. Vedral and P. L. Knight Phys. Rev. A **60**, 194 (1999).

[146] M. Zukowski, A. Zeilinger, M. A. Horne and A. K. Ekert, Phys. Rev. Lett. **71**, 4287 (1993).

[147] R. Horodecki and M. Horodecki and P. Horodecki. Phys. Lett. A **222**, 21 (1996); R. Horodecki and M. Horodecki, Phys. Rev. A **54**, 1838 (1996).

[148] R. Horodecki, P. Horodecki and M. Horodecki, Phys. Rev. A **60**, 1888 (1999).

[149] M. Horodecki, P. Horodecki and R. Horodecki, Phys. Rev. Lett. **78**, 574 (1997).

[150] S. Bose and V. Vedral, Phys. Rev. A **61**, 040101(R) (2000).

[151] N. Gisin, Phys. Lett. A **210**, 151 (1996).

[152] S. Parker, S. Bose and M. B. Plenio Phys. Rev. A **61**, 32305 (2000).

[153] J. Lee, M. S. Kim and H. Jeong, Phys. Rev. A **62**, 032305 (2000).

[154] J. Lee, M. S. Kim and H. Jeong, Phys. Rev. A **62**, 032305 (2000).

[155] Y. Aharonov and D. Albert, Phys. Rev. D **21**, 3316 (1980); *ibid.* **24**, 359 (1981); Y. Aharonov, D. Albert and L. Vaidman, *ibid.* **34**, 1805 (1986).

[156] S. Popescu, Phys. Rev. Lett. **72**, 797 (1994); N. Gisin, Phys. Lett. A **210**, 157 (1996); R. Horodecki, M. Horodecki and P. Horodecki, *ibid.* **222**, 21 (1996).

[157] Lu-Ming Duan, G. Giedke, J. I. Cirac and P. Zoller, e-print quant-ph/9908056 (1999).

[158] L. Mandel, Phys. Scr. **T12**, 34 (1986).

[159] C. T. Lee, Phys. Rev. A **44**, R2775 (1991); N. Lütkenhaus and S. M. Barnett, *ibid.* **51**, 3340 (1995).

[160] J. Janszky, M. G. Kim and M. S. Kim, Phys. Rev. A **53**, 502 (1996).

[161] K. E. Cahill and R. J. Glauber, Phys. Rev. **177**, 1882 (1969).

[162] L.-M. Duan, G. Giedke, J. I. Cirac and P. Zoller, e-print quant-ph/9912017.

[163] W. J. Munro, G. J. Milburn and B. C. Sanders, Phys. Rev. A **62**, 052108 (2000); M. C. de Oliveira and W. J. Munro, Phys. Rev. A. **61**, 042309 (2000).

[164] D. Gottesman and I. L. Chuang, Nature **402**, 390 (1999).

[165] C. Zalka, eprint quant-ph/9811006.

[166] A. Barenco, C. H. Bennett, R. Cleve, D. P. DiVincenzo, N. Margolus, P. Shor, T. Sleator, J. A. Smolin and H. Weinfurter, Phys. Rev. A **52**, 3457 (1995).

[167] R. Landauer, IBM journal of Research and Development **5**, 183 (1961); C.H. Bennett, IBM journal of Research and Development **32**, 16 (1988).

[168] D. P. DiVincenzo, Phys. Rev. A **51**, 1015 (1995).

[169] D. Deutsch, Proc. R. Soc. London A **400**,97 (1985).

[170] D. Deutsch and R. Jozsa, Proc. R. Soc. London A **439**, 553 (1992).

[171] D. P. DiVincenzo, preprint quant-ph/0002077.

[172] N. A. Gershenfeld and I. L. Chuang, Science **275** 350 (1997); I. L. Chuang, N. Gershenfeld , M. G. Kubinee and D. W. Leung, Proc. Roy. Soc. London **A454**, 447 (1998); D. G. Cory, M. D. Price and T. F. Havel, Physica D **120**, 82 (1997); D. G. Cory, A. F. Fahmy, and T. F. Havel, Proc. Nat. Acad. Sci. USA, **94**, 1634 (1997); E. Kinll, I. Chuang and R. Laflamme, Phys. Rev. A **57**, 3348 (1998).

[173] J. I. Cirac and P. Zoller, Phys. Rev. Lett. **74**, 4091 (1995).

[174] I. H. Deutsch and P. S. Jessen, Phys. Rev. A **57**, 1972 (1998); D. Jaksch, H. -J. Briegel, J. I. Cirac, C. W. Gardiner and P. Zoller, Phys. Rev. Lett. **82**, 1975 (1999); D. Jaksch, J. I. Cirac, P. Zoller, S. L. Rolston, R. Côté and M. D. Lukin, Phys. Rev. Lett. **85**, 2208 (2000).

[175] I. L. Chuang and Y. Yamamoto, Phys. Rev. A bf 52 3489 (1995).

[176] B. E. Kane, Nature **393**, 133 (1998).

[177] L.V. Hau, S.E. Harris, Z. Dutton and C.H. Behroozi, Nature **397**, 594 (1999).

[178] T. B. Pittmann, B. C. Jacobs and J. D. Franson, Phys. Rev. Lett. **88**, 257902 (2002); T. C. Ralph, A. G. White, W. J. Munro and G. J. Milburn, Phys. Rev. A **65**, 012314 (2002); T. B. Pittman, B. C. Jacobs and J. D. Franson, Phys. Rev. A **64**, 062311 (2001); T. C. Ralph, N. K. Langford, T. B. Bell and A. G. White, Phys. Rev. A bf 65, 062324 (2002).

[179] P. Michler, A. Kiraz, C. Becher, W. V. Schoenfeld, P. M. Petroff, L. Zhang, E. Hu and A. Imamoglu, Science **290**, 2282 (2000); C. Santori, M. Pelton, G. Solomon, Y. Dale, and Y. Yamamoto, Phys. Rev. Lett. **86**, 1502 (2001); Z. Yuan, B. E. Kardynal, R. M. Stevenson, A. J. Shields, C. J. Lobo, K. Cooper, N. S. Beattie, D. A. Ritchie and M. Pepper, Science **295**, 102 (2002).

[180] A. Kuhn, M. Hennrich and G. Rempe, Phys. Rev. Lett. **89**, 067901 (2002).

[181] G. B. Arfken, *Mathematical Method for Physicists, 3rd edition,* p257 (Academic, New York, 1985).

[182] R. Laflamme, C. Miquel, J. P. Paz and W. H. Zurek, Phys. Rev. Lett. **77**, 198 (1996).

[183] J.-W. Pan, S. Gasparoni, R. Ursin, G. Weihs and A. Zeilinger, Nature **423**, 417 (2003)

[184] Lu-Ming Duan, G. Giedke, J. I. Cirac and P. Zoller Phys. Rev. Lett. 84, 4002 (2000).

[185] Lu-Ming Duan, G. Giedke, J. I. Cirac and P. Zoller Phys. Rev. A **62**, 032304 (2000).

[186] D.E. Browne, J. Eisert, S. Scheel and M.B. Plenio, Phys. Rev. A **67**, 062320 (2003).

[187] J. Eisert, D. Browne, S. Scheel and M.B. Plenio, preprint quant-ph/0307106.

[188] J. Eisert, S. Scheel and M.B. Plenio, Phys. Rev. Lett. **89**, 137903 (2002); J. Fiurasek, Phys. Rev. Lett. **89**, 137904 (2002); .I. Cirac, Phys. Rev. A **66**, 032316 (2002).

[189] R.F. Werner (1989) Phys. Rev. A **40**, 4277 (1989).

[190] X. Wang and B.C. Sanders, Phys. Rev. A **65**, 012303 (2001).

[191] M. Murao, M.B. Plenio, S. Popescu, V. Vedral and P.L. Knight, Phys. Rev. A. **57**, R4075 (1998).

[192] L. Mandel and E. Wolf, *Optical coherence and quantum optics* (Cambridge University Press, 1995).

[193] U. Schöning, *Proceedings of the 40th Annual Symposium on Foundations of Computer Science*, New York, NY, 1999; M. Jerrum, A. Sinclair, E. Vigoda, *Proceedings of the 33rd ACM Symposium on Theory of Computing*, 2001.

[194] E. F. Fama, Financial Analysists Journal, September/October (1965).

[195] A. Ambainis, E. Bach, A. Nayak, A. Vishwanath and J. Watrous, *Proceedings of 33rd STOC* (Assoc. for Comp. Machinery, New York, 2001); D. Aharanov, A. Ambainis, J. Kempe and U. Vazirani, *ibidem*; J. Kempe, quant-ph/0205083.

[196] J. Kempe, quant-ph/0303081 (to appear in *Contemporary Physics*).

[197] B. C. Travaglione, *Phys. Rev. A* **65**, 032310 (2002); W. Dür, R. Raussendorf, V. M. Kendon, and H.-J. Briegel, *Phys. Rev. A* **66**, 052319 (2002); B. C. Sanders, S. D. Bartlett, B. Tregenna and P. L. Knight, *Phys. Rev. A* **67**, 042305 (2003).

[198] Z. Zhao, J. Du, H. Li, T. Yang, Z.-B. Chen and J.-W. Pan, quant-ph/0212149.

[199] P. G. Kwiat, J. R. Mitchell, P. D. D. Schwindt and A. G. White, J. Mod. Opt **47**, 257 (2000).

[200] M. Hillery, J. Bergou and E. Feldman, quant-ph/0302161.

[201] A. M. Childs, E. Deotto, E. Farhi, J. Goldstone, S. Gutmann and A. J. Landahl, *Phys. Rev. A* **66**, 032314 (2002); N. Shenvi, J. Kempe and K. B. Whaley quant-ph/0210064 (to appear in *Phys. Rev. A*).

[202] A. Stefanov, H. Zbinden, N. Gisin and A. Suarez, *Phys. Rev. Lett.* **88**, 120404 (2002).

[203] M. S. Kim, W. Son, V. Bužek and P. L. Knight, *Phys. Rev. A* **65**, 032323 (2002).

[204] M. O. Scully and M. S. Zubairy, *Quantum optics* (Cambridge University Press, 1997).

[205] P. L. Knight, E. Roldan and J. E. Sipe, preprint quant-ph/0304201.

[206] H. Jeong, W. Son, M. S. Kim, D. Ahn and C. Brukner, Phys. Rev. A **67**, 012106 (2003).

[207] C. C. Gerry Phys. Rev. A **59**, 4095 (1999).

[208] B. C. Sanders and G. J. Milburn, Phys. Rev. A **45**, 1919 (1992).

[209] K. S. Lee, M. S. Kim, S. -D. Lee and V. Buzěk, J. Kor. Phys. Soc. **26**, 197 (1993).

[210] F. König, private communication.

[211] N. Korolkova, R. Loudon, G. Gardavsky, M. W. Hamilton and G. Leuchs, J. Mod. Optics. **48** 1339.

[212] *Photonic Crystals Down Under*, http://wwwrsphysse.anu.edu.au/nonlinear /meeting/about.shtml, Nonlinear Optics Group headed by Y. S. Kivshar, Australian National University.

[213] See http://irfibers.rutgers.edu, Laboratory for the Development of Specialty Fiber Optics headed by J. A. Harrington, The State University of New Jersey (Rutgers).

[214] S. Song, C. M. Caves amd B. Yurke, Phys. Rev. A. **41**, 5261 (1990).

[215] M. Dakna, T. Opatrný, L. Knöll and D. -G. Welsh, Phys. Rev. A. **55**, 3184 (1997).

[216] Q.A. Turchette, C.J. Hood, W. Lange, H. Mabuchi and H.J. Kimble, Phys. Rev. Lett. **75**, 4710 (1995).

[217] M. Brune, E. Hagley, J. Dreyer, X. Maître, A. Maali, C. Wunderlich, J.M. Raimond, and S. Haroche, Phys. Rev. Lett. **77**, 4887 (1996).

[218] C. Monroe, D.M. Meekhof, B.E. King and D.J. Wineland, Science **272**, 1131 (1996).

[219] E. Solano, R.L. de Matos Filho and N. Zagury, Phys. Rev. Lett. **87**, 060402 (2001).

[220] N. Korolkova, R. Loudon, G. Gardavsky, M.W. Hamilton and G. Leuchs, J. Mod. Opt. **48**, 1339 (2001).

[221] H. Schmidt and A. Imamoğlu, Opt. Lett. **21**, 1936 (1996); M.D. Lukin and A. Imamoğlu, Phys. Rev. Lett. **84**, 1419 (2000) and references therein.

[222] M. Paternostro, M. S. Kim and G. M. Palma Phys. Rev. A **67**, 023811 (2003).

[223] B. C. Sanders and D. A. Rice, Phys. Rev. A **61**, 013805 (1999).

[224] B. C. Sanders and G. J. Milburn, Phys. Rev. A **45**, 1919 (1992).

[225] A. B. Matsko, I. Novikova, G. R. Welch and M. S. Zubairy Optics Letters **28**, 96 (2003)

[226] T.C. Ralph, A. Gilchrist, G.J. Milburn, W.J. Munro and S. Glancy, preprint quant-ph/0306004.

[227] W. J. Munro, K. Nemoto, G. J. Milburn and S. L. Braunstein, Phys. Rev. A **66**, 023819 (2002).

APPENDICES

Appendix A

Rotations around the x-axis for even and odd cat states

In a few previous papers [116, 117, 227] for a couple of different purposes, the authors approximated the effect of the displacement operator to be a rotation around the x axis of the even- and odd-cat state basis assuming large coherent amplitudes. The action of a classical force was represented by the unitary displacement operator. In this Appendix, we show a mistake in this approximation and correct it.

Their argument [116, 117, 227] can be explained as follows. Two orthogonal cat states are defined as

$$|+\rangle = \mathcal{N}_+(|\alpha\rangle + |-\alpha\rangle), \tag{A.1}$$

$$|-\rangle = \mathcal{N}_-(|\alpha\rangle - |-\alpha\rangle), \tag{A.2}$$

where $|\pm\alpha\rangle$ are coherent states of coherent amplitudes $\pm\alpha$ and $\mathcal{N}_\pm$ are normalization factors. We assume $\alpha \gg 1$ for which the normalization factors $\mathcal{N}_\pm$ approach to $1/\sqrt{2}$. The coherent amplitude α is assumed to be real for simplicity. These assumptions are taken throughout this Appendix following [227].

Consider a displacement operator $D(i\epsilon)$ where ϵ is taken to be real. Then,

the effect of the displacement operator on the even cat state is

$$\begin{aligned} D(i\epsilon)|+\rangle &= D(i\epsilon)\frac{1}{\sqrt{2}}(|\alpha\rangle + |-\alpha\rangle) \\ &= \frac{1}{\sqrt{2}}(e^{i\alpha\epsilon}|\alpha + i\epsilon\rangle + e^{-i\alpha\epsilon}|-\alpha + i\epsilon\rangle). \end{aligned} \tag{A.3}$$

Here, Munro *et al.* made an important approximation as [227]

$$D(i\epsilon)|+\rangle \approx \frac{1}{\sqrt{2}}(e^{i\theta}|\alpha\rangle + e^{-i\theta}|-\alpha\rangle) \tag{A.4}$$

where $\theta = \alpha\epsilon$. If approximation (A.4) is satisfactory, then

$$D(i\epsilon)|+\rangle \approx \cos\theta|+\rangle + i\sin\theta|-\rangle \equiv |+'\rangle \tag{A.5}$$

which corresponds to the rotation around the x axis.

The above argument seems even clearer as follows. The fidelity $|\langle\psi_1|\psi_2\rangle|^2$ between two given states $|\psi_1\rangle$ and $|\psi_2\rangle$ is a measure of closeness between the states. If we assess fidelities between $|\alpha\rangle$ and $|\alpha + i\epsilon\rangle$ and between $|-\alpha\rangle$ and $|-\alpha + i\epsilon\rangle$ for $\alpha \gg 1$, we obtain

$$|\langle\alpha|\alpha + i\epsilon\rangle|^2 = |\langle -\alpha|-\alpha + i\epsilon\rangle|^2 = e^{-\epsilon^2}, \tag{A.6}$$

which depends only on ϵ. Note that only very small amount of ϵ is required to make one cycle for $\alpha \gg 1$. Therefore, we can clearly say

$$|\alpha\rangle \approx |\alpha + i\epsilon\rangle, \tag{A.7}$$

$$|-\alpha\rangle \approx |-\alpha + i\epsilon\rangle, \tag{A.8}$$

which seems to be enough to justify Eq. (A.4).

However, even though Eqs. (A.7) and (A.8) are true from Eq. (A.6), one cannot jump to Eq. (A.4). First, we can directly assess how close the state of the left-hand side and the state in the right-hand side in Eq. (A.4) are as

$$\begin{aligned} |\langle +'|D(i\epsilon)|+\rangle|^2 &= e^{-\epsilon^2}\cos^2\alpha\epsilon(1 + e^{-2\alpha^2})^2 \\ &\approx e^{-\epsilon^2}\cos^2\alpha\epsilon, \end{aligned} \tag{A.9}$$

where we find an periodic term $\cos^2 \alpha\epsilon$ which is not found in Eq. (A.6). For the two states to be close, not only $\epsilon \ll 1$ but also $\alpha\epsilon \ll 1$ is required. However, because α is assumed to be very large, even a small amount of ϵ can cause a significant difference between the two states in Eq. (A.9). For Eq. (A.4) to be true, both α and ϵ should be small. This is in contradiction to the assumption $\alpha \gg 1$, and even impossible because small α may cause large ϵ for a given rotation angle. Therefore, the approximation (A.4) does not hold in general.

Now, we need to obtain a proper approximation of Eq. (A.3) in terms of $|+\rangle$ and $|-\rangle$. It should be noted that $|+\rangle$ and $|-\rangle$ are treated like a two-dimensional basis in this approach. This means the identity $\mathbb{1}$ should be defined as

$$\mathbb{1} = |+\rangle\langle+| + |-\rangle\langle-| = |\alpha\rangle\langle\alpha| + |-\alpha\rangle\langle-\alpha|, \tag{A.10}$$

which is true under the assumption $\mathcal{N}_\pm = 1/\sqrt{2}$. From Eqs. (A.3) and (A.10), we get

$$\begin{aligned} D(i\epsilon)|+\rangle &= \mathbb{1}D(i\epsilon)|+\rangle \\ &= \frac{e^{-\epsilon^2/2}}{\sqrt{2}}\big[(e^{2i\alpha\epsilon} + e^{-2\alpha^2})|\alpha\rangle \\ &\qquad + (e^{-2i\alpha\epsilon} + e^{-2\alpha^2})|-\alpha\rangle\big] \\ &\approx \frac{e^{-\epsilon^2/2}}{\sqrt{2}}(e^{2i\alpha\epsilon}|\alpha\rangle + e^{-2i\alpha\epsilon}|-\alpha\rangle) \\ &\approx \cos\Theta|+\rangle + i\sin\Theta|-\rangle \equiv |+''\rangle \end{aligned} \tag{A.11}$$

where $\Theta = 2\alpha\epsilon$. We can simply check the fidelity

$$|\langle+''|D(i\epsilon)|+\rangle|^2 = e^{-\epsilon^2}|1 + e^{-2\alpha^2}\cos 2\alpha\epsilon|^2 \approx e^{-\epsilon^2} \tag{A.12}$$

which shows that $|+''\rangle$ is the proper approximated state for $D(i\epsilon)|+\rangle$.

Fig. A.1 shows the fidelity between $D(i\epsilon)|+\rangle$ and $|+\rangle$. It is clear that $\Theta = \pi$ makes one cycle, where $\Theta = 2\alpha\epsilon$. It is in agreement with the fact that $0 \le \Theta < \pi$ makes one cycle for a two-level state $|\psi\rangle = \cos\Theta|+\rangle + \sin\Theta|-\rangle$ up to a global phase.

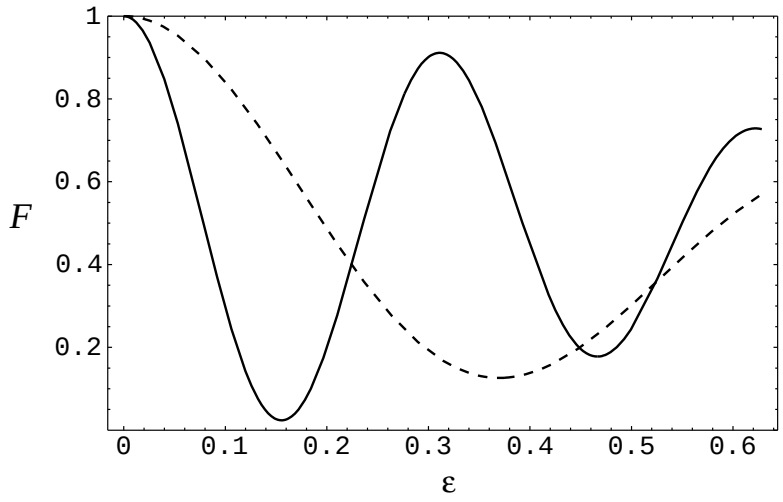

Figure A.1: The fidelity $F = |\langle +|D(i\epsilon)|+\rangle|^2$ against ϵ. $\alpha = 2$ for dashed line and $\alpha = 5$ for solid line. Here, $\Theta = \pi$ makes one cycle with $\Theta = 2\alpha\epsilon$. It is in agreement with the fact that $0 \leq \Theta < \pi$ makes one cycle for $|\psi\rangle = \cos\Theta|+\rangle + \sin\Theta|-\rangle$ up to a global phase.

Appendix B

Positivity of P function and separability for a Gaussian state

Lee *et al.* analysed separability for a Gaussian state with the positivity of the P function [154]. They showed that a mixed two-mode squeezed vacuum in the thermal environment is separable when a positive definite P function can be assigned to it.

A two-mode Gaussian state $\hat{\rho}$ of mode b and c is separable when it is represented by a statistical mixture of the direct-product states;

$$\hat{\rho} = \int d^2\xi \mathcal{P}(\xi)\hat{\rho}_b(\xi) \otimes \hat{\rho}_c(\xi) \tag{B.1}$$

where $\hat{\rho}_{b,c}(\xi)$ are density matrices, respectively, for modes b and c, and $\mathcal{P}(\xi)$ is a probability density function with $\mathcal{P}(\xi) \geq 0$. The states of $\hat{\rho}_b(\xi)$ and $\hat{\rho}_c(\xi)$ can be nonclassical and do not have to have their P functions positive well-defined. However, because they are Gaussian, it is possible to transform them to assign positive well-defined P functions by local unitary transformations[1]. The separable condition, (B.1), can then be written as

$$\hat{\rho}' = \int d^2\zeta_b \int d^2\zeta_c \int d^2\xi \mathcal{P}(\xi) P(\zeta_b;\xi) P(\zeta_c;\xi) \times |\zeta_b\rangle\langle\zeta_b| \otimes |\zeta_c\rangle\langle\zeta_c| \tag{B.2}$$

where $P_b(\zeta_b;\xi)$ and $P_c(\zeta_c;\xi)$ are the P functions, respectively, for the fields

[1] Any local unitary operations do not affect entanglement or separability of a state. By unitary transformations of *squeezing* and *rotation*, any Gaussian state becomes to be represented by its positive well-defined P function [159].

of modes b and c after some local unitary operations. $\hat{\rho}'$ is for the two-mode Gaussian state after the local operations.

We want to prove in this appendix that if and only if a two-mode Gaussian state is separable, a positive well-defined P function $P(\zeta_b, \zeta_c)$ is assigned to it after some local unitary transformations.

Consider the sufficient condition. If a two-mode Gaussian state $\hat{\rho}$ is separable, it can be written as Eq. (B.2) after some local operations. Both $P_b(\zeta_b; \xi)$ and $P_c(\zeta_c; \xi)$ are positive well-defined and $\mathcal{P}(\xi)$ is a probability density function so

$$\int d^2\xi \mathcal{P}(\xi) P(\zeta_b; \xi) P(\zeta_c; \xi) \tag{B.3}$$

is a normalized positive function, which we can take as the positive well-defined P function $P(\zeta_b, \zeta_c)$. We have proved that if a two-mode Gaussian state is separable, it has a positive well-defined P function after some local unitary operations.

Now let us prove the necessary condition. If the locally-transformed two-mode Gaussian state is represented by a positive well-defined P function $P(\zeta_b, \zeta_c)$, the separable condition (B.2) becomes

$$P(\zeta_b, \zeta_c) = \int d^2\xi \mathcal{P}(\xi) P_b(\zeta_b; \xi) P_c(\zeta_c; \xi). \tag{B.4}$$

Further by some additional squeezing and rotation it is always possible to have the rotationally-symmetric variance $[\Delta\zeta_i(\phi)]^2$ for any angle ϕ. After these transformations, the positive well-defined P function $P(\zeta_b, \zeta_c)$ can be written as

$$P(\zeta_b, \zeta_c) = \mathcal{N} \exp\Big[- \sum_{i,j=b,c} \zeta_i N_{ij} \zeta_j^* + \sum_{i=b,c} (\zeta_i \lambda_i^* + \zeta_i^* \lambda_i) \Big] \tag{B.5}$$

where $\mathcal{N}$ is the normalization constant, N_{ij} a Hermitian matrix, and λ_i a complex number. The linear terms of ζ_i are not considered because they do not affect the proof. In fact, they can always be removed by some local displacement operations. Eq. (B.5) can be written as

$$P(\zeta_b, \zeta_c) = \frac{\mathrm{Det} N_{ij}}{\pi^2} \exp\left(- \sum_{i,j=b,c} \zeta_i N_{ij} \zeta_j^* \right) \tag{B.6}$$

where $\mathrm{Det}N_{ij}$ is the determinant of the Hermitian matrix N_{ij}. To find an expression in the form of Eq. (B.4), let us introduce an auxiliary field (ξ, ξ^*) enabling the function $P(\zeta_b, \zeta_c)$ to be represented by a Gaussian integral;

$$P(\zeta_b, \zeta_c) = \frac{\mathrm{Det}N_{ij}}{\pi^3} \int d^2\xi \exp\Big(- |\xi|^2 - E_b(\zeta_b, \xi) - E_c(\zeta_c, \xi)\Big) \tag{B.7}$$

where

$$\begin{aligned} E_b(\zeta_b, \xi) &= \left(N_{bb} + |N_{bc}|^2\right)|\zeta_b|^2 - \zeta_b N_{bc}\xi^* - \zeta_b^* N_{bc}^* \xi & \text{(B.8)} \\ E_c(\zeta_c, \xi) &= (N_{cc}+1)\,|\zeta_c|^2 + \zeta_c\xi^* + \zeta_c^*\xi & \text{(B.9)} \end{aligned}$$

The integrand in Eq. (B.7) can now be decomposed into three Gaussian functions each of which satisfies the normalization condition because

$$N_{ii} > 0 \quad \text{and} \quad \mathrm{Det}N_{ij} > 0 \tag{B.10}$$

for positive well-defined $P(\zeta_b, \zeta_c)$ in Eq. (B.5). Taking

$$\begin{aligned} P_b(\zeta_b; \xi) &= \frac{M_b}{\pi} \exp\left(- M_b|\zeta_b|^2 + \zeta_b N_{bc}\xi^* + \zeta_b^* N_{bc}^*\xi - \frac{|N_{bc}|^2}{M_b}|\xi|^2\right) & \text{(B.11)} \\ P_c(\zeta_c; \xi) &= \frac{M_c}{\pi} \exp\left(- M_c|\zeta_c|^2 - \zeta_c\xi^* - \zeta_c^*\xi - \frac{1}{M_c}|\xi|^2\right) & \text{(B.12)} \\ \mathcal{P}(\xi) &= \frac{M_s}{\pi} \exp\left(-M_s|\xi|^2\right) & \text{(B.13)} \end{aligned}$$

where $M_b = N_{bb} + |N_{bc}|^2$, $M_c = N_{cc} + 1$, and $M_s = \mathrm{Det}N_{ij}/(M_b M_c)$, the P function is finally obtained in the form of Eq. (B.4). It is clear that $\mathcal{P}(\xi)$ is the positive probability density function and the two-mode Gaussian state is separable if it can be transformed to have a positive well-defined P function by some local unitary operations.